Design and Control of Bidirectional DC-DC Converters for Modular Battery Energy Storage Systems

Bortecene Yildirim

B.Sc., M.Sc.

A thesis submitted for the degree of

Doctor of Philosophy

August 2022

School of Engineering

Newcastle University

United Kingdom

Abstract

It has recently been shown that Distributed battery energy storage systems (BESSs) have several advantages over central battery energy storage systems. These include lightening the load on battery management systems (BMSs), reduced converter voltage ratings, increased reliability, and the ability to control individual battery modules` powers. This also gives an opportunity for flexible power sharing amongst different battery modules. However, these systems require numerous additional circuit components, including passive components, switches, and sensing and drive circuits.

This dissertation focuses on creating a more efficient power sharing controller and reducing the number of components used in Distributed BESSs. Power sharing controllers, which consider the state of charge (SoC) of individual battery modules, and the system conversion efficiency, have been proposed. Initially, an adaptive power sharing controller has been presented, whose performance depends on the SoC mismatch level. An efficiency-based optimised power sharing controller is then discussed, whose performance is independent of SoC mismatch level. For this method, the system efficiency is maximised at all battery power conditions, regardless of the degree of mismatch. To demonstrate the proposed algorithms effectiveness, a six-module prototype system, with each module consisting of a half bridge DC-DC converter and a 10 Ah, 12.8 V LiFePo4 battery pack, was constructed for the experimental validation. The results show that the systems conversion efficiency has been improved up to 5.05 % in discharging mode, and 4.8 % in charging mode.

In addition to the power sharing controller, a multi-port converter based Partially-Distributed BESS has also been proposed to reduce the number of circuit components in the structure. In the proposed structure, a group of battery packs is connected to their corresponding multi-port converter via enable / disable switches, with each multi-port converter connected in series. Therefore, different battery charging / discharging currents can be applied to the battery packs connected to the different modules. However, the battery packs connected to the same multi-port converter are charged / discharged with the same current, and therefore, a power sharing controller with a two-level balancing feature is proposed for Partially-Distributed BESSs considering the module-level and pack-level imbalances. The SoC imbalance amongst different modules is corrected using the applied power difference based on the modules relative SoC calculated within the power sharing controller. Pack-level balancing amongst the battery packs that are controlled by the same multi-port converter is achieved using bypassing.

Experimental results for the proposed dual-port converter have been presented in both discharging and charging modes, and the results obtained validate the proposed schemes.

Dedication

I dedicate my dissertation to my wife and my parents.

Acknowledgements

I am very grateful to my supervisors, Dr Mohammed A. Elgendy, Dr Andrew Smith, and Prof Volker Pickert for their encouragement, support, and guidance. I appreciate the time they spent with me and always providing me a new perspective and insight into my research.

I would specially thank Mr. Darren Mackie, Mr. Jeffrey Warren and Mr. Gordon Marshall for their insightful comments and help and for the development of the test-rig, not only for their expertise in electrical engineering but also for their kindnesses and warm-hearted support.

I would like to also acknowledge the Turkish Ministry of National Education for sponsoring this research.

Finally, I would like to thank my parents, and my wife for their support and encouragement.

Table of Contents

List of Figures

List of Abbreviations

AC	Alternating Current
ADC	Analogue-to-Digital Converter
BESS	Battery Energy Storage System
BMS	Battery Management System
DAB	Dual Active Bridge
DBESS	Distributed Battery Energy Storage System
DC	Direct Current
DoD	Depth of Discharge
EMI	Electromagnetic Interference
EMS	Energy Management System
EV	Electrical Vehicle
IC	Integrated Circuit
LiFePo4	Lithium Iron Phosphate
Li-ion	Lithium Ion
MOSFET	Metal Oxide Semiconductor Field Effect Transistor
NaS	Sodium Sulphur
NMC	Nickel Manganese Cobalt
NiMH	Nickel Metal Hydride
OCV	Open Circuit Voltage
PCB	Printed Circuit Board
PWM	Pulse Width Modulation
SC	Switched Capacitor
SoC	State of Charge
SoP	State of Power
SoH	State of Health
SPI	Serial Peripheral Interface
UPS	Uninterruptible Power Supply
VGR	Voltage Gain Ratio

ZVS	Zero Voltage Switching

Chapter 1. Introduction

1.1 Introduction

Battery energy storage systems (BESSs) play a key role in many applications, including portable devices, military applications, smart grids, and electric vehicles (EVs). The integration of the battery management system (BMS) is crucial for a reliable operation, long battery lifetime, and better utilisation of a battery pack. However, management of long battery strings is a challenging issue, especially considering high power applications such as grid storage and electric vehicles. A common solution to the long battery string is to divide it into sub-groups, where each sub-group has an individual BMS IC which is controlled by a central microcontroller. Alternatively, a fully distributed BESS architecture has several further benefits, such as the ability of continuous module / cell level balancing, integration of different battery chemistries and capacities, and improved reliability. This method also gives a degree of freedom for power sharing, which opens the door for power sharing flexibility which can be utilised for system efficiency improvement. However, the fully distributed BESS is expensive as it requires a large number of circuit components. Therefore, any cost reductions and system efficiency improvements obtained by utilising the power sharing flexibility in distributed BESSs are desirable and are the motivations for this research. In this chapter, a brief description of the conventional and distributed BESSs are given, and their challenges are discussed. The main contribution of this dissertation is briefly introduced and linked to the subsequent chapters.

1.2 Conventional Approach for Battery Energy Storage Systems

The deployment of battery energy storage systems (BESSs) is increasing day by day in power systems along with the increased adoption of distributed resources. The stochastic nature of distributed resources creates problems in terms of energy quality, and supply and demand variations. One of the solutions is to integrate the BESSs alongside the distributed resources to help with problems such as fluctuation mitigation, peak shaving, ramp-rate control, and maintaining the power balance [1-5]. A typical connection of a BESS in a DC coupled PV-BESS based microgrid system is illustrated in Figure 1.1.

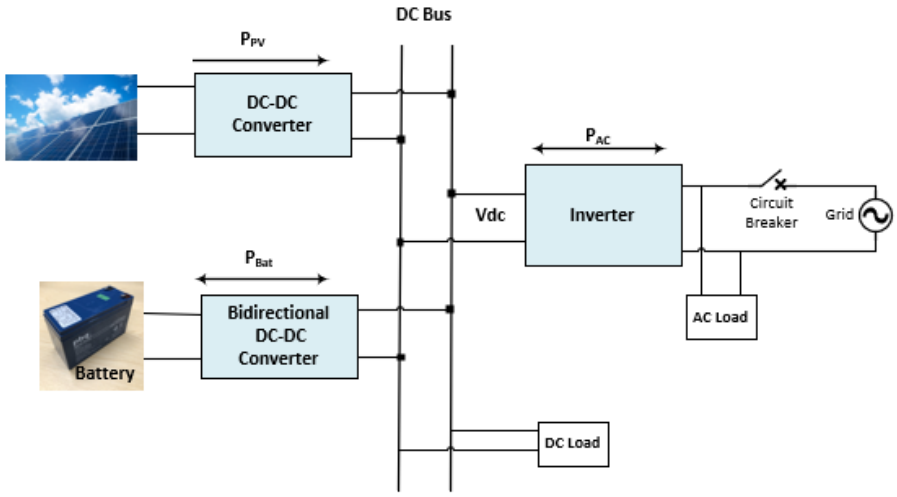

Figure 1.1: A Central Battery Energy Storage System

Battery packs are composed of several series and parallel connected cells, and to satisfy the requirements for applications such as grid storage and EV applications, many cells are connected in series and parallel to increase the voltage and current ratings. For example in [6], 108 series connected LiFePo4 cells are used to form a 350 V battery pack connected to 700 V DC bus, where the battery is utilised for an uninterruptible power supply (UPS) with a load levelling feature.

Similarly, several hundred battery cells are connected in series to increase the voltage level in EVs application, where typical battery pack voltage levels range between 200 V and 800 V [7- 9]. The use of high voltage battery packs in EV applications also provides additional benefits for fast charging, these include the reduction of charging time for the same battery current and power ratings, or a reduction in the cable size and hence conduction loss, for a lower battery current system [8, 9].

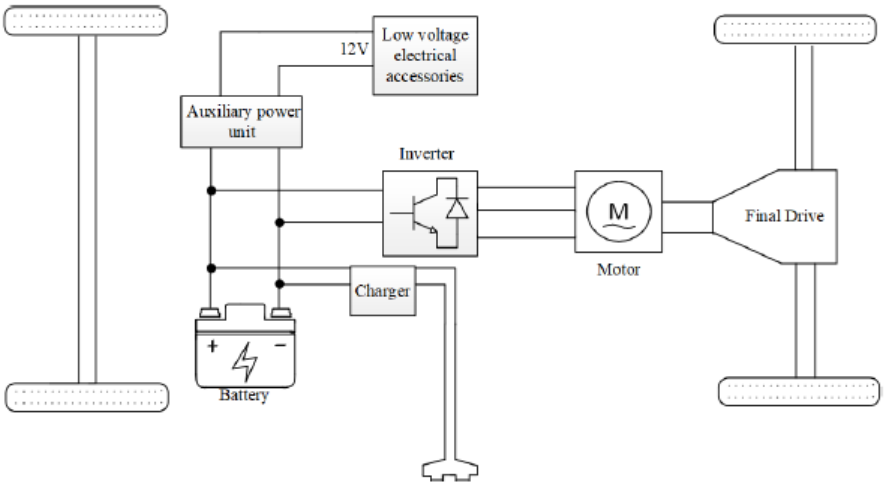

Figure 1.2: General configuration of a battery EV power train [8]

The utilisation of large battery packs is a challenging issue because of the non-uniform characteristics of individual cells. Although a battery pack is composed of the same battery cell technology manufactured by the same company, cell mismatch in a series string is inevitable. It is very unlikely to have identical battery cells at the beginning of their life because of manufacturing processing differences, and as the string performance is decided by the weakest cell in the string, the cell variations can cause capacity reduction during charging, and energy waste during discharging. Cell mismatch also brings additional problems such as overcharge / over-discharge, and safety problems.

To address the abovementioned problems, BMSs are employed for BESSs to increase the usable capacity / energy of a battery pack, and enhance the battery lifespan [10, 11]. The BMS performs crucial tasks such as monitoring individual cell status, estimating important parameters such as State of Charge (SoC), State of Health (SoH), and State of Power (SoP) over voltage and current protection, and cell balancing [12]. The main functions of BMSs are summarised in Fig. 1.3.

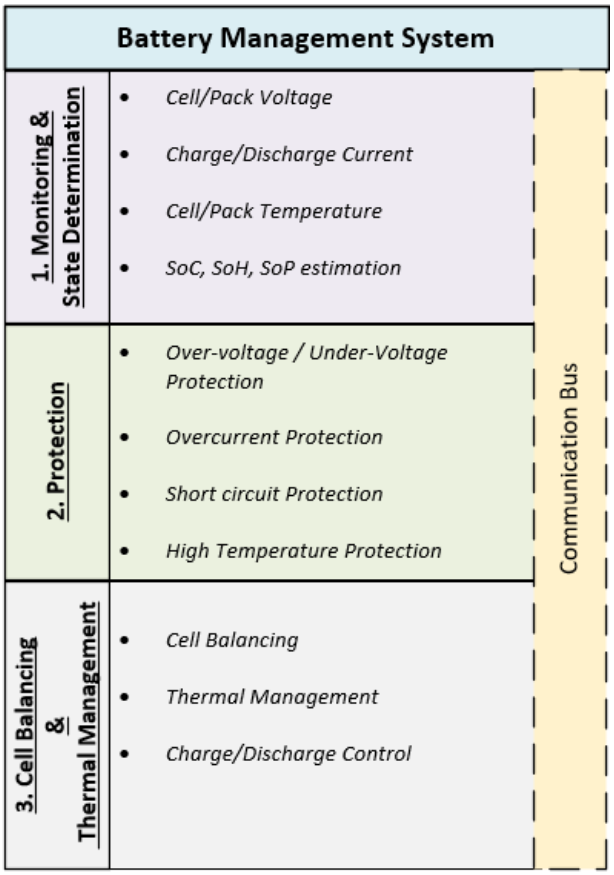

Figure 1.3: Battery Management System Function Overview

The terms for battery cell, battery pack, and battery modules used in this thesis are illustrated in Fig. 1.4. A battery cell represents a single battery cell, a battery pack is a combination of series and/or parallel connected battery cells, and a battery module is a combination of DC - DC converter and a battery pack or a battery cell.

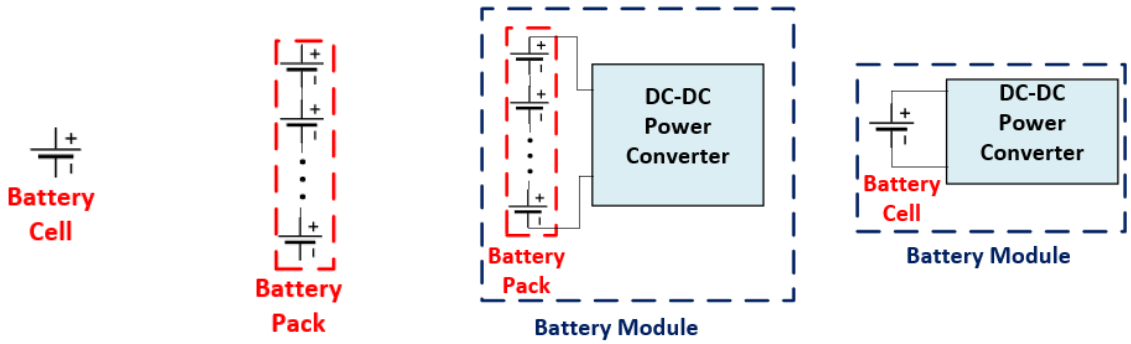

(a) (b) (c) (d)

Figure 1.4: Representation of Batteries (a) Battery Cell (b) Battery Pack or String (c) Battery Module connected to a battery pack (d) Battery Module connected to a battery cell

It is a common technique for large battery packs to manage a group of battery cells separately with individual battery management system boards, which are controlled by a central control unit as shown in Fig. 1.5.

As each BMS board is responsible for between 8 and 12 cells, this small group of cells can be well-managed by the existing balancing topologies in this structure. However, it shows poor performance in trying to correct for the imbalance occurring between battery cells managed by different BMS ICs. Although, the BMS performs balancing functions, each cell is exposed to different ageing due to its slightly different characteristics and the non-uniform thermal distribution occurring throughout the operation of the battery, and the weakest cell limits the performance and lifetime of the whole battery system [11].

The battery pack is connected to the DC bus via a central DC-DC converter which is being used to control the battery charge / discharge powers and to match the battery voltage to the DC bus voltage. This DC-DC converter will be designed to handle the full power of the battery pack. Typically, a high step-down ratio DC-DC converter is used in EV applications to connect the high voltage battery pack, to the low voltage, dc auxiliary loads. In many microgrid applications, the battery voltage is lower than that of the DC bus, so the battery voltage is boosted using the central DC-DC converter. However, the design of high power, efficient, compact, and cost-effective high voltage gain ratio (VGR) DC-DC converters is a research topic beyond the scope of this thesis.

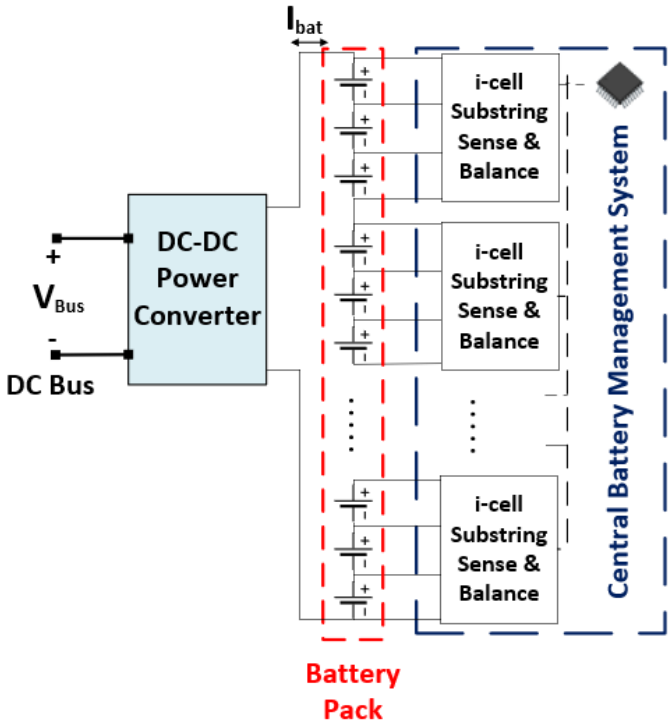

Figure 1.5: A Central Battery Energy Storage System

1.3 Distributed Approach for Battery Energy Storage Systems

In fully-distributed BESSs, the low voltage battery packs are connected to their associated DC-DC converters, and these converters are then connected in series to increase the overall voltage. In this structure, each group of batteries can be managed by its own BMS, and the power sharing controller can manage balancing amongst different battery packs via the different BMSs. Consequently, the additional pack level balancing ability lightens the load on the BMS and balancing circuits and improves the performance of the BESS. The reliability of this system is further improved as any faulty module(s) can be bypassed from the system and replaced without interrupting the overall system operation. The structure is scalable and any applications voltage and power requirements can be achieved by adjusting the number of modules without the need for a high VGR central converter.

In comparison to the central structure, this method allows each battery pack`s power to be controlled separately, allowing the integration of different battery packs with different capacities, chemistries, and SoH for each module.

In the literature, different power sharing controllers have been proposed for fully-distributed BESSs. Huang et al [13], and Li et al [14] reduce the system down the system cell level, where each cell is connected to its corresponding low voltage DC-DC converter to remove the

requirements for additional balancing circuitry. In [15] Altaf et al propose a power sharing controller for simultaneous SoC and thermal balancing of individual cells.

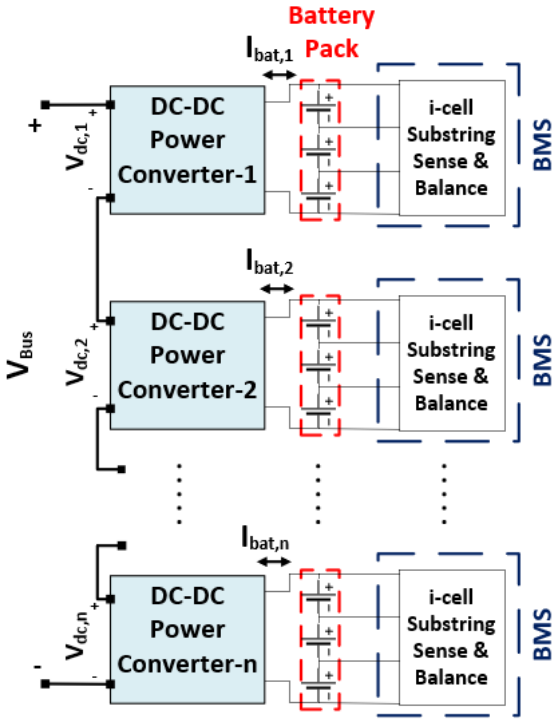

Figure 1.6: The fully-distributed BESS

Li et al [16] are controlling pre-used battery packs to utilise of the individual battery controlling ability, and degree of freedom power sharing, in a fully-distributed BESS. Similarly, pre-used batteries having different chemistries are controlled with the proposed power sharing controller in a fully modularized structure in [17]. A State of Health (SoH) balancing controller is implemented in [18] by adjusting the individual battery pack`s depth of discharge (DoD) in each cycle.

A central multi-port converter has been proposed to modularize battery packs in [19, 20], where each battery pack is connected in series via two complementary switches. In addition, each battery pack has its own balancing circuits and management systems, and any faulty or overcharged / discharged pack can be bypassed. Although this structure lightens the load on the BMS, and increases the system performance and reliability, all of the battery packs are charged / discharged with the same current using a central high current converter, limiting the control flexibility of the system. Unlike the complete modular structure, the battery packs must be of the same chemistry and SoH in this structure. In addition, the whole system relies on a high-voltage central DC-DC converter which makes the reliability of this converter vital.

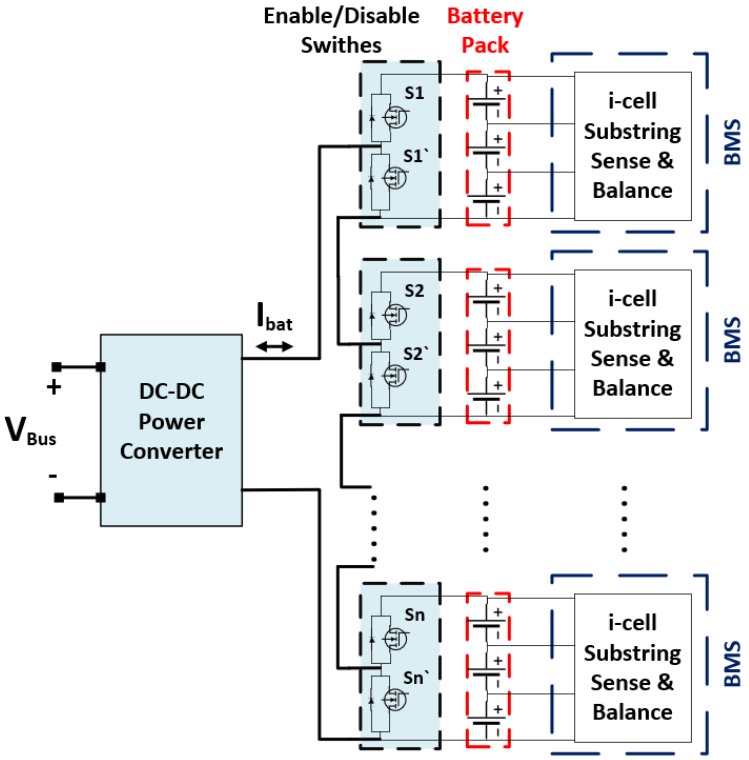

Figure 1.7: Central Multi-Port converter-based BESS

1.4 Thesis Contributions

The contributions of this dissertation are summarised as follows:

1. Power sharing controllers proposed in the literature mainly focus on the balancing of the battery packs` SoC, temperature, and / or SoH in a fully-distributed structure. The converters used in Distributed BESSs are designed to handle the full power of the battery packs, and operate at different power levels depending on the power sharing controller and system battery power demands. Although each converters efficiency curve can be assumed to be the same by assuming identical converters, different module loadings result in different system efficiencies. A typical converter efficiency varies with respect to the load and shows a higher efficiency at some operating areas. For a system having more than one converter, the efficiency can be improved by adjusting individual module powers based on the operational efficiency and total power demand. For example, in parallel connected and interleaved modules, the light load efficiency is improved by deactivation of some module(s) and increasing the active module(s) load. In this dissertation, an efficiency-based optimised power sharing controller is proposed to improve the system conversion efficiency at different battery powers without any additional components or cost increase. The efficiency map of a single converter is

generated from no-load to the full load case, the system efficiency is formulated, and the optimum load for each module is determined using Genetic Algorithm optimisation. In order to respond real time fast changes in the load, a look-up table is constructed using the off-line optimisation algorithm results, and power sharing is achieved by the SoC management loop. The proposed efficiency-based optimised power sharing controller increases the system conversion efficiency at light load, and limits the possible efficiency reduction at heavy load.

2. A partially-distributed BESS based on a multi-port converter is also proposed to reduce the cost of the system without diminishing the advantages of the fully-distributed structure. The fully distributed structure shown in Fig. 1.6 employs numerous components and sensing circuits which increases the system cost. In the alternative central multi-port converter-based BESS (Fig. 1.7), the number of components and sensing circuitry is reduced compared to the fully-distributed BESS. However, the battery packs connected to the same multi-port converter are charged / discharged with the same battery current. This may limit the integration of different capacity and chemistry batteries to the same multi-port converter, as different capacity and chemistry battery packs have different charging and discharging profiles. The proposed partially-distributed structure, shown in Fig. 1.8, has a lower number of components and sensing circuits compared to the fully-distributed structure, reducing the cost and complexity of the system. This partially-distributed structure still maintains the flexibility in terms of different module loading ability and the degree of freedom for power sharing. As each module can be loaded at different power, it also enables integration of different types of batteries controlled by different converters.

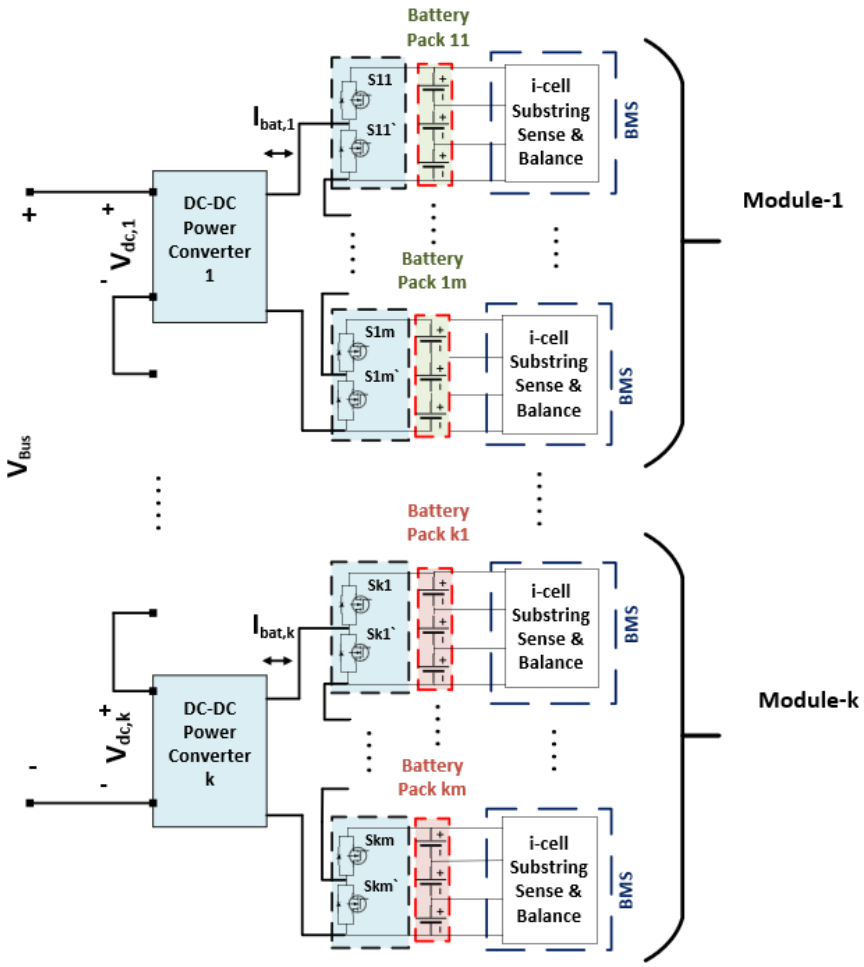

Figure 1.8: A partially-distributed BESS based on a multi-port converter

A power sharing controller with a two-level balancing feature has been proposed here considering module-level and pack-level imbalances. The individual module powers are determined based on the relative values of the individual module capacities and their SoC to the average values, allowing SoC balancing amongst each module. As each battery pack is connected to the same converter, it is charged / discharged with the same power, and there may be some imbalance amongst these battery packs. In the proposed controller, this pack imbalance is corrected by bypassing higher charged battery pack(s) during charging, and lower charged pack(s) in discharging mode. As any bypassed pack(s) affect the module`s voltage, capacity and average SoC, the proposed controller adjusts the individual module`s power demands to maintain SoC balancing during bypassing and reactivation.

1.5 List of Publications

- **B. Yildirim**, M. Elgendy, A. Smith, and V. Pickert, "Evaluation and Comparison of Battery Cell Balancing Methods," in *2019 IEEE PES Innovative Smart Grid Technologies Europe (ISGT-Europe)*, 2019, pp. 1-5.
- **B. Yildirim**, M. A. Elgendy, A. Smith, and V. Pickert, "Adaptive Controller for Power Sharing in Modular Battery Energy Storage Systems," in *The 10th International Conference on Power Electronics, Machines and Drives (PEMD 2020)*, 2020, vol. 2020, pp. 338-342.
- **B. Yildirim**, M. Elgendy, A. Smith, and V. Pickert, "Comparison of Cascaded Modular Converter and Central Multi-Port Converter for Modularization of Battery Packs," in *The 11th International Conference on Power Electronics, Machines and Drives* (PEMD 2022)
- **B. Yildirim,** M. A. Elgendy, A. Smith, and V. Pickert, "Efficiency Optimized Power Sharing Algorithm for Modular Battery Energy Storage Systems," *IEEE Transactions on Industrial Electronics*, pp. 1-10, 2022.
- **B. Yildirim**, M. Elgendy, A. Smith, and V. Pickert, "Partially distributed BESS with two-level balancing ability (Final title to be determined) ," In preparation

1.6 Dissertation Outline

The thesis is organised into 7 chapters as follows:

Chapter 2 presents a detailed literature review covering the state-of-the-art BESSs including BMS and DC-DC converter interfaces. Several SoC estimation methods and cell balancing topologies are discussed and compared, with the advantages and disadvantages of each method highlighted. Common bidirectional DC-DC converter topologies for BESSs are reviewed, and, the challenges of traditional battery systems are summarised.

Chapter 3 introduces distributed BESSs along with different power sharing control methods, and the advantages and disadvantages of distributed BESSs compared to the central converter-based structure are discussed. This chapter presents simulation results for the SoC-based power sharing controllers, and the systems balancing speed and efficiency are discussed. An adaptive power sharing controller, which considers system balancing speed and efficiency is then proposed, and its simulation results are presented and compared to the SoC-based power sharing controller.

Chapter 4 proposes an efficiency-based optimised power sharing controller for a fully-distributed BESS. This method considers the conversion efficiency, battery lifespan, and the management of SoC. The problem formulation, optimisation, and real-time implementation are discussed, and the simulation results are presented.

Chapter 5 proposes a partially-distributed BESS structure based on a multi-port converter along with the power sharing controller. The systems structure is presented along with the design considerations, and the power sharing control is explained in detail. The new structure is compared to the fully-distributed and central multi-port converter based BESSs in terms of number of components, their ratings, sensing circuitry, and reliability. The proposed power sharing controller is then verified via simulation in both charging and discharging modes.

Chapter 6 focuses on the experimental validation of the controllers proposed in this dissertation. This chapter initially gives a brief overview of the experimental system setup. Experimental results for the fully-distributed BESSs using both the SoC based power sharing, and the proposed efficiency-based optimised power sharing, are then presented and compared. Finally, experimental results with a partially-distributed BESS using a dual-port converter are presented using the proposed power sharing controller.

Chapter 7 concludes and summarises this dissertation research work, and recommends potential future research areas.

Chapter 2. Battery Energy Storage Systems (BESSs)

2.1 Introduction

In this chapter, traditional BESSs and their main components, which include the battery pack, battery management system (BMS), and power converter interface, are discussed. Initially, typical battery pack configurations and their structures are described. BMSs and their functions are then explained with special attention paid to SoC estimation methods and cell balancing circuits. Simulation results of some cell balancing topologies are then presented and discussed. Finally, several bidirectional DC-DC- power electronic converters for BESSs are reviewed.

2.2 Architecture of a Battery Energy Storage System

A typical BESS consists of a battery pack, BMS, and a power electronic converter interface as shown in Fig. 2.1. Depending on their chemistry, single battery cell voltages vary between approximately 1 and 4.5 V. For example, nominal cell output voltages are around 1.25 V for nickel metal hydride (NiMH), 2 V for lead acid cells, 2.1 V for sodium sulphur cells (NaS), 3.6 V for lithium nickel manganese cobalt (NMC), and 3.3 V for lithium iron phosphate cells (LiFePo4) [21-24]. Due to the limited voltage and capacity of a single cell, groups of cells are connected in series and parallel to form a battery pack, increasing the battery voltage and capacity, respectively. The power electronic interface controls the charging / discharging power of a battery pack based on the systems demands. Battery management systems (BMSs) monitor the status of each battery cell inside the pack, sensing the cell voltage, current, and temperature, and using these values, they estimate the available pack energy and capacity, and coordinate the system`s operation to ensure reliable battery operation and safety.

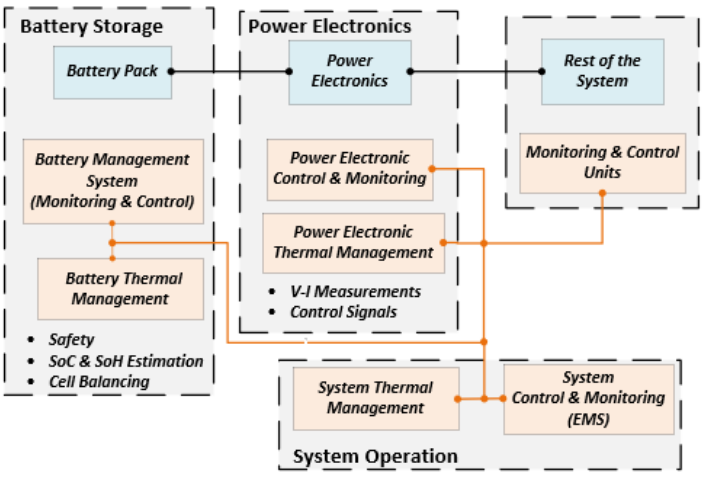

Figure 2.1: A functional block diagram of a Battery Energy Storage System

2.3 Battery Management System (BMS)

A BMS is a key component in battery storage systems, monitoring individual cell voltages, cell currents, cell or pack temperatures, and estimating the cell state of charge (SoC) and state of health (SoH) to ensure safe operation of the battery pack, and to increase its lifespan. Monitoring of the packs individual battery cells gives reliable battery operation, and if there is any undesired circumstance such as overcharging, over-discharging, overcurrent, and / or a high temperature, the BMS stops the systems operation in collaboration with the power converter and system controller. Figure 2.2(a) illustrates a typical implementation of a BMS for a large battery pack. Nowadays, due to the availability of numerous cell management ICs, it is a common practice to manage groups of cells separately, with an overall central controller used for large battery strings. Different manufacturers of these cell management ICs include Linear Technology, Texas Instruments, and Analog Devices [25]. For example, the LTC6804 from Linear Technology can manage up to 12-cells, and can support up to 100 cells using a chain structure as shown in Fig. 2.2 (b). Groups of cell data such as cell voltages, cell currents, and pack temperature, are exchanged with the central controller using built-in isolated serial peripheral interfaces (SPI), and the battery balancing operation mode for each module is determined based on the predefined strategy [26].

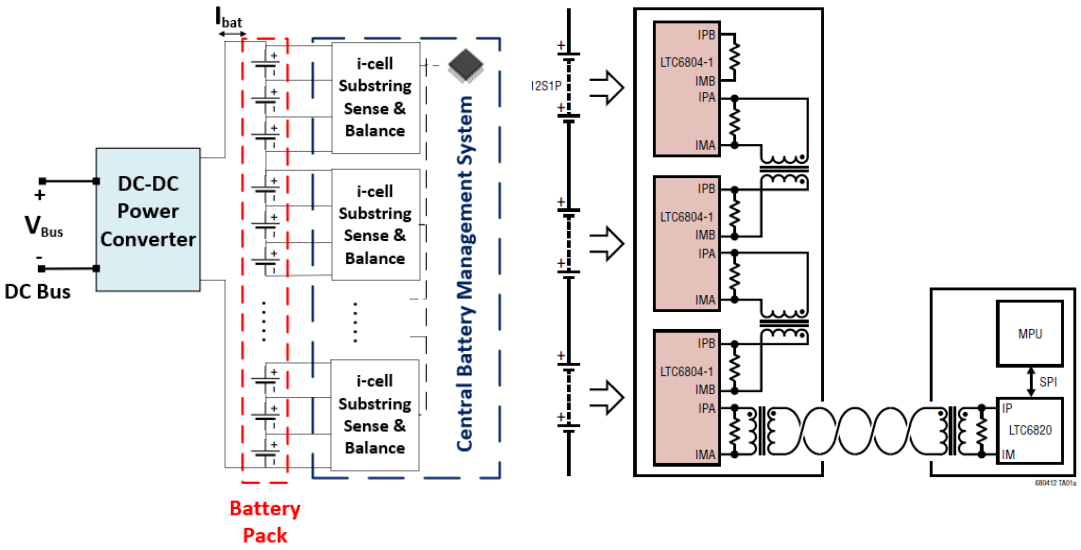

(a) (b)

Figure 2.2: (a) The architecture of a Battery Energy Storage System (b) The Linear Technology multi-cell battery monitor LTC6804 [27]

SoC estimation and cell balancing are the challenging tasks that the BMS must undertake, and the following subsections review some of the methods proposed in the literature concerning these.

2.3.1 State of Charge (SoC) Estimation Methods

The battery SoC can be expressed as the percentage of the remaining available battery capacity over the nominal capacity [28, 29], as depicted in (2.1). A fully charged battery can be stated as having a 100% SoC, while 0% SoC represents an empty cell. It is therefore crucial to estimate the SoC of a battery pack as accurately as possible to allow better battery utilisation and safer operation. The battery voltage and SoC relationship is shown in Fig. 2.3 at different C-rates. Battery C-rate is the ratio of the battery charging / discharging current to its maximum capacity. For example, the C-rate is 1 when a 10 Ah battery pack is charged with 10 A current. However, the nonlinear characteristics of batteries, battery ageing factors, and the different operating conditions, makes SoC estimation challenging [30, 31].

$$SoC_{(t)} = \frac{Q}{Q_n} \times 100\% \tag{2.1}$$

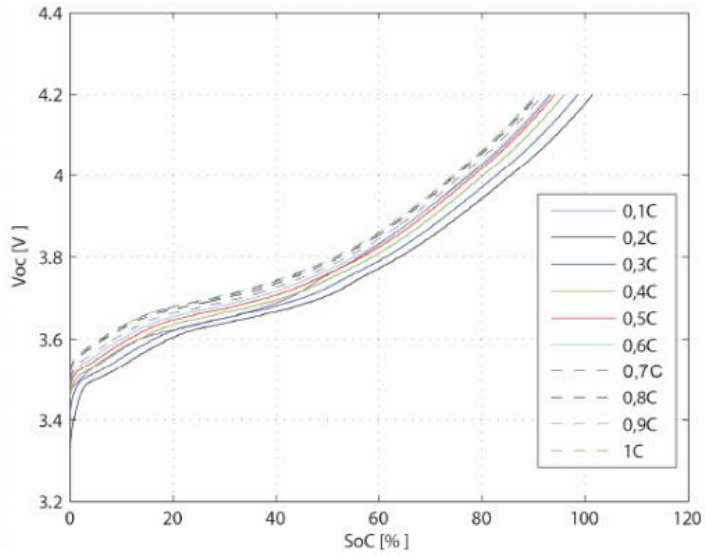

Figure 2.3: OCV-SoC relationship during charge process at different C-rates [42]

There are several well-known SoC estimation methods proposed in the literature. The Coulomb counting method (also known as Ampere-hour method), is a popular and simple SoC estimation technique [32]. It is based on integrating the battery current, which is positive in discharging case in (2.2), over a period of time during either charging / discharging, and it can be expressed as:

$$SoC_{(t)} = SoC_{(0)} - \frac{1}{C * 3600}\int_{t=0}^{t} I_{bat} \times dt \quad (2.2)$$

where C represents the battery capacity and I_{bat} represents the battery current.

The main drawbacks of this method are that it requires knowledge of the initial SoC value and precise current measurement, as any incorrect initial SoC value causes accumulated estimation error [33, 34]. For this reason, re-calibration of the initial SoC is required. In addition, the cell capacity reduction due to ageing also causes estimation error, although this capacity reduction is not as crucial as the initial SoC calibration because ageing is a slow process. The capacity should also be periodically updated. In order to get rid of accumulative errors, it is recommended that the initial SoC be updated at both the fully charged and empty states [32, 35]. The initial battery SoC is calibrated by resetting it to 100% SoC at the fully charged state, and to 0% at the empty state. However, the battery may not be fully charged or discharged which limits its usage for online estimation.

Open Circuit Voltage (OCV) based estimation methods use the relationship between the SoC and OCV of a battery. This relationship is used to create a look-up table which is based on laboratory testing of the battery. The two most common OCV-SoC mapping tests are low current and incremental OCV [36-38]. In the incremental OCV test, the battery is charged up to 100 % SoC, and then discharged using current pulses, with a period of rest between each current pulse to minimise the polarisation effects. The OCV-SoC relationship in charging mode can be obtained using the charging discharging profiles illustrated in Fig. 2.4 [37]. Although good performance is shown in a laboratory environment, precise real world OCV measurement is a challenge as it requires resting the battery for long periods of time [39, 40]. Figure 2.5 shows that the OCV-SoC curve has different relationships at different ambient temperatures [41], and instead of being operated independently, this method is generally applied alongside other techniques to allow correction of any measurement errors and calibrations [30, 35, 40, 42].

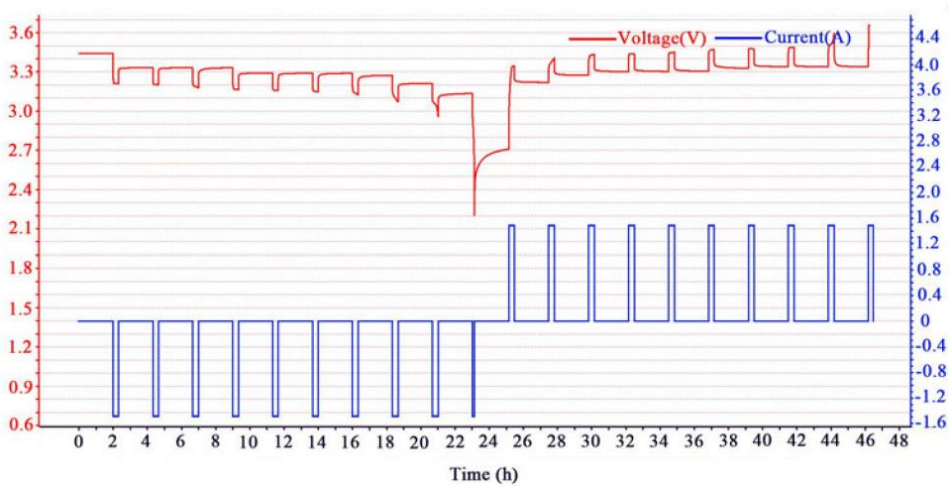

Figure 2.4: The charged discharged profiles of low current OCV test [37]

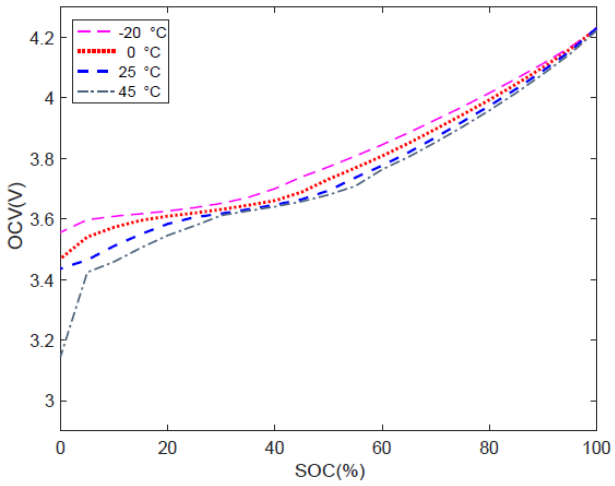

Figure 2.5: Battery OCV-SoC relationship with different temperatures [41]

In model-based estimation methods, the SoC estimation is based on battery model state space equations, and therefore, battery modelling is the basis of model-based estimation methods. Rint, PNGV, and the Thevenin model are the most common battery models used (used in the literature [41-43].

A second order Thevenin equivalent model is illustrated in Fig. 2.6, where R_0 is the internal ohmic resistance, the first RC pair (R_1C_1) represents the contact resistance and capacitance, and the second RC pair (R_2C_2) represents the long transient effects such as concentration polarisation, diffusion, and charge transfer effect [44].

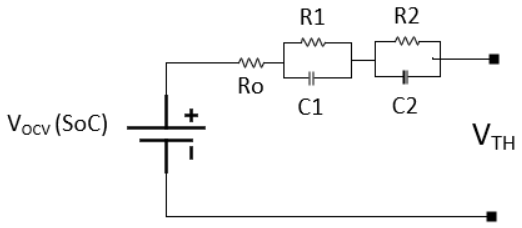

Figure 2.6: Second order battery equivalent circuit model

Although higher order models improve the modelling accuracy, a system second order is commonly used in the literature to reduce the complexity. The models parameters are identified by preliminary tests and are updated with the change of battery operating conditions [31]. From laboratory testing, the relationship between the OCV and SoC can be expressed as an n-order polynomial equation. For example, in [45] the authors use a 6th order polynomial equation to describe this relationship as shown in (2.3)

$$OCV(SoC) = -34.72 \times SoC^6 + 120.7 \times SoC^5 - 165.9 \times SoC^4 + 114.5 \times SoC^3 - 40.9 \times SoC^2 + 7.31 \times SoC + 3.231 \quad (2.3)$$

Many nonlinear state estimation algorithms and adaptive filters such as the Kalman filter [46-48], H ∞ [49], PI observer [50], and sliding mode observer [51, 52] are used in conjunction with the battery model to estimate the internal state conditions of the battery and the SoC. Figure 2.7 shows a simplified diagram of model-based SoC estimation algorithms.

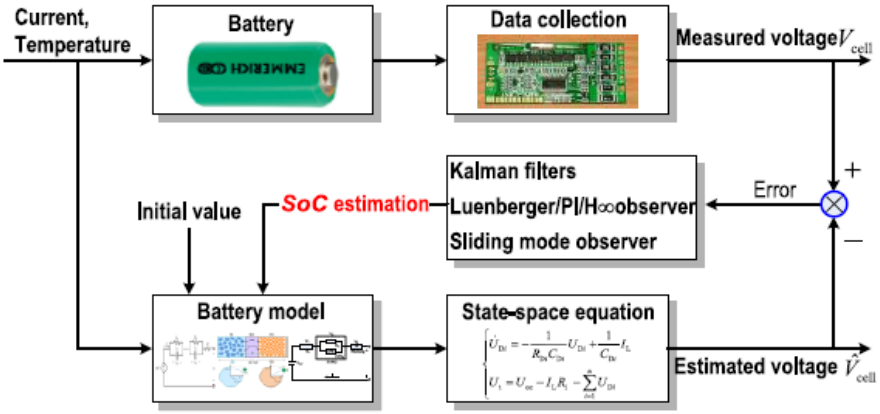

Figure 2.7: Block diagram of Model-based SoC estimation method [30]

The self-correction ability of the closed-loop system improves estimation accuracy and helps to minimise the effect of uncertainties and disturbances [53]. However, as model-based

estimation methods rely on battery modelling accuracy, a higher order model is necessary to describe the complex electrochemical processes occurring within the battery. In addition to the difficulty in accurately modelling the battery considering all of the nonlinear and time-varying characteristics, the higher order model also increases the computational complexity of the system [39, 42, 54].

In data driven SoC estimation methods, the SoC can be estimated using the relationship between the SoC and the battery operating conditions, with the battery terminal voltage, current, and temperature obtained through extensive data training [39, 55]. Many data-driven algorithms, including Artificial Neural Networks [56, 57], Support Vector Machines [58, 59], and Fuzzy Logic controllers [60] have been proposed in the literature to formulate the relationship between the input and output data, and unlike the model-based methods, they do not require extensive knowledge of the battery characteristics. However, extensive knowledge of the training data is required to cover all of the real-time working conditions, as the battery operating conditions may be different from the trained data, and any mismatch between the dataset and real-time operating conditions will reduce the SoC estimation accuracy [54, 61].

2.3.2 Battery Cell Balancing Topologies

Battery pack cell mismatch is inevitable, as each battery cell will have slightly different intrinsic resistances, self-discharge rates, and capacities, due to the inherent manufacturing variations. During the numerous charging and discharging cycles that occur, different power losses arise due to of the intrinsic resistance differences. The thermal variations in the battery pack contributes to the cell mismatches and increases the cell non-uniformity after charging and discharging operations [62 -64].

As a result, the performance of a string battery pack reduces during operation, as it is determined by the weakest cell in the string [65-67]. For example, when a cell reaches its fully charged state before the others, the BMS stops the charging process to prevent overcharging. This results in wasted battery pack capacity as some of the battery cells are still undercharged. [68-70]. Similarly, if a cell is fully discharged earlier than the others, the rest of the available energy from the pack cannot be utilised to prevent over-discharging, resulting in wasted energy. To overcome these problems, BMSs also performs cell balancing functions for series connected cells. In this subsection, different balancing topologies are reviewed and discussed with supporting simulation results presented.

Several cell balancing circuits have been proposed in the literature [71]. According to the method they use to process the redundant energy, cell balancing can be categorised into three main groups: dissipative, energy transferring, and runtime. In the dissipative balancing method, equalisation is achieved by dissipating excess energy from higher charged cells. Figure 2.8(a) shows the implementation of dissipative balancing circuits with fixed shunt resistors. Due to the parallel resistors across each cell, continuous current flows through the resistors, and as the higher charged cells have higher voltages compared to lower charged ones, more energy is dissipated from the higher charged cells, resulting in a convergence of the voltages [72]. However, there is still power flowing through the resistors even when all cells are balanced. To prevent continuous power loss, and to control the balancing circuits, a controllable switch must be placed in series with each resistor as shown in Fig. 2.8(b). Although this is the simplest and cheapest equalisation method, the excess energy is dissipated as heat, resulting in a low energy efficiency. In addition, there is no run time improvement with this method, and some of the available energy from the string cannot be utilised in discharging mode.

(a) (b)

Figure 2.8: Dissipative Balancing Methods, (a) Fixed Shunt Resistor (b) Switched Shunt Resistor

To analyse the dissipative balancing performance, a battery string consisting of 4 series lithium battery cells rated at 3.2 V and 10 Ah was simulated using MATLAB / Simulink. The initial SoC of the individual cells is shown in Table 2.1

Table 2.1: The initial SoC of the individual cells at beginning of the simulation

Cell 1 (%)	**Cell 2 (%)**	**Cell 3 (%)**	**Cell 4 (%)**
70	65	68	60

Dissipative balancing is generally used for charging mode, as there is no advantage in enabling any balancing whilst discharging. In this simulation, the algorithm operates so that when one of the cells reaches its maximum SoC, the BMS stops the charging operation and balancing is enabled until all cell voltages are equal, then charging starts again. Results of the switched shunt resistor balancing method previously shown in Fig. 2.8(b) using 200 mA and 1 A balancing currents are illustrated in Figs. 2.9(a) and 2.9(b) respectively. To adjust the balancing current the value of the parallel resistors has been modified, where the balancing current is inversely proportional to resistor value. With the 200 mA current the balancing takes 5 hours, reducing to 1 hour with a 1 A current. However, the power loss during the balancing is also 5 times higher using the 1 A current compared to that of 200 mA, as shown in Figs. 2.10(a) and (b). It is worth mentioning that with the dissipative balancing method, the final battery pack SoC is equal to that of the weakest cell, which is 90 % in this case presented.

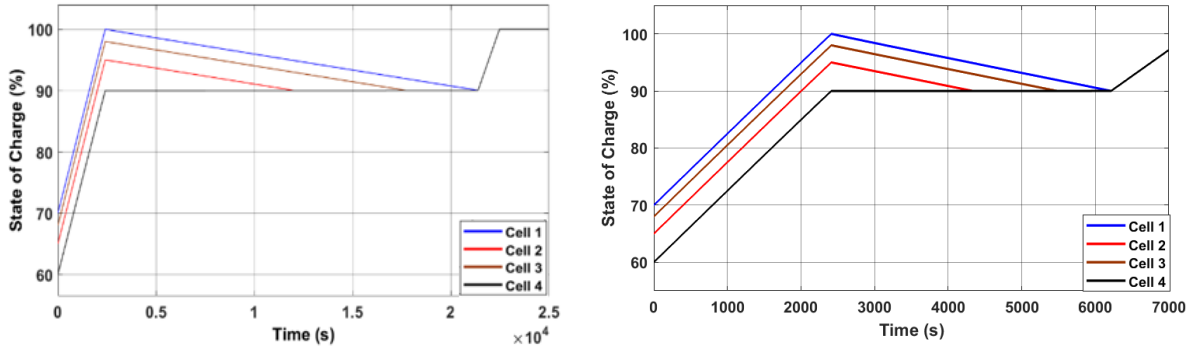

(a) (b)

Figure 2.9: Switched shunt resistor balancing method, (a) Cell SoC with 200 mA balancing current, (b) Cell SoC with 1 A balancing current

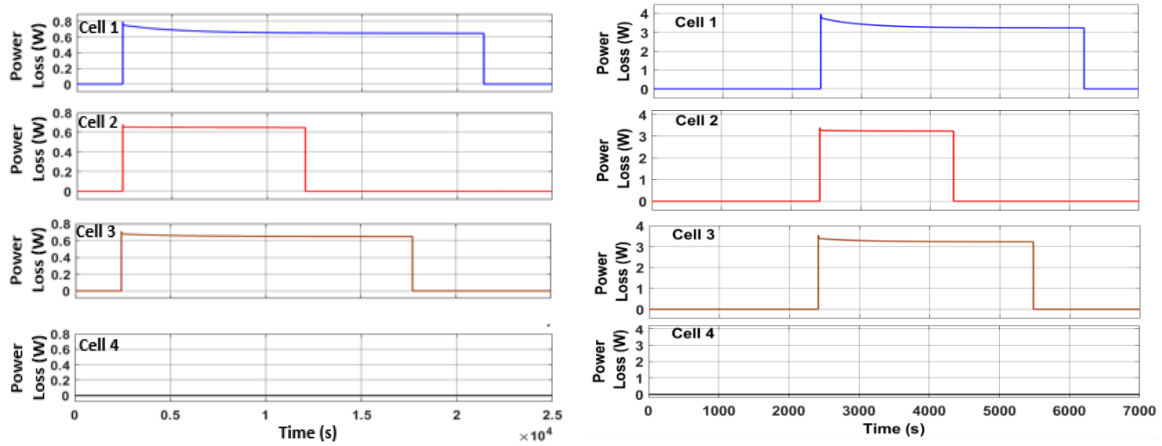

(a) (b)

Figure 2.10: The power loss of each cell, (a) with 200 mA balancing current, (b) with 1A balancing current

Dissipative balancing is the most common method due to its simplicity and cost. However, in practice, the balancing current is restricted to several mA to prevent excessive heat generation, and the resultant balancing speed is slow due to this limited current, especially for higher power applications [73]. Therefore, this balancing method is only satisfactory for lower power applications and for battery strings comprised of very similar SoH cells.

In energy transferring methods, the energy is transferred from higher charged cells to lower charged cells using switches and passive components such as capacitors, inductors, and transformers. The main advantages of this method over dissipating balancing are its higher efficiency and utilisation of the available energy. In the switched capacitor (SC) cell balancing method shown in Fig. 2.11(a), capacitors are connected between the upper and lower cells in one switching cycle, enabling energy exchange between adjacent cells. A disadvantage of this is that the energy exchange is only possible for adjacent cells, so the balancing losses and balancing time increase with string length [74]. Derivatives of the SC method exist, such as the doubled tiered [75] (Fig. 2.11(b)) and chain structures [76, 77] (Fig. 2.11(c)), and these can slightly reduce the balancing time and losses using additional capacitor(s). However, energy transfer is still not possible between arbitrary cells in the string. To address this problem, Ye et al proposed an optimised SC method [78], in which energy transfer is possible between any cells due to the common point of the capacitors as shown in Fig. 2.11(d).

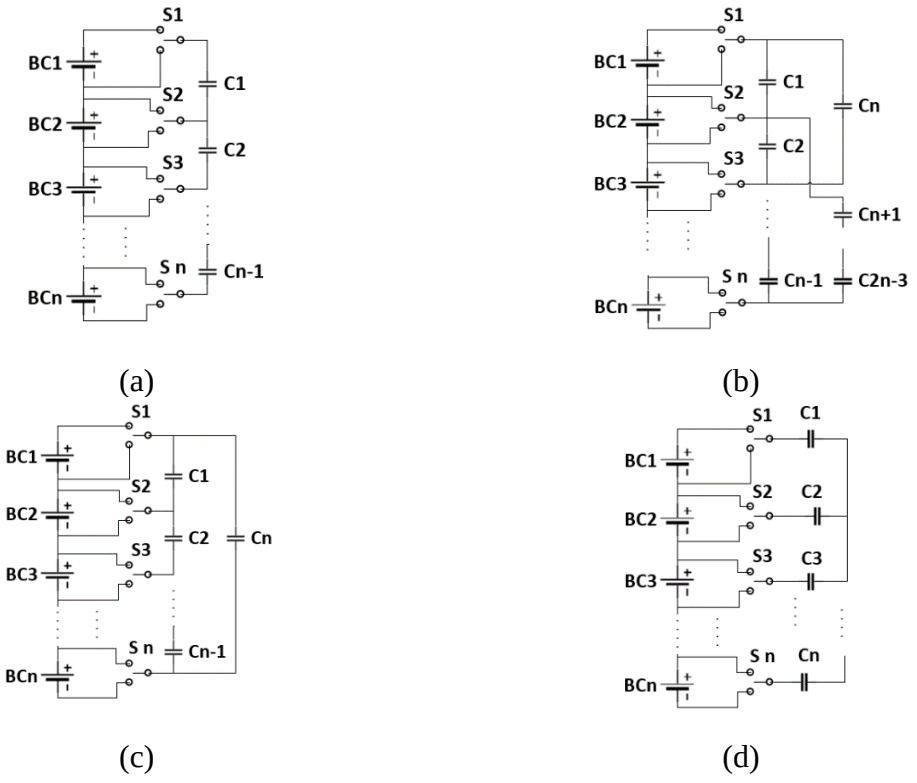

Figure 2.11: Capacitor based energy transferring methods, (a) SC, (b) Double Tiered SC, (c) Chain Structure, (d) Optimised SC

The simplistic control of capacitor-based energy shuttling methods is promising, as all switches are controlled by complementary signals, and no voltage sensing or closed loop control are required [75]. However, they aim to balance cell voltages rather than SoC, which may cause increased unbalance due to the intrinsic cell resistance mismatch, and an increased equalisation time because of the flat discharge curve of the battery. The resistance mismatch is important, especially in pre-used battery cells, which limits this methods application to pre-used battery cells.

The simulations for the SC balancing methods used 470 µF capacitors each having a 20 mΩ equivalent series resistance, and a 50 kHz switching frequency. The initial SoC of the individual cells is the same as for the previous testing (Table 2.1). Figures 2.12(a) and 2.12(b) show the SoC simulation results of the SC and optimised SC balancing methods, respectively. It is evident that unlike the standard SC method, in which energy transfer is only possible between adjacent cells, direct energy transfer between all cells is possible with the optimised SC method. In the conventional SC method (Fig. 2.12(a)), there is still a slight imbalance between the battery cells compared to the optimised, even after 75 hours. Although a relatively faster balancing was achieved with the optimised SC method, the balancing is still very slow, taking approximately 60 hours in this case. Compared to the dissipative method, with the energy transferring method, after the balancing is finished, the average battery and battery pack SoCs are equal if the power losses are ignored, which is 65.75 % in this case

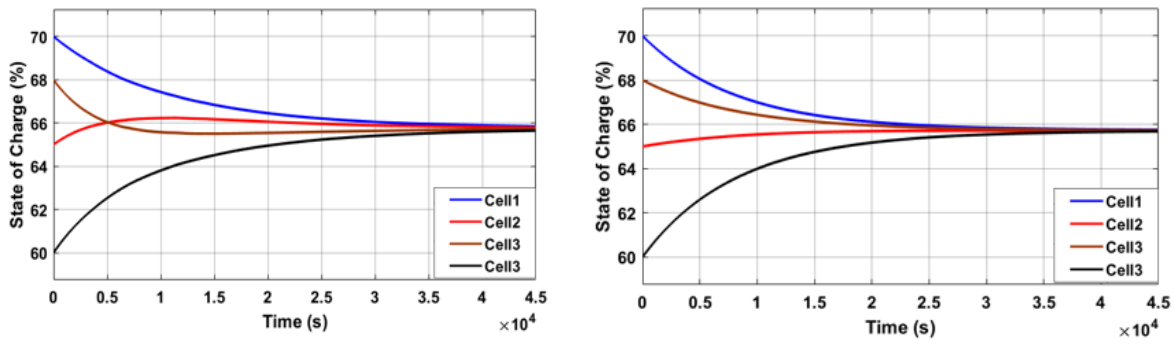

Figure 2.12: The balancing results with capacitive energy transferring method (a) Switched Capacitor, (b) Optimised Switched Capacitor

The multi-inductor energy transferring method [79], which is shown in Fig. 2.13(a), transfers energy between adjacent cells, but as the string length increases, the balancing loss and time also increase in a similar fashion to the SC method. In [80], Park et al proposed the single inductor energy transferring method illustrated in Fig. 2.13(b). In this method, the energy is transferred from the highest charged cell to the lowest charged cell by controlling their corresponding switches. This method allows faster balancing in comparison to the multiple inductor method, but the presence of the diode in the balancing path limits its efficiency, as the diode voltage drop is around 10% - 20% of a single cells voltage [81].

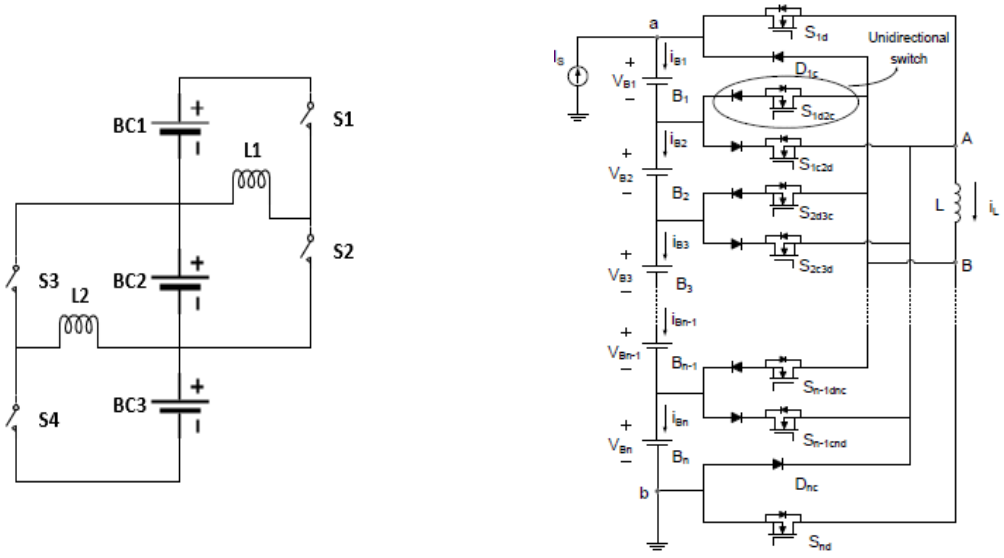

(a) (b)

Figure 2.13: Inductor-based energy transferring methods, (a) Multi-Inductor, (b) Single-Inductor [80]

The multi-winding energy transferring method proposed in [82, 83] and shown in Fig 2.14, is easy to control. In this method, the entire battery pack is connected to the primary winding of a transformer, and a single controllable switch is used to induce currents in the secondary winding of the transformer. The battery cells with lower voltages receive higher currents, and therefore balancing is achieved with a simple control method. However, the design complexity of higher multi-winding transformer systems limits this methods usefulness for a high cell string, and the presence of the diodes also reduces the system efficiency. To increase the efficiency, Li et al [81] and Chen et al [84] utilise bidirectional switches to reduce the conduction losses for the multi-winding transformer method, allowing direct cell-to-cell energy transfer. In these papers, MOSFETs are used for each cell with a common control signal, making the control easier. Although it achieves better efficiency and allows energy transfer

from any cell to any cell, the design complexity of the multi-winding transformer increases with the number of string cells.

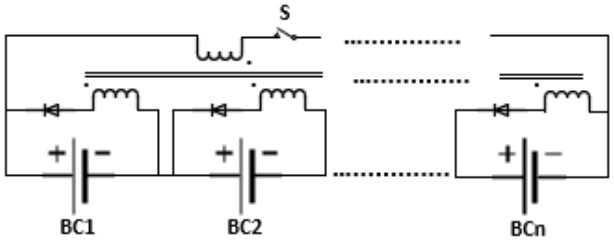

Figure 2.14: Multi-winding transformer-based energy transferring methods

The multiple-transformer based equalisation method [85], uses individual transformers for each battery cell as shown in Fig. 2.15. The control is simple, and each transformer primary winding is connected to the battery pack with a single control switch. Since the induced current in the secondary winding is inversely proportional to the battery SoC, a higher current flows for batteries having lower SoC, due to their lower battery voltage [86]. Conversely, the higher charged cells have less current, as the voltage across these cells is higher. However, the bulky size and cost are the main drawbacks of this multiple-transformer based equalisation method.

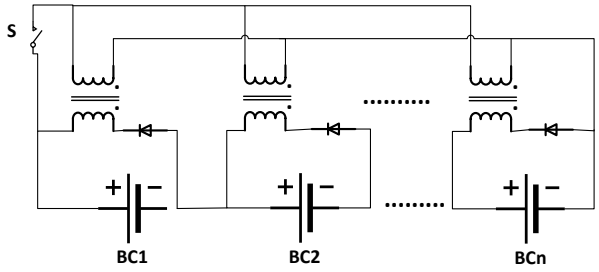

Figure 2.15: Multiple transformer-based energy transferring method

The converter can also be used for an alternative energy-transferring based charge balancing method. Figure 2.16 shows the Cuk converter energy transferring circuitry proposed in [87, 88], where energy transfer is only possible between adjacent cells. The main drawbacks of this balancing circuit are that the equalisation time and power loss increase with string length, owing to the adjacent cell energy transferring capability.

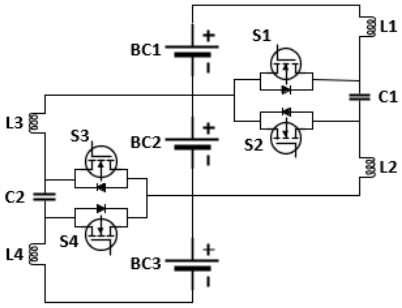

Figure 2.16: Cuk converter for energy transferring

The switched matrix balancing method [89-91] uses multiple cell selection switches, and a central balancing circuit is connected to a pack or a cell with a group of switches. In [91], a central converter method is used (Fig. 2.17), where the cell selection switches are employed to transfer energy from anywhere in the battery pack to any cell for a long battery string. The overall battery is modularized, and each battery group is monitored by cell monitoring ICs. A central microcontroller collects the cell information from the ICs, determines the switching pattern for the battery equalisation, and the energy is transferred from the battery pack to any cell using the selected switches. Besides balancing relatively quickly and efficiently, this method only utilises one converter which reduces the number of passive components. However, it employs many switches in proportion to the number of series connected cells, leading to increased control complexity [92].

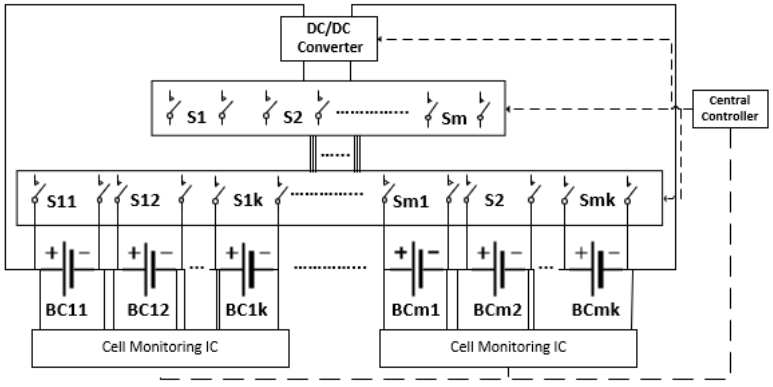

Figure 2.17: Modularized charge balancing with cell selection switches

In the runtime balancing method [13, 93, 94], each individual cell is connected to a low power converter, which constitutes a module, and each converter is connected in series to increase the overall voltage as shown in Fig. 2.18. No central power converter is required in this method to adjust the charging / discharging power of the battery. Instead, the power processing and cell balancing functions are integrated within the systems structure using two cascaded control loops [93, 95, 96]. The cell balancing control loop generates reference DC bus side voltages for each module by comparing their corresponding battery pack`s SoC to the average SOC value. Each individual modules voltage is then regulated by the local controller, which is controlled by the DC bus side voltage control loop. For this control, the higher charged cells release more power than the lower ones in the discharging mode, and lower charged cells are charged at higher powers in the charging mode. This enables balancing of the cells while the battery is operating, hence it is called 'runtime balancing'.

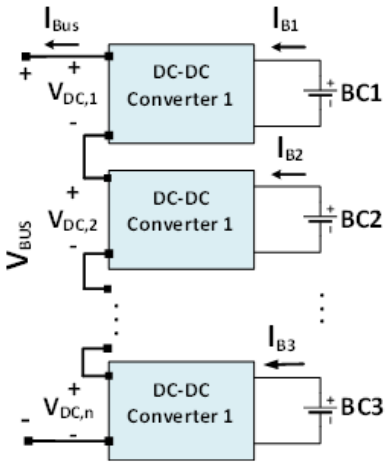

Figure 2.18: The structure of runtime balancing method

The runtime balancing method was modelled and simulated in MATLAB / Simulink to allow for a comparative analysis. A bidirectional half bridge DC-DC Buck-Boost converter, with a 250 kHz switching frequency, 6.8 µH inductor, and a 33µF capacitor was used in the simulation. The initial cell conditions are the same as for the previous testing (Table 2.1). The battery cells were first discharged with an 0.8 C battery power, i.e. 8A total battery current, and the results are shown in Fig. 2.19.

At the start of the simulation, as the SoCs of cells 1 and 3 are higher than the average SoC, the DC bus side voltages of these modules are also higher than the equal sharing voltage, which is 6V in this case. On the other hand, the modules 2 and 4 have lower voltages, due to having lower SoC values than the average. Figure 2.19(b) shows the SoC of each battery cell during

discharging. The sum of the module voltages is always equal to the DC bus voltage, which is 24 V in this case, and this is illustrated in Fig. 2.19(c). All cells are balanced at around 1400 s, and each module shares the power evenly, and each modules voltage at the series connected side is 6V.

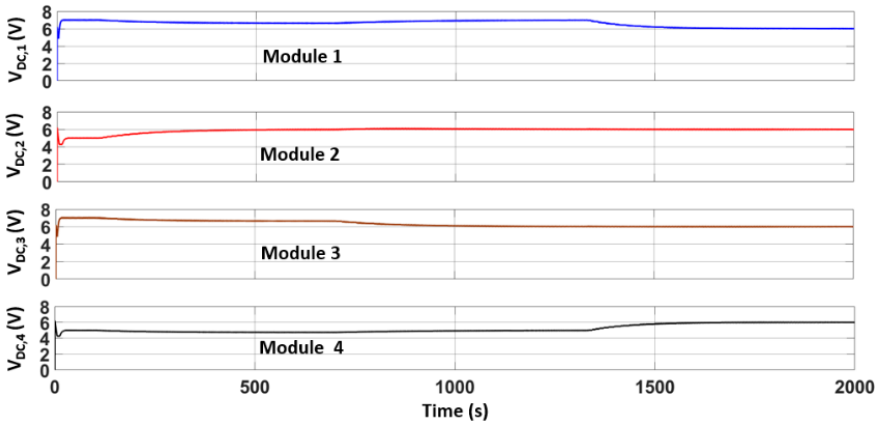

(a)

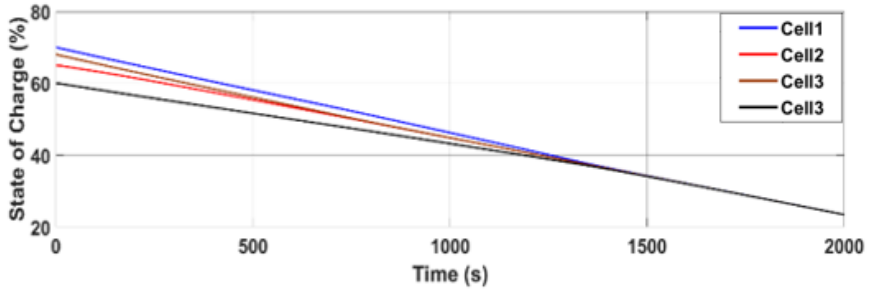

(b)

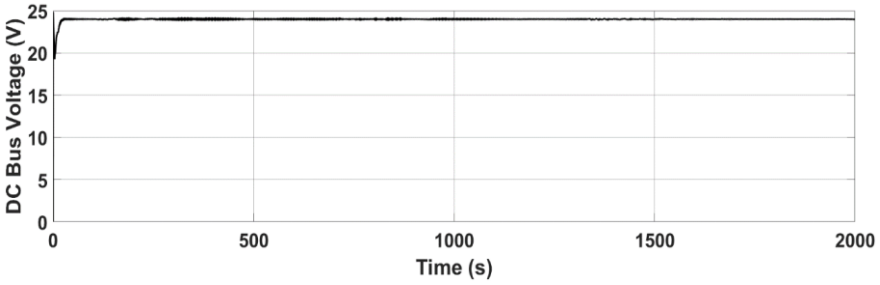

(c)

Figure 2.19: Runtime Balancing Method in discharging mode with 0.8 C battery power, (a) Modules Voltages, (b) Cell SoC, (c) DC Bus voltage

In Fig. 2.20, discharging mode simulation results for a 0.2 C battery power are shown. The same initial SoC values were implemented. Here, unlike the 0.8 C discharge condition, where all cells were balanced at around 1400 s, the cells are still not balanced after 2000 s due to the low 0.2 C discharge power. However, the SoC of cell 2 is equal to the average SoC at around

1200 s, and its DC bus side voltage is 6 V. It is also worth noting that the DC bus voltage is maintained at 24 V during the balancing as shown in Fig. 2.20(c).

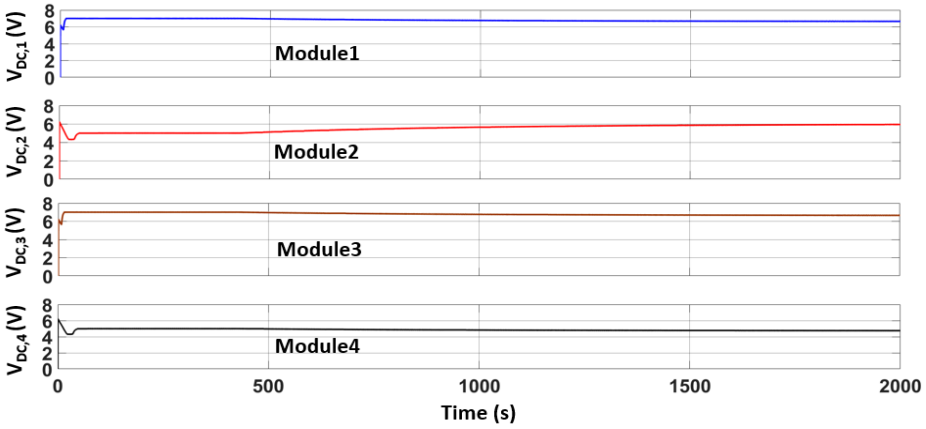

(a)

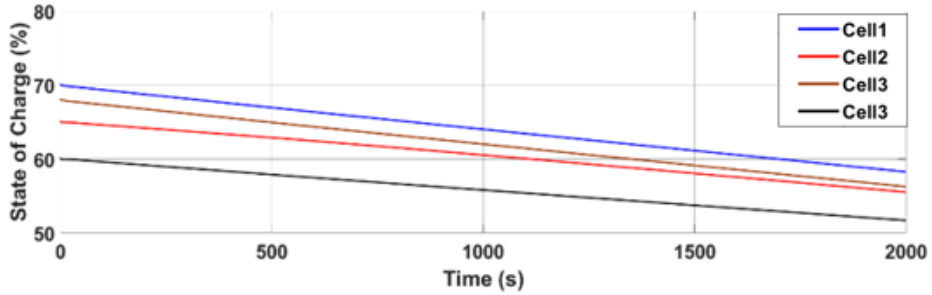

(b)

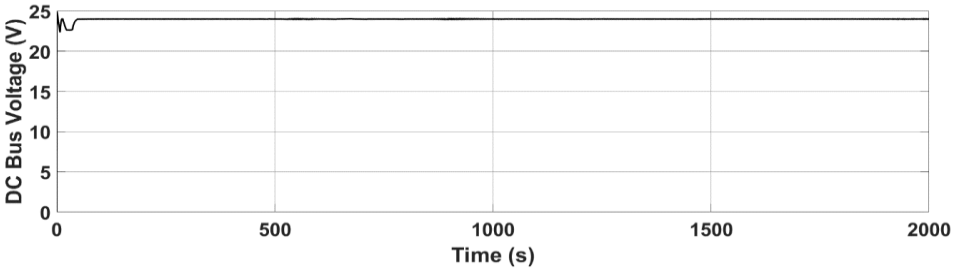

(c)

Figure 2.20: Runtime Balancing Method in discharging mode with 0.2 C battery power, (a) Modules Voltages, (b) Cell SoC, (c) DC Bus voltage

Charging mode runtime balancing results are presented in Fig 2.21, the initial cell SoCs are shown in Table 2.2. In charging mode, the higher charged cells 1 and 3 are charged with a lower power than cells 2 and 4. After balancing, all of the modules DC bus side voltages and charging powers are equal, and the DC bus voltage is maintained at the desired 24 V during the operation.

Table 2.2 The initial cells SoC at the beginning of the simulation in charging mode

Cell 1 (%)	Cell 2 (%)	Cell 3 (%)	Cell 4 (%)
30	25	28	20

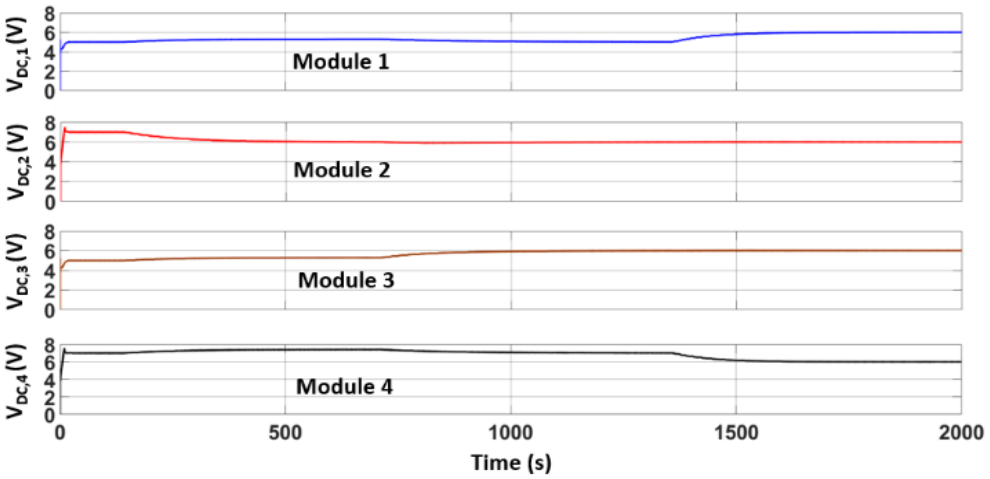

(a)

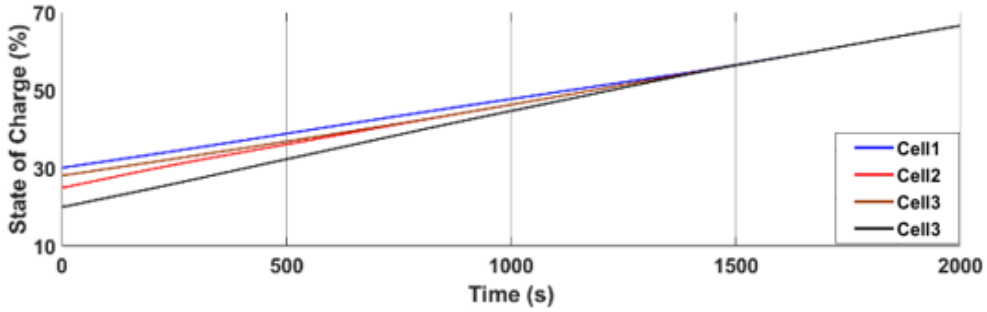

(b)

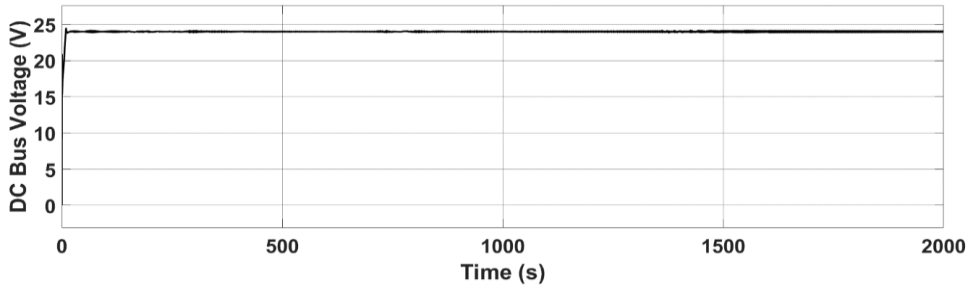

(c)

Figure 2.21: Runtime Balancing Method in charging mode with 0.8 C battery power, (a) Modules Voltages, (b) Cell SoC, (c) DC Bus voltage

In comparison to the energy transferring and dissipative balancing methods previously discussed where all battery cells are charged / discharged with the same battery power, this structure enables continuous adjustment of the individual cell charge / discharge powers. In addition, the length of the string does not affect the performance of the runtime balancing method. Therefore, this is an appropriate structure for a system based on pre-used batteries where a high imbalance is expected, as the continuous balancing capabilities during battery operation prevents divergence of the cell voltages, even if the battery pack is composed of different SoH cells. The main drawbacks of this runtime balancing method are its high cost, and the requirement of a relatively complex controller.

2.4 DC-DC Converter Interfaces

The battery storage systems are interfaced with the DC bus via bidirectional DC-DC converters. The converters control the charging / discharging current of the battery packs based on commands from the systems controllers, such as the energy management system (EMS), and they match the battery pack voltages to the DC bus voltage. In most applications, the Boost converter is preferred in order to use lower voltage battery packs, this allows better utilisation of battery packs with fewer series connected cells as mentioned in Section 2.3 [97]. There are two main types of bidirectional converter: isolated and non-isolated, and the choice depends on the requirements of galvanic isolation and the necessary voltage gain (VGR) [97, 98]. Transformerless converters can be preferred for their simple, cost effective, and efficient structures when galvanic isolation is not necessary, but the isolated topologies allow higher voltage gains because of the transformer turn ratios, as well as providing additional safety due to the galvanic isolation. In this section, some of the most common bidirectional DC-DC converter topologies are reviewed.

The bidirectional half bridge converter is shown in Fig. 2.22. It operates as a Boost converter in discharging mode and a Buck converter in charging mode. Due to the low number of components, low cost, and easy control, it is an attractive converter for many applications. However, the voltage gain conversion ratio is limited due to the hard switching and high conduction loss, limiting its use for high gain systems. Although, many research papers incorporating coupled inductors [99-102], have been proposed to increase the voltage gain, this additional circuitry increases the systems cost and control complexity.

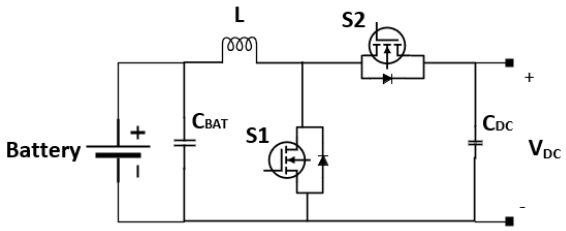

Figure 2.22: Bidirectional Half Bridge Buck-Boost Converter

A cascaded Buck-Boost converter is a cascaded connection of bidirectional Buck and Boost converters as shown in Fig. 2.23. It can operate in either Buck and Boost modes in both directions of operation, i.e. the DC bus side voltage can be higher or lower than that of the battery voltage [103, 104]. Similarly, the battery side voltage can be reduced (Buck) or increased (Boost) during charging. For this converter only one switch operates at the switching frequency in each operating mode, whilst the rest being either on or off [105]. The bidirectional Buck and Boost capabilities makes this topology suitable for applications where there is a high chance of overlap between the DC bus and battery voltages [106]. For example, in a low voltage DC microgrid system the DC bus voltage can be as low as 24 V [107], whilst the battery pack voltages may be higher or lower depending on the SoC value. In such a scenario, the cascaded Buck -Boost topology may be a suitable candidate with its low number of components and simple control structure.

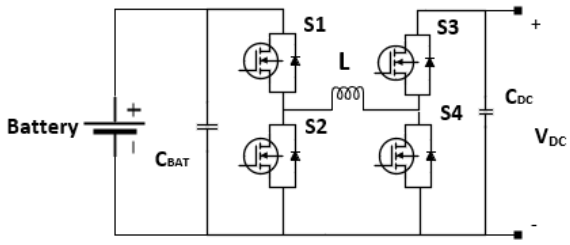

Figure 2.23: Cascaded Buck-Boost Topology

A SEPIC-Zeta converter is shown in Fig. 2.24, where it behaves as a SEPIC converter in discharging mode, and a Zeta converter in charging mode. In order to achieve a high VGR it operates at extreme duty ratios [108]. A coupled inductor SEPIC - Zeta converter is proposed in [109], where a 500 W system with a 24 V input and 400 V output was tested. Although, this method increases the voltage gain, the additional circuitry increases the number of components, drive circuitry, cost, and control complexity.

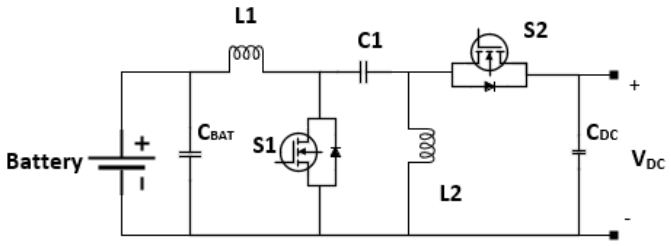

Figure 2.24: SEPIC - Zeta Converter

Isolated converters use the transformer for galvanic isolation, and these topologies are good candidates for applications where safety is a major concern such as Electric Vehicles and aircraft [110]. A dual active bridge (DAB) converter is shown in Fig. 2.25, which has a bidirectional Buck-Boost capability. The first converter stage on the left-hand side performs DC-AC conversion, the high frequency transformer then controls the secondary side AC voltage depending on the turns ratio, and then AC-DC rectification is performed on the right hand side. Resonant circuits and the transformer are used to increase the efficiency via Zero Voltage Switching (ZVS), and in [111], a 97 % peak efficiency is obtained in both charging and discharging modes. The direction of the power can be controlled using simple phase shift control methods [112, 113], and some other modulation techniques such as dual-phase shift [114], and triple-phase shift [115] have been proposed to increase the efficiency over wide voltage gains, but at the expense of increased control complexity. However, the high number of switches, its bulky size, cost, and complicated control are the main drawbacks of this topology.

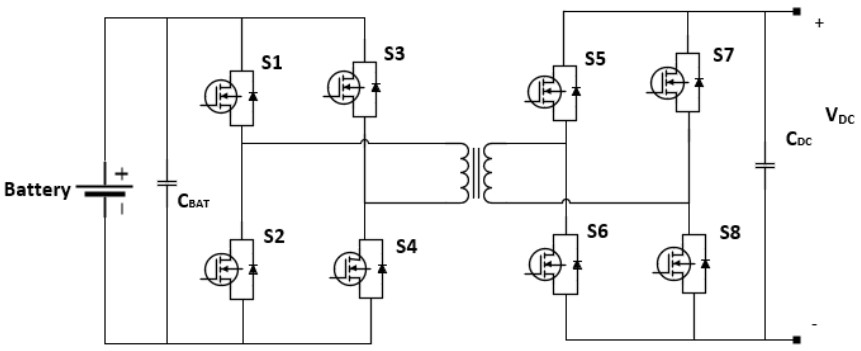

Figure 2.25: Dual Active Bridge Converter

Compared to the DAB topology, the isolated dual half bridge topology (Fig. 2.26) uses 4 switches [116]. Resonant half bridge topologies have also been proposed for battery and fuel cell applications [117-119], looking to increase the efficiency and reduce the switching losses. In [120], a voltage gain of 31.25 was achieved with a dual half bridge converter, using a 32:1 transformer, 12.8 V batteries, and a 400 V DC bus.

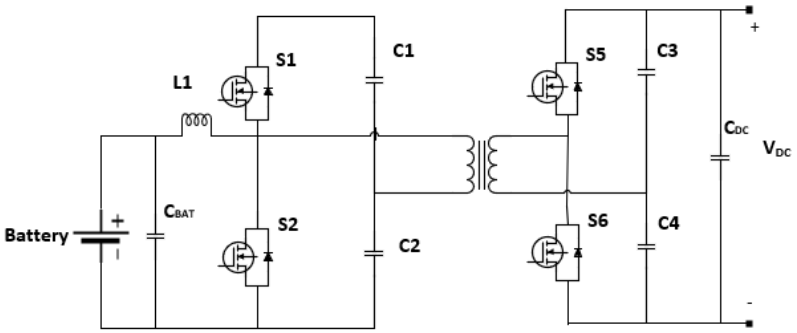

Figure 2.26: Dual Half Bridge Converter

The combination of a full bridge and half bridge topology is shown in Fig. 2.27. Here, one side of the transformer is connected to a full bridge, and the other side is connected to a half bridge. Morrison and Egan [121] use this topology for UPS systems. In [122], the full bridge half bridge topology is used with series resonant circuitry to increase the efficiency over wide range of battery voltages, and a 97.8% peak efficiency is obtained in both discharging and charging modes.

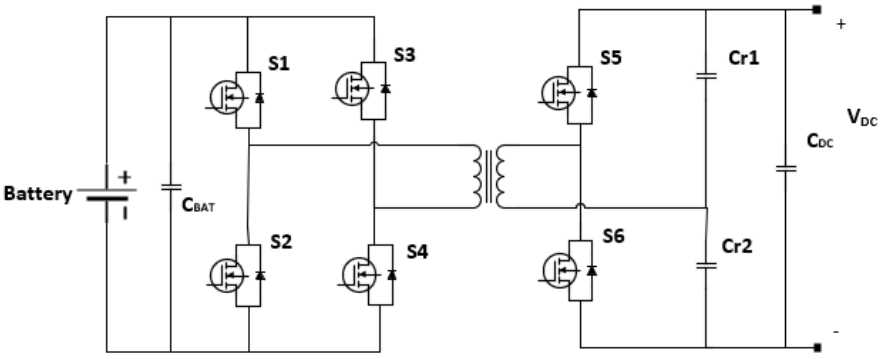

Figure: 2.27: Full Bridge - Half Bridge Converter

Many review papers for bidirectional DC-DC converter topologies have been written [110, 123-125], and Table 2.3 gives examples of proposed bidirectional DC-DC converter topologies, listing the required number of components, VGR, peak efficiency stated, and the presence of galvanic isolation. High voltage gain bidirectional DC-DC converter topologies for energy storage systems are well-summarised in [123], and it is found that only the isolated topologies can achieve gains greater than 20.

Currently, bidirectional DC-DC converters for storage systems is an important research topic, and the trade-off between the efficiency over a wide range of operating points, high voltage gain, size, and cost is attracting for many researchers.

Table 2.3 Comparison of some bidirectional DC-DC converter topologies proposed in the literature

Topology	**Number of Components**			**Voltage Conversion Ratio**	**Efficiency (%)**		**Isolation**
	Switches / Diodes	Inductor	Capacitor		Charging	Discharging	
Buck / Boost with Coupled Inductor[100]	3	2	3	300/40	95	91.5	No
Buck / Boost with Coupled Inductor[101]	3,1	2	2	200/24	96	86	No
Buck / Boost with Coupled Inductor[102]	3,3	2	4	200/24	92	96	No
SEPIC / Zeta with coupled inductor [109]	4	2	5	400/24	92.6	94.3	No
LLC Resonant DAB [111]	8	2	3	400/75	97	97	Yes
Triple-Phase Shift Control with LLC Tank DAB [115]	8	3	2	270/30	96	96	Yes
Isolated Half Bridge[116]	4	1	6	300/48	NA	NA	Yes
Isolated Half Bridge[119]	4	2	6	144/60	93	NA	Yes
Isolated Half Bridge[120]	4	-	4	400/12.8	88	88	Yes
Isolated Half Bridge [118]	4	2	5	NA	91.5	95.7	Yes
Full Bridge–Half Bridge with resonance [122]	6	1	4	400/250-415	97.8	97.8	Yes

2.5 Summary and Conclusion

This chapter has discussed conventional battery storage architectures, along with the BMS and power converter interfaces. As a common solution, long battery strings are divided into submodules with adjacent BMS ICs. These are then controlled by a central controller unit which may also require additional electromagnetic interference (EMI) filters. This means that the traditional approach to the management of long battery strings increases the cable connections and wiring harnesses.

In conventional BESSs, it is desirable to have as many identical cells as possible in the string, as the lifetime of the whole battery system relies on the weakest cell. Although cell balancing topologies improve the battery packs performance, increasing the number of cells in a battery string also increases the chance of cell mismatch, and reduces the balancing performance of cell balancing topologies, and string lifetime.

In state-of-the-art BESSs, a central power electronic converter interface is used, and significant efforts have been made to increase the voltage gain and / or efficiency, leading to additional circuits, increased control complexity, and cost. In addition, the whole battery pack is still being charged / discharged with the same battery power, leading to different cell temperatures caused by their inherently different intrinsic resistances, and this in turn may increase the level of mismatch in the string. Unlike the central structure, the distributed BESS allows control of individual pack powers. Recently, many authors have published on distributed BESS, discussing their benefits which depend on the systems structure and control methods. In the next chapter, distributed BESSs are introduced, with their advantages and disadvantages over the state-of-the-art BESSs discussed.

Chapter 3. Distributed Battery Energy Storage Systems and Control Methods

3.1 Introduction

The distributed battery structure is achieved by connecting each battery pack to their corresponding converter, and connecting the converters in series. In this chapter, the modular structures for battery energy storage systems are investigated, with their advantages and disadvantages mentioned. The operational range of the distributed BESS is analysed and discussed along with the systems performance, including the balancing speed and efficiency. Based on the discussion, an adaptive power sharing controller is proposed that improves the light load performance of the system. Simulation results are presented for both the SoC-based power sharing and proposed adaptive power sharing controllers, allowing the performance for both control methods to be compared.

3.2 System Structure

The distributed battery storage system is illustrated in Fig. 3.1 [14, 126]. In this system, each battery pack is connected to a low power DC-DC converter, and each converter is connected in series at the DC bus side. The overall voltage of the system is increased by the cascaded connection of the converters, and the independent connection of the battery packs allows individual control of the battery packs` powers. The system is also scalable, and voltage and power levels can be achieved for any system by increasing the number of cascaded connected modules and the capacity of the cells. This can be implemented either at cell-level, i.e., the converter is connected to individual battery cells as shown in Fig. 3.1(b), or at pack level, in which each converter is connected to a battery pack as illustrated in Fig 3.1 (a).

With the cell level integration, complete cell balancing is achieved using the SoC-based power sharing controller, and no additional balancing is required [94]. On the other hand, when it is implemented for battery pack, balancing circuits are necessary for each individual battery pack to equalize the cells in the pack. As each balancing circuit is responsible for a small number of series connected cells, low voltage battery packs can be well managed using the available balancing methods. Compared to the central structure mentioned in Chapter 2, the reliability is further improved as any faulty module(s) can be bypassed, and hence the overall reliability is improved.

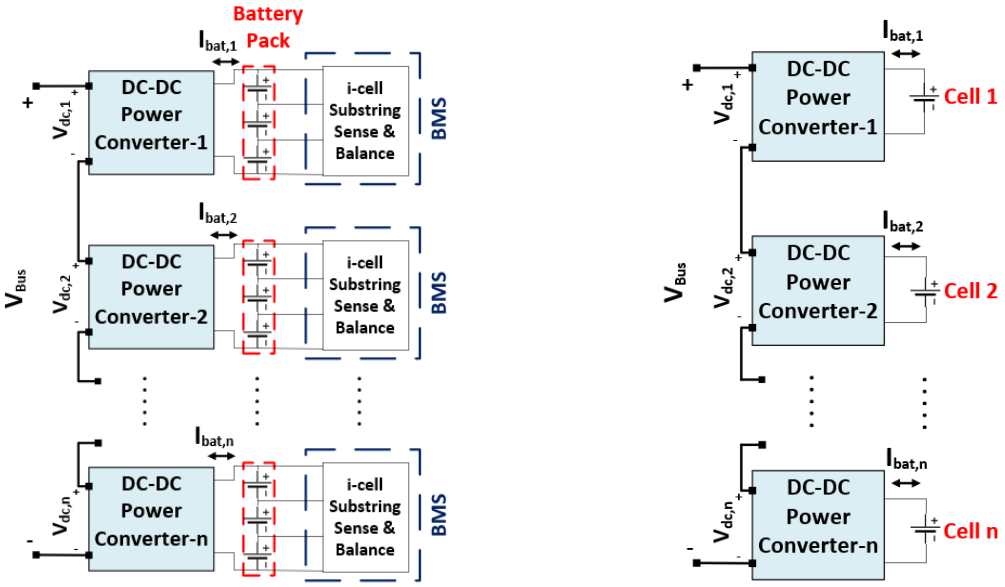

(a) (b)

Figure 3.1: The distributed battery storage system (a) Pack Level Modularization (b) Cell Level Modularization

The advantages of the distributed battery storage structure are summarised as follows:

- The cascaded connection of the DC-DC converters increases the system voltage level. This enables the use of low voltage batteries for each converter without the requirements of a high voltage gain converter. Each BMS is responsible for low number of cells, and therefore the workload on the balancing circuits and BMSs are reduced, and the low voltage battery packs can be well managed by the available balancing circuits.
- The independent connection of the battery packs to their corresponding converters enables different loadings to be applied to each battery pack, which brings several additional advantages. During operation, continuous SoC balancing of the cell / pack is achieved along with the power processing function by adjusting each modules power. Thermal balancing can also be achieved using this structure, and the relatively flexible power sharing feature can be utilized for different battery pack capacities and / or chemistries. The proposed power sharing controller also allows SoH balancing for pre-used batteries.
- The system is scalable, and the desired voltage and power levels can be achieved for any system by increasing the number of cascaded connected modules and the capacity of the cells. This is possible without changing the design of the modules.

- The reliability of the system is also improved compared to the central BESS. In the conventional BESS, when one of the cells is faulty, the operation of the complete system has to be stopped. This new structure can bypass any faulty module(s), with the rest of the modules still supporting the system.

3.3 Control Methods for Distributed BESS

In the literature, distributed BESSs are investigated for many different applications with different power sharing controllers. The distributed battery storage system is used for cell level integration in [14, 93, 96] with cell voltage balancing controllers in both charging and discharging modes. A local controller is used for each module, and this communicates with the global controller via a communication bus, sending out the status of the battery pack and regulating the battery power based on the commands from the global controller. The global controller determines the operating points of each module based on the information from each local controller. A bypassed command is generated for any faulty or unsafe cells, and the active modules share the power based on their cell voltage with respect to average value.

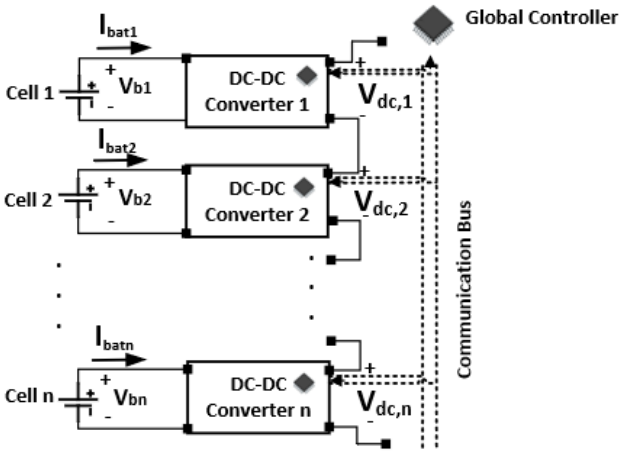

Figure 3.2: The distributed control architecture with a global controller

The individual modules powers are determined by the power command generation block diagrams. Figure 3.3 illustrates the power command generation block diagrams and local controllers in discharging mode. Each cell voltage is compared to the system average cell voltage to create power differences. These individual differences are added to equal DC bus voltages ($V_{DC,ref}/N_{act}$) to generate individual DC bus side voltages for each module from $V_{dc,ref1}$ to $V_{dc,refn}$. The local controller then adjusts the individual DC bus side voltages of each module. Therefore, the higher voltage cells are discharged with higher power, and lower charged cells are discharged with lower power in discharging mode, in which SoC balancing and battery discharging functions are achieved simultaneously.

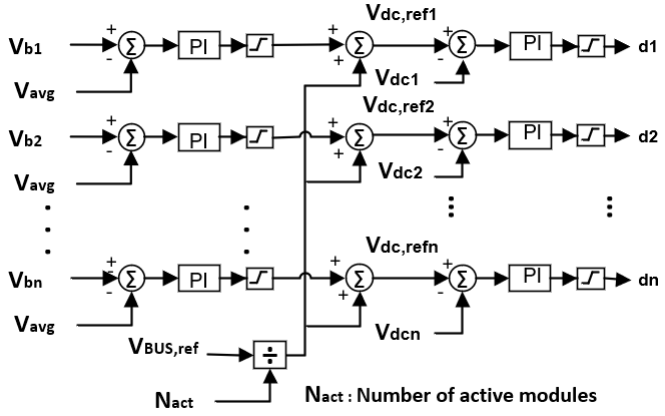

Figure 3.3: The controller block diagrams in discharging mode

A central power sharing controller is proposed in [13, 95] for simultaneous SoC balancing and DC bus voltage regulation. Two closed loop controllers are implemented in both the discharging and charging modes, as shown in Fig. 3.4. The SoC balancing controller decides the voltage loop multiplier value ($\alpha_{v,x}$) by comparing each battery pack`s SoC with the average value. The value of the voltage loop multiplier is always higher than zero. When any battery pack has a higher SoC than that of average, the voltage loop multiplier will be greater than one in discharging mode, and it is less than one for a module whose corresponding battery pack`s SoC is less than the average value. In the output voltage regulation loop, each module`s reference value is multiplied by its corresponding multiplier, and the reference voltage value ($V_{dc,refx}$) for each module is decided based on equation 3.1. To ensure the DC bus voltage is always equal to $V_{Bus,ref}$, the reference DC bus voltage is divided by the sum of the voltage loop multipliers, M_v. Fig. 3.5 shows the power sharing controller in charging mode. The SoC balancing loop generates voltage loop multipliers for each module by comparing their associated battery pack`s SoC to the average. The average battery current and modules dc bus side voltages are then controlled as shown in Fig.3.6.

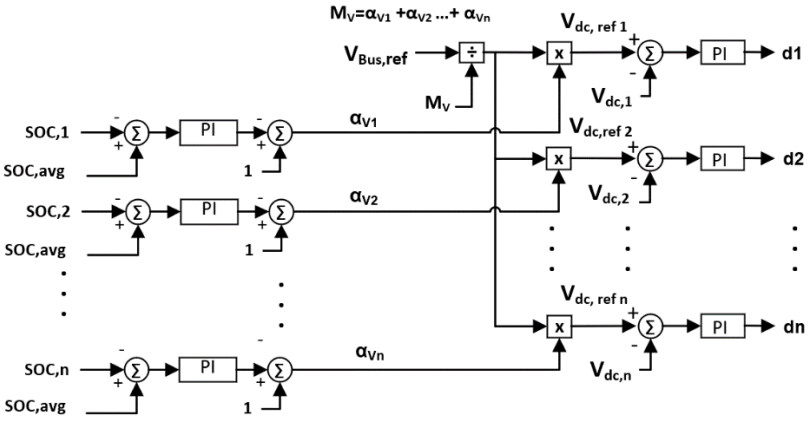

Figure 3.4: The power sharing controller block diagrams in discharging mode,

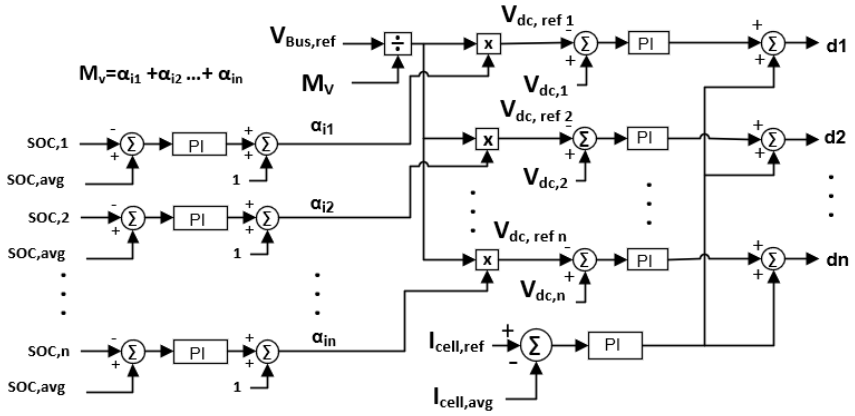

Figure 3.5: The power sharing controller block diagrams in charging mode

$$V_{dc,refx} = \frac{V_{Bus,ref}}{M_v} \times \alpha_{Vx} \tag{3.1}$$

Besides the SoC based power sharing controller, many different control methods have been proposed in the literature. Temperature variations amongst different cells increases the non-uniformity in the string, and reduces the battery lifespan, and thermal balancing control algorithms have been proposed in [15, 127] for distributed battery storage systems.

The individual power sharing capability of the distributed BESS makes it a suitable structure for a system consisting of different capacity battery packs. The increasing number of electric vehicles (EVs) worldwide is also increasing the number of retired battery packs. In EV systems, when the cell SoH reaches 80% of its initial capacity, the battery is assumed to have reached the end of its life for vehicle applications [128]. Currently, there is a growing interest to utilise these retired batteries in stationary applications as the performance of the retired batteries is still satisfactory for these. However, the increased mismatch of these battery cells may reduce their performance for stationary applications when the traditional central structure is used. However, the different SoH packs / cells can be well managed by the distributed BESS with its continuous balancing feature and improved reliability due to bypassing. Each battery pack is charged / discharged at different rates depending on their relative capacity and SoC, and any faulty or overcharged / over-discharged modules can be bypassed from the system. Power sharing controllers are proposed in [16, 17, 129] for retired battery packs with different SoH. The power sharing controller determines the individual modules power based on their relative capacity and SoC, and the results show that the SoC of each battery pack is well-balanced, whilst the DC bus voltage is regulated at the desired voltage level. As a long-term balancing objective, the SoH balancing can also be achieved by adjusting individual battery pack`s depth

of discharge (DoD) in each charge / discharge cycle. An example of this was proposed in [130].

In general, two cascaded controllers are implemented to control the individual battery packs. The outer controller determines the operational range of any module based on the aim of the controller, while the inner loops are used to adjust the individual modules power.

3.4 Operational Range of the Distributed BESS

In the distributed BESS, each module consists of a DC-DC converter and a battery pack / cell. Although the modules voltage ratings are reduced, the modules converter should be capable of handling the full current of the battery packs. The whole systems battery power is shared amongst the different modules, and the DC bus side voltage of each converter determines the individual modules powers.

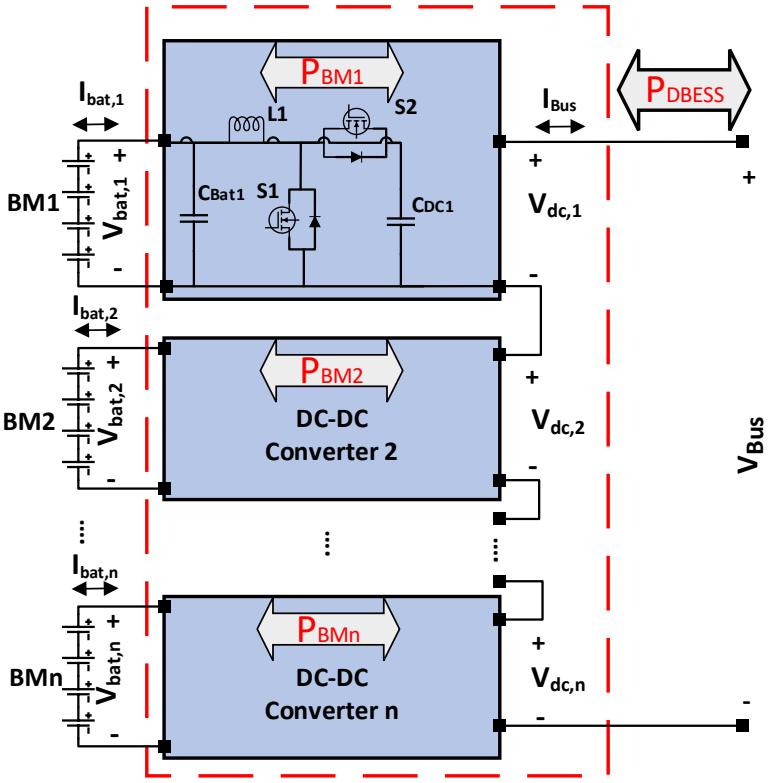

Figure 3.6: The power distribution in distributed BESS

Each modules battery and DC bus side powers can be expressed as follows:

$$P_{bat,x} = V_{bat,x} \times I_{bat,x} \tag{3.2}$$

$$P_{dc,x} = V_{dc,x} \times I_{Bus} \tag{3.3}$$

If a lossless system is assumed, the battery side power will be equal to the DC bus side power of the module, therefore:

$$I_{bat,x} \times V_{bat,x} = I_{Bus} \times V_{dc,x} \tag{3.4}$$

Considering the DC bus side current (I_{Bus}) is same for all modules at the series connected side, the individual modules` battery current is directly proportional to their corresponding DC bus side voltages for a system having identical battery voltages (V_{bat}), which can be expressed as follows:

$$I_{bat,1} : I_{bat,2} : \ldots . : I_{bat,n} = V_{dc,1} : V_{dc,2} : \ldots . : V_{dc,n} \tag{3.5}$$

The operational range of any converter in the distributed BESS is illustrated in Fig. 3.7. In a balanced condition all modules share the power evenly (P_{eq}), and their DC bus side voltage is $V_{dc,eq}$. When any modules DC bus side voltage is higher than that of the average value, its corresponding battery current and power demands will also be higher than those of the average value. In contrast, when a modules DC bus side voltage is lower than that of the average value, it is loaded with a power lower than the average. The DC bus side voltage of any bypassed module and its corresponding power is zero. The intended power sharing of the different modules is accomplished within this operational range based on the aim of the controller.

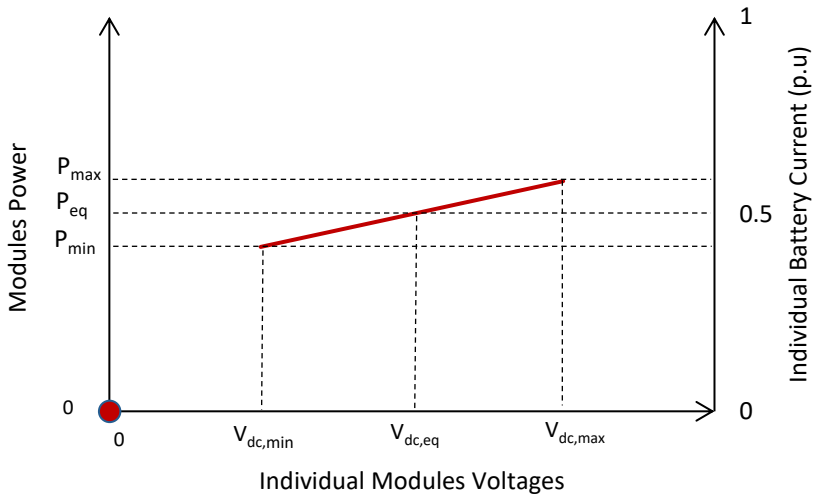

Figure 3.7: Operational Range of distributed BESS

An individual modules power ($P_{BM,x}$) with respect to the total battery power (P_{DBESS}) can be calculated from the ratio of its DC bus side voltage to the DC bus voltage. Therefore, the power requirements from an individual module, and the battery current for a given total battery power, can be estimated using (3.6) and (3.7), respectively.

$$P_{BM,x} = \frac{V_{dc,x}}{V_{Bus}} \times P_{DBESS} \tag{3.6}$$

$$I_{batx} = \frac{I_{Bus} \times V_{dc,x}}{V_{bat,x}} \tag{3.7}$$

In the next section, the DBESS using the SoC-based power sharing controller is simulated in MATLAB / Simulink, and the systems performance is analysed and discussed for different initial SoC mismatch and power levels. The operational range of the modules, the balancing speed, and the systems conversion efficiency, are also investigated at different battery power levels.

3.5 Simulation Results of Distributed BESS

The simulation parameters of the SoC-based power sharing are shown in Table 3.1. Six modules are used for the simulation. Each module consists of 6-battery packs with different initial SoC values, and 6 bidirectional half bridge DC-DC converters are used as shown in Fig. 3.8. The converter operates in Buck mode in the charging mode, and Boost mode in discharging. Li-ion batteries are used in the simulation, and their voltage and capacity are 24 V, 30 Ah respectively. The distributed BESS is connected to a 400 V DC bus. The simulation was carried out at different battery powers and initial SoC mismatches were used to investigate the performance of the system at different power levels. The distributed BESS was discharged at 65 %, 15% and 50% of its total battery rated power for a specific period of time intervals. The battery discharging power was controlled by connecting and disconnecting parallel resistive load at the DC bus. The simulation parameters are summarised in Table 3.1.

Table 3.1. Simulation Parameters

	Voltage (V)	**Capacity (Ah)**	**Initial SoC (%)**
Battery Module 1	24	30	80
Battery Module 2	24	30	75
Battery Module 3	24	30	78
Battery Module 4	24	30	79
Battery Module 5	24	30	76
Battery Module 6	24	30	76.5
Battery Discharging Power	**Time (s)**	**Value (%)**	
	0-1000	65	
	1000-2000	15	
	2000-4000	50	

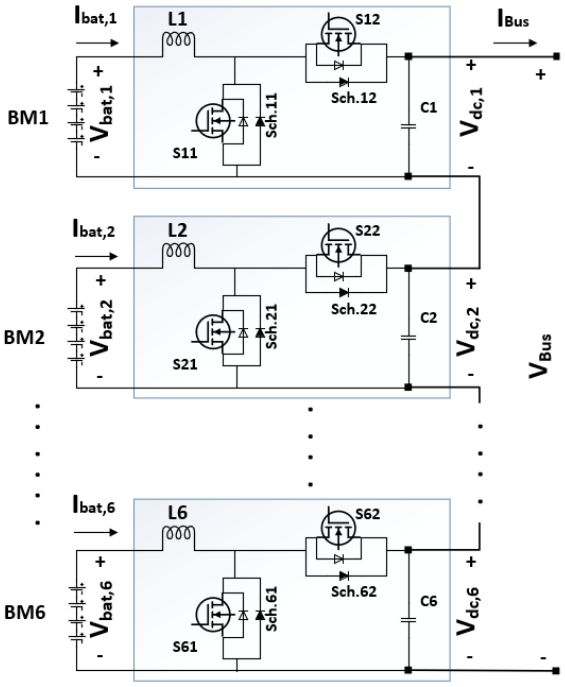

Figure 3.8: The distributed BESS with half-bridge Buck Boost converter

Figure 3.9 shows the simulation results with the SoC based power sharing controller in discharging mode. The SoC-based power sharing controller used in this simulation was shown in Fig. 3.4. For this discharging condition, batteries with higher SoC release more power as their DC bus side voltages are higher than the others. From Fig. 3.9(a) it can be seen that the

battery module 1 has the highest SoC, and thus has the highest DC bus side voltage. The relative DC bus side voltages of any module with respect to the equal sharing voltage ($V_{dc,x} - V_{dc,eq}$) is illustrated in Fig. 3.9(d). It can be seen that the difference is directly related to the SoC difference, and it is large when there is a high mismatch as shown in Figs. 3.9(d) and 3.9(e). When the battery modules` SoC converge, the voltage difference reduces irrespective of battery load, and all module voltages are equal when there is no mismatch between any battery modules. The DC bus voltage in all cases is equal to the reference bus voltage, which is 400 V in this case (Fig. 3.9(b)).

For the same capacity of battery packs, C, the SoC difference of any module with respect to average SoC, $\Delta SoC_{x(t)}$, at any time can be estimated using (3.8), in which the battery current is positive in discharging case. In the distributed BESS, the balancing speed is directly proportional to the difference of discharging current of any module with respect to the average value. For the same capacity of battery packs, it is also directly related to the power differences of any modules with respect to average module`s power.

$$\Delta SoC_{x(t)} = \Delta SoC_{xi} - \frac{1}{C \times 3600} \times \int_0^t \Delta I_{bat,x(t)} \times dt \tag{3.8}$$

$$\Delta I_{bat,x(t)} = I_{bat,x(t)} - I_{bat,eq(t)} \tag{3.9}$$

where ΔSoC_{xi} is the initial SoC mismatch of module `$x$` with respect to average *SoC*, and $\Delta I_{bat,x(t)}$ is the instantaneous battery current difference of module `$x$` with respect to average current, *C* is the battery capacity.

When a lossless system is assumed, and the battery voltage variations for different discharging current are ignored, substituting (3.7) and (3.9) into (3.8) yields:

$$\Delta SoC_{x(t)} = \Delta SoC_{xi} - \frac{1}{C \times 3600} \times \int_0^t \frac{(V_{dc,x(t)} - V_{dc,eq(t)})}{V_{bat(t)}} \times I_{Bus(t)} \times dt \tag{3.10}$$

$$V_{dc,eq(t)} = \frac{V_{Bus}}{N_{act(t)}} \tag{3.11}$$

where $V_{dc,eq(t)}$ is the DC bus voltage level at which active modules share DC bus voltage evenly, and $N_{act(t)}$ is the number of active modules at the specific time t.

As can be understood from (3.10) the power differences among the modules are directly related to the SoC mismatch level, as the SoC differences control the dc bus side voltage of each module, and total battery power. Therefore, the highest power difference is created at the beginning of the simulation, which is the highest SoC mismatch point, and the highest battery power point as shown in Fig. 3.9(g).

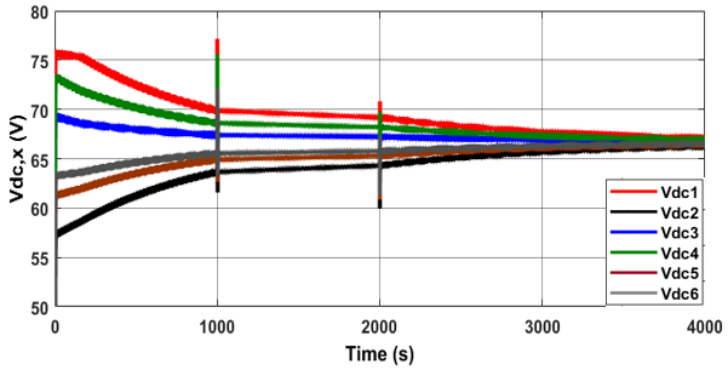
Vdc,x (V)
Time (s)
Vdc1
Vdc2
Vdc3
Vdc4
Vdc5
Vdc6

(a)

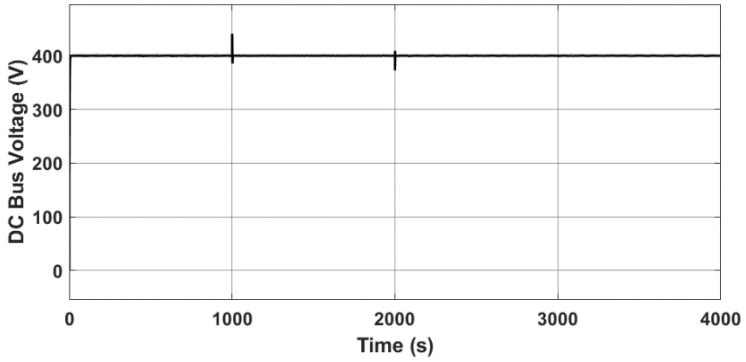
DC Bus Voltage (V)
Time (s)

(b)

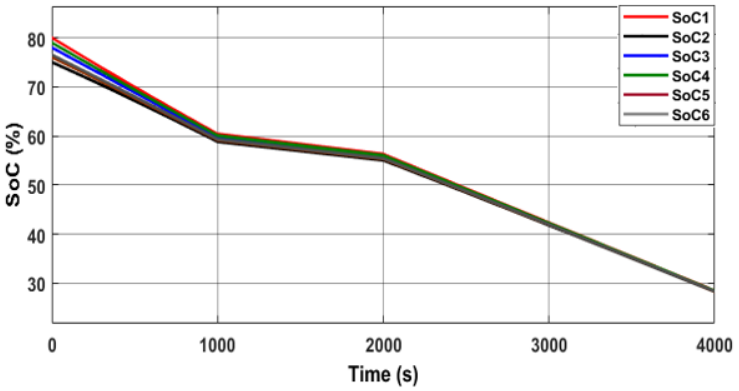
SoC (%)
Time (s)
SoC1
SoC2
SoC3
SoC4
SoC5
SoC6

(c)

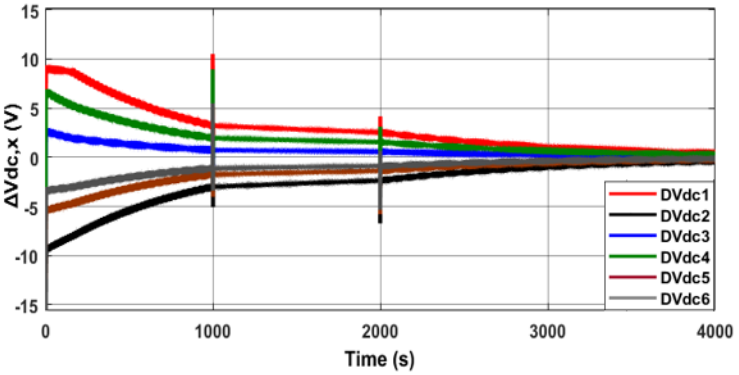
ΔVdc,x (V)
Time (s)
DVdc1
DVdc2
DVdc3
DVdc4
DVdc5
DVdc6

(d)

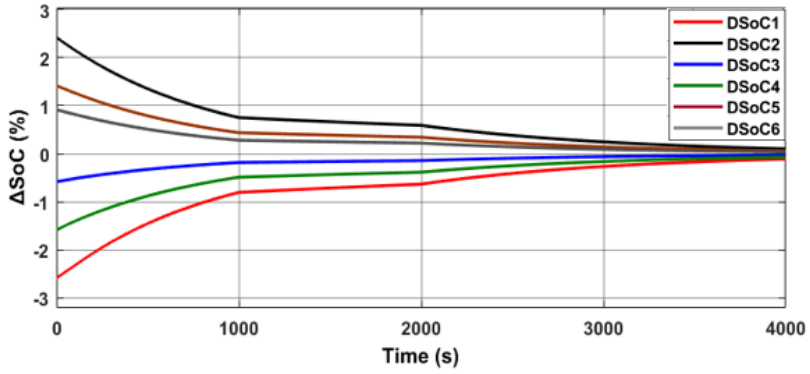

(e)

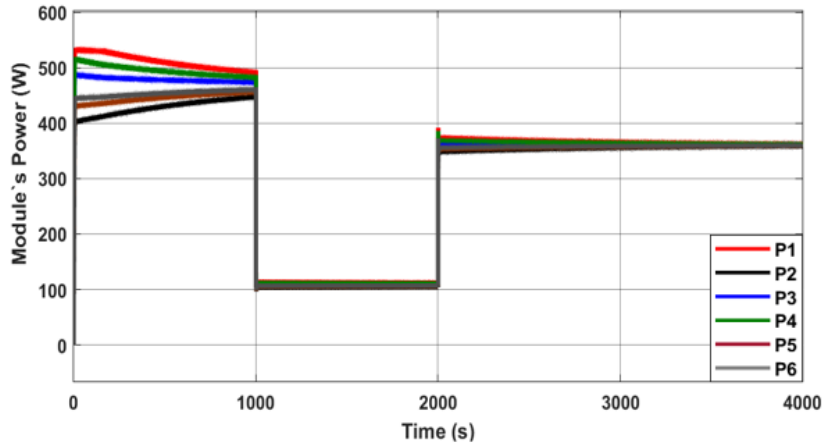

(f)

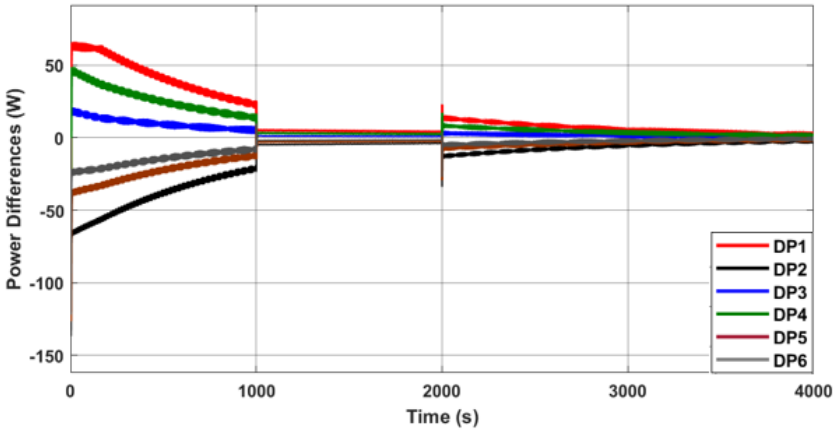

(g)

Figure 3.9: SoC-based Power sharing controller with different battery discharge powers, (a) Modules DC bus side voltages, (b) DC bus voltage, (c) SoC of each module, (d) Difference between modules` voltage and voltage at equal power sharing, (e) Differences between modules` SoC and average SoC, (f) Modules power, (g) Difference between modules` power and equal power

Figure 3.10 shows the power differences of any module at different battery power and voltage difference levels. A higher balancing speed is achieved at higher battery powers with the same SoC differences. The individual modules power, and their relative power are illustrated in Figs. 3.9(e) and 3.9(f), respectively. As Fig. 3.9(d) shows, the SOC convergence is slow at 15% rated power (1000-2000 s), whilst they converge relatively fast at 65% (0-1000 s), and 50% (2000-4000 s) rated power, and most of the balancing occurs in the heavy load areas.

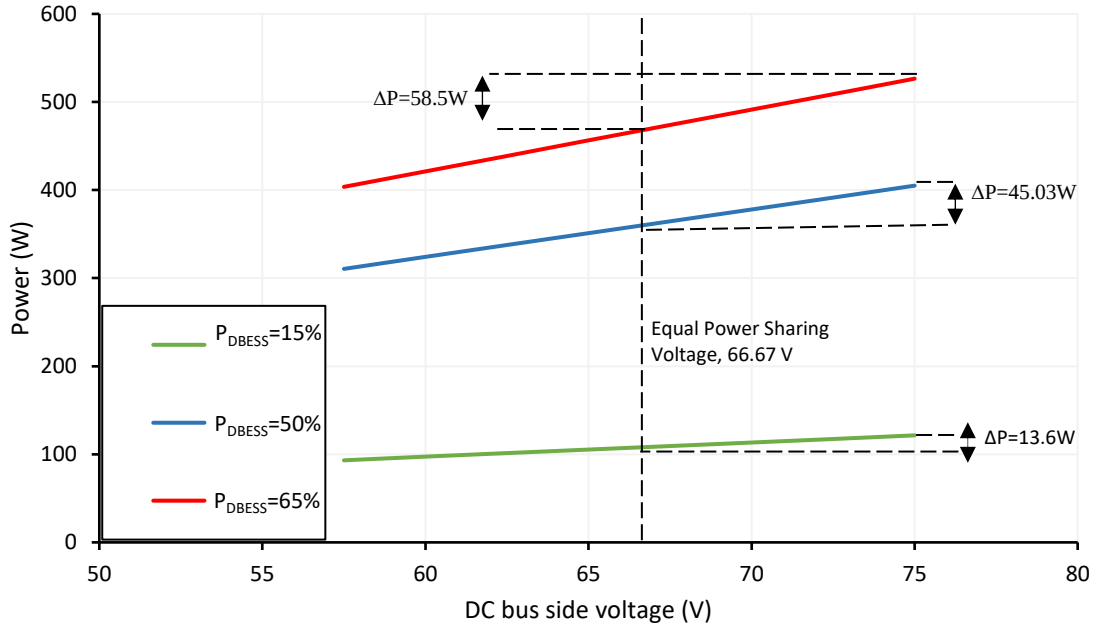

Figure 3.10: The power differences at different DC bus side voltage and battery power

The system operating efficiency can be estimated by the average conversion efficiency of the individual modules, and it can be estimated at any time using (3.12). The weighting factor of each module is directly proportional to its DC bus side voltages, as the current at the DC bus side is the same for all modules. Thus, the module with higher DC bus side voltages, will have higher weighting factor.

$$\eta_s = \sum_{x=1}^{n} \eta_x \times w_x \tag{3.12}$$

$$w_x = \frac{V_{dc,x}}{V_{Bus}} \tag{3.13}$$

where η_x and w_x are the efficiency and weighting factor of converter 'x', respectively, and η_s is the system conversion efficiency.

In general, the converter efficiency varies at different load and voltage levels, and different loads also affect the weighting factors of individual modules, and the total system conversion efficiency. To understand the effects of power sharing on the system conversion efficiency, an efficiency map is generated using suitable standard components.

3.6 Efficiency Analysis of Distributed Battery Energy Storage System

In the power loss calculation, a bidirectional half-bridge DC-DC converter is considered. The loss components consist mainly of two parts, namely conduction and switching losses. The MOSFET loss ($P_{M,c}$) and diode conduction loss ($P_{D,c}$) are calculated using (3.14), and (3.15), respectively.

$$P_{M,c} = I_{bat,rms}^2 \times R_{ds,on} \times d \tag{3.14}$$

$$P_{D,c} = I_{bat,rms} \times V_{DS,F} \times (1 - d) \tag{3.15}$$

where $I_{bat,rms,}$ is the rms currents, and $R_{ds,on}$ and $V_{DS,F}$ are the on-state MOSFET resistance, and diode forward voltage drop, respectively. d is the duty ratio.

The inductor conduction loss is calculated using (3.16):

$$P_L = I_{bat,rms}^2 \times DCR \tag{3.16}$$

$$I_{bat,rms} = \sqrt{I_{bat}^2 + \frac{I_{ripple}^2}{12}} \tag{3.17}$$

where DCR is the DC resistance of inductor, and I_{ripple} is the peak-to-peak inductor current ripple which can be calculated using (3.18) for a boost converter.

$$I_{ripple} = \frac{V_L \times d}{L \times f_{sw}} \tag{3.18}$$

where f_{sw} is the switching frequency, and L is the inductance. V_L represents the voltage across the inductor.

The voltage and current overlap loss during the switching transition can be expressed as

$$P_{V-I} = \frac{(V_{DC} + V_{DS,F}) \times I_{bat}}{2} \times f_{sw} \times (t_r + t_f) \tag{3.19}$$

where t_r and t_f are the rise and fall time of switching transitions respectively.

The gate charge loss (P_G) and output capacitance loss ($P_{COSS,FET}$) of the MOSFET can be calculated using (3.20) and (3.21) respectively:

$$P_G = Q_g \times V_{GS} \times f_{sw} \tag{3.20}$$

$$P_{COSS,FET} = \frac{1}{2} \times C_{OSS} \times \left(V_{DC} + V_{DS,F}\right)^2 \times f_{sw} \tag{3.21}$$

where C_{OSS} and Q_g are the MOSFET output capacitance and total gate charge, and V_{GS} is the gate-source voltage applied to the MOSFET.

The reverse recovery loss of the diode (P_{RR}) is calculated using (3.22).

$$P_{RR} = Q_{RR} \times V_{DC} \times f_{sw} \tag{3.22}$$

where Q_{RR} represents the reverse recovery charge of diode.

Therefore, the total converter loss is the sum of individual loss components and can be expressed as

$$P_{tot} = P_{M,c} + P_{D,c} + P_L + P_{V-I} + P_G + P_{COSS,FET} + P_{RR} \tag{3.23}$$

where P_{tot} is the total converter`s loss

The efficiency map of a single converter is generated at different battery power and voltage levels and illustrated in Fig. 3.11, whilst Table 3.2 shows the components used for this efficiency calculation. The components` parameters used in the efficiency calculation are listed in Table B1 in Appendix B. To reduce the conduction loss of the nonsynchronous converter an antiparallel Schottky diode was used as shown in Fig. 3.8. The converter was designed to handle the maximum battery current and voltage ratings of the module, which were 75 V, and a maximum discharging current of 1C (i.e. 30 A for a 30 AH battery).

Table 3.2. The component list used in the efficiency calculation

Component	**Manufacturer**	**Part Number**	**Ratings**	
			Voltage (V)	**Current (A)**
MOSFETs	VISHAY	SIR606BDP	100	38.7
Schottky Diode	VISHAY	V40PW10C	100	40
Inductor	Wurth Elektronik	7443763540220	-	40.6

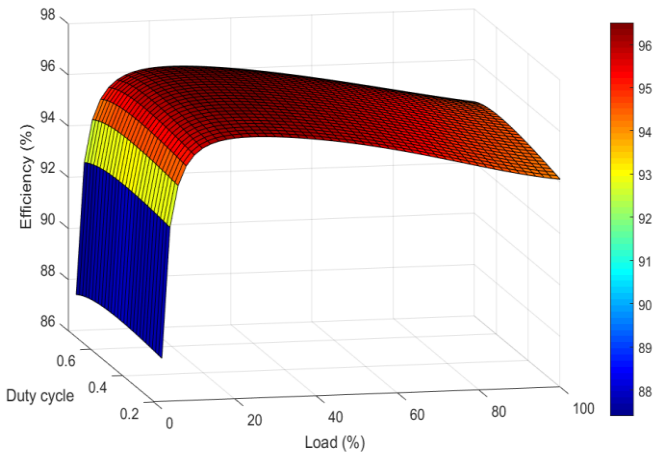

Figure 3.11: The efficiency map of the designed converter

The converter efficiency at different power and duty ratios with a switching frequency of 100 kHz is shown in Fig. 3.11. The efficiency increases from no load to the peak efficiency point, which is at around 25 % load in this case. After the peak efficiency, the efficiency reduces as the conduction loss increases with the increase in current. In the light load area, the highly loaded modules will have both higher weighting factors and a higher efficiency. Therefore, in the light load area the higher power sharing ratio increases the system efficiency. This can be found from equations (3.12) and (3.13) which means more power is processed more efficiently. Higher loaded modules have a higher weighting factor, but with a corresponding lower efficiency, and therefore the higher power sharing results in the systems conversion efficiency reducing after the peak efficiency point.

The power sharing methods proposed in the literature do not consider the systems efficiency, but they do consider specific aims, including SoC balancing for same or different capacity battery packs, temperature balancing, or SoH balancing. For example, in the SoC balancing controller, the power differences amongst the modules depends only on the SoC differences of each module, with the system conversion efficiency and balancing speed varying with the different distributed BESS power levels. Although fast balancing is achieved at higher battery powers, the higher power differences after the peak efficiency cause a reduction in the systems conversion efficiency, whilst the systems light load efficiency and balancing speed increases with the higher power sharing ratios.

In the next section, a simple adaptive power sharing controller considering the systems efficiency and balancing speed is proposed. The simulation was carried out with the same initial battery pack mismatches and battery powers used for the SoC balancing method.

3.7 Adaptive Power Sharing Controller for Distributed BESS

When there are mismatches amongst modules, there are also inherent power difference, which requires the use of SoC balancing. This balancing causes a different loading to appear on each module and has an impact on the systems conversion efficiency. The power differences are created in the SoC balancing loop, and the ability to adjust the power difference level can be utilised to improve the system conversion efficiency based on the efficiency map of the system without any additional hardware.

With the proposed adaptive power sharing controller, the voltage loop multipliers, which generate voltage difference at the DC bus side, and thus the power difference between modules, are decided by both the SoC difference and the battery load, as shown in Fig. 3.12. To do this, a 2D lookup table, whose inputs are the SoC difference, and the battery load, is used. Whilst the voltage difference is kept as high as possible at light load, it is gradually reduced with increasing battery load and reduced SoC difference.

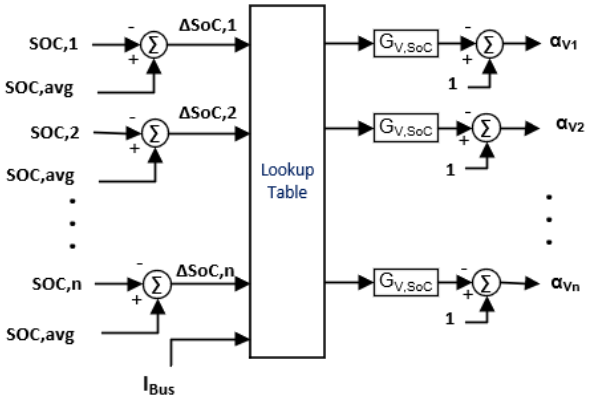

Figure 3.12: The decision of voltage loop multipliers with adaptive power sharing controller

Figure 3.13 shows the simulation results of the proposed adaptive power sharing controller. To increase the system conversion efficiency and the balancing speed, the voltage difference is kept as high as possible in the light load area, without violating the converter voltage ratings. This is shown in Figs. 3.13(a) and 3.13(d). The upper voltage limit at the series connected side is decided by the voltage rating of the converter, which is 75 V in this case. Compared to the SoC-based power sharing controller, where the individual DC bus side voltage difference at the series connected side is 9 V at 65 % load, for the same SoC differences, it is 2.5 V with the adaptive power sharing method. This can be observed in Fig. 3.13(d). This smaller voltage difference means that the efficiency reduction compared to the SoC based power sharing controller is limited, as the narrower voltage ranges limit the efficiency reduction at heavy load area. However, the balancing speed is also reduced because of the lower voltage differences at the DC bus side.

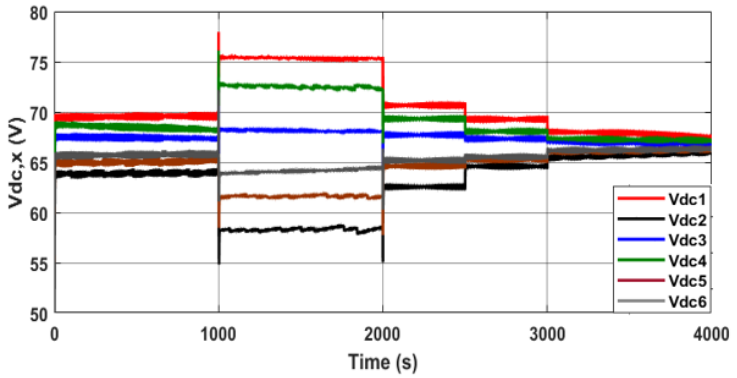
Vdc,x (V)
Time (s)
Vdc1
Vdc2
Vdc3
Vdc4
Vdc5
Vdc6

(a)

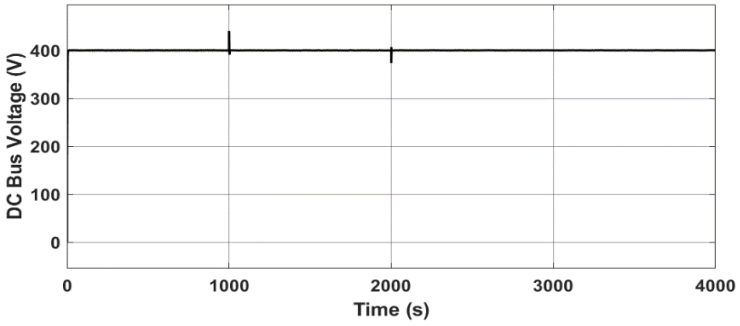
DC Bus Voltage (V)
Time (s)

(b)

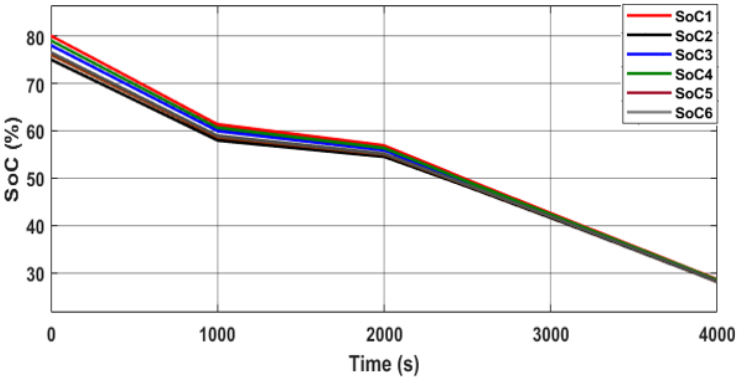
SoC (%)
Time (s)
SoC1
SoC2
SoC3
SoC4
SoC5
SoC6

(c)

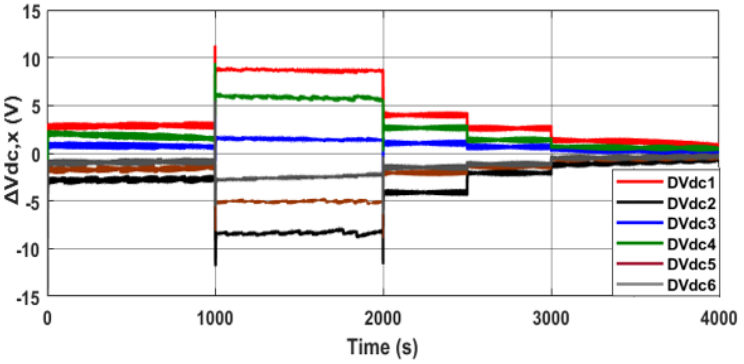
ΔVdc,x (V)
Time (s)
DVdc1
DVdc2
DVdc3
DVdc4
DVdc5
DVdc6

(d)

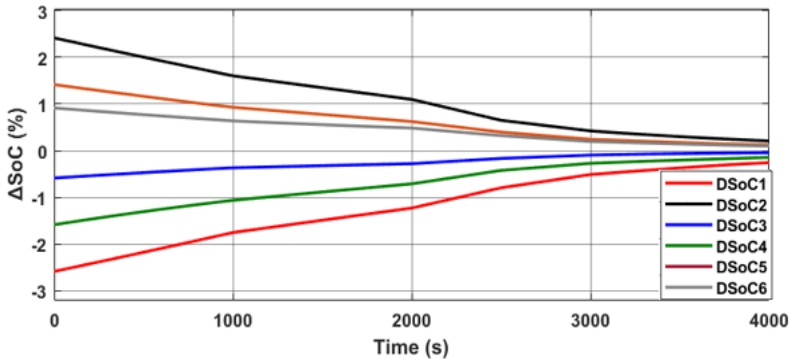

(e)

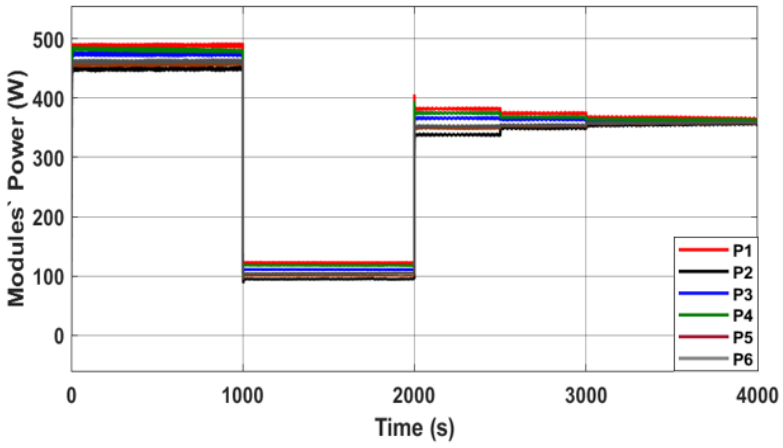

(f)

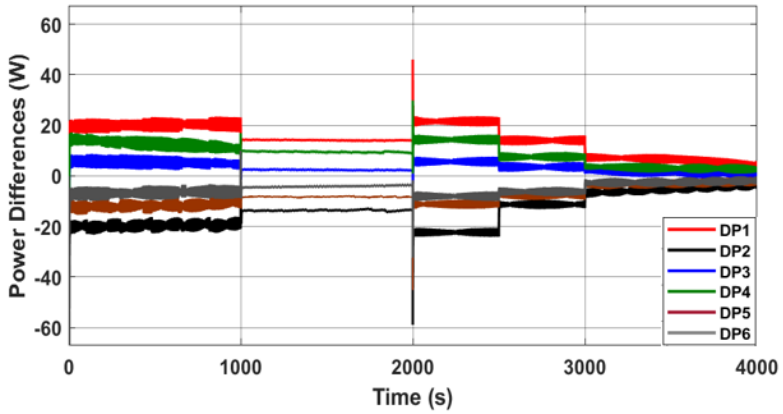

(g)

Figure 3.13: Adaptive power sharing controller with different battery discharge power, (a) Modules DC bus side voltages, (b) DC bus voltage, (c) SoC of each module, (d) Difference between modules` voltage and voltage at equal power sharing, (e) Differences between modules` SoC and average SoC, (f) Module`s power, (g) Difference between modules` power and equal power

Figures 3.13(f) and (g) show the individual modules powers and power differences. The individual power difference with respect to equal sharing case is limited to 20 W at heavy load in the proposed adaptive power sharing controller, whereas it is more than 50 W at the beginning of the simulation using the conventional power sharing controller (Fig. 3.9(g)).

The system conversion efficiency with both control methods is estimated for this simulation case study using (3.12) and (3.13) and illustrated in Fig. 3.14. The equal sharing efficiency is also included to show the effect of the power sharing ratios on the system conversion efficiency at different power levels, and the limitation of the SoC based power sharing controller. In comparison to the equal sharing case, the light load efficiency is increased in both control methods. However, the efficiency improvement in the SoC-based controller depends on the SoC mismatch level and only limited efficiency improvement may be obtained. With the higher allowable voltage differences, a higher efficiency improvement is achieved with the adaptive power sharing controller as shown in Fig. 3.14. The efficiency reduction is also higher with the SoC based power sharing controller when there are high mismatches amongst the modules. The efficiency reduction is also limited with the proposed controller with the lower power sharing ratios, but with the expense of a reduced speed of balancing.

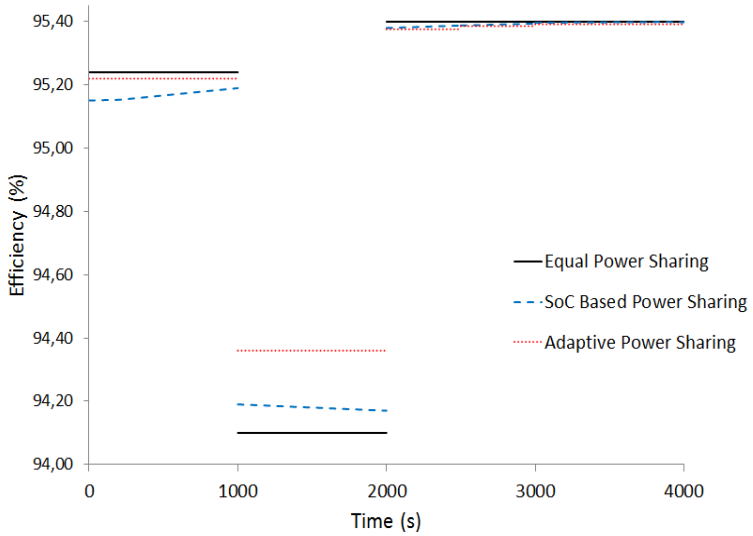

Figure 3.14: Comparison of system efficiency with SoC based controller and adaptive controller

3.8 Summary and Conclusion

This chapter discussed the distributed BESS and existing control methods. The power sharing controllers available in the literature are aimed at specific targets. For example, in the SoC-based power sharing the aim of the controller is to balance the SoC of each module while processing the battery power. This implies operating the modules at different powers and consequently different efficiencies.

The system performance in terms of balancing speed and efficiency was analysed for a SoC-based power sharing controller. An adaptive power sharing controller was then proposed to improve the light load efficiency and balancing speed, and to limit the efficiency reduction at the heavy load area. The results show that a higher conversion efficiency is obtained with the proposed adaptive power sharing controller compared to the SoC-based power sharing controller.

However, the effectiveness of the proposed adaptive power sharing controller depends on the SoC mismatch level, and the power sharing ratios can be adjusted via the SoC differences. In fact, the fast and continuous balancing feature of the distributed BESS prevents divergence of the battery pack`s SoC in the module when the battery packs consist of the same type, capacity, and SoH. In this case, the modules share the power evenly, and the proposed controller may not be effective for a system where the expectation of a high imbalance is low. On the other hand, the proposed adaptive power sharing controller can be effective for a system where continuous imbalance is expected, such as in retired / re-used battery systems. As continuous balancing is required for distributed BESS consisting of pre-used batteries, the adaptive power sharing ability can be utilised to achieve better efficiency at different battery powers compared to the SoC-based power sharing controller. In the next chapter, an efficiency-based optimised power sharing controller is proposed and discussed which is applicable for a system using similar SoH cells.

Chapter 4. Efficiency-Based Optimised Power Sharing Controller for Distributed BESS

4.1 Introduction

The performance of the adaptive power sharing controller proposed in the previous chapter depends on the SoC mismatch which limits its usage and performance. In this chapter an efficiency-based optimised power sharing controller for distributed BESSs is proposed whose effectiveness is independent of SoC imbalance level. The bypassing ability of distributed BESSs is utilised to increase the light load efficiency compared to the adaptive power sharing controller. An off-line Genetic Algorithm is used to determine the number of bypassed modules with respect to the battery power. To deal with fast changes in the battery load, a lookup table is generated based on the off-line Genetic Algorithm optimisation results, and this is used for the real-time implementation. A SoC management algorithm is also implemented to ensure the modules SoC are close to each other in all operating cases. Simulation results are presented which validate the proposed controller.

4.2 The Operational Range of a Modular Converter with Bypassed Modules

A distributed BESS has the ability to bypass any module contained within the system, with the rest of the modules supporting the systems requirements. When any module is bypassed, there will be voltage and power / capacity drops in the system which needs to be compensated by the remaining active modules. This means that the rest of the active modules will increase their operating voltage and current in order to compensate for the voltage and power drops in the system. The active modules` equal sharing voltage and power with $n_{bp}$ bypassed modules can be calculated using (4.1), and (4.2), respectively. The active modules` voltage and power will be $(n/(n-n_{bp}))$ times higher than that of the case without any bypassed modules. Figure 4.1 illustrates the shifting of the operating voltage and power of the individual modules when bypassing occurs for a given total battery power.

$$V_{dc,eqbp} = \frac{V_{Bus}}{n - n_{bp}} \tag{4.1}$$

$$P_{BM,bp} = \frac{P_{DBESS}}{n - n_{bp}} \tag{4.2}$$

where n_{bp} is the number of bypassed modules, and $V_{dc,eqbp}$ and $P_{BM,bp}$ represent the modules DC bus side voltage and corresponding module power in the equal sharing case with n_{bp} bypassed modules.

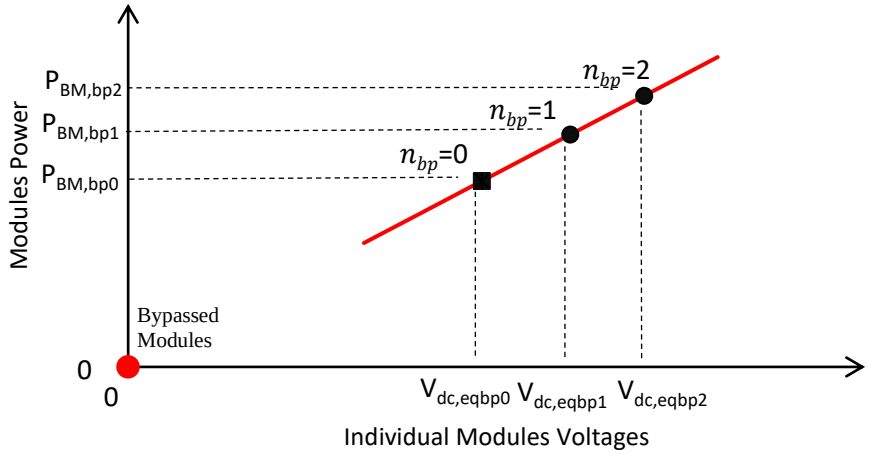

Figure 4.1: The effect of bypassing on individual the converter voltages and powers

Bypassing of any module causes a high (dV/dt) which in turn creates a surge current (4.3) from the capacitor connected to the DC bus side of each converter. The high current damages the bypassing switches and avoiding the surge current is necessary to protect the components of the converter modules.

$$i_C = C \times \frac{dV}{dt} \tag{4.3}$$

where i_C is the capacitor current, C is the capacitance.

In addition, the battery should also be isolated from the rest of the system after bypassing occurs. Although, each converter topology has different fault tolerance abilities, and some of them inherently block the system, a bidirectional half bridge Buck-Boost converter is used in this thesis and is considered for the following analysis. The following two things should be considered carefully in order not to damage the circuit components.

1. During bypassing the energy of the capacitor should be discharged carefully or blocked,
2. After bypassing the battery should be isolated from the system,

In the literature different bypassing methods have been proposed [131]. In order to limit the current from the DC bus side capacitor when bypassing occurs, a resistor is placed in series with a MOSFET as illustrated in Fig. 4.2. As the resistor causes a high conduction loss, it is bypassed after the capacitor is discharged [131]. This can be achieved by either placing and

controlling another parallel switch (S5) or turning-on the converter switches at the same time (S1 and S2). The battery is isolated from the system with the isolation switch S3. In normal operating condition S3 is always on, and it is turned off when the battery is bypassed.

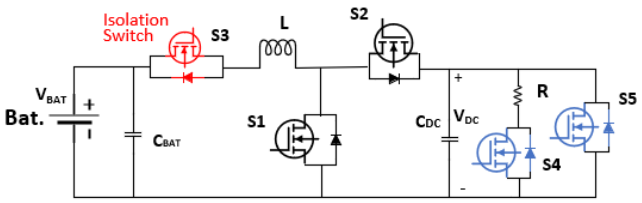

Figure 4.2: Bypassing with two switches and resistor

In [132] two additional complementary switches are placed at the DC bus side of the converter as shown in Fig. 4.3. In this H-bridge configuration switch S3 is always on, and S4 is always off when the module is connected to the rest of the system, i.e. when the module is active [132]. When bypassing occurs, the bottom switch (S4) is turned-on and S3 is turned-off. With this method, the capacitor voltage is blocked, and the battery is isolated from the system.

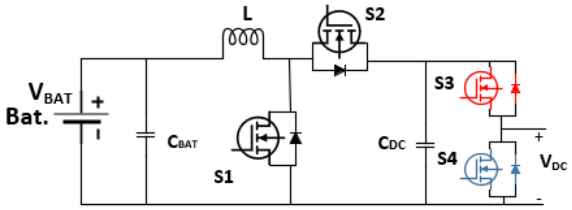

Figure 4.3: Bypassing with H-bridge configuration

In [133] the converter switches are used to control the system current during bypassing. By controlling the current of the switches in switches` active region, the capacitor discharge current is kept within the safe operating area of the switches. The isolation switch is still required to isolate the battery from the DC bus during the bypassing event. Although, this method requires only one additional component to isolate the battery, it increases the control complexity.

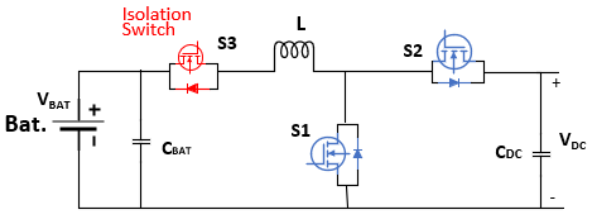

Figure 4.4: The use of converter switches for bypassing

In the literature, the bypassing ability of distributed BESSs is used to improve the systems reliability and to maintain system operation. Any faulty modules are bypassed during charging / discharging and the other modules increase their voltage and current levels to compensate for this loss. In some cases when there is a high mismatch the bypassing command is used to increase the balancing speed, an example of which is discussed in [93]. Here, the bypassing feature of the distributed BESS is utilised to improve the light load efficiency. In the next section an optimisation algorithm is used to determine the number of active modules at different battery power levels based on the systems efficiency curve.

4.3 Problem Formulation & Optimisation

The converters in distributed BESSs are designed to handle the full power available from the batteries, and the battery power varies depending on the power requirements of the system. Typically, the Energy Management System (EMS) determines the battery power, and the battery converter operates at different power levels for different periods of time depending on the required battery power. The individual converter efficiency also varies within this wide range of operating modes, and the different loads applied to each module for a given battery power affects the total system conversion efficiency. Therefore, the flexible power sharing feature of the distributed BESS can be utilised to improve the system`s energy conversion efficiency. A Genetic Algorithm is used to determine the power sharing ratios at different loads within the system constraints, and the loss components of the bidirectional half bridge DC-DC converter are integrated in the optimisation problem, along with the system constraints.

4.3.1 Efficiency Map of Synchronous Bidirectional Buck-Boost Converter

The converter loss components are the same as those for the nonsynchronous converter used in Chapter 3, except that a switching dead time transition now occurs in the MOSFET body diodes. Although the following calculations are carried out in the Boost operating mode, the same procedure was applied for the Buck mode. The control and synchronous MOSFETs` conduction losses, are calculated using (4.4) and (4.5), where S1 and S2 stand for the boost and buck switches, respectively. The inductor conduction losses is calculated using (4.6), where the rms current can be estimated using (4.7) [134]. It is worth mentioning that the inductor core loss is very low compared to its conduction loss and it is neglected to simplify the calculations.

$$P_{con,s1} = I_{bat,rms}^2 \times R_{ds,on} \times d \tag{4.4}$$

$$P_{con,s2} = I_{bat,rms}^2 \times R_{ds,on} \times (1 - d) \tag{4.5}$$

$$P_L = I_{bat,rms}^2 \times DCR \tag{4.6}$$

$$I_{bat,rms} = \sqrt{I_{bat}^2 + \frac{I_{ripple}^2}{12}} \tag{4.7}$$

The switching loss consists of V-I overlap loss (P_{V-I}), dead-time loss (P_{dt}), reverse recovery loss (P_{RR}), output capacitance loss ($P_{COSS,FET}$) and gate charge loss (P_G). The calculations for these loss components are shown in (4.8) to (4.12) below:

$$P_{V-I} = \frac{(V_{dc} + V_{DS,F}) \times I_{bat}}{2} \times f_{sw} \times (t_r + t_f) \tag{4.8}$$

$$P_{dt} = V_{SD} \times I_{bat} \times f_{sw} \times (t_{dtr} + t_{dtf}) \tag{4.9}$$

$$P_{RR} = Q_{RR} \times V_{dc} \times f_{sw} \tag{4.10}$$

$$P_{COSS,FET} = C_{OSS} \times V_{DC}^2 \times f_{sw} \tag{4.11}$$

$$P_G = (Q_{g1} + Q_{g2}) \times V_{GS} \times f_{sw} \tag{4.12}$$

where t_{dtr} and t_{dtf} are the dead times when the current rising from low to high and falling from high to low during switching, respectively.

The converter loss is the sum of the individual component losses (4.13) and the efficiency of the converter can be calculated using (4.14):

$$P_C = P_{con,s1} + P_{con,s2} + P_L + P_{V-I} + P_{dt} + P_{rr} + P_{COSS} + P_G \tag{4.13}$$

$$\eta_c(\%) = \frac{P_{in} - P_C}{P_{in}} \times 100\% \tag{4.14}$$

The efficiency maps of a single converter in the Boost (battery discharging) and Buck (battery charging) modes are presented in Figs. 4.5(a) and 4.5(b) respectively. For these results, each module`s DC bus side voltage was varying between 12.8 and 40 V, the currents between 0 and 10 A, and the battery voltage was 12.8 V. The switching frequency was set at 250 kHz and the converters` components used for the efficiency calculations are shown in Table 4.1. The parameters of the converters` components are also shown in Table B2, in Appendix B. In both cases the efficiency is low at light load due to the higher switching loss contribution, and it has

a peak efficiency around 30 % load. After the peak efficiency point, the efficiency reduces slightly because of the quadratic relationship between the conduction losses and current.

Table 4.1. The component list used in the efficiency calculation

Component	**Manufacturer**	**Part Number**	**Ratings**	
			Voltage (V)	**Current (A)**
MOSFETs	VISHAY	TK18E10K3	100	18
Inductor	Vishay	IHLP-8787MZ5A		15.4

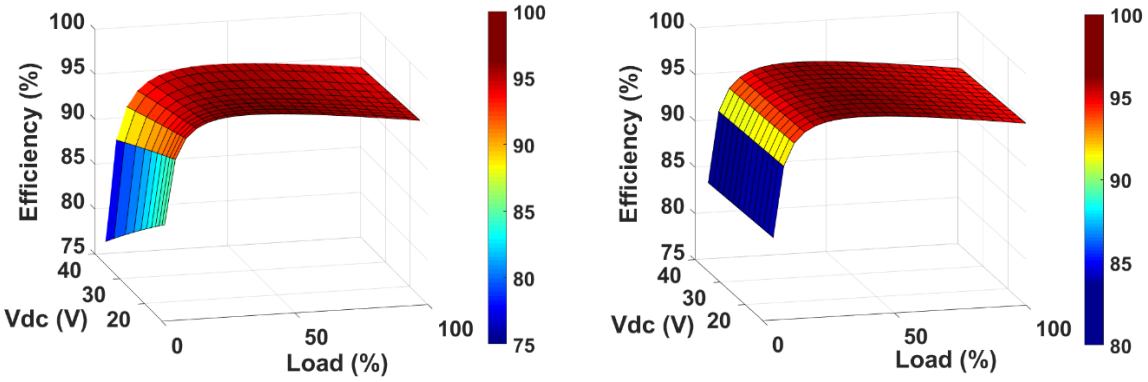

(a) (b)

Figure 4.5: The efficiency map of a single converter, (a) in discharging mode, (b) in charging mode

4.3.2 Problem Formulation

The objective is to minimise the total system conversion loss as defined in (4.15) considering the loss components represented in (4.13).

$$min.fobj = \sum_{x=1}^{n} P_{c,x} \tag{4.15}$$

The system parameters and limitations for this optimisation are summarised in Table 4.2. The number of modules used for this case study is 6, and the DC bus voltage is 120 V. The rated voltage and capacity of each battery pack is 12.8 V and 10 Ah, respectively, and the recommended maximum continuous charge / discharge currents are 5 A and 10 A. Therefore, the maximum continuous discharging power of the system is 768 W and the maximum

continuous charging pow.er is 384 W for the 6 modules. The designed converter voltage rating is 40V, and the current rating is 10A.

Table 4.2. System Specifications

System Parameters		**Value**
Number of Modules, n		6
DC Bus Voltage, V_{Bus} (V)		120
Discharging Power, $P_{s,d}$ (W)		768
Charging Power, $P_{s,c}$ (W)		384
Battery Parameters	Rated Voltage, V_{Bat} (V)	12.8
	Capacity, C, (Ah)	10
	Maximum Continuous Discharge Current, $I_{bat,max}$ (A)	10
	Maximum Continuous Charge Current, $I_{bat,max}$ (A)	5
Converter Parameters	Maximum Voltage, $V_{dc,max}$ (V)	40
	Minimum DC Bus Side Voltage, $V_{dc,min}$ (V)	0/12.8
	Current Ratings, (A)	10
	Maximum duty ratio, d_{max}	0.8

The constraints of the problem are formulated from (4.16) to (4.19). In distributed BESSs the sum of the module voltages is equal to the DC bus voltage (4.16), and the maximum DC bus side voltage of each module should be limited to the converter voltage limits, which is 40 V in this case. The minimum DC bus side voltage can be either 0 V for a bypassed case, or it is equal to the battery voltage with a Boost converter, which is 12.8 V in this system. The maximum current of the individual module should not exceed the converter current ratings, and as the converter is designed to handle the full battery power, this is restricted by the maximum charge / discharge current of the individual battery packs. In the optimisation, the battery lifespan is considered, and it is important not to exceed the recommended charging / discharging current of each battery pack. Therefore, in order not the degrade the battery life, the maximum charge / discharge current is restricted by the maximum continuous battery charge / discharge current shown in the battery datasheet of 5 A and 10 A, respectively.

$$\sum_{x=1}^{n} V_{dc,x} = V_{Bus} \tag{4.16}$$

$$V_{dc,min} \leq \{V_{dc,1}, V_{dc,2}, \dots, V_{dc,n}\} \leq V_{dc,max} \tag{4.17}$$

$$0 \leq \{I_{bat,1}, I_{bat,2}, \dots, I_{bat,n}\} \leq I_{bat,max} \tag{4.18}$$

$$0 \leq \{d_1, d_2, \dots, d_n\} \leq d_{max} \tag{4.19}$$

Consider:

$$I_{bat,1} : I_{bat,2} : \dots . : I_{bat,n} = V_{dc,1} : V_{dc,2} : \dots . : V_{dc,n} \tag{4.20}$$

The DC bus side voltages are the decision variables. When the number of bypassed modules increases, the remaining active modules` voltages and currents also increase. Therefore, the number of bypassed modules is restricted by the converter voltage and current ratings. Figure 4.6 illustrates the operational range of the distributed BESS for the presented case study, this was created using equation (3.4) shown below again for ease.

$$I_{bat,x} \times V_{bat,x} = I_{Bus} \times V_{dc,x} \tag{3.4}$$

This figure shows the discharging mode relationship between the DC bus voltage and the battery current for total battery powers (P_{DBESS}) between 20 % and 100 %. The battery voltage is assumed to be 12.8 V and constant for simplicity.

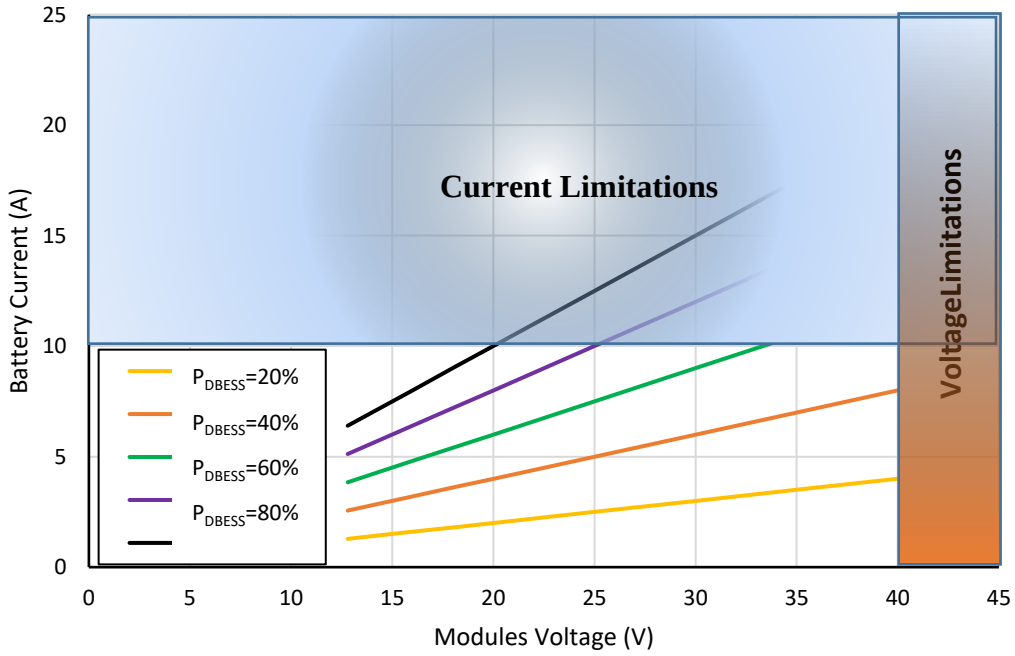

Figure 4.6: The constraints of the distributed BESS

From Fig. 4.6 it is clear that when the total battery power increases, greater current variations occur for the same voltages because of the higher contribution of the I_{bus} (as shown in (3.4)).

Although, it depends on the designed converter ratings, the main limitation for the number of bypassed modules in this case study is the converter voltage rating at light load. When the total battery power increases, the converter DC bus side voltage operating range should also be restricted to not exceed the recommended battery discharging current. For example, at 40 % battery power (orange line), a battery pack can be discharged with a maximum of 8 A when it operates at its maximum DC bus voltage (40 V). At 60 % battery power (green line), the individual battery pack`s discharge current will be 10 A with a 33.33 V DC bus voltage. At this power, the discharging current will be 12 A when it operates at its maximum DC bus voltage, exceeding the recommended maximum discharge current. This is even worse at the full discharging power, i.e., when P_{DBESS} is equal to the 100 %, as all of the individual battery discharge currents will be 10 A with a 20 V DC bus voltage, and no balancing can be achieved at this point. Therefore, the constraints used in the problem formulation avoid operating the modules at undesirable voltage and current levels, and keeps the operation point of each battery pack and converter within the designed voltage and current ratings.

4.3.3 Efficiency Optimisation

In this implemented scheme, a Genetic Algorithm with a population size of 400 was used to obtain the global optimal solution at each battery power. The optimisation algorithm was run from 0 % to 100 % load in 5% steps. A smaller step size would have increased the optimisation accuracy, but at the expense of a large lookup table and consequently increased memory requirements. Figure 4.7 which is showing the discharging mode condition, demonstrates how the module voltages vary depending on the number of bypassed module(s) and load used. The results show that the modules have a tendency to move closer to their peak efficiency points with bypassing used, as many modules as possible at light load, which is restricted by converter voltage limits.

When getting closer to the system peak efficiency point, the number of bypassed modules reduces. With up to 15% battery power, 3 modules are bypassed from the system, and the rest of the active modules operate at their highest powers for a given total battery power. Here, the DC bus side voltages are 40 V. At 20 % battery power, 2 modules are bypassed, and the active modules are loaded at 30% of their full power rating. The DC bus voltages for this condition is 30 V. With 25 % load, only 1 module is bypassed, and the 5 active modules are operating at their highest efficiency point. After the 30 % battery power, which is the peak efficiency point,

the efficiency reduces, with the modules sharing the power equally and no modules being bypassed.

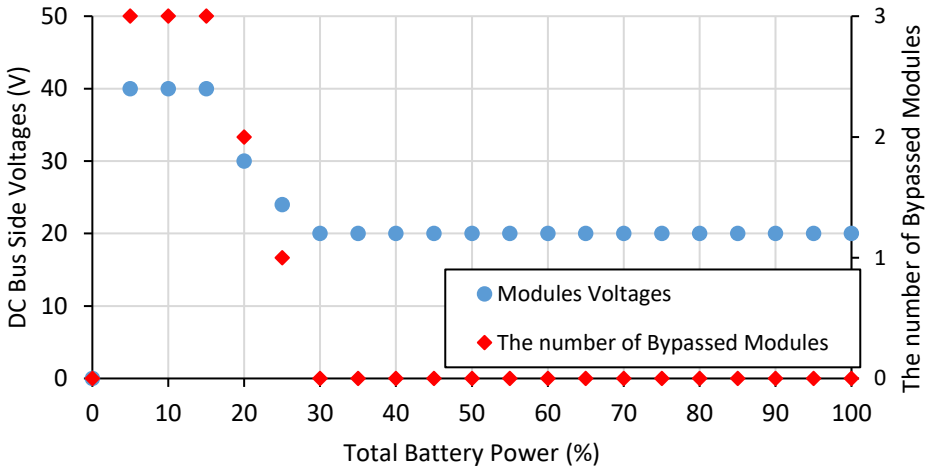

Figure 4.7: The DC bus side voltages of active modules and number of bypassed modules in discharging mode at different battery powers

Figure 4.8 shows the change of the active modules` powers compared to the equal sharing case. It is worth mentioning that although the active modules` loads are doubled at 5 % and 10 % battery power, they do not operate at their maximum efficiency point, as the active modules maximum power is restricted by the converter voltage ratings.

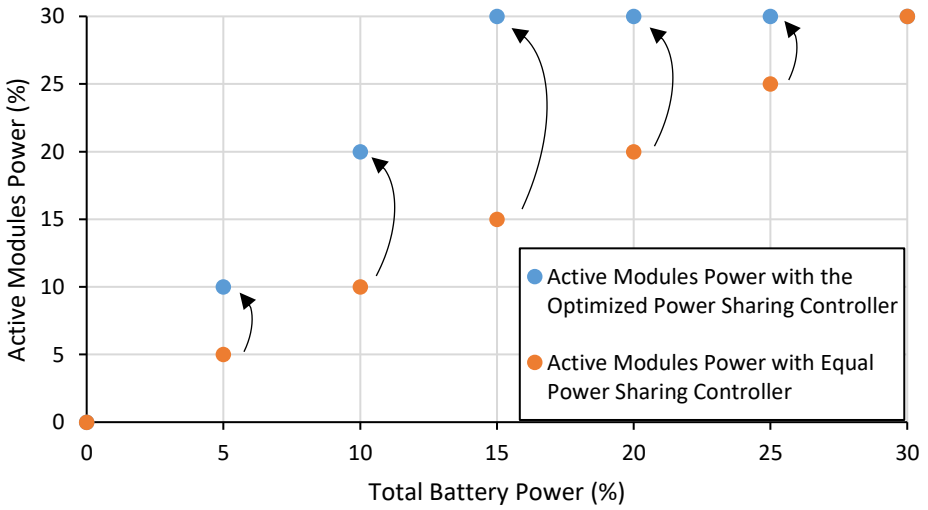

Figure 4.8: The change of individual modules` powers at different battery powers

Figure 4.9 shows the number of bypassed modules and the DC bus side voltages of active modules at different battery charging power. Due to the continuous battery current charging limit, the maximum operation of the converter is half of its rated power in this mode. In a similar manner, the system has a tendency to move closer to the peak efficiency point. Up to 15% battery power, 3 modules are bypassed and active modules operate at their maximum power for the instantaneous total battery power. At 20 % battery power 2 modules are bypassed, whilst 1 module is bypassed at 25 % battery power to increase the active modules power and light load efficiency. After the peak efficiency points, all modules are active and the power is evenly shared for the minimum system conversion loss.

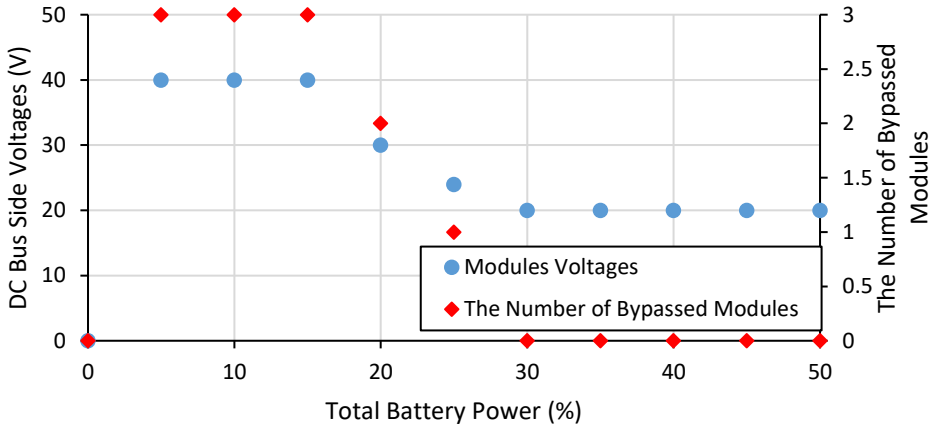

Figure 4.9: The DC bus side voltage of active modules and number of bypassed modules in charging mode at different battery power

4.4 Real-Time Implementation

The proposed efficiency-based optimisation method is achieved off-line, and to deal with the fast changes of battery power in real time, a lookup table is used for the real time implementation. The real-time power allocation method for the efficiency-based optimised power sharing controller is shown in Fig. 4.10. In the lookup table, 'n' bypass commands are generated for 'n' modules based on the off-line Genetic Algorithm optimisation results. Up to 15 % battery power, 3 module bypass commands ($\beta_{a1}, \beta_{a2}, \beta_{a3}$) are set to 1, and the rest are set to 0. With 20 % battery power, β_{a1} and β_{a2} are set to 1, while the rest are set to 0. As there is only 1 module bypassed at 25% battery power, only β_{a1} is set to 1 at this point.

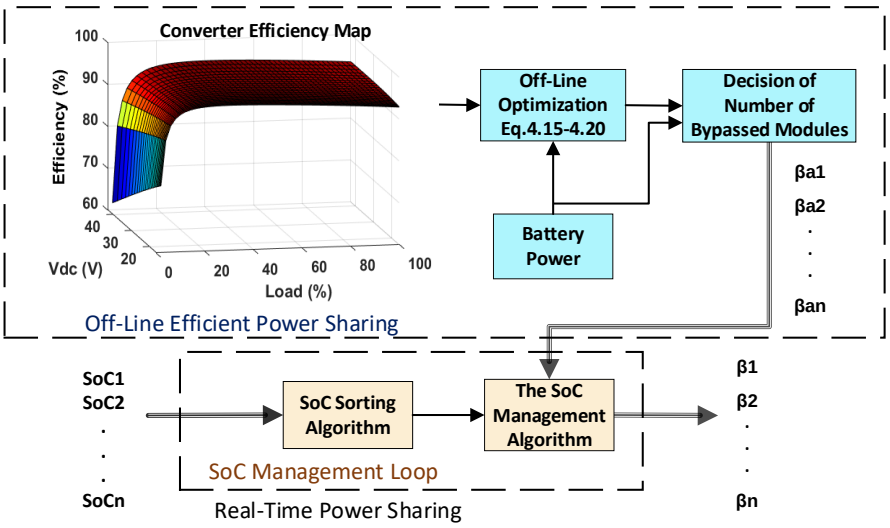

Figure 4.10: The real-time power allocation for efficiency-based optimised power sharing controller in distributed BESS

These arbitrary bypass commands are shared amongst the modules based on the modules SoC values and the SoC management loop. Inside the SoC management loop, the modules` SoCs are sorted and the modules (if any) to be bypassed are determined based on their relative SoC ($SoC_x - SoC_{avg}$) and mode of operation. Therefore, the bypassed commands for corresponding modules (β_1 to β_n) are finally decided upon within this loop. Flowcharts for the discharging and charging cases are shown in Figs. 4.11 and 4.12, respectively. In charging mode, the module(s) with higher SoC are bypassed, whilst the lower SoC module(s) are selected for bypassing in discharging mode. To prevent frequent changing of the bypassed modules, the efficiency-based optimised power sharing controller does not ensure that the modules SoCs are equal. Instead, each module`s SoC is kept within a predefined limit with respect to the average SoC. When any bypassed modules relative SoC reaches the predefined threshold value, it will be reconnected, and another active module is bypassed. The threshold value is set to 1, and when one of the bypassed modules relative SoC ($SoC_x - SoC_{avg}$) reaches 1% in discharging mode, the corresponding module is activated in order to prevent further divergence of the battery SoC, and the module with the next lowest SoC amongst the remaining active modules is bypassed. Likewise, in charging mode, the bypassed module is swapped when any bypassed modules relative SoC is equal to minus 1.

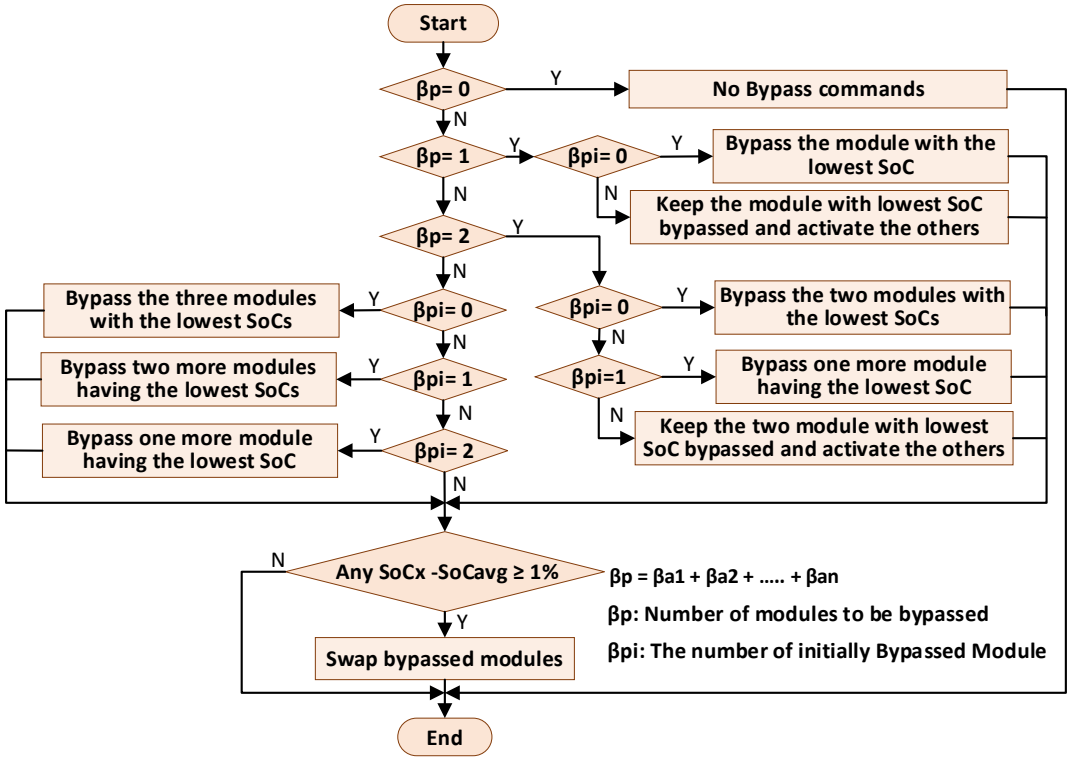

Figure 4.11: The SoC management algorithm in discharging mode

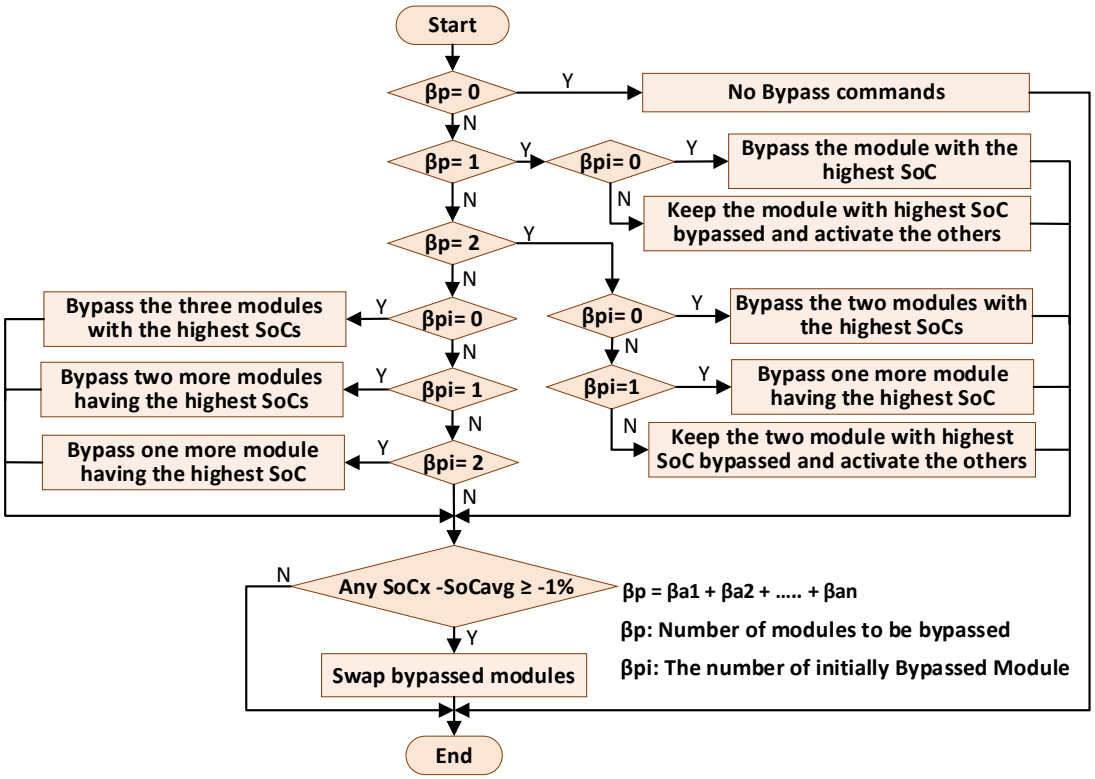

Figure 4.12: The SoC management algorithm in charging mode

In addition, when the number of bypassed modules changes (i.e., the battery power changes), the previously bypassed modules are kept in the bypassed state as long as their relative SoC is within the limit. For example, in discharging mode, when the battery power changes from 15 % to 20 %, the number of required bypassed modules reduces from 3 to 2. The previously bypassed modules may not be the lowest SoC battery packs, but their relative SoC may be still within the (1%) limit. For this condition, instead of changing the status of all of the bypassed modules, only 1 additional bypassed module is activated and two of them stay in their bypassed condition as long as their relative SoC is within the predefined limit. This also prevents frequent changing of the bypassed modules during power transitions.

After the decision for which modules are bypassed, the power sharing controllers are implemented in the discharging and charging modes. The conventional SoC-based power sharing controller proposed in [13] is modified in this section. Since the SoC balancing loop creates power differences amongst the modules, this will cause shifting of the modules` desired operating points, and the optimum efficiency will not be achieved. Therefore, in this efficiency-based optimised power sharing controller two parameters have been added to the block diagrams shown in Fig 4.13.

The first parameter is the SoC balancing loop enabling / disabling parameter (Δ), and the second is the modules bypass / activate parameter (β_x). As the SoC management is accomplished by the proposed algorithm, the enable / disable multiplier Δ is set to 0 and the SoC balancing loop is disabled.

The power management for the discharging and charging cases is achieved using the control block diagrams shown in Figs. 4.14 and 4.15, respectively. Here, the individual modules DC bus side reference voltages ($V_{dc,ref1}$ to $V_{dc,refn}$) are multiplied with their associated bypassed commands (β_1 to β_n) determined in the SoC management loop. The reference DC bus side voltage for an arbitrary module 'x' ($V_{dc,refx}$) is computed using (4.21). The individual modules DC bus side voltages are then regulated based on the generated reference value in discharging mode as shown in Fig. 4.14.

For charging operation, the power sharing controller can be realised by applying a voltage equal to the bus voltage (V_{Bus}) at the bus side, and the average charging current controller is also included as shown in Fig. 4.15.

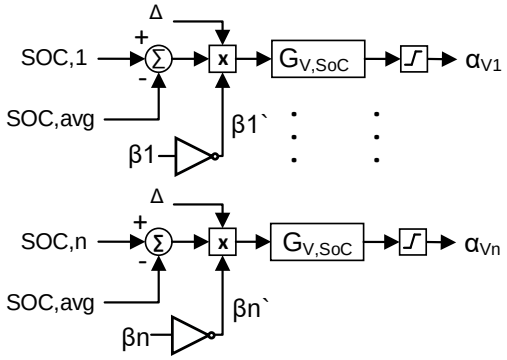

Figure 4.13: The block diagram of SoC balancing controller

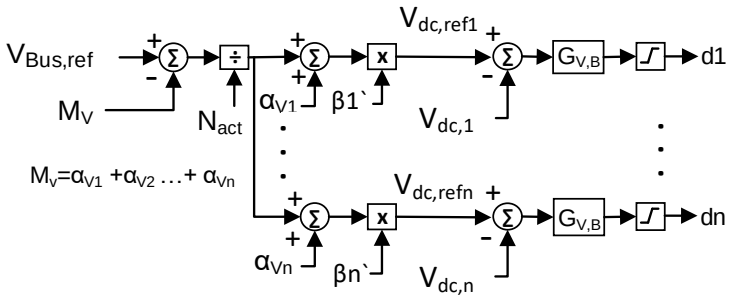

Figure 4.14: Modules DC bus side voltage control during discharging

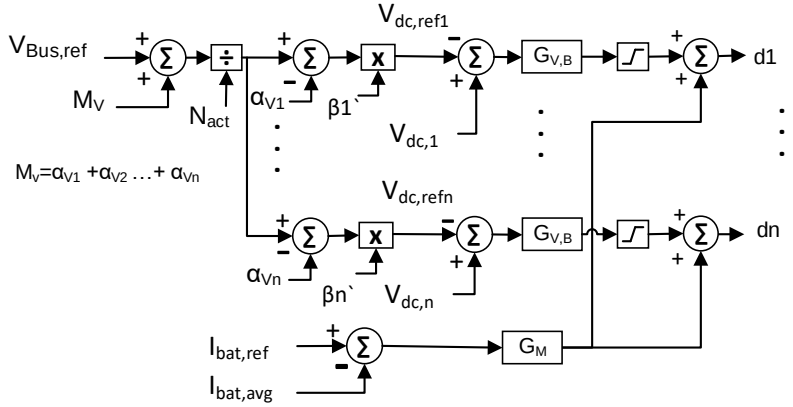

Figure 4.15: Modules DC bus side voltage control and average charging current control during charging

$$V_{dc,refx} = \frac{V_{Bus,ref}}{N_{act}} \times \beta_x^{`} \tag{4.21}$$

$$I_{bat,avg} = \frac{1}{N_{act}} \times \sum_{x=1}^{n} I_{bat,x} \tag{4.22}$$

$$N_{act} = n - \sum_{x=1}^{n} \beta_x \tag{4.23}$$

$$M_V = \sum_{X=1}^{n} \alpha_{Vx} \tag{4.24}$$

where N_{act} is the number of active modules, and $I_{bat,avg}$ is the average battery current. M_V is the sum of the correction values.

For the conventional SoC-based power sharing controller, the value of the enable / disable multiplier(Δ) is set to 1 and it has no effect on the SoC balancing loop. The outer SoC balancing loop compares the individual modules SoC with the average, and determines the individual module DC bus side voltages by adding a correction value (α_{vx}). The sum of the α_{vx} parameters (M_v) is extracted / added from / to the reference bus voltage ($V_{Bus,ref}$) in the discharging / charging modes to keep the DC bus voltage at the desired value. The reference DC bus side voltage for an arbitrary module x ($V_{dc,refx}$) is calculated using (4.25) and (4.26) in the discharging and charging modes, respectively.

$$V_{dc,refx} = \left[\frac{V_{Bus,ref} - M_v}{N_{act}} + \alpha_{Vx}\right] \times \beta_x^{`} \tag{4.25}$$

$$V_{dc,refx} = \left[\frac{V_{Bus,ref} + M_v}{N_{act}} - \alpha_{Vx}\right] \times \beta_x^{`} \tag{4.26}$$

4.5 Simulation Results

The SoC-based power sharing controller and the proposed efficiency-based optimised power sharing controller were both simulated using MATLAB / Simulink. The simulation parameters of the system are shown in Table 4.3. Six modules were used for the simulations, with each module consisting of 6-battery packs with different initial SoC values, and 6 bidirectional half bridge Buck-Boost converters. 12.8 V, 10 Ah, Li-ion batteries were used in the simulations, and the distributed BESS is connected to a 120 V DC bus. Batteries were discharged and charged at variable power level. While the maximum discharging current is 10 A, the maximum charging current was set to 5 A.

Table 4.3. Simulation Parameters

System Parameters	**Value (%)**	
	Discharging	**Charging**
Initial SoC of Battery-1	90	53
Initial SoC of Battery-2	88	54
Initial SoC of Battery-3	86	55
Initial SoC of Battery-4	87	53.5
Initial SoC of Battery-5	87.5	52
Initial SoC of Battery-6	89	52.5
Time (min)	**Battery Discharge-Power**	**Battery Charge-Power**
0-8	10	10
8-16	20	20
16-24	25	25
24-32	40	30
32-40	70	40
40-48	100	50

The simulation was carried out at different battery powers with initial SoC mismatches. In discharging mode, the battery packs operate as a power source, and they supply parallel resistive loads connected to the DC bus side of the system. These parallel resistive loads are then controlled to discharge with the desired power level. In the charging mode, a 120 V voltage source is connected to the DC bus side, and to charge the battery modules with different charging currents, the reference charging current is controlled.

4.5.1 Simulation Results with SoC-based Power Sharing Controller with Variable Discharging Power

Figure 4.16 shows the simulation results with SoC-based power sharing controller. Depending on the SoC of each module, the modules DC bus side voltages vary to perform the balancing function during discharging. Modules 1, 2, and 6 have higher SoCs than the average, and their

corresponding DC bus side voltages are also greater than equal sharing voltage as illustrated in Fig. 4.16(a). Therefore, these modules are discharged with battery currents higher than the average current as illustrated in Fig. 4.16(b). In contrast, the modules with a SoC lower than the average (modules 3, 4, and 5) have lower DC bus side voltages and are discharged with less current. As the modules are converging, the voltage differences reduce, and they share the DC bus voltage and total battery power evenly when the modules SoCs are balanced. Figure 4.16(c) shows the SoC of each module, where they are balanced at around 2000 s. After this point, each module is discharged with the same power. The DC bus voltage is always maintained at 120 V as shown in Fig. 4.16(d). In the SoC-based power sharing controller the voltage difference only depends on the SoC mismatch amongst the modules for the SoC balancing.

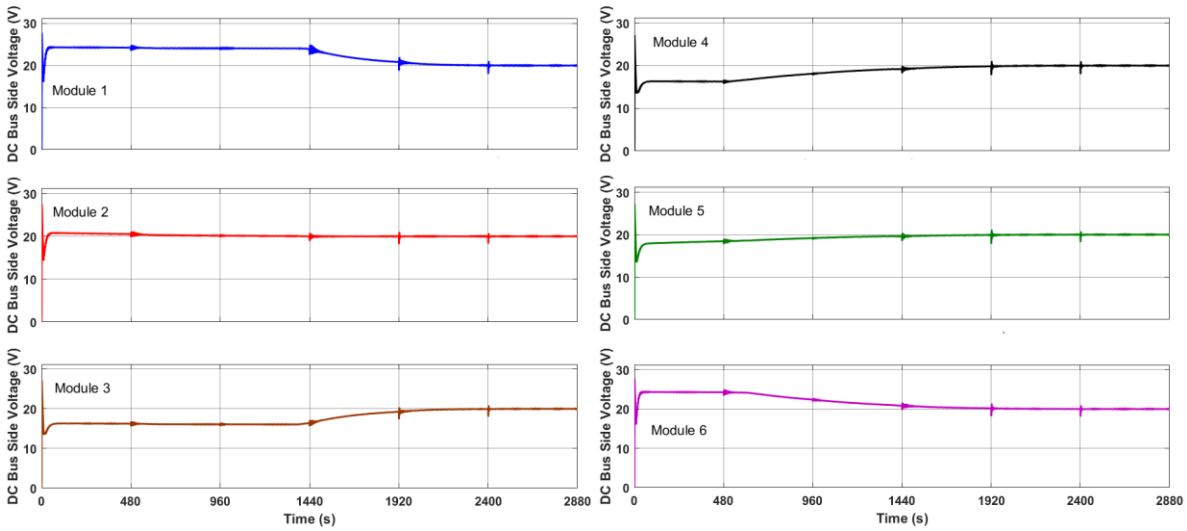

(a)

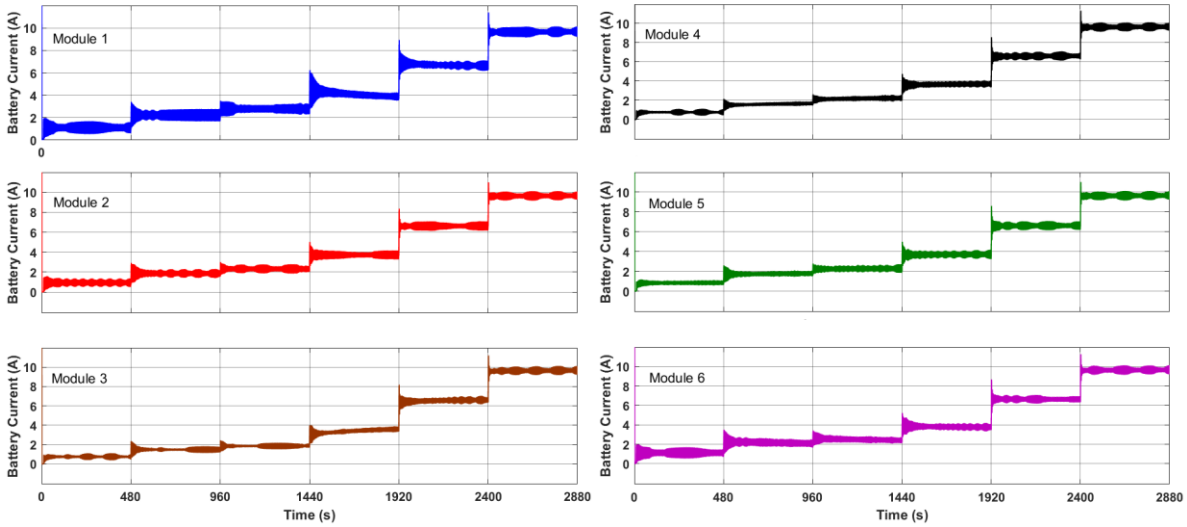

(b)

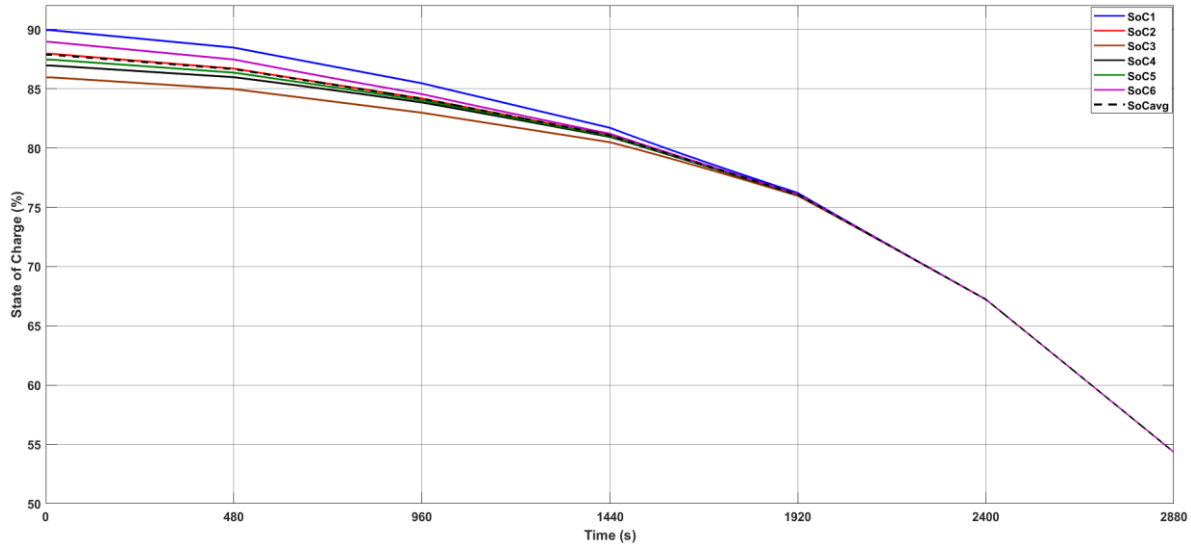

(c)

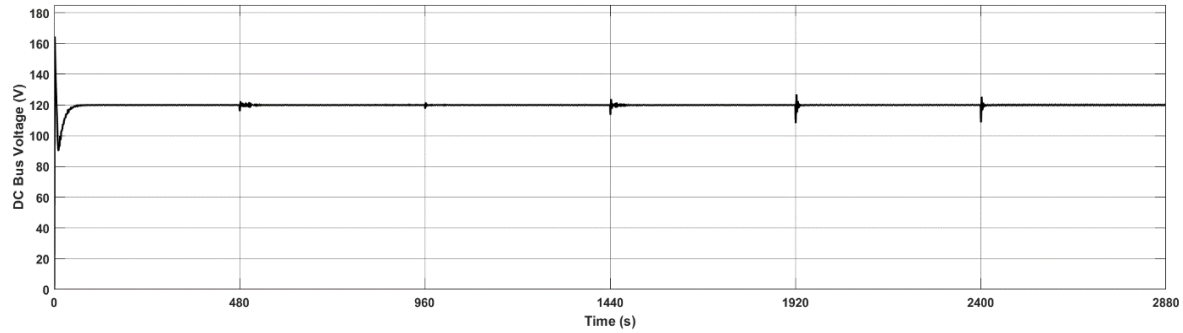

(d)

Figure 4.16: SoC-based power sharing controller with variable battery discharging current, (a) Module DC bus side voltages, (b) Battery packs discharging currents, (c) SoC of each module, (d) DC bus voltage

4.5.2 Simulation Results with the Efficiency-based Optimised Power Sharing Controller with Variable Discharging Power

Simulation results for the efficiency-based optimised power sharing controller are shown in Fig. 4.17. At 10% battery power, 3 modules with the lowest SoC (modules 3, 4, and 5) are bypassed from the system, and the rest of the modules are active. Figure 4.17 (a) shows the DC bus side voltage of each module. As the DC bus voltage is 120 V for this system, the active modules DC bus voltages are 40 V, and they share the power evenly. In this case, each active module is discharged with 2 A as shown in Fig. 4.17(b), i.e., the individual active modules` power is 20% of their rated power. Although, a higher efficiency could be obtained if higher individual modules powers were used, the voltage ratings of the system limit the individual battery power to 20% load in this case. When the battery power is increased from 10% to 20% at 480 s, one additional module is activated, with each active module now operating at 30% of

their rated load. During this transition, Module 5 has the highest SoC amongst the 3 bypassed modules, so this module is activated. At 20 % total battery power (between 480 and 960 s,) 2 modules are bypassed from the system, and the active modules are now discharged with a 3 A battery current. At 25% total battery power, only 1 module is bypassed, and the 5 modules are operating at 30% battery power. After the peak efficiency power, (1440 s), the modules share the power evenly to limit the reduction in the systems conversion efficiency. Figure 4.17(c) shows the SoC of each module, and although they are not perfectly balanced, they are very close to each other, and any modules relative SoC ($SoC_x - SoC_{avg}$) is always less than 1% in this case.

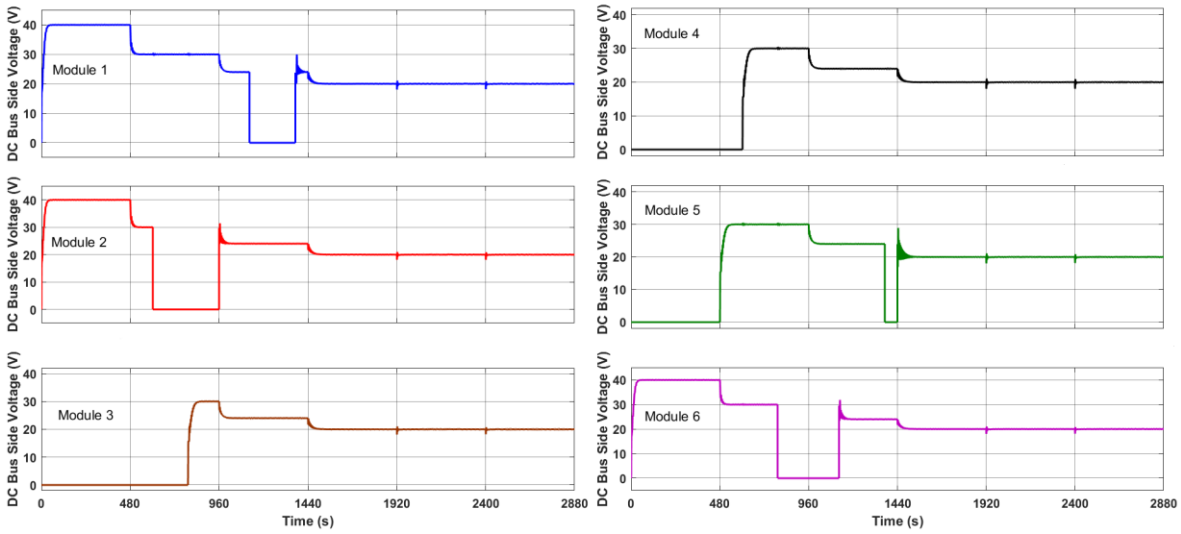

(a)

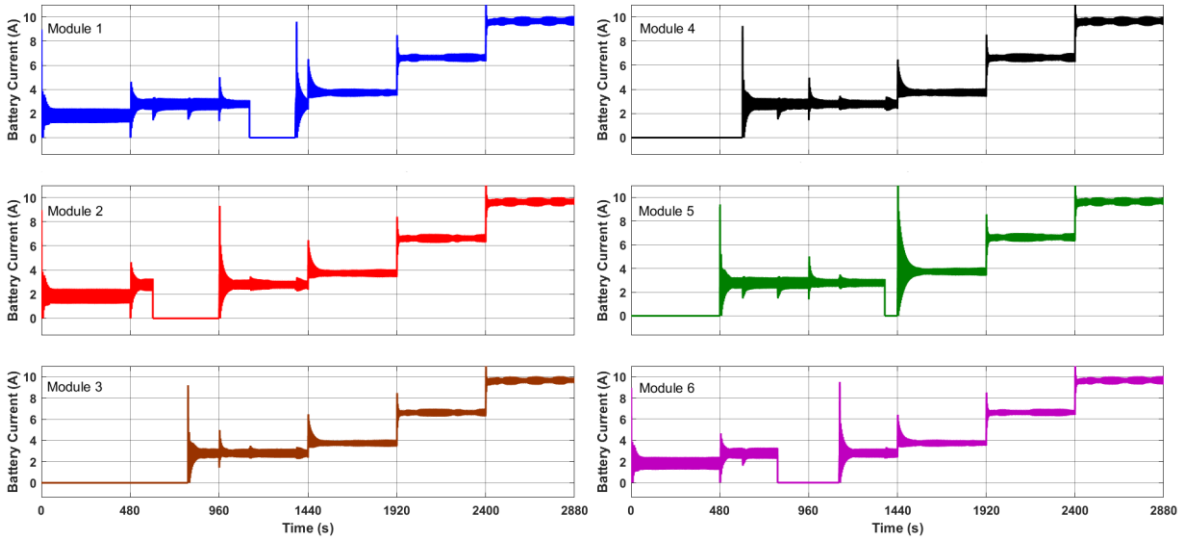

(b)

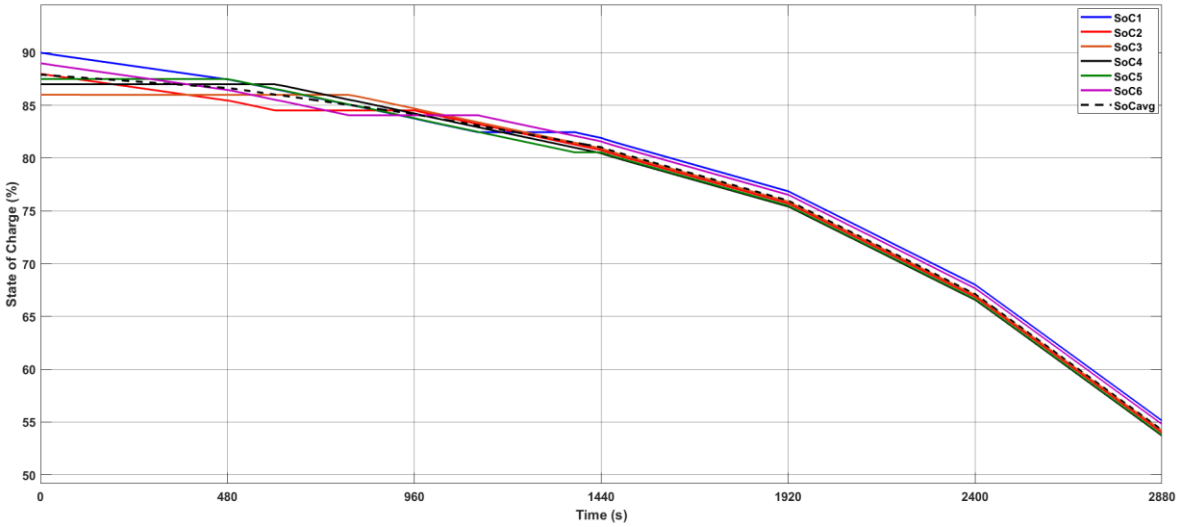

(c)

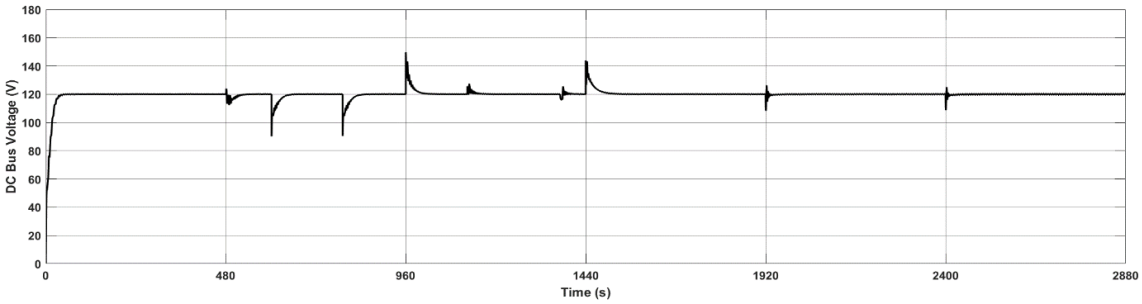

(d)

Figure 4.17: Efficiency-based optimised power sharing controller with variable battery discharging current, (a) Modules DC bus side voltages, (b) Battery packs discharging currents, (c) SoC of each module, (d) DC bus voltage

In each bypassing event, when any bypassed modules relative SoC reaches 1 %, the corresponding module is activated in order to prevent further divergence of the battery SoC, and the module with the lowest SoC amongst the active modules is bypassed. At around 600 s, the relative SoC of the bypassed Module 4 reaches the predefined turn on value, and it is activated so the predefined SoC differences are not exceeded. At the same time, the module with the lowest SoC (Module 2) is bypassed. Similarly, other modules are bypassed at different times, with Modules 3 and 6, 6 and 1, and 1 and 5 swapping at 791, 1124, and 1371 s, respectively.

The system efficiency with both control methods is estimated using (3.12) and is presented in Fig. 4.18 for discharging mode. The efficiency with the equal power sharing method is also included to show the effect of the power sharing ratios on the system efficiency at different power levels. This graph demonstrates the limitation of the SoC-based power sharing

controller. With the proposed efficiency-based power sharing control method, the system efficiency is increased by 5.05% compared to the equal sharing method at 1% battery power, and 0.6% at 10%, 20%, and 25% battery power, respectively. The light load efficiency is also improved with the SoC-based power sharing controller, with a maximum 1.7 % increase at 10% load. This is because the voltage difference at the DC bus side is limited in the SoC-based power sharing controller and it is ±4 V in the case study. In addition, the module power differences in the SoC-based power sharing controller depends on the battery packs` SoC mismatch levels. Therefore, when all battery packs are balanced, there will be no light load efficiency improvement with the SoC-based power sharing, and the conversion efficiency will be the same as the equal power sharing method. In addition, if there is a SoC mismatch, the SoC-based controller has a lower system efficiency than that of the equal sharing case after the peak efficiency point, 28% battery power in this case. This efficiency reduction is prevented when the optimised power sharing controller is used.

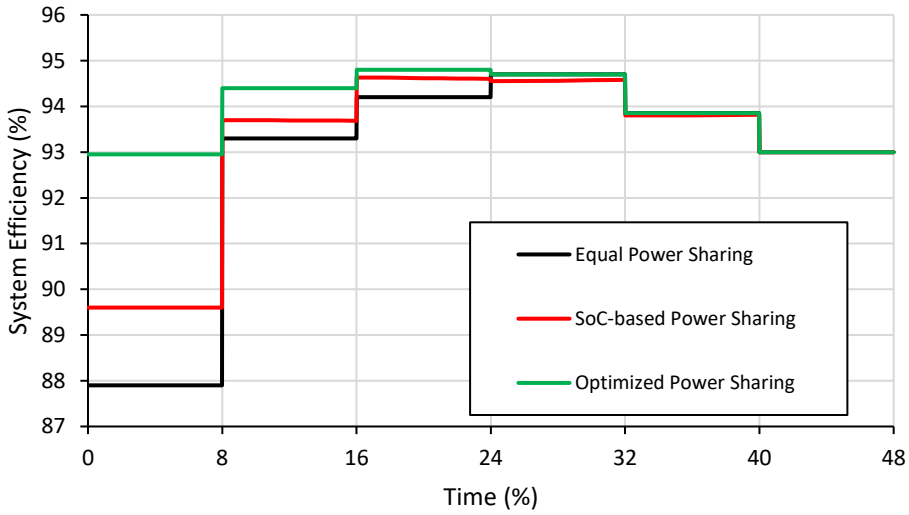

Figure 4.18: Estimated system efficiency for this case study in discharging mode

The estimated operational system efficiencies of the SoC-based, efficiency-based, and equal power sharing controllers are shown in Fig. 4.19 from no load to full load at discharging mode. In the SoC-based power sharing controller the system efficiency varies between the SoC-based power sharing efficiency curve and equal power sharing efficiency curve depending on the SoC mismatch level.

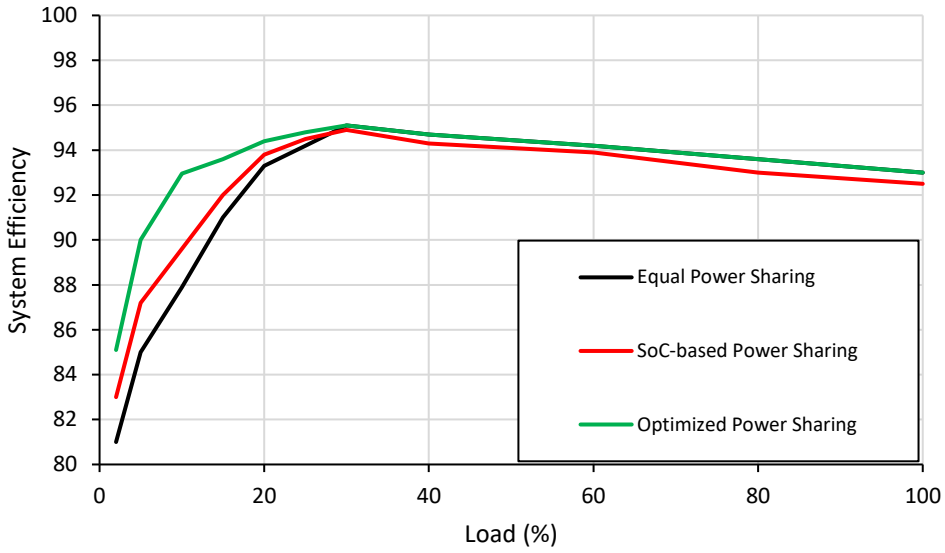

Figure 4.19: Operational system efficiency at full load range in discharging mode

4.5.3 Simulation Results with SoC-based Power Sharing Controller with Variable Charging Power

In the charging mode, a 120V DC power supply is connected to the DC bus, and the total DC voltage is shared among the modules based on the SoC of each module using the power sharing controller previously presented in Fig. 4.15. Figure 4.20 shows simulation results for this SoC-based power sharing controller in the charging mode. To perform the SoC balancing, the modules with a SoC lower than the average are charged with higher currents in the charging mode, and vice versa. In Fig. 4.20(a), modules 1, 5, and 6 have lower SoCs than the average and their corresponding DC bus side voltages are bigger than the equal sharing voltage. This means they are charged with higher currents as shown in Fig. 4.20(b). Modules 2, 3, and 4, have lower DC bus side voltages and are charged with lower battery currents. In the SoC-based power sharing controller, the voltage differences depend on the SoC mismatch level regardless of the total battery power, and when the modules are converging, the voltage differences reduce. When the module SoCs are balanced, each module shares the DC bus voltage and total battery power evenly. Figure 4.20(c) is showing the SoC of each module. On this graph they are balanced at around 2100 s, and after this, each module is charged with the same battery current. The sum of the individual modules voltages is always 120 V as shown in Fig. 4.20(d).

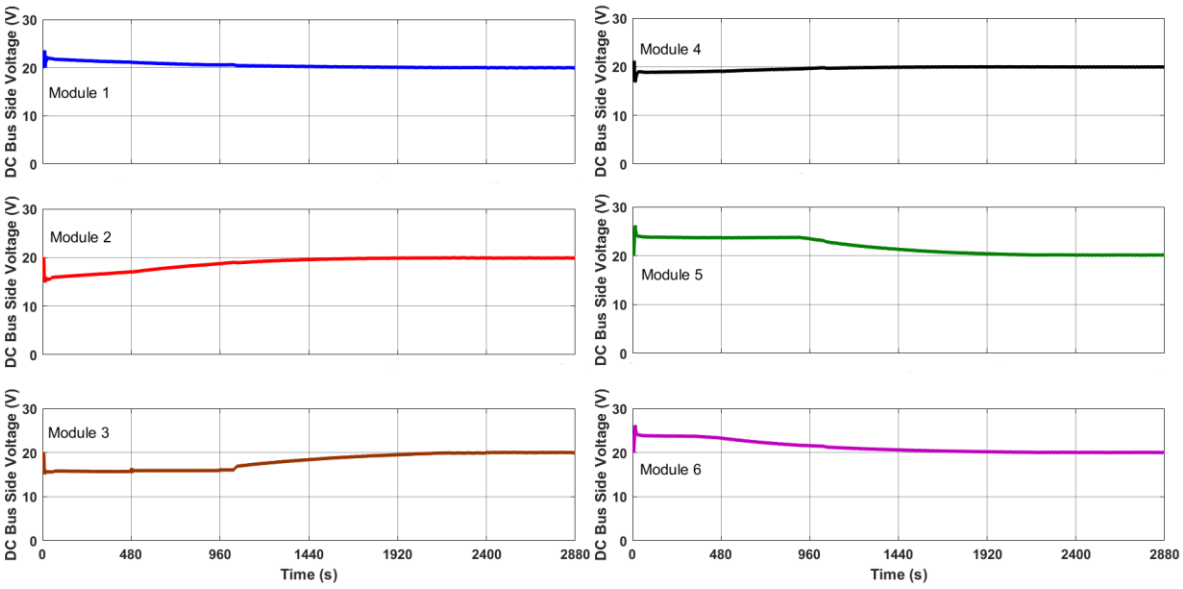
Module 1
Module 2
Module 3
Module 4
Module 5
Module 6
DC Bus Side Voltage (V)
Time (s)

(a)

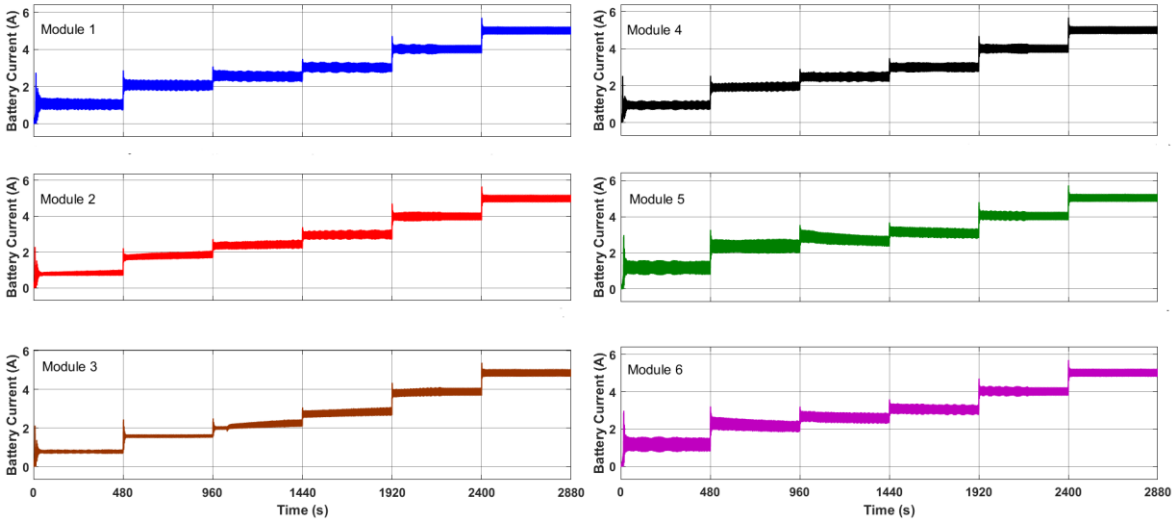
Module 1
Module 2
Module 3
Module 4
Module 5
Module 6
Battery Current (A)
Time (s)

(b)

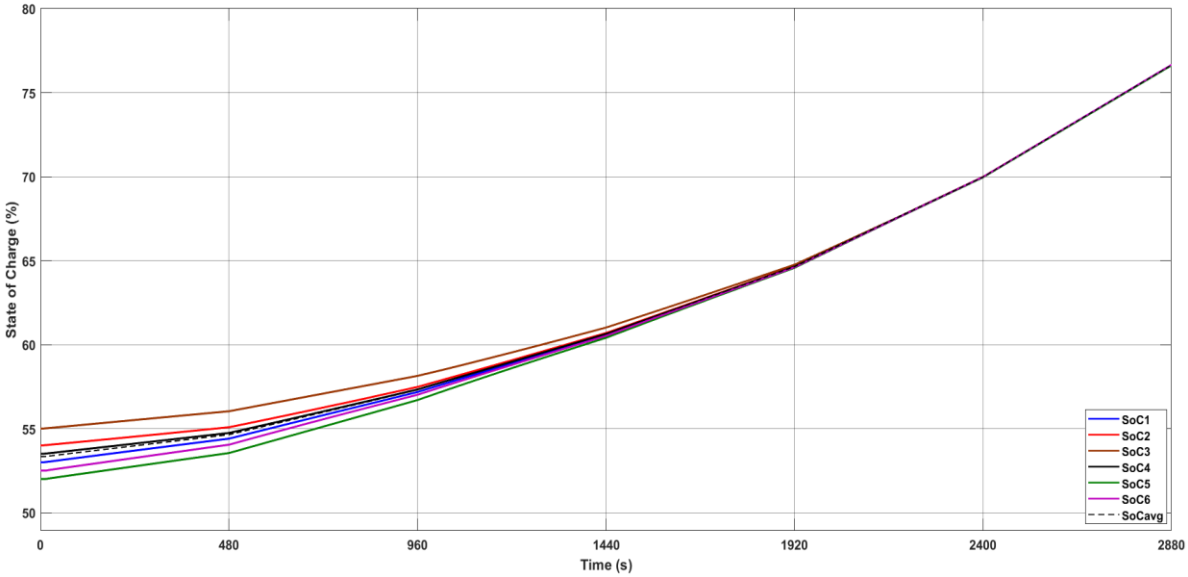
State of Charge (%)
Time (s)
SoC1
SoC2
SoC3
SoC4
SoC5
SoC6
SoCavg

(c)

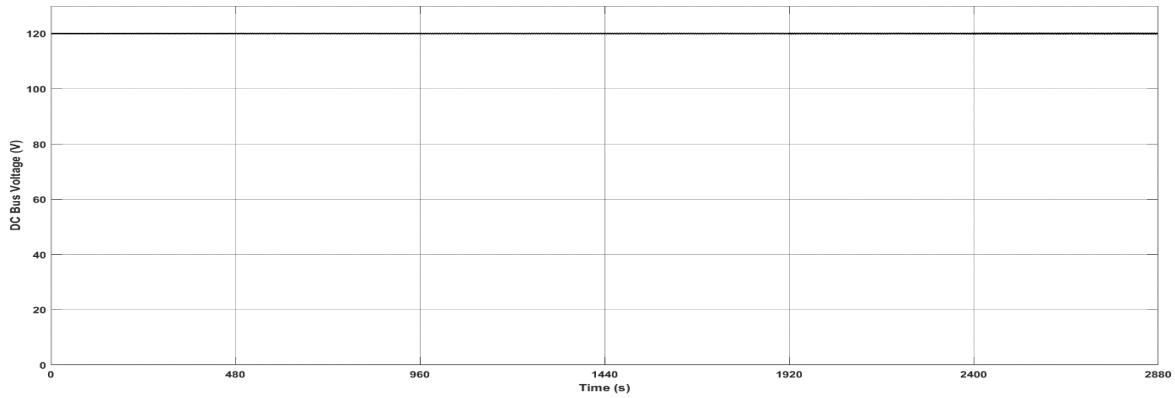

(d)

Figure 4.20: SoC-based power sharing controller with variable battery charging current, (a) Modules DC bus side voltages, (b) Battery packs charging currents, (c) SoC of each module, (d) DC bus voltage

4.5.4 Simulation Results with the Efficiency-based Optimised Power Sharing Controller with Variable Charging Power

Simulation results for the efficiency-based optimised power sharing controller are shown in Fig. 4.21. At 10% battery power, 3 modules with the highest SoC (modules 2, 3, and 4) are bypassed from the system, the other modules are charged with a 2 A battery current, and a 40 V DC bus side voltage is occurring. At 480 s, the total battery power increases to 20 %. In a similar way to the discharging case, at 20 % total battery power (between 480 and 960 s) 2 system modules are bypassed, and the active modules are charged with a 3 A battery current, 30 % of their rated power. During the battery power transition at 480 s, Module 2 has the lowest SoC amongst the 3 bypassed modules, so this module is now activated. At 25% total battery power, only 1 module is bypassed, while the remaining 5 modules now operate at 30% battery power. During the power transient at 960 s, the bypassed Module 6 is now activated. After the peak efficiency power (1440 s), all modules are active, and each module shares the power evenly to limit any reduction in the systems conversion efficiency. With the proposed SoC management algorithm each modules` SoC is kept close to each other, as a bypassed module is activated when its relative SoC reaches -1%. At around 430 s, the relative SoC of the bypassed Module 4 reaches the predefined turn on value, and it is activated in order not to exceed the predefined SoC difference. At the same time, the module with the highest SoC (Module 1) is bypassed. Similarly, different modules are bypassed at different times, with Modules 3 and 6, 1 and 5, 5 and 2, and 2 and 4 swapping at 740, 800, 1120 and 1400 s, respectively.

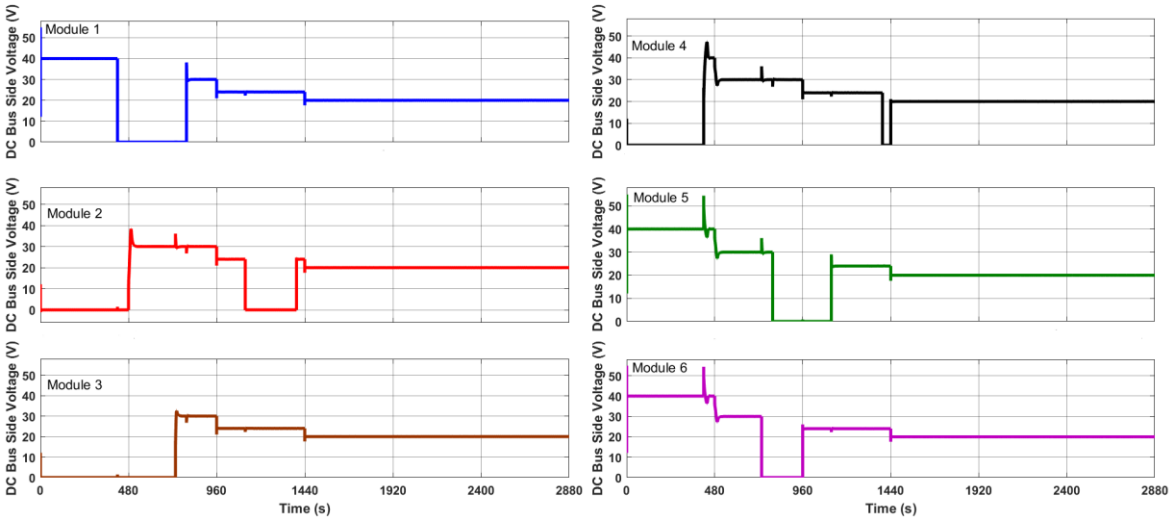
Module 1
Module 2
Module 3
Module 4
Module 5
Module 6
DC Bus Side Voltage (V)
Time (s)

(a)

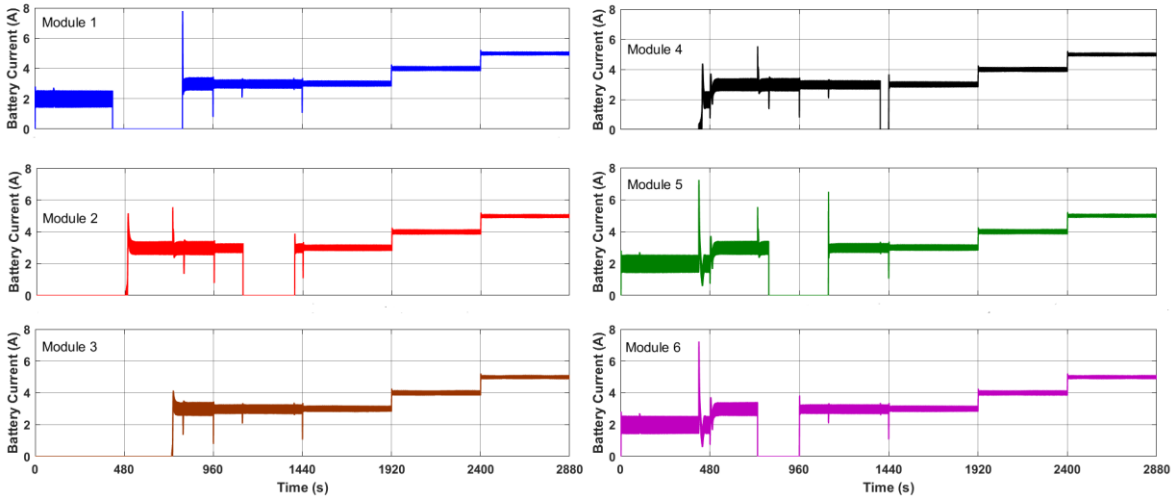
Module 1
Module 2
Module 3
Module 4
Module 5
Module 6
Battery Current (A)
Time (s)

(b)

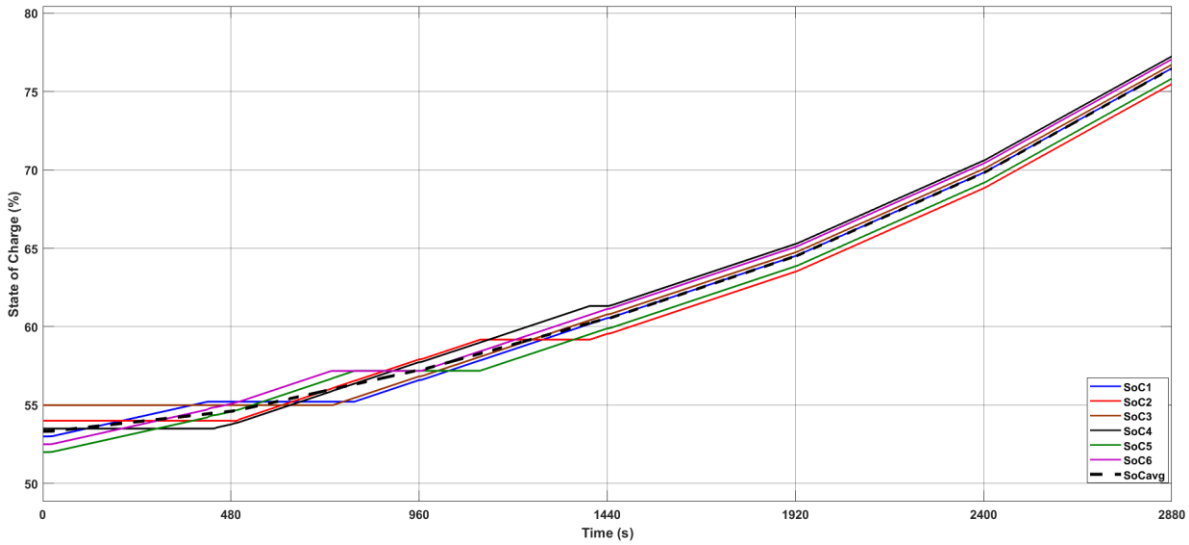
State of Charge (%)
Time (s)
SoC1
SoC2
SoC3
SoC4
SoC5
SoC6
SoCavg

(c)

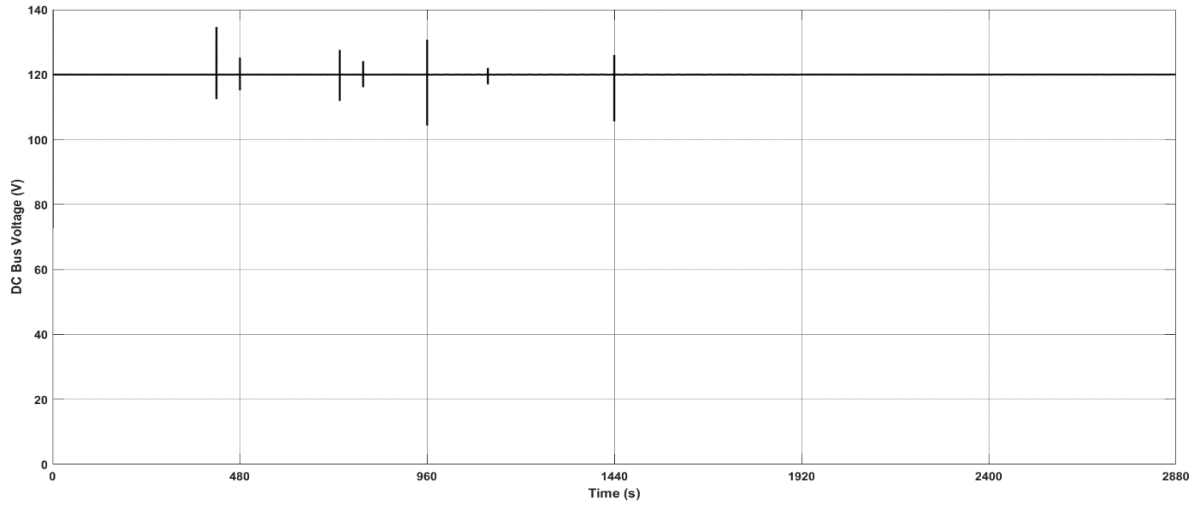

(d)

Figure 4.21: Efficiency-based optimised power sharing controller with variable battery charging current, (a) Modules DC bus side voltages, (b) Battery packs charging currents, (c) SoC of each module, (d) DC bus voltage

Figure 4.22 shows the estimated system efficiencies for the charging case. A limited efficiency improvement of 1.5% is achieved at 10% load using the SoC-based power sharing controller compared to the equal power sharing case. However, up to an 4.8% efficiency improvement can be achieved with the efficiency optimised controller at the same battery power regardless of the cell mismatch level, and any possible efficiency reduction at heavy load is prevented with the proposed power sharing controller. The operational system efficiencies of the SoC-based, efficiency-based, and equal power sharing controllers are shown in Fig. 4.23 for the charging mode. In a similar way to the discharging case, the SoC-based power sharing controller efficiency varies between the SoC-based power sharing curve and equal power sharing curve depending on the mismatch level. However, the optimised power sharing controller has a higher charging efficiency at light load, and the same efficiency as the equal power sharing after the peak efficiency point.

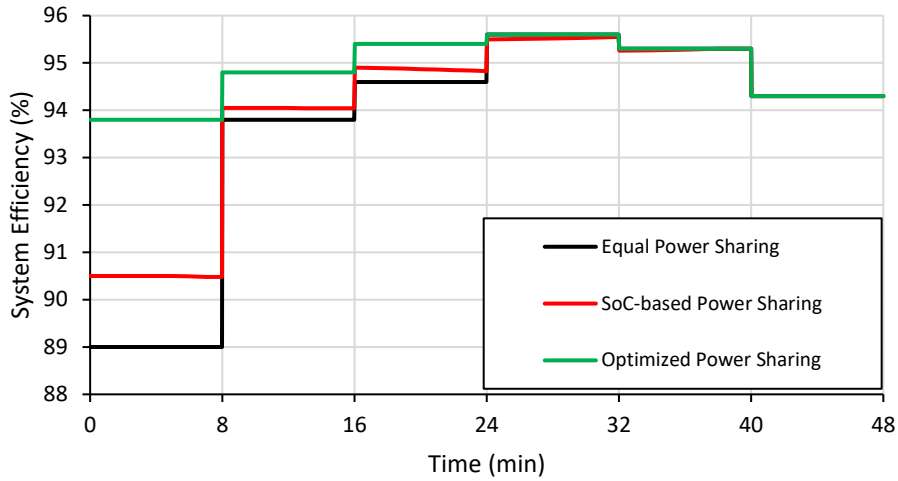

Figure 4.22: Estimated System efficiency for this case study in charging mode

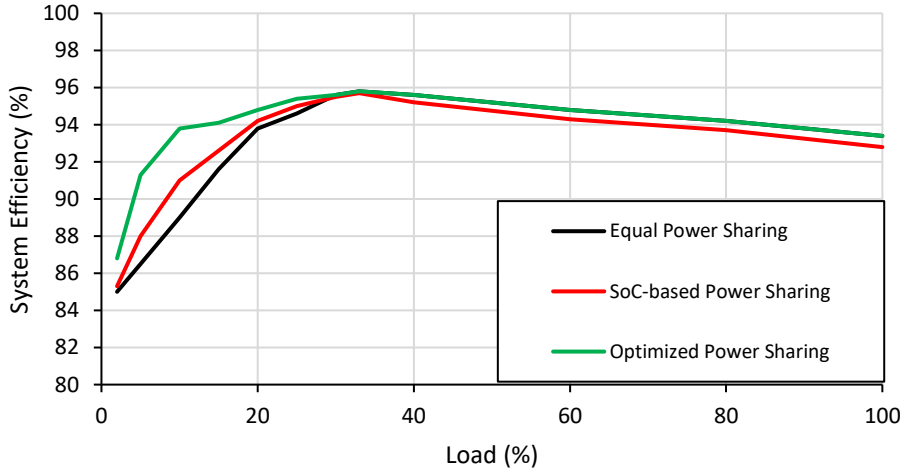

Figure 4.23: Operational system efficiency at full load range in charging mode

4.6 Discussion on Total System Efficiency

The distributed BESSs losses mainly consist of two loss components, which are battery losses and converter losses. Overall loss minimisation is examined in [135] and [136] to decide upon the optimum charging strategy of a Li-ion battery used for EV application. In [135] the converter and battery losses are formulated separately, and two local optimum charging strategies are found for each loss component, i.e., considering only battery efficiency, and considering only charger (converter) efficiency. After determining the dominant loss component, the optimum charging strategy is adapted for the battery charging. The experimental results in [135] show that with two series connected batteries giving a 40 Ah capacity, the overall efficiency is the same as the converter only optimisation results. This is

because the battery resistance is negligible with a low number of series connected cells, and the converter loss will be the dominant loss component.

Similarly, in [136], battery resistance variations with respect to the battery SoC and charging rates are formulated to help determine the optimum charging currents for Li-ion batteries at different SoC levels. The complete charging loss of the system is examined with an on-board charger as shown in Fig. 4.24, for a 34 Ah, 12 kWh lithium NMC battery. The results show that the battery losses dominate the total system loss, so an adaptive charging strategy is applied considering only the battery efficiency, and this has a very low effect on the converter efficiency. Compared to the previous case, the numerous series connected cells affect the battery resistance for the different SoC and charging current values, which in turn affects the power loss.

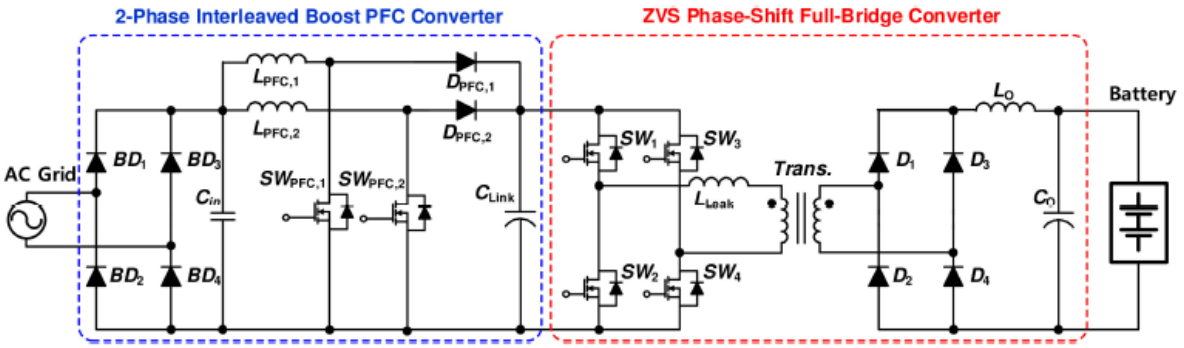

Figure 4.24: The configuration of on-board charger [136]

Compared to the central BESS used in EV applications, where battery pack voltages are several hundred volts, the distributed BESS consists of low voltage battery packs. Therefore, the number of series connected cells and series resistances are very small compared to the battery packs used in the central structure. With these considerations, in this chapter the battery losses are neglected, and the converter efficiency is assumed to be the dominant loss component of the system. Therefore, only converter losses are considered in the proposed efficiency-based optimised power sharing controller.

4.7 Summary and Conclusion

This chapter proposed an efficiency-based optimised power sharing controller which maximises the energy conversion efficiency of the fully distributed BESS without degrading the battery lifespan. Real-time optimum power sharing is undertaken based on a simple look-up table, whose data is generated using an off-line Genetic Algorithm optimisation method considering the converters power loss components. To demonstrate the proposed algorithms effectiveness, a six-module prototype system was simulated using MATLAB / Simulink, with each module consisting of a half-bridge converter and a 10 Ah, 12.8 V, LiFePo4 battery. Simulations were undertaken at different battery power levels in both charging and discharging modes, using the proposed efficiency-based optimised power-sharing and the conventional SoC-based power-sharing methods. The results obtained show that the proposed power-sharing control significantly improves the light load efficiency compared to the conventional and equal power sharing methods. In addition, compared to the SoC-based power sharing controller, where the system efficiency reduces with SoC mismatches after the peak efficiency point, the efficiency reduction disappears due to the equal sharing in the proposed method. Instead of keeping all of the modules SoC at an equal state, this strategy keeps all of the SoC values within a tight tolerance (1%), improving the total system conversion efficiency. In Chapter 6, the proposed efficiency-based optimised power sharing controller is experimentally validated using the same simulation parameters shown in this chapter.

Chapter 5. Partially-Distributed Battery Energy Storage System

5.1 Introduction

The advantages of the distributed BESS were summarised in Chapter 3. However, despite these many advantages, the high cost of the distributed BESS is a significant disadvantage, and any possible cost reduction is desirable. In this chapter, a partially-distributed BESS based on multi-port converters is proposed which reduces the number of components and sensing circuits required compared to the fully distributed system. The structure of this proposed multi-port partially-distributed BESS is introduced, and it is also compared to the fully-distributed BESS, and a BESS based on a central multi-port converter. A power sharing controller with a two-level balancing feature is also proposed which considers the module and pack-level imbalances. Simulation results are also included which validate this method.

In the fully-distributed BESS (Fig. 5.1), the long battery string is modularised. Here, each low voltage battery pack is connected to its corresponding converter, and each converter is connected in series at the DC bus side. As each module consists of an individual battery pack and a DC-DC converter, numerous components and sensing circuits are required in this system, and therefore, the fully-modularised BESS is a relatively expensive system.

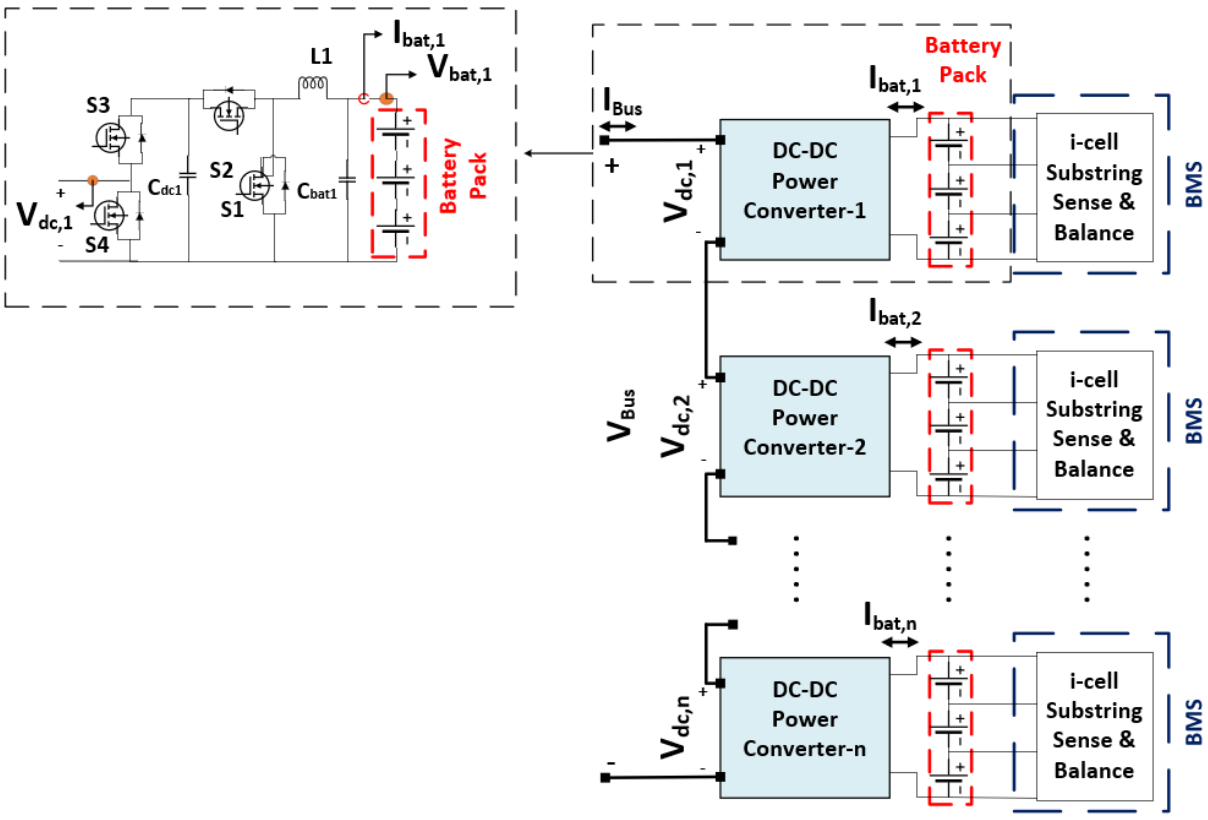

Figure 5.1: Fully-distributed BESS

Recently, BESSs based on the multi-port converter principle have been proposed in [19, 20] and an example is shown in Fig. 5.2. In this structure, a central multi-port converter with enable / disable switches is used to control the charging / discharging powers of the low voltage battery packs. The upper (*Sx*) and lower (*Sx`*) switches for an arbitrary battery pack x operate as a complementary pair. When the upper switch is on and the bottom switch is off, the corresponding battery pack is connected to the system, and vice versa. It is worth mentioning that the same charging / discharging current is applied to all of the battery packs in this structure, and a central high-power converter controls the full BESSs power. However, as the long battery string is modularised, each low voltage battery pack can be connected / disconnected to / from the system via the enable / disable switches. Although, the same charging current for each pack limits the control flexibility of this structure, the bypassing ability adds an additional balancing function amongst the battery modules and this increases the system reliability. In comparison to the fully-distributed BESS, it has a smaller number of components and sensing circuits, which in turn reduces the cost of the system.

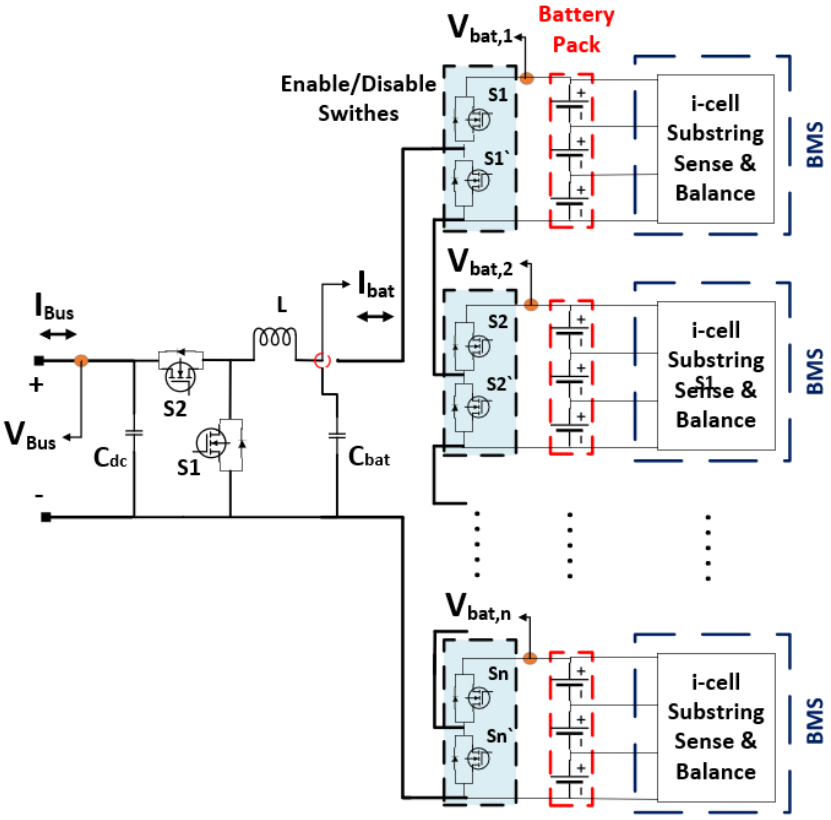

Figure 5.2: BESS based on a central multi-port converter

5.2 The Proposed Partially-Distributed BESS based on a Multi-Port Converter

The proposed partially-distributed BESS is shown in Fig. 5.3. In the partially-distributed BESS, a multi-port converter is used for a group of battery packs, with the converters connected in series at the DC bus side in a similar way to the fully-distributed BESS. The battery packs connected to the same multi-port converter are charged / discharged with the same battery current as in the BESS based on multi-port converter, but different battery modules can be charged / discharged with different currents. For example, looking at Fig. 5.3, 'm' battery packs from battery pack-11 to battery pack-1m within module-1 are charged / discharged with the same battery power, but different charging / discharging currents can be applied to the battery packs from module-1 to module-k, as they are controlled by different multi-port converters.

It is desirable that the battery packs within any module are identical as the same battery charging / discharging current is applied, but the groups of battery packs connected to the different multi-port converters can have different chemistries, capacities, and/or SoH, as the module level power controlling ability can control the charging / discharging currents of these different modules.

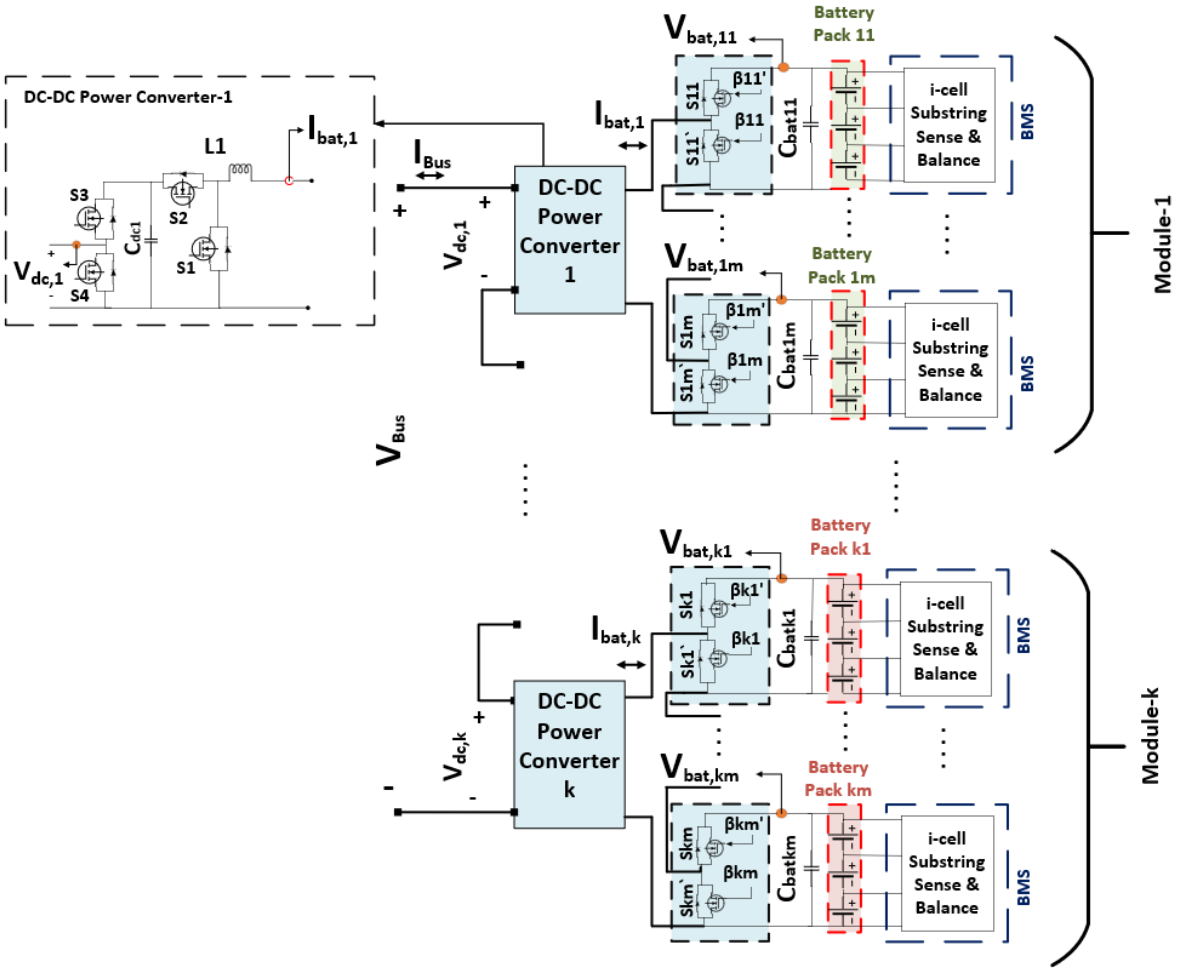

Figure 5.3: Partially-distributed BESS based on a multi-port converter

As shown in Fig. 5.4, for the fully-distributed BESS, `$n$` number of battery packs are used with `$n$` single-port converters ($m = 1$), whilst in the central multi-port converter based BESS, a single multi-port converter with a port number equal to the number of individual battery packs ($m = n$) is used. The proposed partially-distributed BESS is between these two topologies. With a two-port converter, the number of converters needed will be the half that used in the fully-distributed BESS, and with the increase in the number of converter ports, the required number of converters reduces even further.

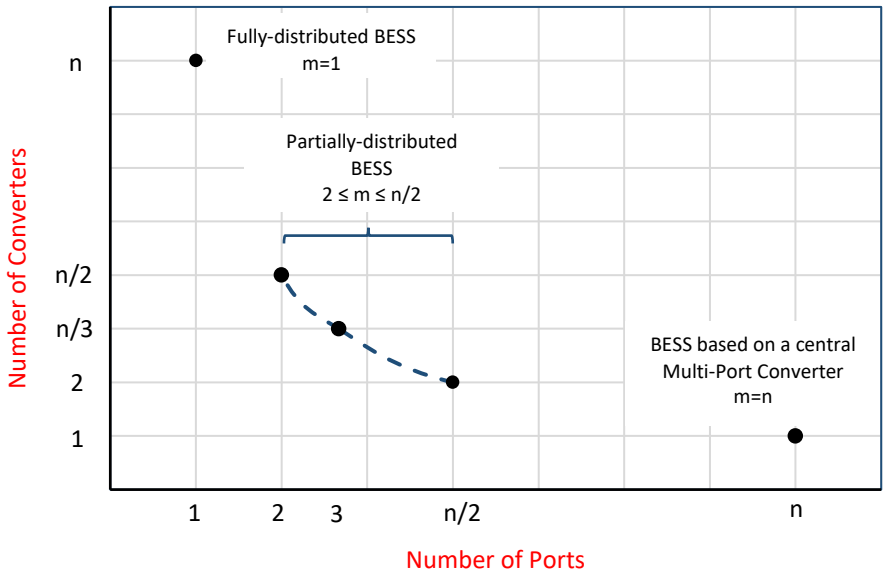

Figure 5.4: The number of converters with respect to the number of ports (k=n/m)

5.3 Comparison of Structures

In this section, the proposed partially-distributed BESS is compared to the previous published methods, looking at the number of components and their ratings, the reliability, efficiency, and the degree of freedom for power sharing. The number of switches and passive components varies depending on the converter type and bypass arrangement used for each module, and in the following analysis, the bi-directional half bridge Buck-Boost converter is assumed for all of the structures. The bypassing for the fully-distributed, central multi-port converter, and partially-distributed BESSs is based around two series complementary switches, and their circuit diagrams are shown in Figs. 5.1, 5.2, and 5.3, respectively.

It is worth noting that in the central multi-port converter based BESS, a single battery side capacitor (C_{bat}) is used, and bypassing / enabling of the battery modules results in a voltage drop / increased voltage across the capacitor, which may cause high current flows during this event. Therefore, inrush current limiting methods may also be required for that structure. To

avoid this problem in the proposed partially-distributed BESS, the battery side capacitors are modularised and placed close to their corresponding battery packs as shown in Fig. 5.3.

5.3.1 The Number of Components and Ratings

The following analysis gives a brief summary of the number of circuit components used in each structure, including the number of switches and passive components, their ratings, and the voltage and current sensing circuits. The number of switches used in the fully-distributed BESS is `$4n$` for `$n$` battery packs. The DC bus voltage is the sum of the individual module voltages, and each module should also operate at higher voltage value than the equal sharing case to allow the balancing function to be performed. Additional modules are usually included in systems for redundancy purposes, but for simplicity they are ignored in this analysis. Due to this simplification, the minimum voltage ratings of the switches in the fully-distributed BESS (including additional voltage to perform balancing (V_{bal})) is ($V_{Bus}/n + V_{bal}$). The converter switches must also withstand the maximum charging / discharging currents of the battery packs ($I_{bat,max}$). As the DC bus current flows through the bypass switches in the fully-distributed BESS, the current rating of the bypass arrangement switches is (P_{max}/V_{Bus}).

In the central multi-port converter based BESS, there are `$2n$` bypass switches for `$n$` battery packs, and `2` switches for the central multi-port converter. While the voltage rating of the bypass switches is equal to the battery pack voltage, the bus side converter switches` voltage ratings are equal to the DC bus voltage (V_{Bus}).

Similarly, there are `$2n$` bypass switches for `$n$` battery packs in the proposed partially-distributed BESS, and each multi-port converter has `4` switches, therefore, `$4n/m$` converter switches are used for `$n/m$` multi-port converters. In total, $2n + 4n/m$ switches are used. The voltage ratings of the enable / disable switches are equal to the battery pack voltages, and the converter switches must handle the maximum voltage of the corresponding converter ($V_{bus} \times m/n + V_{bal}$).

In the fully-distributed BESS, `$2n$` capacitors and `$n$` inductors are used for `$n$` battery packs. The battery side capacitors` voltage rating is equal to the battery voltage ($V_{bat}$), and the DC bus side capacitors` voltage rating is ($V_{bus}/n + V_{bal}$).

The central multi-port converter based BESS uses only `2` capacitors and `1` inductor. The capacitor voltage rating is equal to the total battery voltage ($V_{bat,tot}$), and the DC bus side capacitors` are rated at the DC bus voltage (V_{bus}).

In the proposed partially-distributed BESS, for the `$n/m$` multi-port converters, `$n$` capacitors (rated at the battery voltage) are used for `$n$` battery packs, and `$n/m$` capacitors rated at ($V_{bus} \times m/n + V_{bal}$) are used at the DC bus side. The inductor must withstand the maximum charging / discharging current of the battery in each structure, which is ($I_{bat,max}$).

The inductance and capacitance values are calculated using (5.1) and (5.2), respectively. From these equations, the capacitance (C) and inductance (L) values depend on the switching frequency (f_s), and the allowable voltage and current ripples (ΔV and Δi). The lower voltage ratings of the fully-distributed BESS also enable operation at higher switching frequencies, which reduces the value and size of the passive components. In contrast, the higher voltage ratings increase the size of the passive components used in the central multi-port converter based BESS. Although a higher switching frequency may reduce the size of the passive components, the converter efficiency reduces with the increase in switching frequency), and especially with increased voltage ratings, as the voltage current overlapping loss during a switching transition directly proportional to the switching frequency and voltage. This may require advanced heatsinks which in turn increases the cost of the system. In the proposed-partially distributed BESS, the voltage ratings of the individual modules depend on the number of ports, and the size of the passive components increases with the increase of number of ports.

$$L = \frac{V_L \times d}{\Delta i \times f_s} \tag{5.1}$$

$$C = \frac{i_c \times d}{\Delta V \times f_s} \tag{5.2}$$

where d is the duty ratio, and V_L and i_c represent the voltage across the inductance and the capacitor current, respectively.

In the fully-distributed BESS, `$n$` current sensing circuits are used to sense the battery currents, and `$2n$` voltage sensing circuits are required to sense the DC bus and battery side voltages for the `$n$` battery packs. In the central multi-port converter BESS only a single current sensing circuit and `$n + 1$` voltage sensing circuits are required. The required number of current sensing circuits in the partially-distributed BESS is equal to the number of multi-port converters, `$k$` which is `$n/m$`, and to sense the `$n$` battery pack and `$n/m$` DC bus side voltages, `$n + n/m$` voltage sensing circuits are used. Table 5.1 summarises the components and their ratings for these three topologies.

Table 5.1 The components and ratings for three topologies

	PARAMETERS	Fully Distributed BESS	Central Multi-Port Converter based BESS	Partially Distributed BESS
Battery Parameters	Battery Voltage (V)	V	V	V
	Battery Capacity (Ah)	C	C	C
	Battery Energy (Wh)	VC	VC	VC
	Number of Battery	n	n	n
	Total Battery Energy (Wh)	nVC	nVC	nVC
Converter Parameters	Number of Converters	n	1	n/m
	Number of Switches	$4n$	$2\ (n+1)$	$2n\ (1+2/m)$
	Voltage Ratings of Battery Side Switches (V)	$-$	V_{bat}	V_{bat}
	Voltage Ratings of Converter Switches (V)	$V_{Bus}/n+\ V_{bal}$	V_{Bus}	$V_{Bus}*m/n+\ V_{bal}$
	Current Rating of Converter Switches (A)	$I_{bat,max}$	$I_{bat,max}$	$I_{bat,max}$
	Current Rating of Enable/Disable Switches (A)	$-$	$I_{bat,max}$	$I_{bat,max}$
	Current Rating of Module Bypass Switches (A)	P_{max}/V_{Bus}	$-$	P_{max}/V_{Bus}
	Number of Inductor	n	1	n/m
	Current Rating of Inductor (A)	$I_{bat,max}$	$I_{bat,max}$	$I_{bat,max}$
	Number of Capacitor	$2n$	2	$n+n/m$
	Voltage Rating of Battery Side Capacitor (V)	V_{bat}	$V_{bat,tot}$	V_{bat}
	Voltage Rating of DC Bus Side Capacitor (V)	$V_{Bus}/n+\ V_{bal}$	V_{Bus}	$V_{Bus}*m/n+\ V_{bal}$
	Number of Current Sensing Circuitry	n	1	n/m
	Number of Voltage Sensing Circuitry	$2n$	$n+1$	$n+n/m$

5.3.2 Reliability

The ability to perform the desired functions for a specific period of time is known as the reliability of a component or a system [137]. The reliability of a BESS is an important issue, and the reliability of each structure with different number of battery packs will be estimated using reliability block diagrams. The reliability of the submodules in the reliability block

diagrams will be calculated using the assumed failure rates of the components, and the failure rate and reliabilities for a component or system can be calculated using (5.3), and (5.4), respectively [137].

$$\lambda = \sum_{i=1}^{n} N_i \times \lambda_{g,i} \times \pi_{Q,i} \tag{5.3}$$

$$R_{(t)} = e^{-\lambda \times t} \tag{5.4}$$

where λ_g and π_Q are the generic failure rate and quality factor, respectively, and N is the quantity of the component. R represents the reliability of a component or a system.

For this analysis, the same failure rates presented in [137] are used for the following calculations, and the failure rate of each component per hour is shown in Table 5.2. The reliability of the battery, bidirectional DC-DC converter, and bypass arrangement were calculated using (5.4) for 50000 hours with the assumption of unity quality factor. The estimated reliability of the corresponding systems are also shown in Table 5.2.

Table 5.2 The failure rate and reliability of each component

Components	**Failure Rate (failures/hour)**	**Reliability (p.u.)**
MOSFET	1.1×10^{-9}	
Diode	7.5×10^{-9}	
Inductor	2.0×10^{-10}	
Capacitor	2.5×10^{-9}	
Battery	1.0×10^{-5}	0.6065
Bi-directional Buck-Boost Converter	1.99×10^{-8}	0.9990
Bypass Arrangement	1.72×10^{-8}	0.9991

After the individual component and submodule reliabilities are found, reliability block diagrams and equations (5.5) and (5.6) are used to estimate the series and parallel subsystems connections, respectively [137, 138]. To evaluate the reliabilities, the reliability block diagrams of each structure are generated and shown in Fig. 5.5, where R_{Bat}, R_{BDCC}, and R_{BP} are the reliabilities of the battery, bi-directional DC-DC converter, and bypass arrangements, respectively.

$$R_{series} = \prod_{i=1}^{n} R_i \tag{5.5}$$

$$R_{parallel} = 1 - \prod_{i=1}^{n} (1 - R_i) \tag{5.6}$$

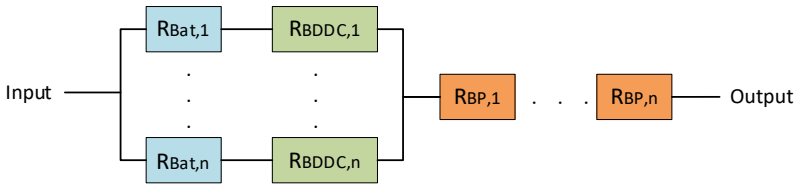

(a)

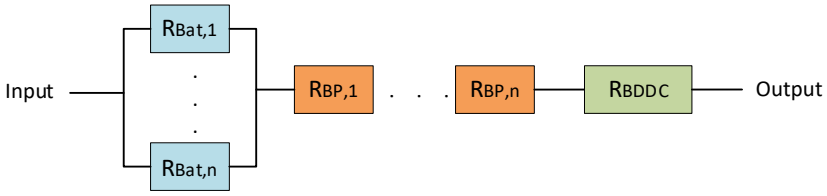

(b)

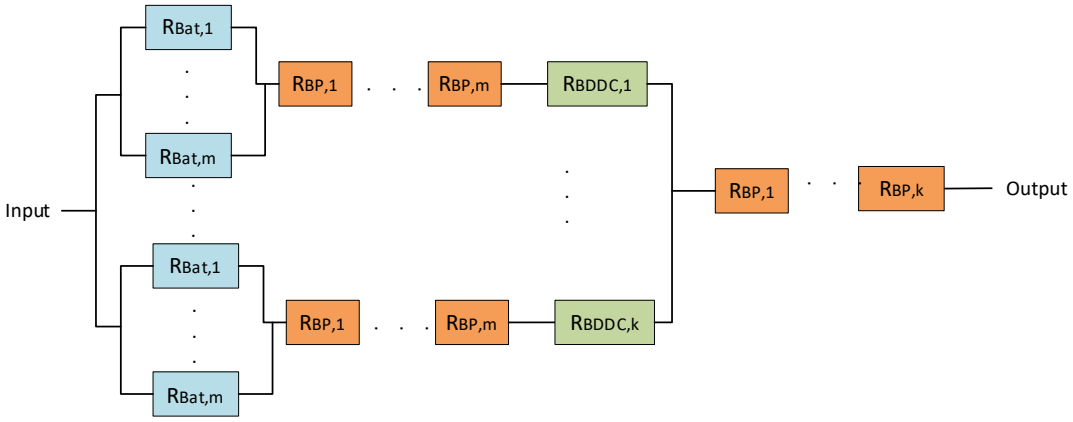

(c)

Figure 5.5: The Reliability Block Diagrams, (a) Fully-distributed BESS, (b) Central multi-port converter based BESS, (c) Partially-distributed BESS (k=n/m)

Fundamentally, increasing the number of series connected modules reduces the system reliability, as any fault in any of the subcomponents in the series structure results in loss of the complete system. Conversely, parallel components or submodules can compensate for the faults of other parallel connected components or submodules, hence increasing the number of parallel components or systems increases the system reliability.

In each structure, the battery packs are independently connected to the system, i.e., during any undesired operating conditions the battery can be bypassed by controlling the bypass arrangement switches. Therefore, the battery packs are connected in parallel and the associated bypass arrangements are connected in series in the reliability block diagrams. Compared to the fully-distributed and partially-distributed BESSs, the central multi-port converter based BESS relies on a single converter which makes the reliability of the central converter vital. The reliability functions of the fully-distributed BESS, central multi-port converter based BESS, and partially-distributed BESS for `n` battery packs are derived using (5.5) and (5.6), and are shown in (5.7), (5.8) and (5.9), respectively.

$$R_{FDB} = (1 - (1 - R_{Bat} \times R_{BDCC})^n) \times R_{BP}^n \tag{5.7}$$

$$R_{CMB} = (1 - (1 - R_{Bat})^n) \times R_{BP}^n \times R_{BDCC} \tag{5.8}$$

$$R_{PDB} = \left(1 - (1 - R_{BP}^m \times R_{BDCC} \times \ (1 - (1 - R_{Bat})^m)\ )^{n/m}\right) \times R_{BP}^{n/m} \tag{5.9}$$

where R_{FDB} , R_{CMB} ,and R_{PDB} represent the reliability of fully-distributed BESS, central multi-port converter based BESS, and partially-distributed BESS, respectively.

The reliabilities of each structure with different numbers of battery packs, and different numbers of converter ports for the partially-distributed BESS, are presented in the Table 5.3. Figure 5.6 shows the reliability of each structure with different numbers of battery packs. The term $1 - R_{bat}$ represents the battery reliability. When the number of battery packs increases, the reliability of battery increases due to the parallel connections, and the system reliability reaches its peak value with 8 modules for the fully-distributed BESS and central multi-port converter based BESS. However, the increased number of modules increases the number of series connected bypass arrangements, and this reduces the system reliability even though the battery reliability increases. With a low number of battery packs the bypass arrangement's reliability is high, but the battery reliability is low. On the other hand, as the number of series bypass arrangement circuits ($R_{BP}^{n/m}$) is less in the proposed partially-distributed BESS, a better reliability is achieved for a higher number of modules with this method. The reliability of the partially-distributed BESS is calculated with 2-port, 4-port, and 8-port converters. The results (Fig. 5.4) shows that the reliability of the partially-distributed BESS with a 2-port multi-port converter reduces earlier and with a sharper curve than that of the 4-port and 8-port counterparts. Therefore, higher reliability is achieved with a higher number of ports for a high number of battery packs thanks to the reduced dependence on the bypass arrangement circuits.

Table 5.3 The reliability of each structure with different number of battery packs

Number of Battery Pack (n)	Reliability				
	Fully-Distributed BESS	Central multi-port converter based BESS	Partially-distributed BESS		
			m=2	m=4	m=8
4	0.9724	0.9715	0.9735		
8	0.9922	0.9913	0.9958	0.9974	
16	0.9857	0.9847	0.9928	0.9964	0.9906
32	0.9716	0.9706	0.9857	0.9928	0.9963
64	0.9440	0.9431	0.9716	0.9857	0.9928
128	0.8911	0.8903	0.9440	0.9716	0.9857

.

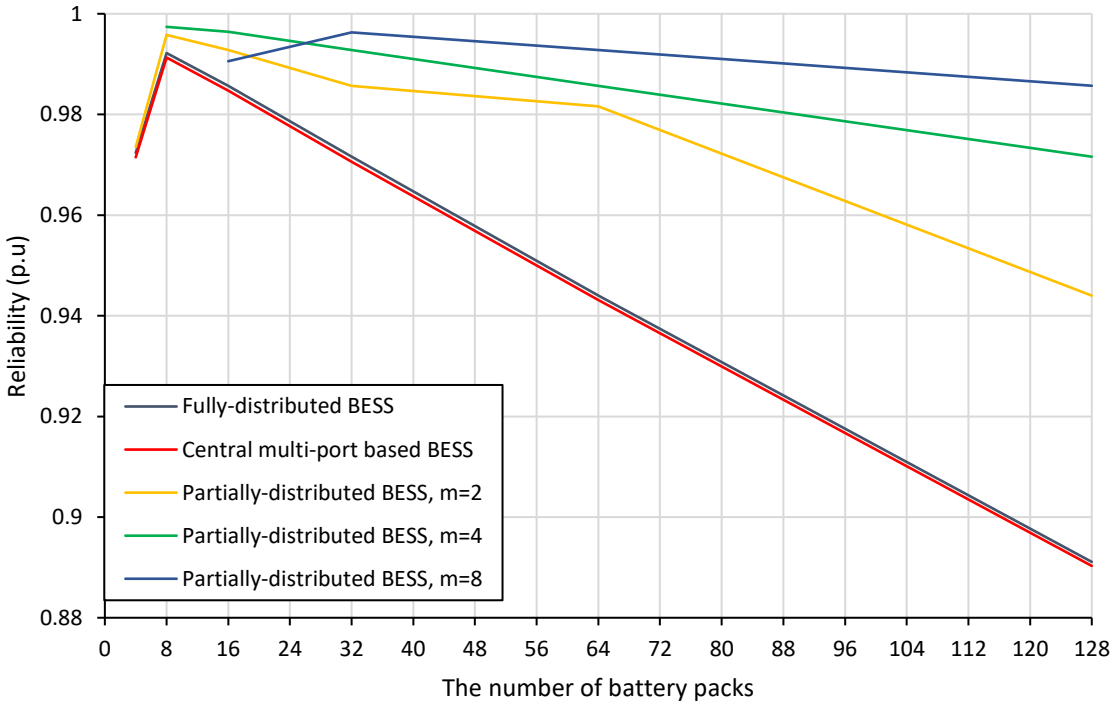

Figure 5.6: The reliability of each structure with different number of battery packs

5.3.3 Efficiency

A comparison of the efficiency of each structure is a challenging task, as the efficiency depends on many factors including the power converter topologies, switching techniques, the individual components used in each structure, the number of modules, the power sharing ratios, and the

system structure. In the following analysis the efficiency block diagrams for each structure are generated, and a brief discussion on the system connection types and number of modules is analysed. The efficiency block diagrams for each case are shown in Fig. 5.7. Typically, the efficiency of the system is the multiplication of each cascaded connected submodules efficiency.

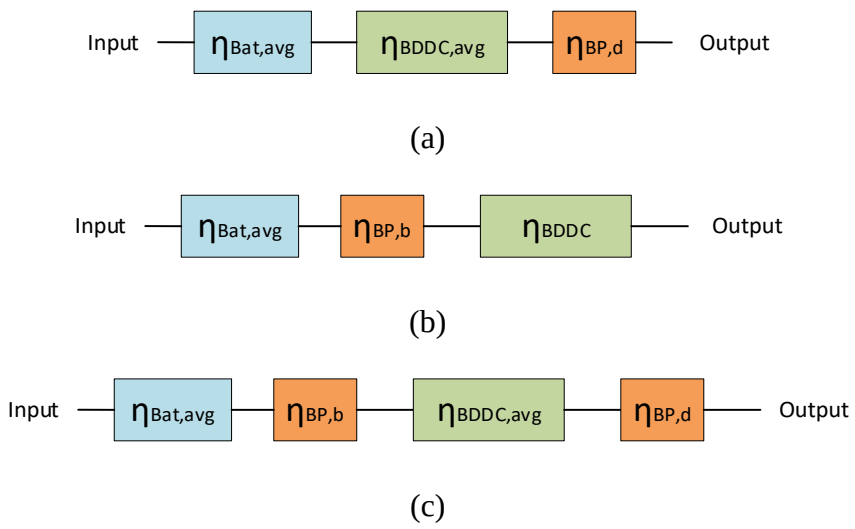

Figure 5.7: The Efficiency Block Diagrams, (a) Fully-distributed BESS, (b) Central multi-port converter based BESS, (c) Partially-distributed BESS

Assuming that the total battery voltage and current is the same for each structure, the desired battery voltage and power can be achieved with different numbers of modules (`n`). Either a higher number of low voltage battery packs or a smaller number of high voltage battery packs can be used. Although, the battery packs voltage reduces with an increased number of modules, the total number of series connected cells in the system is the same for the desired total battery pack voltage. Therefore, it can be assumed that the number of battery packs (`n`) has no effect on the battery efficiency in each structure when the resistance between each connection wires are ignored.

The efficiency of the fully-distributed BESS (η_{FDB}) can be calculated using (5.10). In the fully-distributed BESS, `n` bidirectional DC-DC converters are used for `n` battery packs, and the average converter efficiency ($\eta_{BDDC,avg}$), and average battery efficiency ($\eta_{Bat,avg}$) for each can be used in the block diagram. When the number of battery packs increases, the number of converters and bypass circuits in the fully-distributed BESS also increase. The total battery power is divided into more converters, and the average conversion efficiency can be used to estimate the conversion efficiency. The average conversion efficiency of bidirectional DC-DC converters can be estimated using (3.12) as discussed in Chapter 3. On the other hand, the

increased number of modules increases the number of bypass arrange configurations. This means the same current flows through more bypass arrangement circuits increasing their total conduction loss. The position of the bypass arrangement circuits also affects the power loss.

When the total battery voltage is boosted, the DC bus side current will be lower, and the connection of the bypass circuits at the DC bus side reduces the system conversion loss because of the lower current, and vice versa. Ideally, ultra-low series resistance (R_{ds}) switches should be used to reduce the total bypass arrangement loss. In the fully-distributed BESS the bypass circuits are placed at the DC bus side, and the efficiency ($\eta_{BP,d}$) can be calculated using (5.11). This equation depends on the number of modules, and an increased number of modules reduces the bypass switches efficiency.

$$\eta_{FDB} = \eta_{Bat,avg} \times \eta_{BDDC,avg} \times \eta_{BP,d} \tag{5.10}$$

$$\eta_{BP,d} = \frac{V_{Bus} - I_{bus} \times R_{ds} \times n}{V_{Bus}} \tag{5.11}$$

where $\eta_{BP,d}$ represents the efficiency of bypass circuits located at the DC bus side of converter.

A single converter is used in the central multi-port converter based BESS (η_{CMB}), and its efficiency can be calculated using (5.12) by multiplying the average battery efficiency, bypass arrangement circuit efficiency, and the single converter efficiency. In this case the bypassing circuit is placed at the battery side, and its efficiency (5.13) depends on the number of battery packs.

$$\eta_{CMB} = \eta_{Bat,avg} \times \eta_{BDDC} \times \eta_{BP,b} \tag{5.12}$$

$$\eta_{BP,b} = \frac{V_{bat,tot} - I_{bat} \times R_{ds} \times n}{V_{bat,tot}} \tag{5.13}$$

Where η_{BDDC} represents the DC-DC converter efficiency, and $\eta_{BP,b}$ represents the efficiency of bypass circuits located at the battery side of converter.

The efficiency of the partially-distributed BESS (η_{PDB}) can be calculated using (5.14) by multiplying each series connected subsystems` efficiency. In a similar way to the fully-distributed BESS, the average converters efficiency is calculated using (3.12). In this structure, the bypassing circuits are placed at both the battery and DC bus sides. The inclusion of more bypass circuits increases the total bypass arrangement loss in the partially-distributed BESS

which can be estimated using (5.15). It is the sum of the `$n$` bypass losses for the `$n$` battery packs, and the `$k$` bypass losses used for the `$k$` modules .

$$\eta_{PDB} = \eta_{Bat,avg} \times \eta_{BP,b} \times \eta_{BDDC,avg} \times \eta_{BP,d} \tag{5.14}$$

$$\eta_{BP,b} + \eta_{BP,d} = \frac{V_{bat,tot} - I_{bat} \times R_{ds} \times n}{V_{bat,tot}} + \frac{V_{Bus} - I_{Bus} \times R_{ds} \times k}{V_{Bus}} \tag{5.15}$$

5.3.4 Power Sharing Flexibility

In this section the degree of freedom for power sharing amongst the different battery packs for each structure is evaluated and compared. The independent connection of the battery packs in the fully-distributed BESS enables individual battery power control, and this has several advantages including adding additional balancing functions, lightening the load on the battery balancing circuits, utilising different chemistry and SoH batteries, and even balancing the battery SoH.

In the central multi-port converter based BESS, all of the battery packs are charged / discharged with the same battery power when the enable / disable switches are fully on / off. Any mismatch amongst the battery packs can be corrected using the bypassing ability. Although the bypassing can be utilised to correct any imbalance among the battery packs, the same battery charging / discharging current limits its control flexibility. For example, the battery packs used in the structure should ideally be the same chemistry, as different chemistry battery packs may require different charging / discharging currents and voltage limits. It may also be challenging to control pre-used and different SoH battery packs with this structure, as high imbalance is expected among different SoH packs. Managing different SoH batteries with this structure will cause frequent module bypassing, resulting in a system voltage and capacity drop, which may in turn require overdesign of the system to compensate for these reductions. Therefore, the central multi-port converter based BESS can be suitable for the battery packs where high imbalance is not expected, and any imbalance amongst different battery packs can be corrected with the bypassing ability.

In the proposed partially-distributed BESS, each battery pack being controlled by the same converter is charged / discharged with the same battery power. Therefore, it is desirable that the battery packs in the same module have a similar chemistry and SoH. This is the same as for the central multi-port converter based BESS, however, the charging / discharging currents

of the battery packs within the different modules can now be controlled. Therefore, the characteristic of the partially-distributed BESS is similar to the fully-distributed BESS in the module level, and battery packs with different chemistry, capacity, and SoH can be used for the module level.

The comparison of each structure is summarised in table 5.4. The fully-distributed BESS has the highest degree of freedom for power sharing, however, it is also the most expensive structure, as it requires numerous components and sensing circuits. The central multi-port converter based BESS is the cheapest structure, but its power sharing ability is limited, whilst the fully-distributed and central multi-port converter based BESSs have good reliability thanks to their bypassing capabilities. Typically, the partially-distributed BESS requires fewer components than the fully-distributed BESS, and is therefore cheaper. It also has a higher degree of freedom for power sharing compared to the central multi-port based BESS, and it shows better reliability that the other methods, especially for a high number of modules. It is worth mentioning that the cost, reliability, efficiency, and the power sharing capability vary in the proposed partially-distributed BESS depending on the port number for each multi-port converter. An increased number of ports reduces the system cost, but it also reduces the power sharing capability for the same number of battery packs.

Table 5.4 The comparison of each structure

PARAMETERS	Fully-distributed BESS	Central Multi-Port converter based BESS	Partially-distributed BESS
Cost	Very Expensive	Moderate	Expensive
Reliability	Good	Good	Very Good
Efficiency	Good	Good	Good
The degree of freedom for power sharing	Very Good	Poor	Moderate

5.4 Proposed Power Sharing Controller for Partially-Distributed BESS in Discharging Mode

The aim of the proposed power sharing controller is to achieve simultaneous SoC balancing and DC bus voltage regulation, and for the partially-distributed BESS, a two-level balancing feature is proposed considering the module and pack-level imbalances. The SoC imbalance amongst the different modules is corrected based on the charging / discharging powers determined by the power sharing controller. The pack-level balancing amongst any battery

packs controlled by the same multi-port converter is achieved by bypassing. In the proposed power sharing controller, the module-level and pack-level balancing are decoupled. Figure 5.8 shows the proposed power sharing controller in discharging mode which consists of two closed loop controllers. The outer SoC balancing loop compares an individual module`s average SoC to the system`s average SoC, and determines the individual module`s reference DC bus side voltage ($V_{dc,refx}$) by adding a correction value (α_{Vx}). The inner voltage control loop regulates the individual modules DC bus side voltages. To ensure the DC bus voltage is always maintained at the desired level, the sum of the correction values (M_V) is extracted from each module.

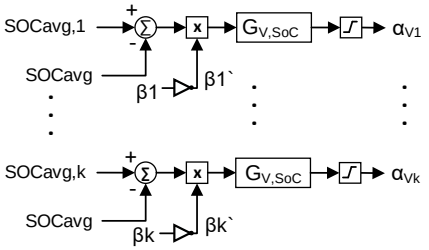

(a)

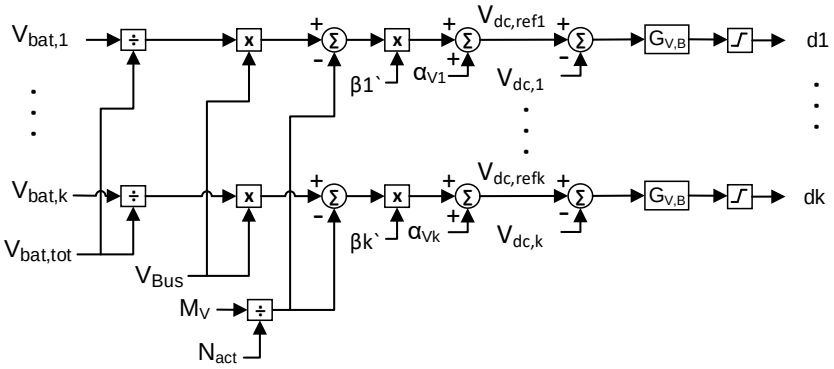

(b)

Figure 5.8: The power sharing controller block diagrams in discharging mode, (a) SoC balancing controller (b) Modules DC bus side voltage control loop

As the module-level and pack-level balancing control is decoupled, the bypassed packs are not taken into account in the power sharing controller. Therefore, in the proposed power sharing controller, the module-level power sharing is realized based on the average SoC of each module. For an arbitrary xth module, the average SoC can be calculated as follow:

$$SoC_{avg,x} = \frac{1}{N_{act,x}} \times \sum_{y=1}^{m} SoC_{xy} \times \beta_{xy}^{`} \tag{5.16}$$

$$SoC_{avg} = \frac{1}{N_{act}} \times \sum_{x=1}^{k} SoC_{avg,x} \times \beta_x^{`} \tag{5.17}$$

where $SoC_{avg,x}$ and SoC_{avg} are the average SoC of x^{th} module, and the system average SoC respectively. $N_{act,x}$ and N_{act} represent the number of total active battery packs within the x^{th} module, and the number of active modules, respectively. SoC_{xy} represents the SoC of a y^{th} battery pack within the module x^{th}. $\beta_x^{`}$ and $\beta_{xy}^{`}$ are the complementary bypass commands for the x^{th} module, and the y^{th} battery pack within the x^{th} module , respectively.

The desired DC bus voltage of the x^{th} module is calculated as follow:

$$V_{dc,refx} = \sum_{x=1}^{k} \left[\left(\frac{V_{bat,x}}{V_{bat,tot}} \times V_{Bus} - \frac{M_V}{N_{act}} \right) \times \beta_x^{`} + \alpha_{Vx} \right]$$	(5.18)
$$M_V = \sum_{x=1}^{k} \alpha_{Vx}$$	(5.19)

The reference DC bus voltage of arbitrary module *'x'* is directly proportional to the ratio of the modules` battery voltage ( $V_{bat,x}$) to the total battery voltage of the system ($V_{bat,tot}$). As any bypassed pack(s) affect the modules` voltage, capacity, and average SoC, the proposed controller readjusts the individual module`s power accordingly to maintain SoC balancing during bypassing and after reactivation. The total battery voltage of arbitrary module *'x'* can be calculated using (5.20)

$$V_{bat,x} = \sum_{y=1}^{m} V_{bat,xy} \times \beta_{xy}^{`} \tag{5.20}$$

where $V_{bat,xy}$ is the voltage of the y^{th} battery pack within the x^{th} module.

The total system battery voltage is the sum of all of the active battery modules voltages, and can be calculated as follows:

$$V_{bat,tot} = \sum_{x=1}^{k} V_{bat,x} \times \beta_x^{`} \tag{5.21}$$

Although the expected mismatch level amongst battery packs within the same module is low as they ideally have same chemistry, capacity, and SoH, the different aging mechanisms due to the same charging / discharging current may increase the mismatch level during operation. Therefore, the battery pack bypassing ability of the multi-port converter is utilised to address

the SoC imbalance amongst the battery packs within the same module. The pack-level balancing algorithm in discharging mode is shown in Fig. 5.9. The balancing algorithm sorts all of the battery packs SoC, and the mismatch level between the highest and lowest SoC battery packs is identified. If the mismatch level is above a predefined threshold value, the battery pack having the lowest SoC value is bypassed in discharging mode. The threshold value depends on the designers preferences, and a smaller value can be used with an associated increased bypassing frequency. The number of simultaneous bypassed packs can also be limited in the pack-level SoC balancing algorithm, considering the capacity and voltage reduction caused by the bypassed battery packs. In this design, a single battery pack is bypassed for a specific period of time to limit the capacity and voltage drop. The balancing time is very fast using the bypassing method, and this time depends on the initial SoC mismatch (ΔSoC_0), capacity of the battery packs, and the battery charge / discharge currents, which can be understood from (5.22), where the battery current is positive in discharging case.

$$\Delta SoC_t = \Delta SoC_0 - \frac{1}{3600 \times C} \int_0^t I_{bat.(t)} \times dt \tag{5.22}$$

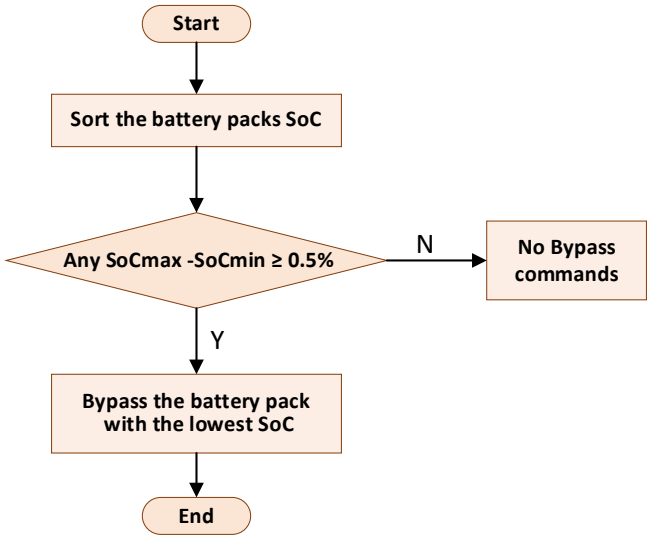

Figure 5.9: The SoC balancing algorithm for the battery packs within the same module in discharging mode

5.5 Proposed Power Sharing Controller for Partially-Distributed BESS in Charging Mode

Figure 5.10 shows the proposed power sharing controller for the partially-distributed BESS in charging mode. The power sharing controller can be realised by applying a voltage equal to the bus voltage (V_{Bus}) at the bus side. The outer SoC balancing loop determines the individual modules power differences by comparing each modules average SoC to the systems average. In a similar method to the discharging mode, the reference DC bus voltage of each module is directly proportional to the ratio of the modules` battery voltage to the total battery voltage of the system. The total bus voltage shared amongst the modules is directly proportional to the module`s battery voltages, and the sum of the voltage correction values (M_v) is added to each module to maintain the DC bus voltage at the desired level. The DC bus side voltage of an arbitrary module 'x' can be computed using (5.23). Unlike the discharging case, in charging mode, the correction value is extracted from the reference DC bus side voltages of each module to balance the SoC of each module. In addition, to ensure the charging current of each module is well-regulated, an additional current loop is included in the system in a similar way to that proposed by Huang in [13].

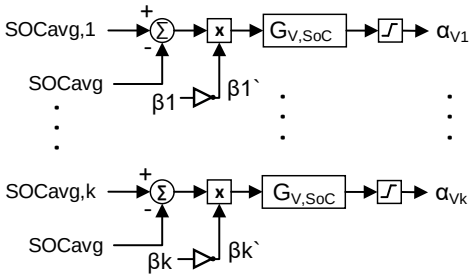

(a)

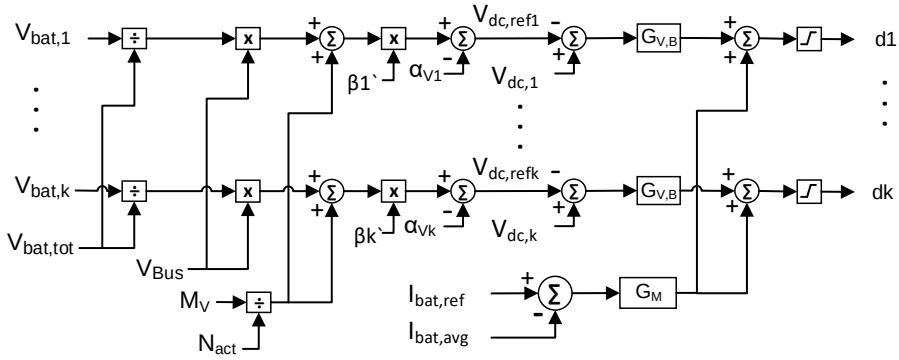

(b)

Figure 5.10: The power sharing controller block diagrams in charging mode, (a) SoC balancing controller, (b) Modules DC bus side voltage and average charging current control loop

$$V_{dc,refx} = \sum_{x=1}^{k} \left[\left(\frac{V_{bat,x}}{V_{bat,tot}} \times V_{Bus} + \frac{M_V}{N_{act}} \right) \times \beta_x^{`} - \alpha_{Vx} \right] \tag{5.23}$$

$$I_{bat,avg} = \frac{1}{N_{act}} \times \sum_{x=1}^{k} I_{bat,x} \tag{5.24}$$

where $I_{bat,avg}$ and $I_{bat,x}$ are the average battery currents of the system and x^{th} module, respectively.

The pack-level balancing algorithm for the charging mode is shown in Fig. 5.11. Unlike the discharging case, in charging mode, the highest SoC battery pack is bypassed when the threshold value is reached.

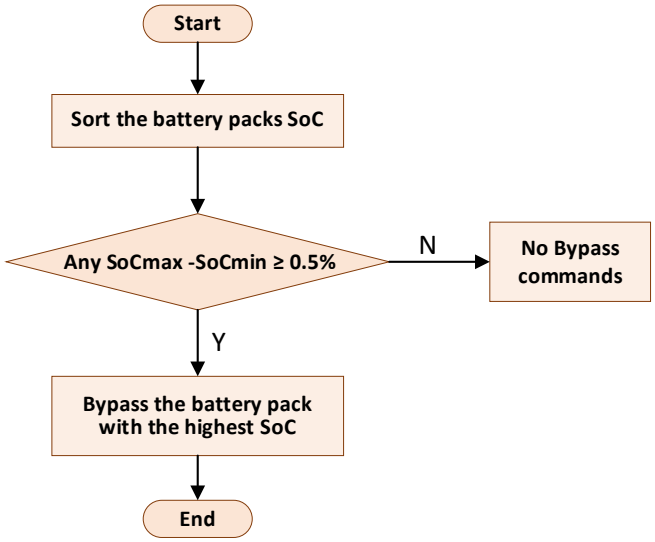

Figure 5.11: The SoC balancing algorithm for the battery packs within the same module in charging mode

5.6 Simulation Results

The proposed power sharing controller for the partially-distributed BESS was simulated using MATLAB/Simulink. The simulation parameters of the system are shown in Table 5.5. Six battery packs are controlled with three dual-port DC-DC converters, and each module consists of 2-battery packs and a dual-port bidirectional half bridge Buck-Boost converter. Li-ion batteries are used in the simulation, and their voltage rating and capacity are 12.8 V and 10 Ah respectively. The distributed BESS is connected to a 120 V DC bus.

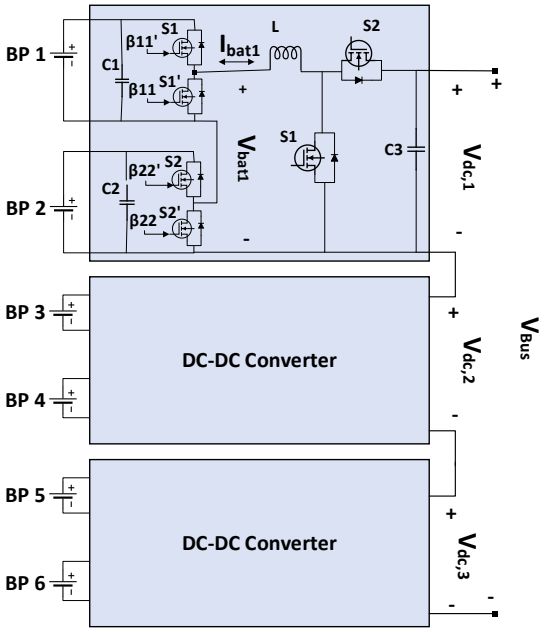

Figure 5.12: The dual-port converter based partially-distributed BESS

Table. 5.5 Simulation parameters

Parameter	**Value**	
	Discharging	**Charging**
DC Bus Voltage (V)	120	120
Average Discharge Current (A)	6	3
Initial SoC of Battery-1 (%)	70	30
Initial SoC of Battery-2 (%)	90	30
Initial SoC of Battery-3 (%)	75	28
Initial SoC of Battery-4 (%)	80	35
Initial SoC of Battery-5 (%)	85	32
Initial SoC of Battery-6 (%)	85	42

5.6.1 Discharging Mode

In this section, the proposed two-level balancing power sharing controller is demonstrated in discharging mode. The SoCs of the battery packs controlled by same converter are balanced using the bypassing feature, whilst module-level balancing is realised by controlling the

discharge power of each module based on their relative SoC. Therefore, in this structure, any imbalance amongst battery packs 1-2, 3-4, and 5-6 is removed using the bypassing feature, and any imbalance between modules 1, 2 and 3 is removed with the proposed power sharing controller.

Figure 5.13 shows the simulation results of the partially-distributed BESS in discharging mode. At the beginning of the simulation, battery pack 1 is bypassed to balance battery packs 1 and 2. The DC bus side voltages of each module are regulated based on the number of active battery packs and average SoC. As shown in Fig. 5.13 (a), module 1 has the lowest DC bus side voltage, and module 3 has the highest DC bus side voltage between 0 and 870 seconds. Battery pack 2 is discharged with the highest current as shown in Fig. 5.13 (b), since it has the greatest average SoC amongst all of the modules (Fig. 5.13 (c)). When the SoCs of battery packs 1 and 2 are equal at around 870 seconds, battery pack 1 is activated, and battery pack 3 is bypassed to balance battery packs 3 and 4. The DC bus voltages of each module are re-regulated to maintain module level balancing as shown in Fig. 5.13 (a). In this case, module 1 is discharged with the highest discharging current with a highest DC bus side voltage to perform module-level balancing, as it has the highest SoC without having any bypass pack. In contrast, module 3 is discharged with the lowest current as shown in Fig. 5.13 (b). When the SoCs of battery pack 3 and 4 are balanced at around 1150 seconds, battery pack 3 is activated, and each modules DC bus side voltage is re-regulated to perform module-level balancing. All of the modules are balanced at around 3300 seconds with each module sharing the power equally. The DC bus voltage is always regulated at 120 V in discharging mode as shown in Fig. 5.13 (a).

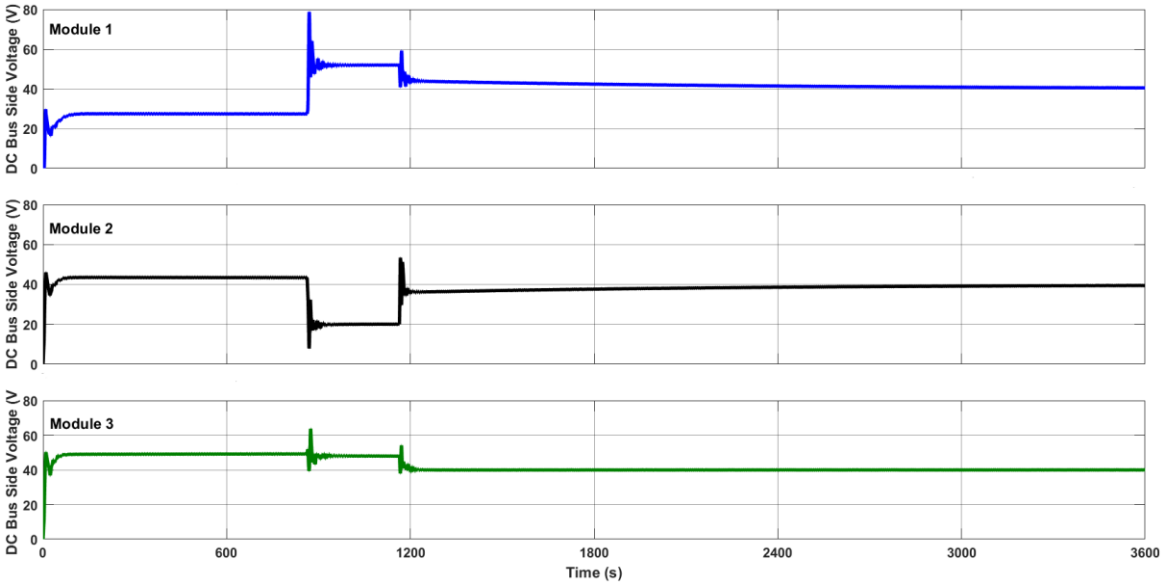

(a)

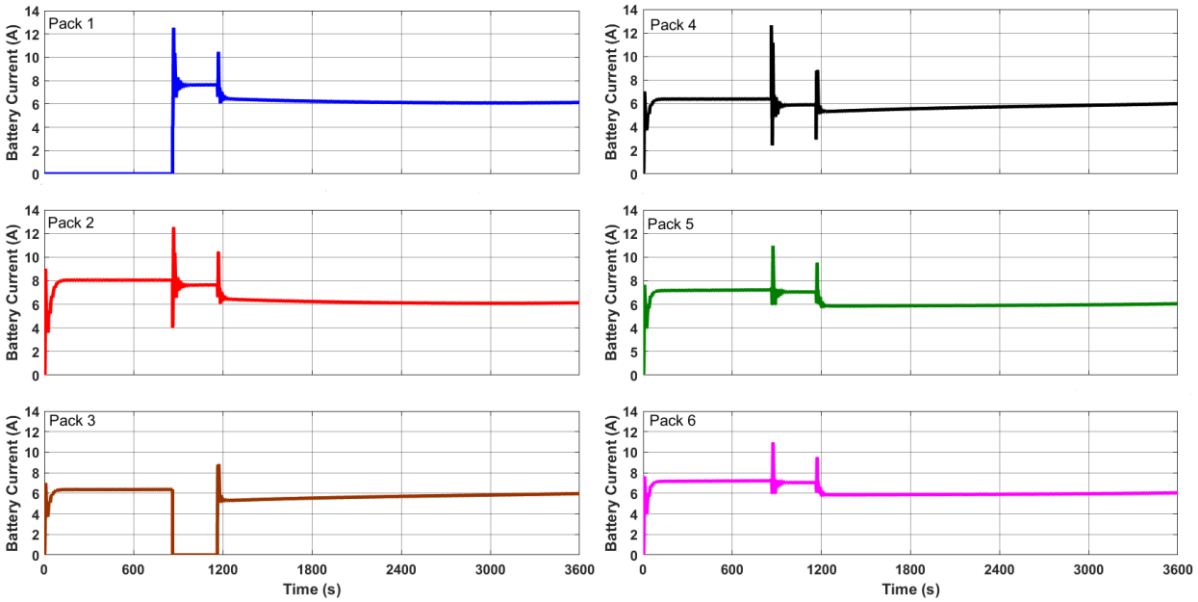

(b)

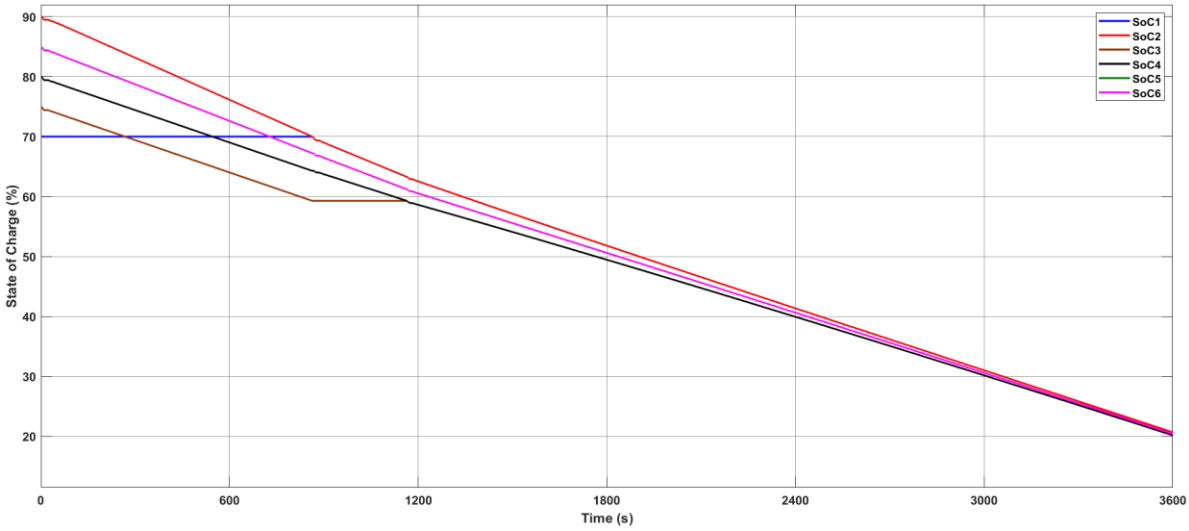

(c)

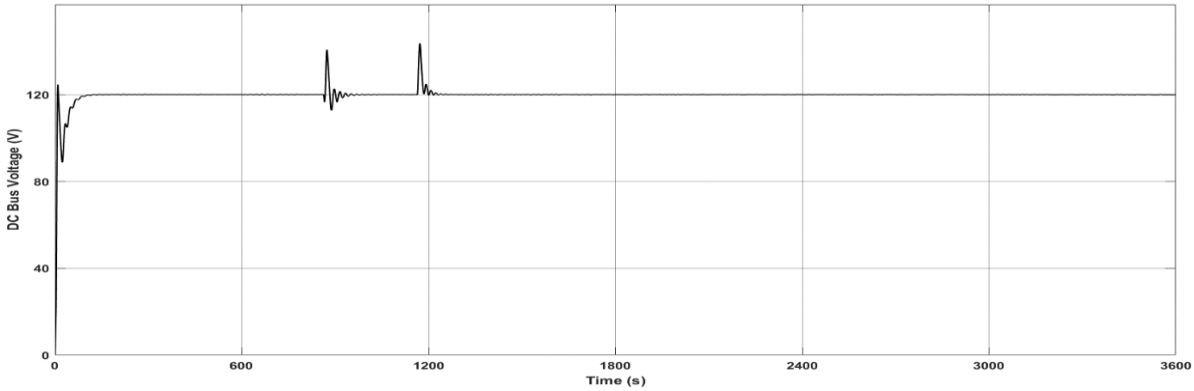

(d)

Figure 5.13: Simulation results of partially-distributed BESS in discharging mode, (a) Modules DC bus side voltages, (b) Battery packs discharging currents, (c) SoC of each module, (d) DC bus voltage

5.6.2 Charging Mode

Figure 5.14 shows the simulation results of the partially-distributed BESS in charging mode. Initially, to balance battery packs 5 and 6, battery pack 6 is bypassed between 0 and 580 seconds for the pack-level balancing. To perform module-level balancing, the modules with the higher average SoCs are charged with less current, and vice versa in charging mode. Battery module 1 (packs 1 and 2) has the lowest average SoC so it is charged with the highest battery current as shown in Fig. 5.14(b). The DC bus side voltages of each module depends on the module`s battery voltage and SoC. As module 3 has one bypassed pack, it has the lowest DC bus side voltage between 0 and 580 s as shown in Fig. 5.14(a). Module 1 has the lowest average SoC without any bypassed battery packs, so its bus side voltage is the greatest in this period. When the SoCs of battery packs 5 and 6 are equal, battery pack 6 is activated, and battery pack 4 is bypassed to balance battery packs 3 and 4. The DC bus voltages of each module are then re-regulated to maintain the module level balancing as shown in Fig 5.14(a). In this case, module 2 has the lowest DC bus side voltage. When the SoCs of battery packs 3 and 4 are equal, battery pack 4 is activated at around 900 s, and the modules DC bus side voltages are regulated again. All modules are balanced at around 4000 s, and after that point, all modules DC bus side voltages are equal to each other (Fig. 5.14(a)), and they are all charged with an equal charging current (Fig. 5.14(b)).

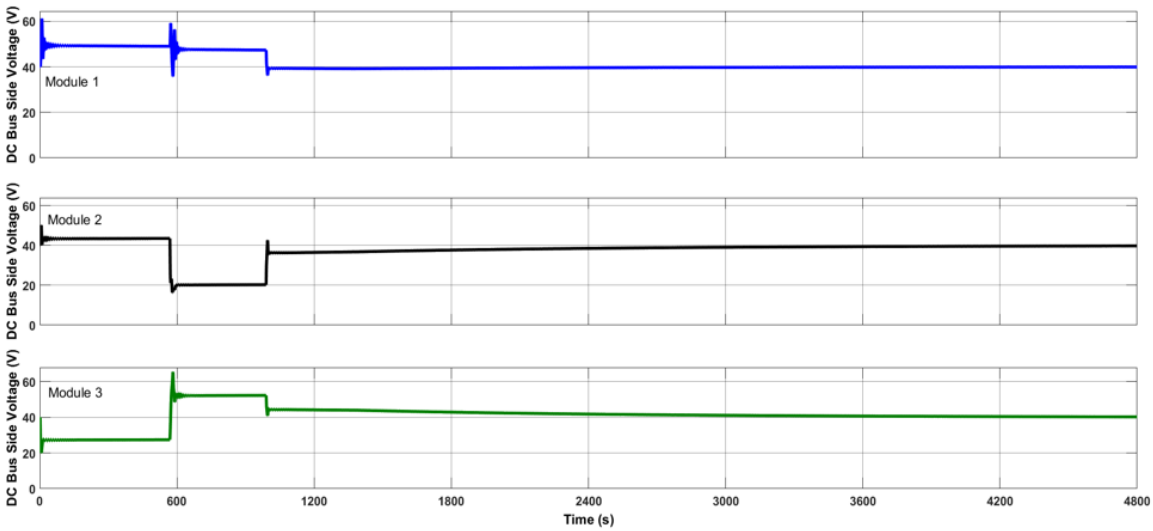

(a)

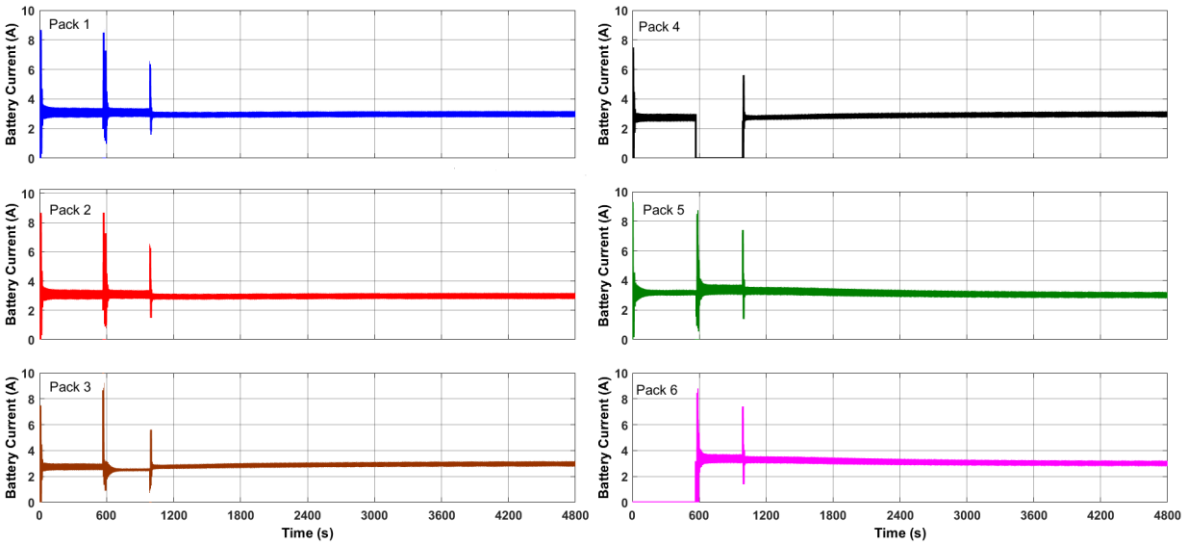

(b)

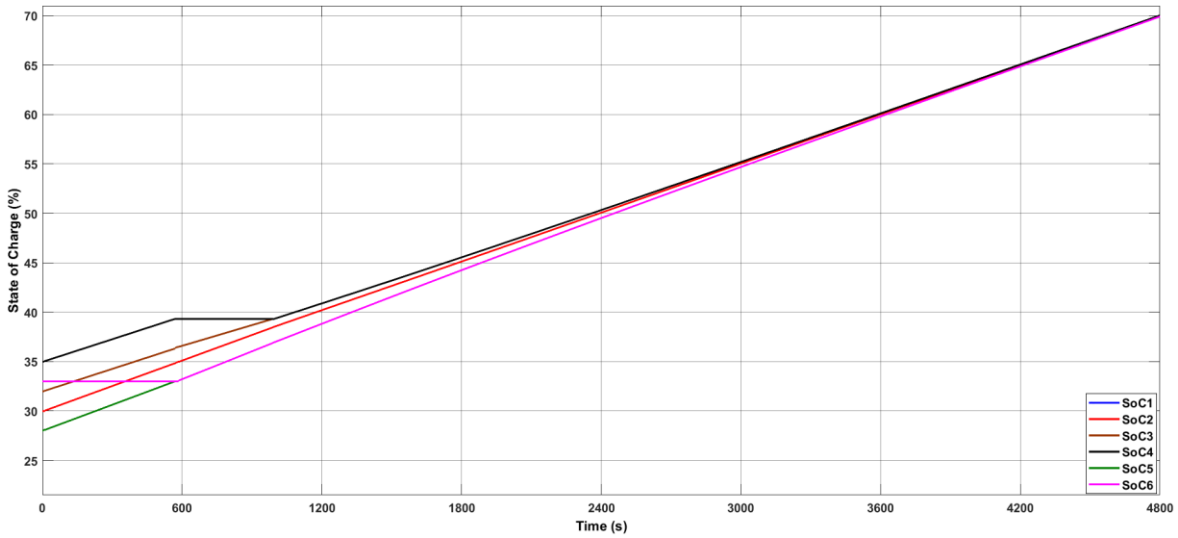

(c)

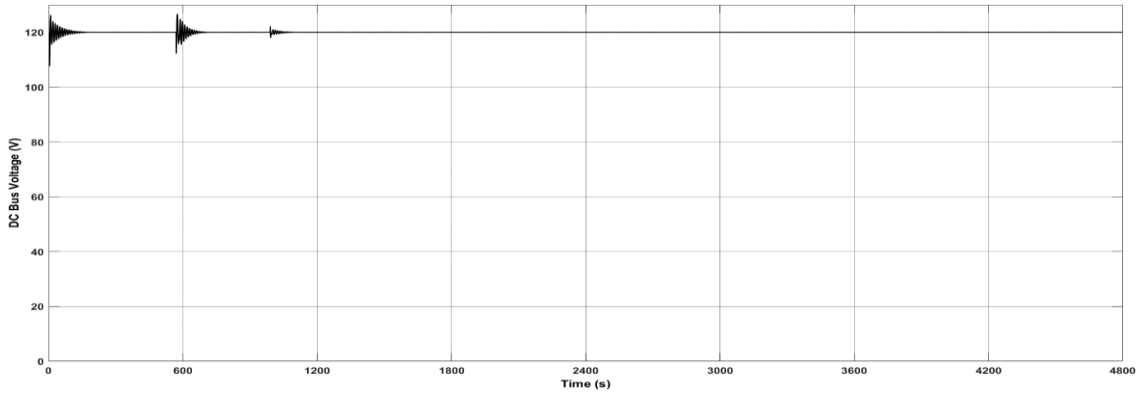

(d)

Figure 5.14: Simulation results of partially-distributed BESS in charging mode, (a) Modules DC bus side voltages, (b) Battery packs charging currents, (c) SoC of each module, (d) DC bus voltage

5.7 Summary and Conclusion

In this chapter, a partially-distributed BESS was proposed. The proposed structure requires fewer components and sensing circuits than the fully-distributed BESS, and hence it is also cheaper. The proposed structure has a higher reliability than its counterparts due to the reduced dependency of the system on the series connected submodule reliabilities. A power sharing controller with a two-level decoupled balancing function was proposed in both discharging and charging modes, and the simulation results validate the proposed control methods in both of these conditions.

Chapter 6. Experimental Prototypes and Results

6.1 Introduction

In this chapter, scaled-down laboratory prototypes are developed for both the fully-distributed and partially-distributed BESSs. The experimental setup is described in detail along with the components used, such as the battery, DC-DC converters, controller, and auxiliary circuits. In the first part, the fully-distributed BESS with a single-port converter is experimentally tested. To validate the effectiveness of the proposed power sharing controller described in Chapter 4, the battery is charged and discharged at different power level with both the conventional SoC-based power sharing controller, and the proposed efficiency-based optimised power sharing controller. The proof of concept of the proposed partially-distributed BESS is then demonstrated, along with the proposed power sharing controller in both charging and discharging modes.

6.2 Laboratory Prototype Development

A scaled down experimental prototype is developed and constructed in this chapter. The system specifications are summarised in Table 6.1. The enclosure including control board, gate drivers, battery packs, single-port DC-DC converter, and dual-port DC-DC converter is shown in Fig. 6.1. The detailed information regarding each component is given in the following subsections.

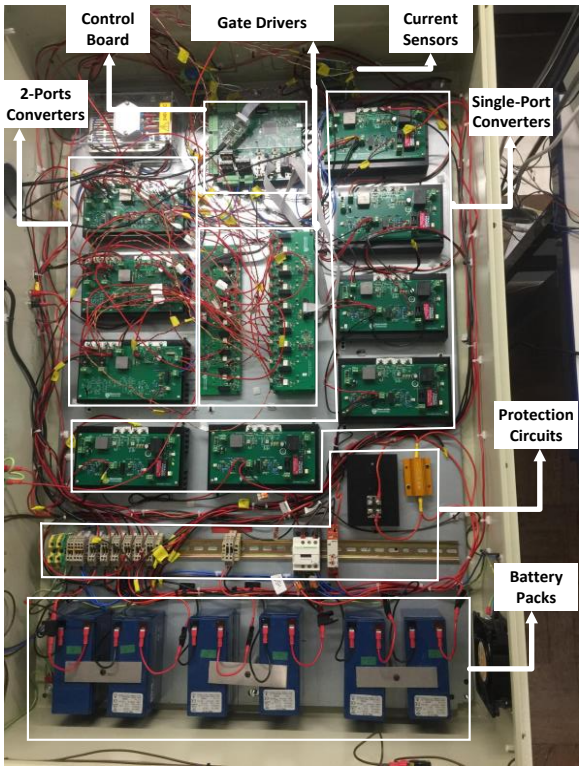

Figure 6.1: Experimental Setup

Table 6.1 System Specifications

Number of Battery	6
Number of Single-Port Converter	6
Number of Dual-Port Converter	3
DC Bus Voltage (V)	120
Maximum Discharging Power (W)	768
Maximum Charging Power (W)	384
Microcontroller	TMS320F28377d
Data Acquisition	Agilent 34970A

6.2.1 Battery Packs

In this experiment, six lithium iron phosphate (LiFePo4) batteries are used. The rated voltage and capacity of each battery is 12.8 V and 10 Ah, respectively. The recommended maximum discharging / charging currents are 10A and 5A, respectively. Each battery pack has an individual BMS inside, and protection and passive balancing circuitry. Battery discharging and charging profiles are shown in Figs. 6.3, and 6.4, respectively. The parameters of the battery pack are summarised in Table 6.2.

Figure 6.2: Battery Pack

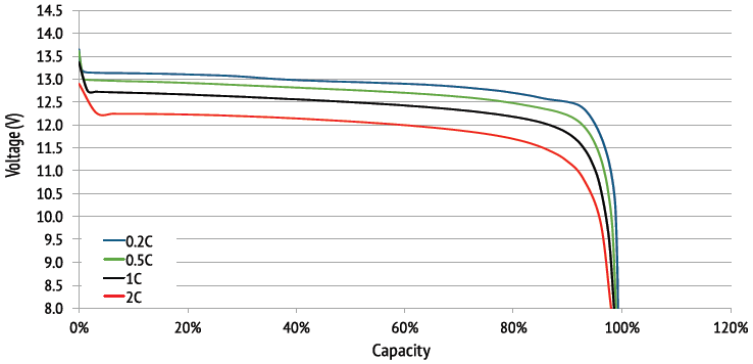

Figure 6.3: Battery discharge voltage characteristics at various discharge rate

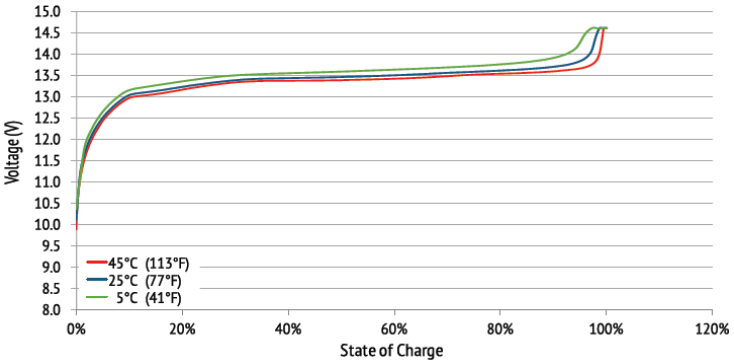

Figure 6.4: Battery charge voltage characteristics at various temperatures with 0.2C charging rate

Table 6.2 Battery Parameters

Parameters	Values
Nominal Voltage (V)	12.8
Nominal Capacity (Ah)	10
Energy (Wh)	128
Maximum Continuous Discharge current (A)	10
Recommended Continuous Charge Current (A)	5

6.2.2 Single-Port Bidirectional DC-DC Buck-Boost Converters

In the fully-distributed BESS, each single battery pack is controlled by its associated converter. Therefore, six single-port bidirectional DC-DC Buck-Boost converters were developed for the fully-distributed BESS. A picture of the designed single-port bidirectional DC-DC Buck-Boost converters is shown in Fig. 6.5, and the manufacturers and part numbers for the major components are shown in the Table 6.3. A 250 kHz switching frequency was used for this converter, and a 33 µH power inductor with a rated current of 15.5 A, and a 47 µF DC bus side

capacitor with a rated voltage of 100V were used. A 10 µF capacitor with a rated voltage of 25 V was also placed at the battery side of the converter. The voltage and current ratings of the selected TK18E10K3 MOSFET are 100V and 18 A, respectively. To allows safe bypassing of any module, a double throw single pole (DTSP) relay was used.

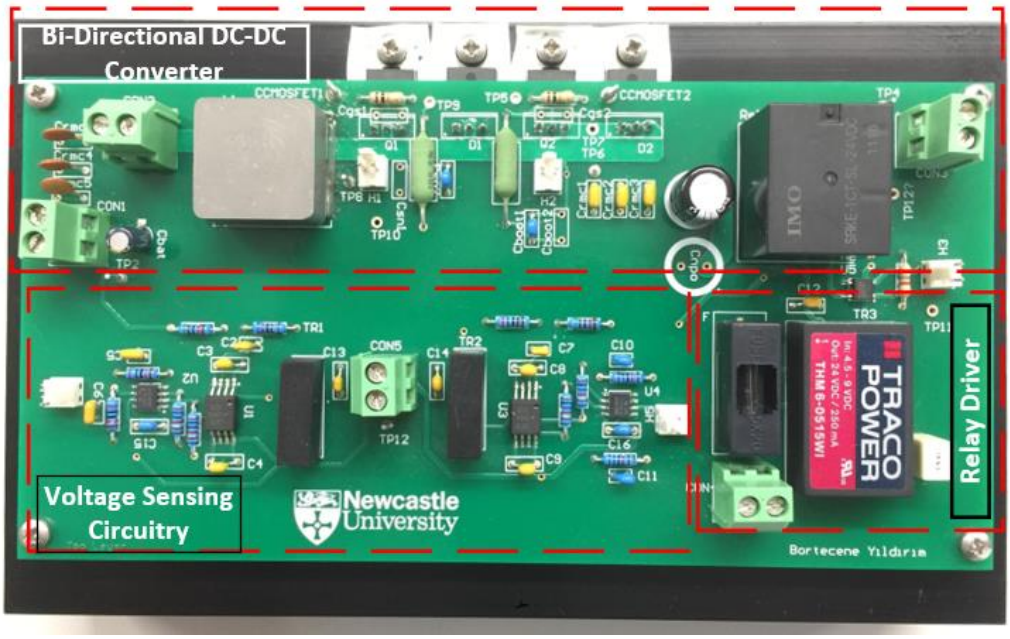

Figure 6.5: Single Port Bidirectional DC-DC Converter with voltage sensing circuitry

The voltage sensing circuits are integrated onto the converter PCB. This sensing is achieved using an ACPL-C87B isolation amplifier. The differential output signal of this amplifier is converter to the single ended signal using an OPA237 op-amp as shown in Fig. 6.6. This construction gives a wide range of operational accuracy due to the gain adjustment.

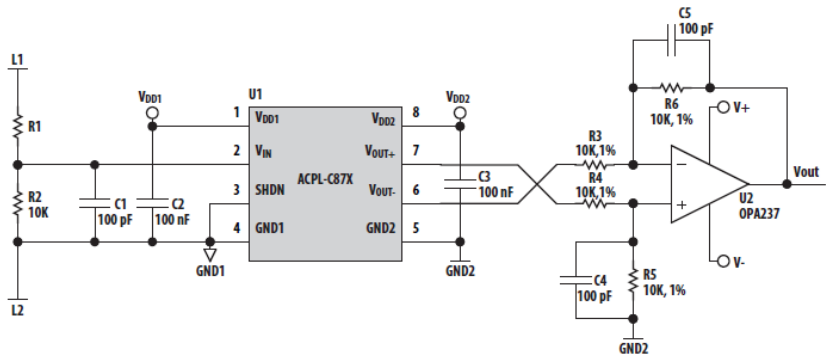

Figure 6.6: The voltage sensing circuitry [139]

Table 6.3 The component list used in Single-Port DC-DC Converter

Parts		**Model**	**Manufacturer**
MOSFET		TK18E10K3	Toshiba
Schottky Diode		NTST20100CTG	On-Semiconductor
Inductor		IHLP-8787MZ5A	Vishay
Capacitor	DC Bus Side	ECA-2AHG470	Panasonic
	Battery Side	ECA-1VM100B	Panasonic
Relay		SRKE-1CT-SL-24VDC	IMO
Isolation Amplifier		ACPL C87B	Broadcom
Operational Amplifier		OPA237	TI

6.2.3 Dual-Port Bidirectional DC-DC Buck-Boost Converter

In the partially-distributed BESS, a group of battery packs are controlled by their corresponding multi-port converter. For the experimental validation of the proposed partially-distributed BESS and power sharing controller, three dual-port converters were designed. Figure 6.7 presents a photograph of the designed dual-port converter, and Table 6.4 shows the major components used. The converter was designed to operate with a switching frequency of 250 kHz, the inductor used was 75 µH with a 10.6 A saturation current, and the DC bus side capacitor was 68 µF with a voltage rating of 160V. The rated voltage and current of the high switching frequency MOSFET were 150 V and 21 A, respectively. Each converter contains two voltage sensing circuits (which are the same as used for the single-port converter in Fig. 6.6), and a single current sensing circuit.

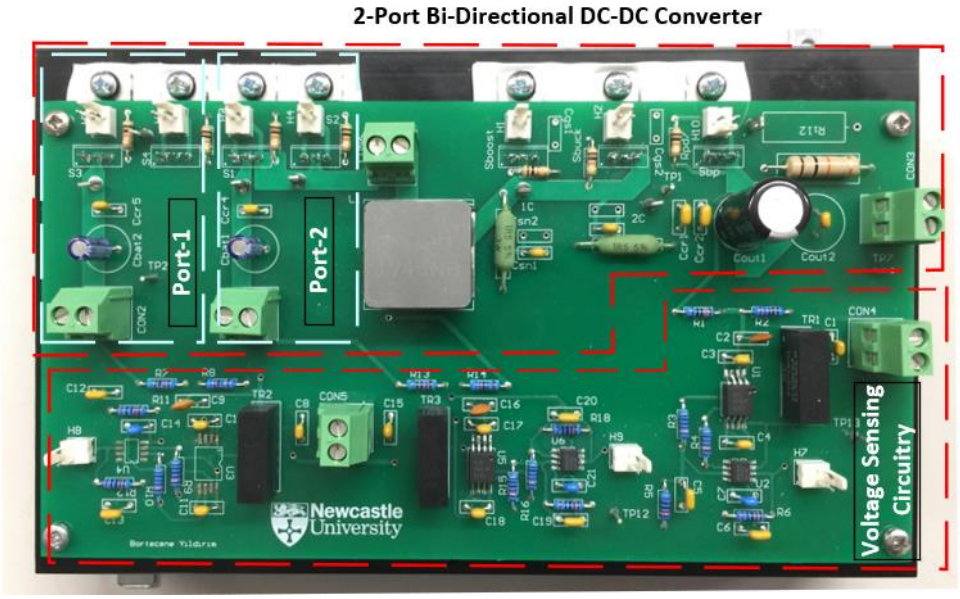

Figure 6.7: Dual-Port Bidirectional DC-DC Converter with voltage sensing circuitry

Table 6.4 The components used in the Dual-Port DC-DC Converter

Parts		Model	Manufacturer
MOSFET	Bypass/Enable Switches	IRFB7437PbF	Infineon
	High Frequency Switches	IPP530N15N3GXKSA1	Infineon
Inductor		IHLP8787MZER750M5A	Vishay
Capacitor	DC Bus Side	EEU-ED2C680B	Panasonic
	Battery Side	ECA-1VM100B	Panasonic

6.2.4 Control Board & Gate Driver & Current Sensor

The control board used in these experiments was based around the Texas Instruments TMS320F28377d 32-bit microcontroller, which has 24 PWM outputs, and 16 analogue-to-digital converter (ADC) input channels with 12-bit resolution for single ended signal conversion capability. The control board is shown in Fig. 6.8.

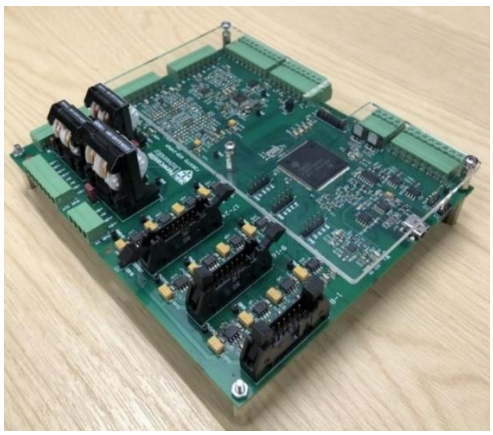

Figure 6.8: Control Board Interface

The external gate driver boards shown in Fig. 6.9 have 8 gate driving circuits. Two of them operate in complementary or independent mode. The output voltages of the driver circuits can be ±15 V or +15 V, -5 V, +15 V, or 0 V. In these experiments ±15 V was used to drive the power MOSFETs. CAS 16-NP current transducers were used for the external current sensing, and their PCB is illustrated in Fig. 6.10.

Figure 6.9: The gate driver circuitry

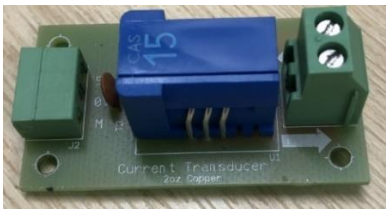

Figure 6.10: Current Sensing Circuitry

The complete test bench with all components is shown in Fig. 6.9. During the discharging of the battery, a DC load was connected, and the battery operates as a power source. During charging, a DC power supply was connected to the DC bus, and the battery behaves as a load. A data-logger (Agilent 34970A) was used to collect the system data during the long charging / discharging operations.

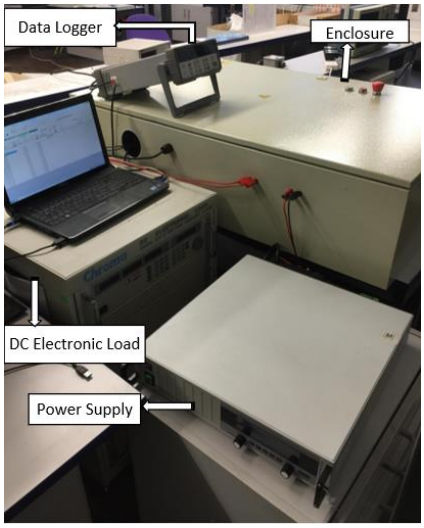

Figure 6.11: The complete test bench

6.3 Experimental Results with Single Port DC-DC Converter

The open loop waveforms of the designed single-port bidirectional DC-DC converter are shown in Fig. 6.12, with a battery side voltage of 13.2 V, and DC bus side voltage of 20.6 V. The rms value of the input current is 2.27 A, with an 880 mA current ripple.

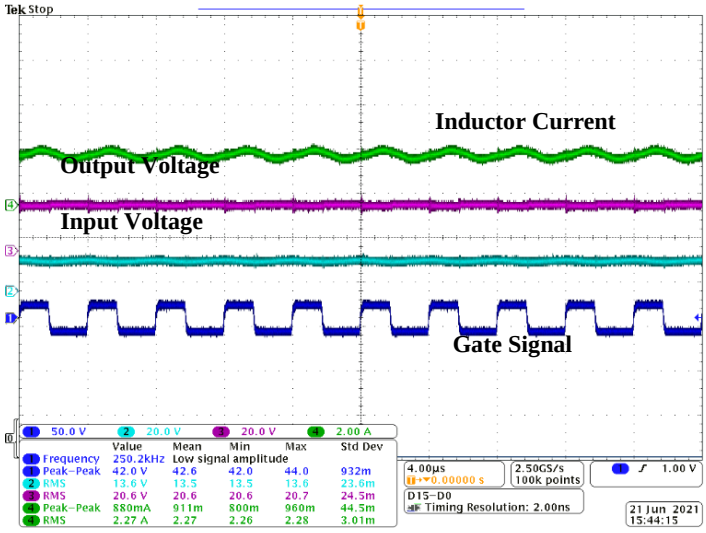

Figure 6.12: The single-port DC-DC converter open loop waveform in Boost mode of operation

In the following two subsections (6.3.1 and 6.3.2), the fully-distributed BESS, consisting of six single-port Buck-Boost converters and six LiFePo4 battery packs, is tested with constant charging / discharging powers and the SoC-based power sharing controller. The power sharing is realised using the control block diagrams explained in Chapter 4. The coulomb counting method was used for the SoC estimation in the experiments. The battery packs` SoC has been initialized before each test. The battery current has been sensed at every 1 s, for the coulomb counting estimation.

6.3.1 The Cell Balancing Function with Constant Battery Power in Discharging Mode

The experimental parameters and initial SoCs of the battery modules are shown in Table 6.5. The maximum SoC mismatch in this case is 8 %, which occurs between battery-1 and battery-3. The battery modules are discharged with 60 % rated battery discharge current, i.e., 6 A average battery current, by supplying a 460W load. The desired DC bus voltage is 120 V.

Table 6.5 The experimental parameters for constant current discharging mode

Parameter	**Value**
DC Bus Voltage (V)	120
Average Discharge Current (A)	6
Initial SoC of Battery-1 (%)	90 %
Initial SoC of Battery-2 (%)	87 %
Initial SoC of Battery-3 (%)	82 %
Initial SoC of Battery-4 (%)	85 %
Initial SoC of Battery-5 (%)	84 %
Initial SoC of Battery-6 (%)	86 %

Figure 6.13 shows the experimental results for the SoC-based power sharing controller in the constant discharge power mode. For the purpose of SoC balancing, the modules share the power based on their relative SoC with respect to the average SoC. As the SoCs of modules 1, 2, and 6 are higher than the average, the DC bus side voltages of these modules(V_{dc1}, V_{dc2}, and V_{dc6}) are higher than the equal sharing voltage as illustrated in Fig. 6.13(a). The voltages of modules 3, 4, and 5 (V_{dc3}, V_{dc4}, and V_{dc5}) are lower than that of the equal sharing voltage, as their SoCs are less than the average SoC. The individual module battery currents are illustrated in Fig. 6.13(b). The module with the highest SoC compared to the average has the highest discharging current, and vice versa. The individual module SoCs converge with the created power difference during discharging, and at around 28 minutes they are all balanced as shown in Fig. 6.13(c). After reaching the equal SoC, their DC bus side voltages are also equal to each other, and they share the power evenly so that the balanced state is preserved. It is worth noting that the DC bus voltage is always equal to its reference value of 120V as shown in Fig. 6.13(a).

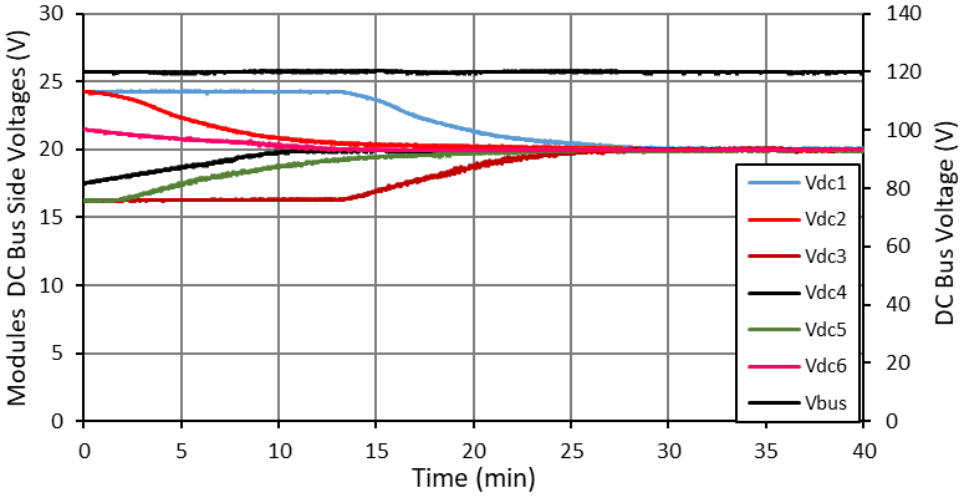

(a)

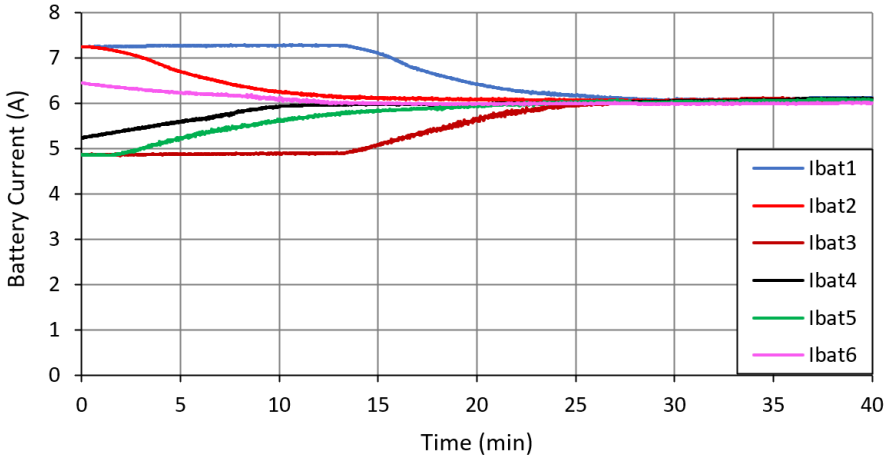

(b)

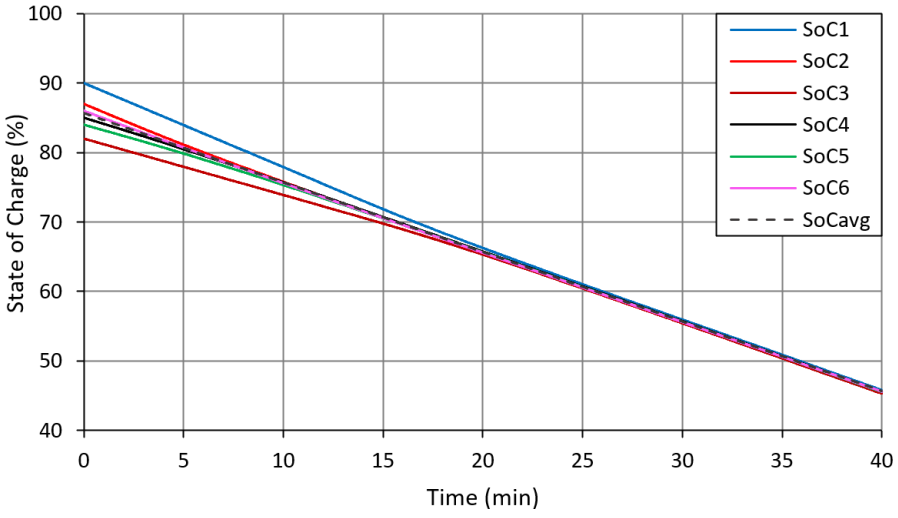

(c)

Figure 6.13: Experimental results in discharging mode with 6 A average battery current, (a) Modules DC bus side voltages, (b) Individual Modules battery discharging currents, (c) Individual battery packs SoC

6.3.2 The Cell Balancing Function with Constant Current Charging Mode

In this experiment, the fully-distributed BESS is charged with a 2.5 A average charging current. A DC power supply is connected to the DC bus side of the system to charge the batteries by applying a voltage equal to the bus voltage (120 V), with the batteries behaving as a load. The experimental parameters and initial SoCs of the battery modules are shown in Table 6.6. The maximum mismatch in this case is 3 %, which is between battery module 1 and battery module 4.

Table 6.6 The experimental parameters for the continuous current charging mode

Parameter	**Value**
DC Bus Voltage (V)	120
Average Charge Current (A)	2.5
Initial SoC of Battery-1 (%)	60
Initial SoC of Battery-2 (%)	59
Initial SoC of Battery-3 (%)	59.5
Initial SoC of Battery-4 (%)	57
Initial SoC of Battery-5 (%)	58.5
Initial SoC of Battery-6 (%)	57.5

Figure 6.14 shows the experimental results of the SoC-based power sharing controller in constant current charging mode. In the charging mode, the modules with the lowest SoC are loaded with higher charging powers for the purpose of SoC balancing, and vice versa. Since, the SoCs of modules 1, 2, and 3 are higher than the average, the DC bus side voltages of these modules (V_{dc1}, V_{dc2}, and V_{dc3}) and their battery currents (I_{bat1}, I_{bat2}, and I_{bat3}) are lower than the equal sharing case as shown in Figs. 6.14(a) and 6.14(b), respectively. As the SoC of modules 4, 5, and 6 is less than the average , they have higher DC bus side voltages (V_{dc4}, V_{dc5}, and V_{dc6}) and are charged by higher battery currents (I_{bat4}, I_{bat5}, and I_{bat6}) .

The DC bus voltage is shared amongst the modules, and the sum of the modules DC bus side voltages is always 120V as shown in Fig. 6.14(a). The SoC of each module converges during charging, and they are balanced at around 35 minutes as shown in Fig. 6.14(c). It is worth mentioning that the charging balancing time takes longer than discharging, even with a smaller mismatch level. This is because the balancing time depends on the power differences created amongst the modules, and the charging current is much lower (2.5 A) compared to the 6 A discharging current.

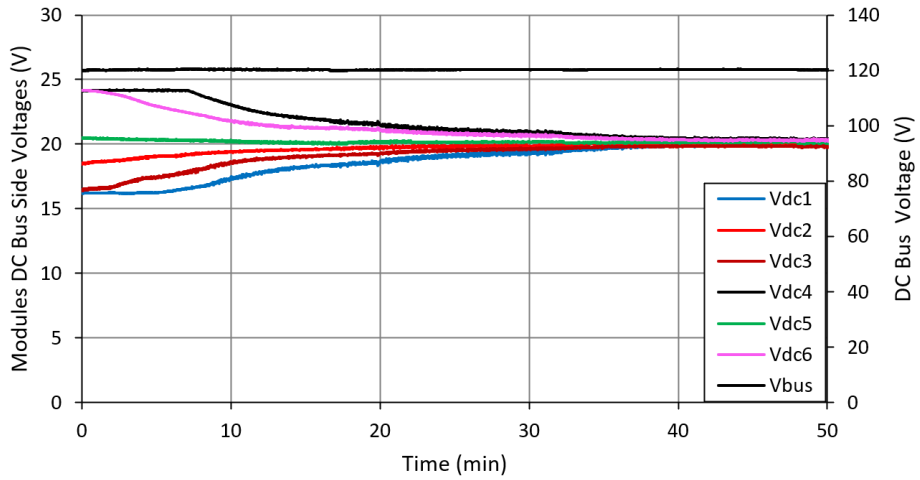

(a)

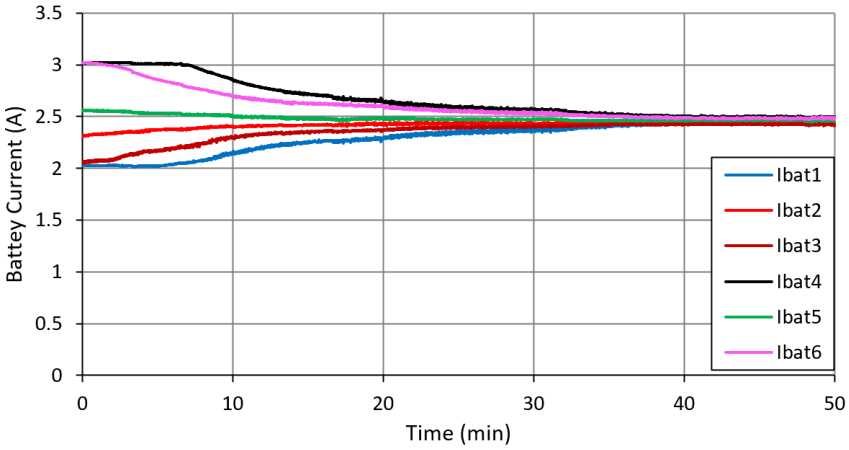

(b)

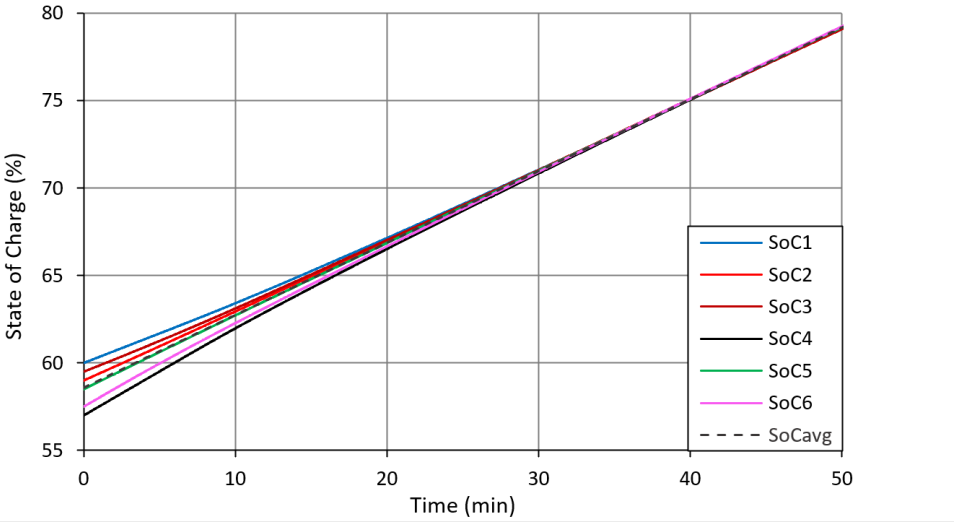

(c)

Figure 6.14: Experimental results in charging mode with 2.5 A average battery current, (a) Modules DC bus side voltages, (b) Individual Modules battery charging currents, (c) Individual battery packs SoC

6.4 Experimental Results of SoC-based Power Sharing Controller with Different Battery Power

The fully-distributed BESS are discharged and charged with different battery power in the following subsections 6.4.1.and 6.4.2, respectively. The results with the SoC-based power sharing controller are presented in this section. The same experimental parameters and initial SoC used in the simulation in chapter 4 are used and listed in Table 6.7.

Table 6.7 The experimental parameters with different battery charging / discharging power

System Parameters	**Value**	
	Discharging	**Charging**
Initial SoC of Battery-1 (%)	90	53
Initial SoC of Battery-2 (%)	88	54
Initial SoC of Battery-3 (%)	86	55
Initial SoC of Battery-4 (%)	87	53.5
Initial SoC of Battery-5 (%)	87.5	52
Initial SoC of Battery-6 (%)	89	52.5
Time (min)	**Battery Discharge-Power (%)**	**Battery Charge-Power (%)**
0-8	10	10
8-16	20	20
16-24	25	25 `
24-32	40	30
32-40	70	40
40-48	100	50

6.4.1 The SoC-based Power Sharing Controller with Variable Discharging Power

In discharging mode, the total battery load is changed by changing the load power connected to the DC bus. Figure 6.15 shows the experimental results with the SoC-based power sharing controller in discharging mode. The fully-distributed BESS is discharged with 10%, 20%, 25%, 40%, 70% and 100% power of its rated power in each 8 minutes intervals in this discharging experiment. The individual modules DC bus side voltages along with the DC bus voltage of the system is illustrated in Fig. 6.15(a). The DC bus side voltages of each module vary depending

on the corresponding battery modules` SoC. Modules 1,2, and 6 have higher SoC than that of the average, and their DC bus side voltages are also bigger than that of the equal sharing cases. Regardless of the total battery power, the modules with higher SoC are discharged with higher battery current than that of the average discharging current. The DC bus side voltage is maintained at the desired level as shown in Fig. 6.15 (a). On the other hand, the average battery discharging current increases with the increase of the total battery power as shown in Fig. 6.15(b). As the balancing speed directly related to the power differences among the modules, the balancing speed increases with the increase of discharging battery current. All modules are balanced at around 35 minutes and they share the total battery power equally after 35 minutes to maintain the balanced state.

6.4.2 The SoC-based Power Sharing Controller with Variable Charging Power

The fully-distributed BESS is charged with the SoC-based power sharing controller using variable average charging current. The average charging current is set to 1 A ,2 A, 2.5 A, 3 A, 4A and 5A for 8 minutes intervals to apply the same test condition with the simulation case used in chapter 4. Figure 6.16 shows the experimental results with the SoC-based power sharing controller in charging mode. During the charging mode, the DC bus voltage is maintained at 120 V by the power supply, and shared among the individual modules. The individual modules DC bus side voltages are related to the relative SoC of each module with respect to the average SoC and independent of the total charging current. In the charging case, the modules with the lower SoC are charged with higher current, and vice versa. Since the SoCs of modules 1,5 and 6 are less than that of the average, the DC bus side voltages of these modules are higher than equal sharing voltages as shown in Fig. 6.16(a). When the battery packs converge the relative SoC differences reduces, and modules DC bus side voltages also converges. Figure 6.16(b) illustrates the individual modules battery current. Each module`s battery current is directly related to the DC bus side voltage of each module and the individual modules battery current increases at each 8 minutes interval with the increase of average charging current. Figure 6.16(c) shows the SoC of each module. The balancing speed increases with increased battery power, and at around 38 minutes all of the modules are balanced. After that point, each module DC bus side voltages and battery current are equal to each other to preserve the balanced condition. The sum of the modules DC bus side voltages is always 120 V as shown in Fig. 6.16(a).

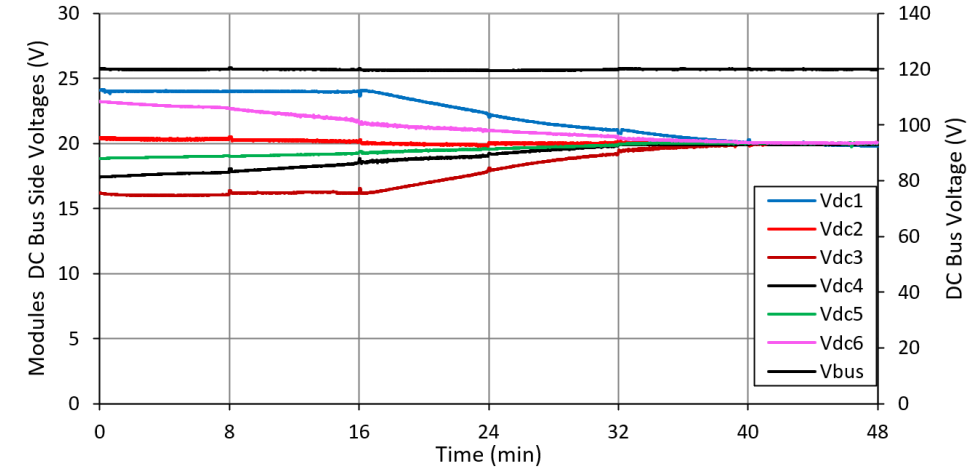

(a)

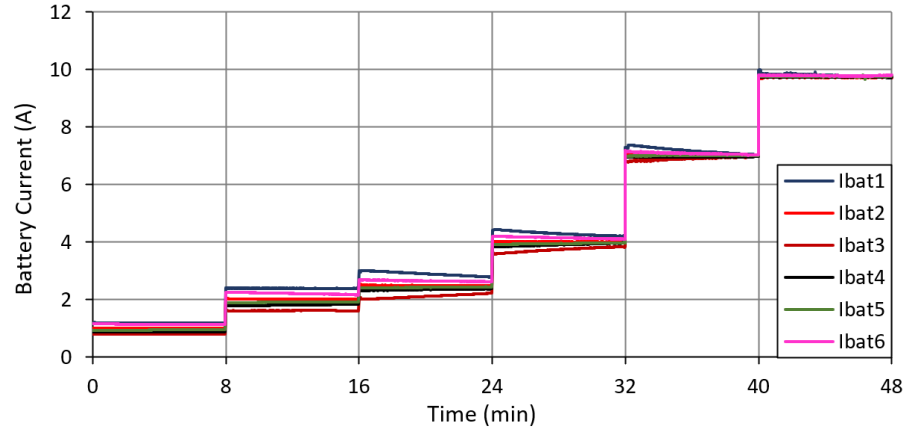

(b)

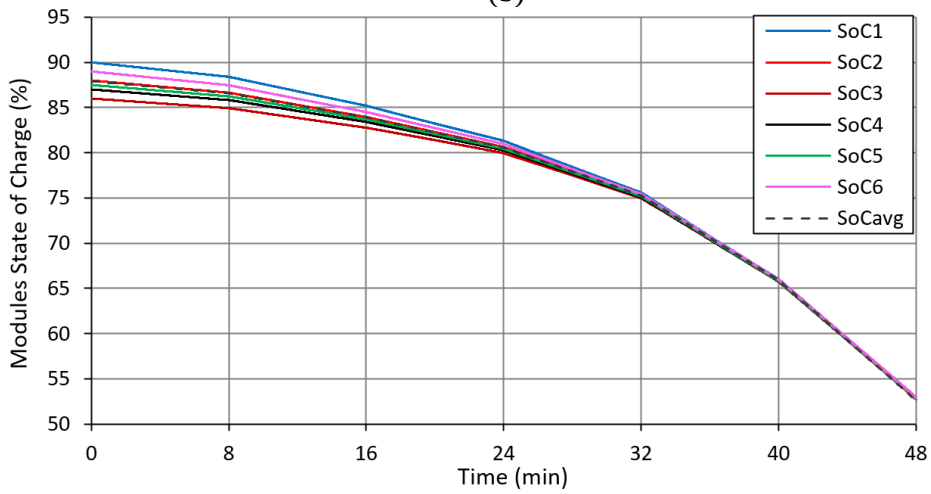

(c)

Figure 6.15: Experimental results with SoC-based power sharing controller in discharging mode, (a) Modules DC bus side voltages, (b) Individual Modules battery discharging currents, (c) Individual battery packs SoC

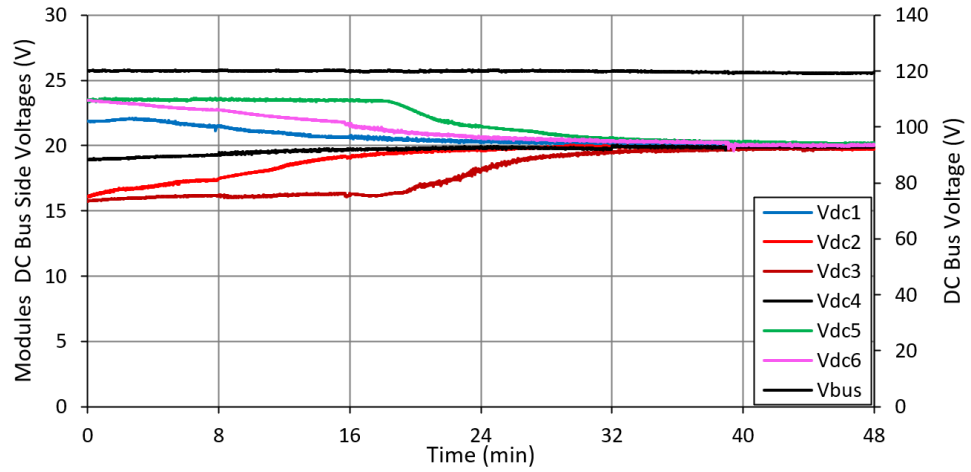

(a)

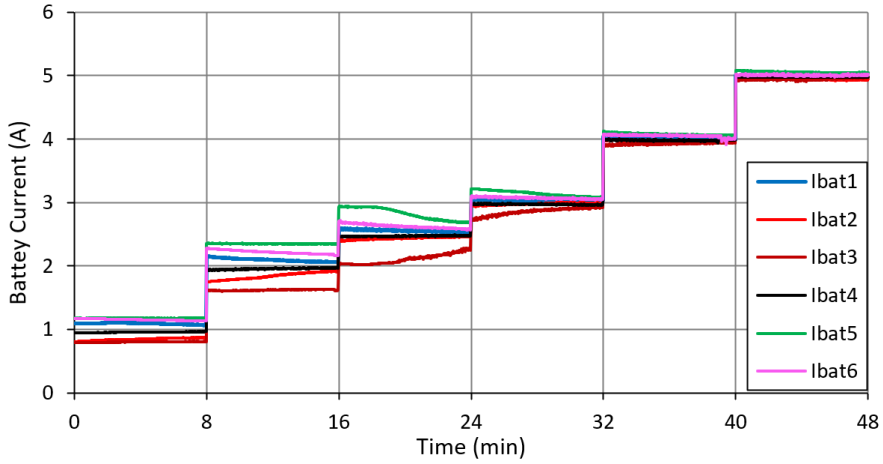

(b)

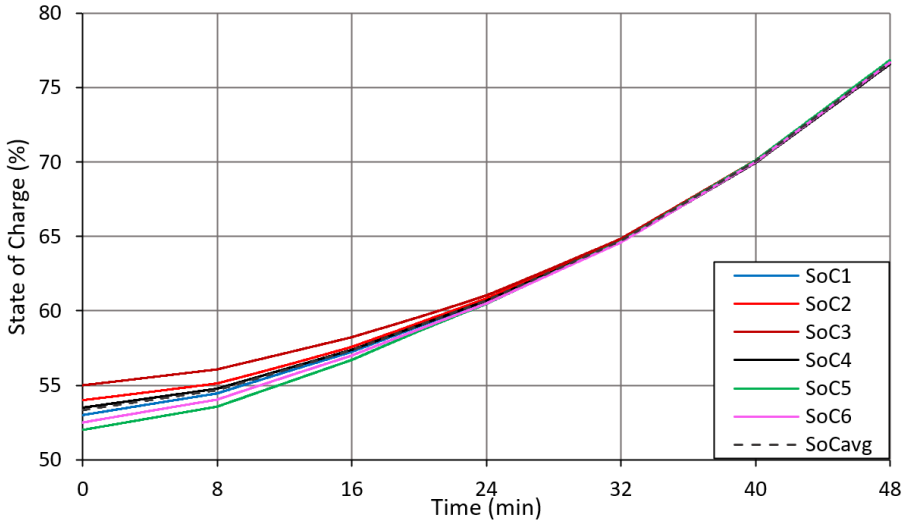

(c)

Figure 6.16: Experimental results with SoC-based power sharing controller in charging mode, (a) Modules DC bus side voltages, (b) Individual Modules battery charging currents, (c) Individual battery packs SoC

6.5 Experimental Results of Efficiency-based Optimised Power Sharing Controller with Different Battery Power

To verify the effectiveness of the proposed efficiency-based optimised power sharing controller in chapter 4, the fully-distributed BESS are discharged and charged with different battery power in the following subsections 6.5.1.and 6.5.2, respectively. The same test conditions used in the SoC-based power sharing controller in section 6.4 are applied. The experimental parameters are listed in Table 6.7.

6.5.1 The Efficiency-based Optimised Power Sharing Controller with Variable Discharging Power

Results for the efficiency-based optimised power sharing controller in discharging mode are presented in Fig. 6.17. For this test, the maximum number of bypassed modules was kept at 3 in order not to exceed the voltage rating of the active modules. Based on the optimised power sharing controller with the load requiring 10% of the systems battery power, the 3 modules with the lowest SoC are bypassed in discharging mode. In this case, the 3 active modules are loaded at 20% (instead of loading the 6 modules at 10%) as can be seen from the Fig. 6.17(b). When the battery power is increased from 10% to 20% at 8 minutes, one additional module is activated, with each active module operating at 30% of their rated load. During this transition, module 5 has the highest SoC amongst the 3 bypassed modules, so this module is activated. At around 10 minutes, the relative SoC of the bypassed module 4 reaches the predefined turn on value, i.e. when $SoC_4 - SoC_{avg} = 1\%$, and it is activated in order not to exceed the predefined SoC differences. At the same time, the module with the lowest SoC (module 2) is bypassed. Similarly, different modules are bypassed, with modules 3 and 6, 6 and 1, and 1 and 5 swapping at around, 12, 18, and 23 minutes, respectively. Between 16 and 24 minutes, five modules support the DC bus voltage, each providing 30% of their active module power. After the peak efficiency point (24 minutes), all modules share the power evenly, and each module`s relative SoC difference is less than 1%, as shown in Fig. 6.17(c). Rather than keeping all modules SoC at equal state, this strategy keeps all modules very close to each other. The DC bus voltage is maintained at 120 V all the time as shown in Fig. 6.17(a).

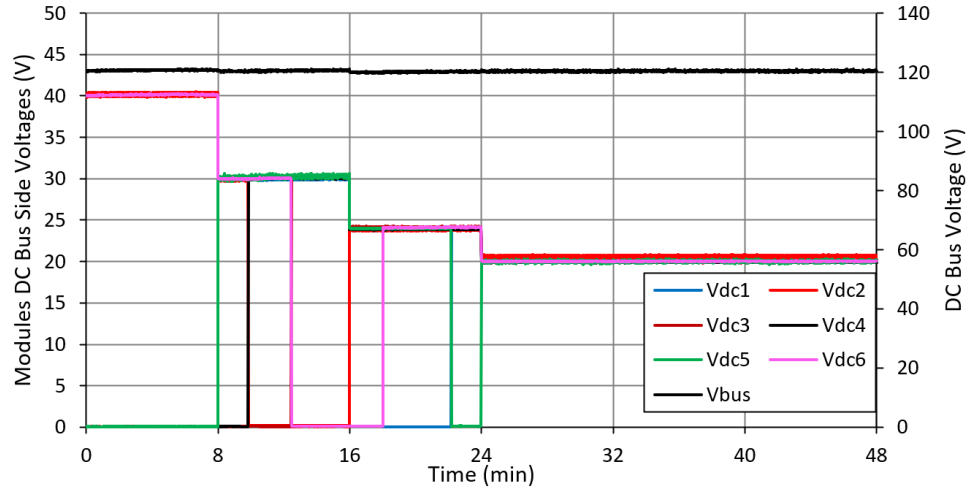

(a)

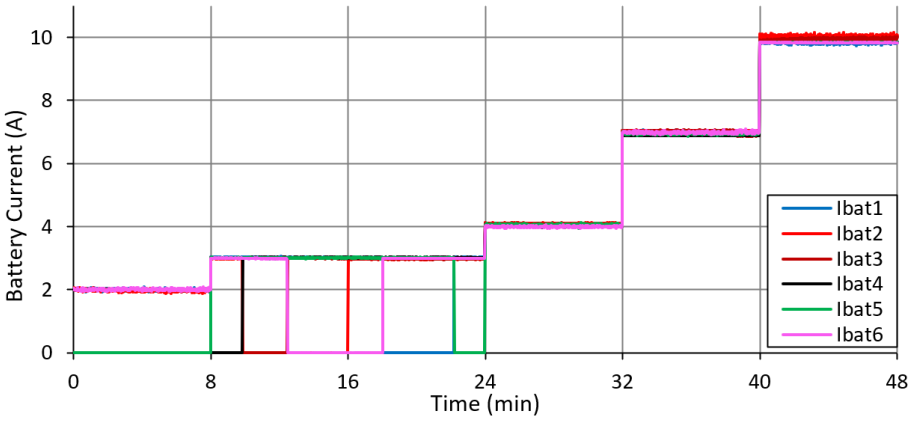

(b)

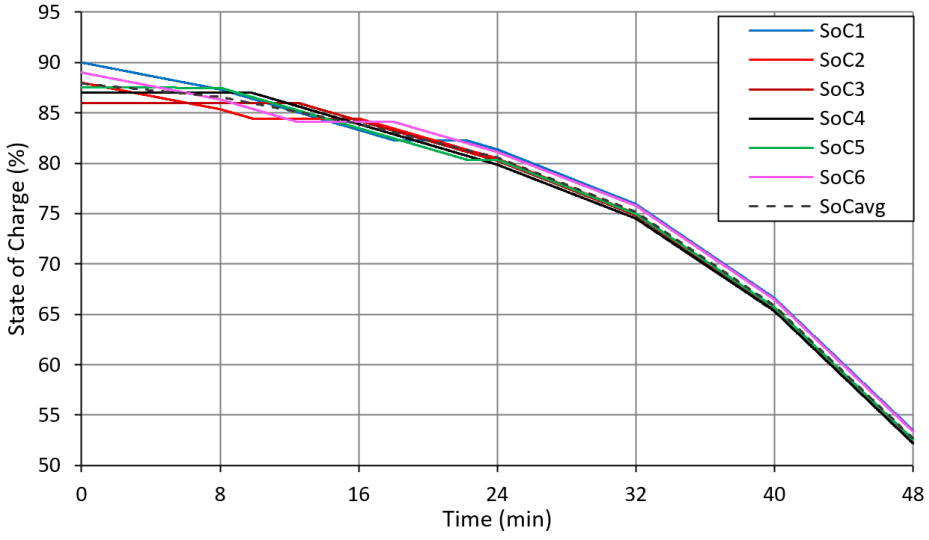

Figure 6.17: Experimental results with efficiency-based optimised power sharing controller in discharging mode, (a) Modules DC bus side voltages, (b) Individual Modules battery discharging currents, (c) Individual battery packs SoC

6.5.2 The Efficiency-based Optimised Power Sharing Controller with Variable Charging Power

Results for the efficiency-based optimised power sharing controller in charging mode are presented in Fig. 6.18. Similar to the discharging case, the maximum number of bypassed modules was kept at 3 to not exceed the voltage rating of the active modules. As the battery recommended maximum continuous charging current is 5 A, the maximum average charging current is also set to 5A in order not to degrade the battery lifespan. At 10 % battery load, the 3 modules with the highest SoC, modules 2,3 and 4, are bypassed. The rest of the active modules DC bus side voltage is 40 V, and their battery current increased to 2A between 0-8 minutes. At 20% total battery power, the lowest SoC module (module 2) among the bypassed module is activated, and each active modules are charged with 3A charging current as shown in Fig. 6.18(b). At 16 minutes the total battery power changes from 20% to 25%, and 5 modules need to be charged based on the optimisation result. At this point, another bypassed module with a lowest SoC (module 6) is activated, and five active modules are charged with 3 A charging current. The swapping of the bypassed modules occurs during the charging event to preserve the predefined SoC mismatch level based on the SoC management loop mentioned in chapter 4. Different modules are bypassed and activated, with modules 1 and 4, 6 and 3, 5 and 1, 2 and 5, and 4 and 2 swapping at around, 7, 12, 13, 18, and 23 minutes, respectively. After the 3A average charging current (24 minutes), all modules share the power evenly, and each module`s relative SoC difference is less than 1%, as shown in Fig. 6.18(c). The sum of the modules DC bus side voltages is always 120 V as shown in Fig. 6.18(a).

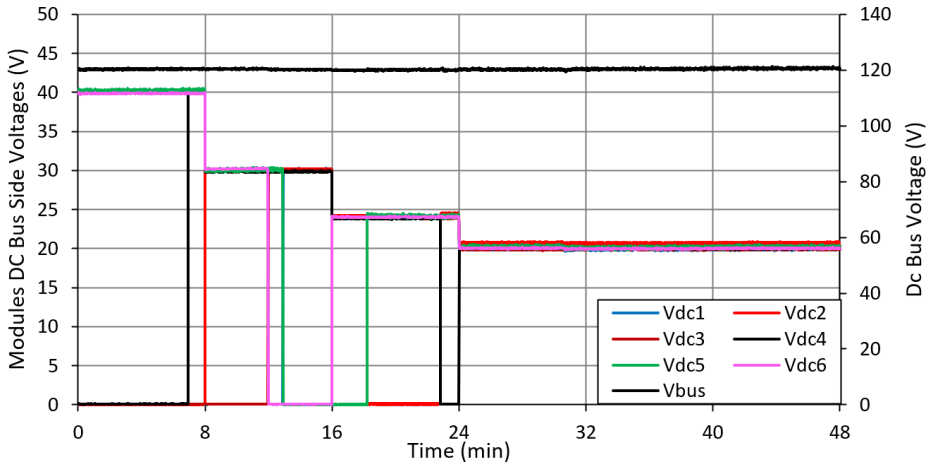

(a)

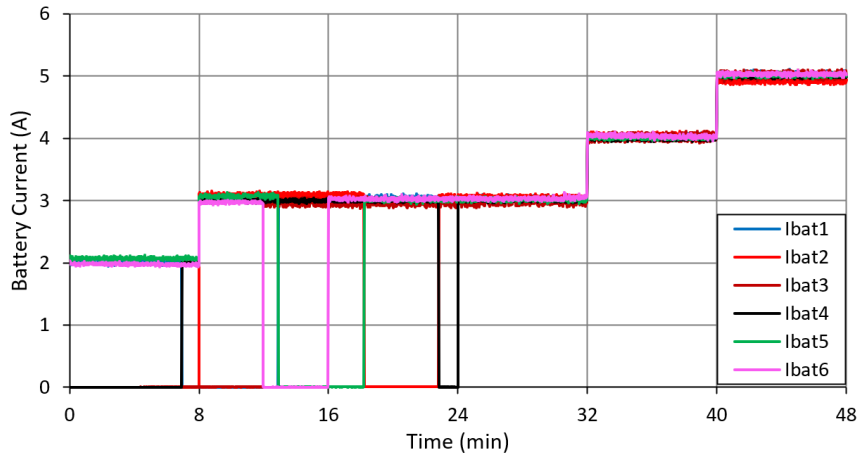

(b)

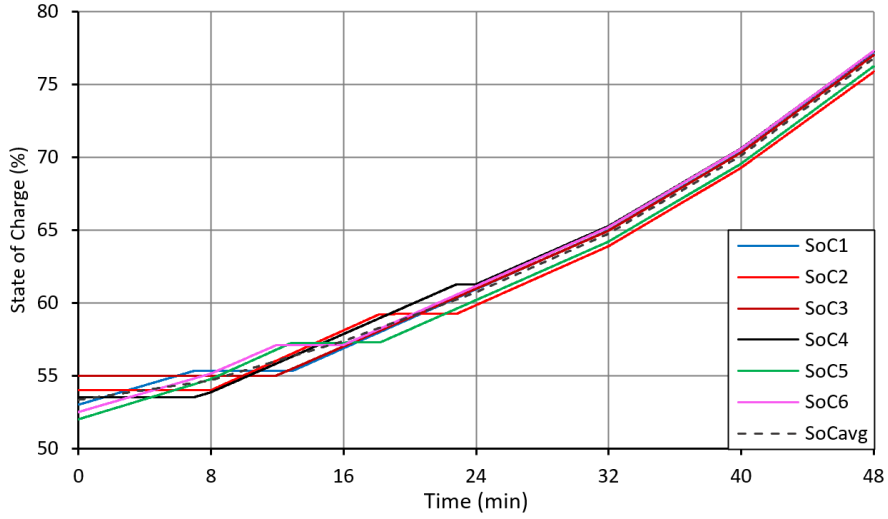

(c)

Figure 6.18: Experimental results with efficiency-based optimised power sharing controller in charging mode, (a) Modules DC bus side voltages, (b) Individual Modules battery charging currents, (c) Individual battery packs SoC

6.6 Experimental Results of Partially-Distributed BESS with Dual-Port DC-DC Converter

In this section the proposed partially-distributed BESS is experimentally tested with the designed dual-port converters shown in Fig. 6.7. The complementary gate signals for the battery pack enable / disable switches are illustrated in Fig. 6.19. In order to prevent short circuit 1 µs dead-time is used during transition.

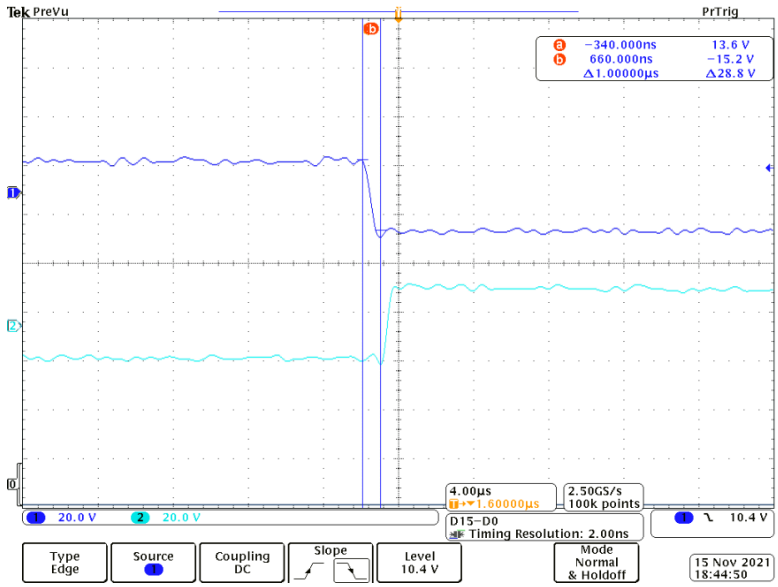

Figure 6.19: The complementary signals for the enable/disable switches with 1 µs dead-time

The open loop waveform of the designed dual-port half bridge converter is shown in Fig. 6.20, with an input voltage of 22.7 V, and output voltage of 44.6 V.

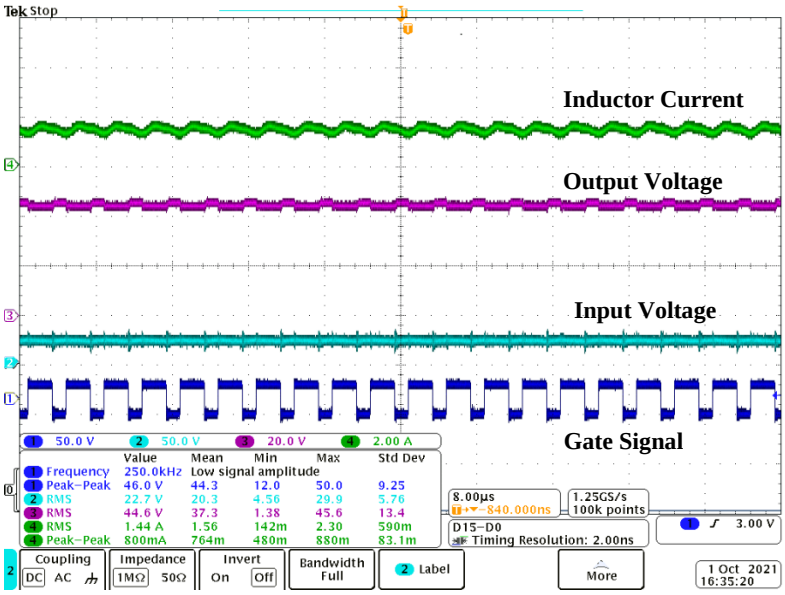

Figure 6.20: The dual-port DC-DC converter open loop waveform in boost mode of operation

The effectiveness of the power sharing controller proposed in chapter 5 is demonstrated with the bypassing of a battery pack in the system. Figure 6.21 shows the bypassing event of one

battery pack from the system. There are six battery packs connected to their associated dual-port converters. Before bypassing all 3 modules share the power evenly and each modules DC bus side voltages are 40 V to support 120 V DC bus. When battery pack 3 in the second module is bypassed, the battery side voltage of that module is halved. To compensate the voltage drop, and maintain the DC bus voltage at the desired level, each module increases their DC bus side voltages. The DC bus side voltage of each module is directly proportional to the battery side voltages ($V_{bat,x}$). In this case there are `5` active battery packs after bypassing, meaning that the DC bus side voltage of each module increases by `6/5` times, and modules 1,2 and 3 voltages are 48 V, 24 V, and 48 V, respectively.

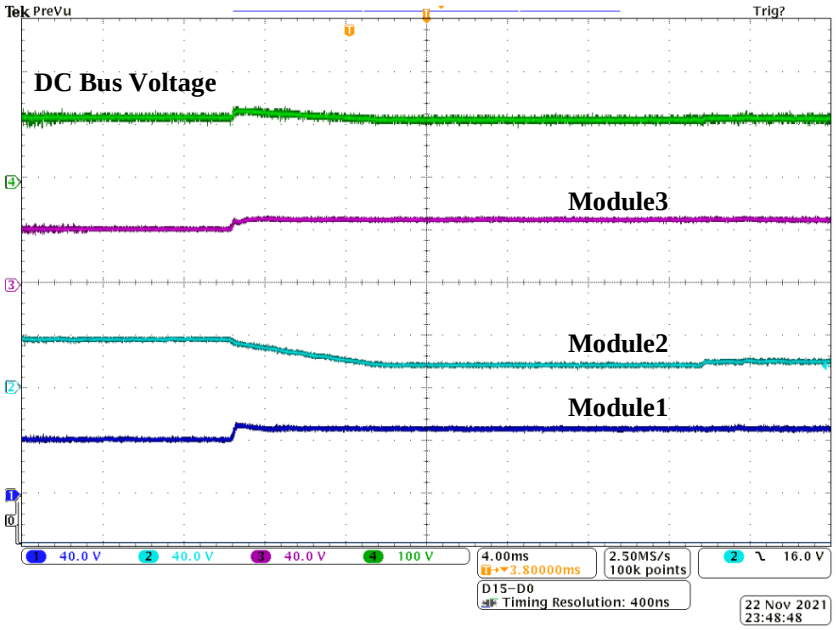

Figure 6.21: The bypassing a battery pack from the system

Figure 6.22 shows the activation of the battery pack 3 in the second module. During bypassing, the battery voltage of module 1 ($V_{bat,1}$) and 3 ($V_{bat,3}$) is two times higher than that of the module 2 ($V_{bat,2}$), resulting in their corresponding DC bus side voltages is also two times higher than that of the second module. When battery pack 3 in the second module is activated, the battery side voltage of that module is doubled, and the system total battery side voltages ($V_{bat,tot}$) increases by `6/5` times. Consequently, DC bus side voltages of each module reduce by 6/5 times. It is worth noting that the second module DC bus side voltage increases, as its battery side voltage($V_{bat,2}$) is doubled, but the VGR of that module reduces by 6/5 times.

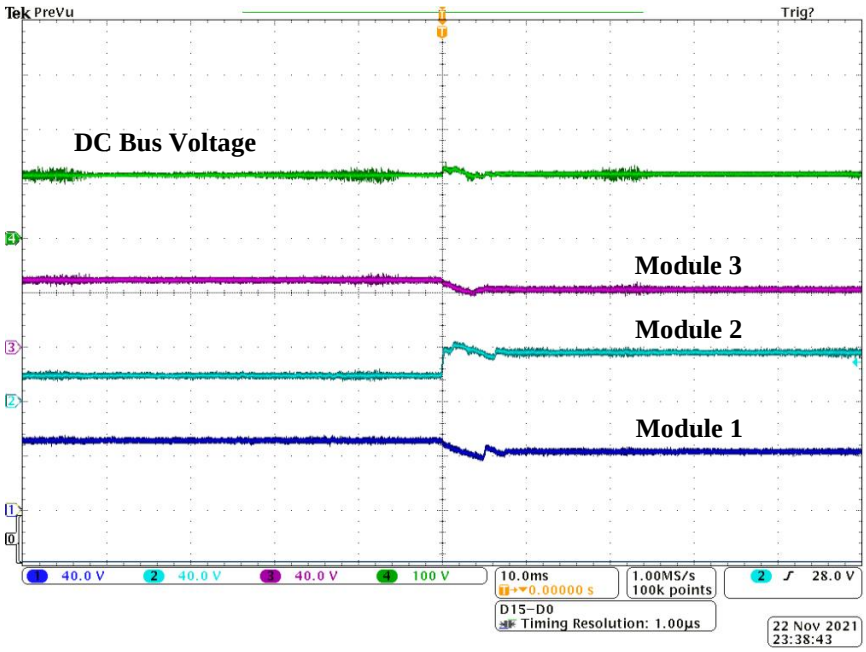

Figure 6.22: The activation of a battery pack in the system

In the following subsections 6.7.1-6.7.2 the two-level SoC balancing functions proposed in chapter 5 are validated for the partially-distributed BESS in discharging and charging mode.

6.6.1 Power Sharing Controller for the Partially-Distributed BESS in Discharging Mode

In discharging mode, the aims of the controller are to regulate DC bus voltage and balance the SoC of each battery packs. The two-level decoupled balancing algorithm is implemented, where the module-level balancing is realized by the power sharing controller, and pack-level balancing is achieved by bypassing of the battery packs connected to the same dual-port converter as mentioned in chapter 5. The experimental parameters and initial SoC of each battery pack are listed in Table 6.8. In this experiment battery packs 1-2 (module-1), battery packs 3-4 (module-2), and battery packs 5-6 (module-3) are connected to their associated dual-port converters, and any mismatch among these battery packs are corrected by bypassing.

Table 6.8 The experimental parameters for partially-distributed BESS in discharging mode

Parameter	Value
DC Bus Voltage (V)	120
Average Discharge Current (A)	6
Initial SoC of Battery-1 (%)	70
Initial SoC of Battery-2 (%)	90
Initial SoC of Battery-3 (%)	75
Initial SoC of Battery-4 (%)	80
Initial SoC of Battery-5 (%)	85
Initial SoC of Battery-6 (%)	85

Figure 6.23 shows the experimental results of the partially-distributed BESS with proposed power sharing controller in discharging mode. At the beginning of the experiment, battery pack-1 is bypassed to balance battery packs 1 and 2. When having a bypassed battery pack, the DC bus side voltages of each module increase to compensate the voltage drop, where DC bus side voltage of the module with a bypassed pack is lower compared to the others. The DC bus voltage of each module is proportional to the ratio of the module's battery voltage to the total battery voltage $\left(\frac{V_{bat,x}}{V_{bat,tot}}\right)$. The correction values (α_{Vx}) is also included to achieve module-level SoC balancing. As one of the battery packs in the first module is bypassed, module 1 has the lowest DC bus side voltages between 0 and 15 minutes. On the other hand, it is discharged with the highest discharging current as shown in Fig. 6.23(b), as it has the highest average SoC (SoC_{avg1}) among all. The DC bus side voltage of module 3 is the highest one between 0-15 minutes, since there is no bypassed battery pack in module 3 and its average SoC is also higher than that of the second module. When the SoCs of battery packs 1 and 2 are equal at around 15 minutes, the battery pack 1 is activated, and battery pack 3 is bypassed to balance the battery packs 3 and 4. The DC bus voltages of each module are re-regulated to maintain module level balancing as shown in Fig. 6.23(a). After 15 minutes, the first module is discharged with the highest discharging current with a highest DC bus side voltage to perform module-level balancing, as it has the highest SoC without having any bypass pack. In contrast, module 3 is discharged with the lowest current as shown in Fig. 6.23(b). The battery pack 3 is activated at around 20 minutes, when the SoC of battery pack 4 is equal to the SoC of battery pack 3, and each modules DC bus side voltages are re-regulated to perform

module-level balancing. All modules are balanced at around 55 minutes, and each module shares the power equally. The DC bus voltage is always regulated at 120 V in discharging mode as shown in Fig. 6.23(a).

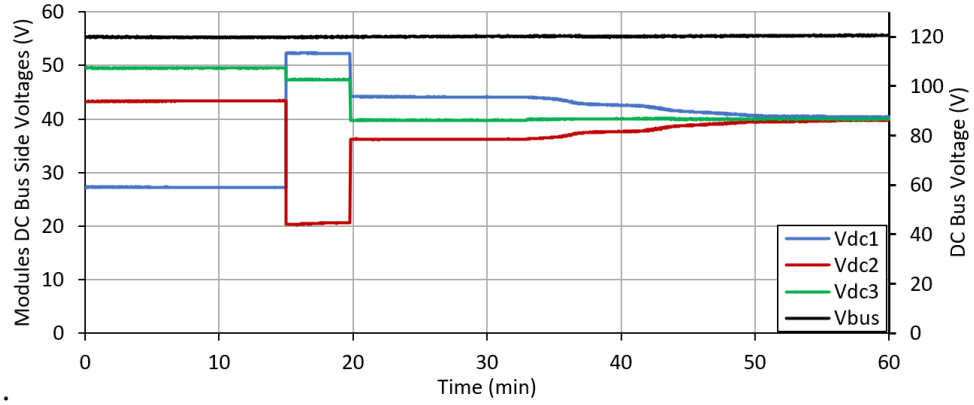

(a)

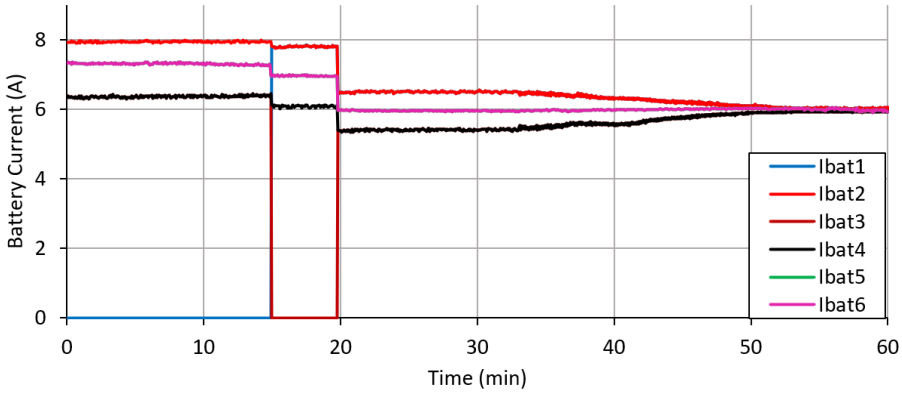

(b)

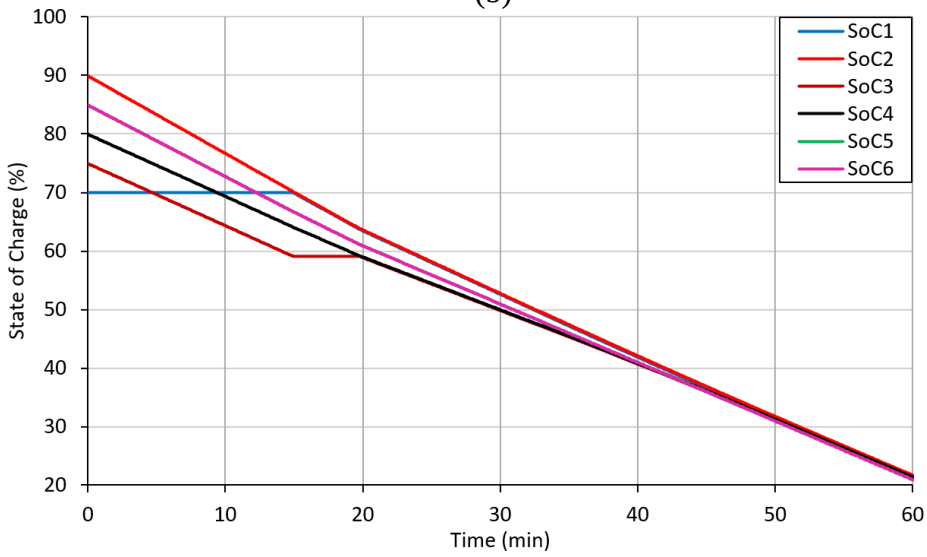

(c)

Figure 6.23: Experimental results of partially-distributed BESS in discharging mode, (a) Modules DC bus side voltages, (b) Battery Packs discharging currents, (c) Battery packs SoC

The bypassed battery packs have no effect for the module-level balancing controller and each active battery packs are discharged proportional to their average SoC ($SoC_{avg,x}$). As the pack-level and module-level balancing are decoupled the bypassed packs are not considered in the calculation of average SoC. Since the average SoC of module 1 ($SoC_{avg,1}$) is the highest one, it is discharged with the highest battery current, the second module is discharged with the lowest current as it has the lowest average SoC. Figure 6.23(c) shows the SoC of each battery packs. It can be seen that the battery packs 1 and 2, and 3 and 4 are balanced by bypassing at around 15 minutes, and 20 minutes respectively. On the other hand, all modules are balance at around 55 minutes with the proposed power sharing controller, and each modules DC bus side voltages and battery current are equal to each other after 55 minutes to preserve the balanced condition.

6.6.2 Power Sharing Controller for the Partially-Distributed BESS in Charging Mode

In this experiment the partially-distributed BESS is charged with 3 A average charging current. A DC power supply is connected to the DC bus side of the system to charge the batteries by applying voltage equal to the bus voltage (120 V). Table 6.9 shows the experimental parameters and initial SoC of battery packs.

Table 6.9 The experimental parameters for partially-distributed BESS in charging mode

Parameter	**Value**
DC Bus Voltage (V)	120
Average Discharge Current (A)	3
Initial SoC of Battery-1 (%)	30
Initial SoC of Battery-2 (%)	30
Initial SoC of Battery-3 (%)	32
Initial SoC of Battery-4 (%)	35
Initial SoC of Battery-5 (%)	28
Initial SoC of Battery-6 (%)	33

Figure 6.24 shows the experimental results of the partially-distributed BESS with proposed power sharing controller in charging mode. The pack-level balancing is used for the battery packs 5 and 6, and 3 and 4. Different from the discharging case, the battery pack with the higher SoC is bypassed in the charging mode. Between 0 and 9 minutes, the battery pack 6 is bypassed to balance battery packs 5 and 6, and the power is shared among the modules based on the modules average SoC ($SoC_{avg,x}$) to perform module-level SoC balancing. Module 1 has the highest DC bus side voltage between 0-9 minutes as its average SoC is lower than that of the module 2. On the other hand, module 3 has the lowest DC bus side voltage as battery pack 6 is bypassed between 0 and 9 minutes. Although the third module DC bus side voltage is lower than that of the other module, it is charged with the higher current due to having lower average SoC ($SoC_{avg,2} < SoC_{avg,1} = SoC_{avg,3}$). After the SoC of battery packs 5 and 6 are equalized at around 9 minutes, the battery pack 4 is bypassed, and battery pack 3 and 4 are balanced at around 15 minutes. The DC bus side voltages of each module regulated accordingly to perform module-level balancing. While the third module has the highest DC bus side voltage between 9 and 15 minutes, the second module has the lowest DC bus side voltage. After 15 minutes all battery pack are active, and all of the modules are balanced at around 70 minutes, and they are charged with the equal charging currents.

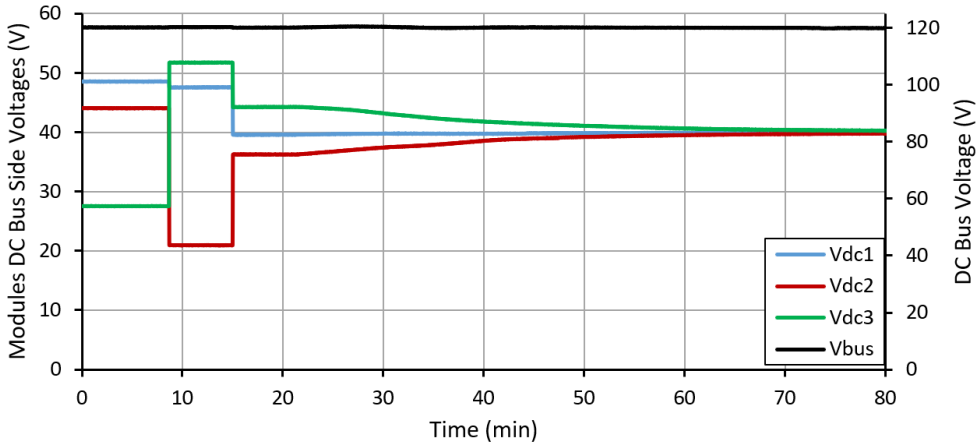

(a)

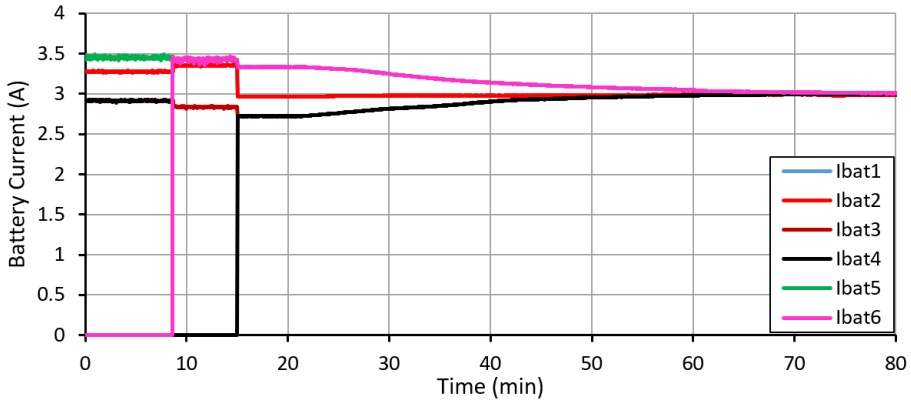

(b)

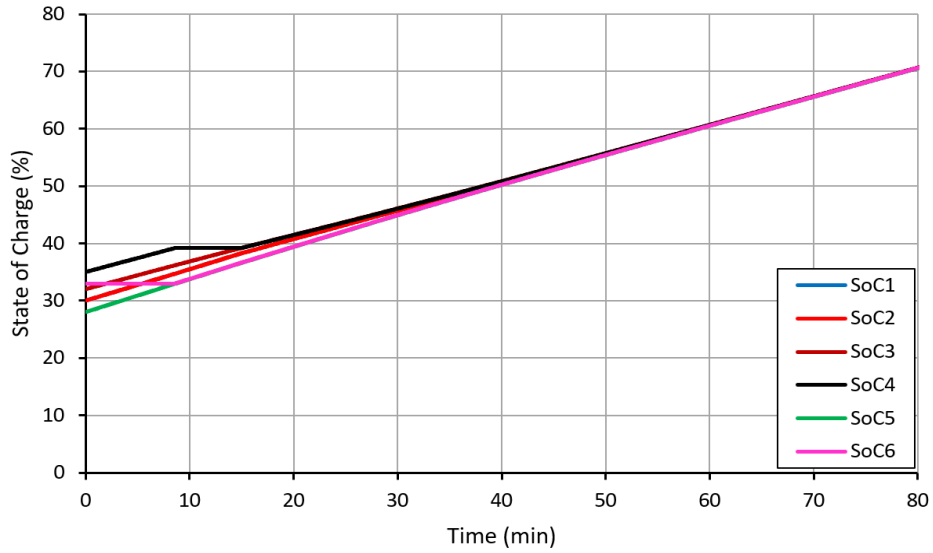

(c)

Figure 6.24: Experimental results of partially-distributed BESS in charging mode, (a) Modules DC bus side voltages, (b) Battery Packs charging currents, (c) Battery packs SoC

6.7 Summary and Conclusion

In this chapter, the experimental prototypes for the fully-distributed BESS, and partially-distributed BESS are presented. The individual components including battery storage systems, DC-DC converter, voltage/current sensing circuitries, and control board are demonstrated in detail. The proposed power sharing control methods are validated experimentally for both fully-distributed BESS and partially-distributed BESS.

Chapter 7. Conclusions and Future Work

7.1 Summary and Conclusion

The central BESS along with its main components including battery packs, BMS, and DC-DC converter are introduced in chapter 2. A battery pack consists of numerous series and parallel connected cells to meet the voltage and power demand of a specific system. A central high power DC-DC converter processes the full power of the battery, and high gain converter may be required depending on the system requirements. Accordingly, many effords have been devoted to increase the voltage gain of the DC-DC converter, and some of them are covered in chapter 2. The long battery strings bring other concerns caused by the cell nonuniformity. The management of the long battery string is a challenging task and cell management ICs are necessary to fully utilise the battery pack, and improve its lifespan. In a traditional approach, the battery strings are managed by cell management ICs, which are connected to the central control units. The main challenges of the traditional approach to the management of long battery strings are the increased cable connections, wiring harnesses, and performance reduction of available cell balancing topologies. Besides, the reliability of the central BESS reduces with the increase of the number of series connected cells.

The distributed-BESS reduces the voltage ratings of the battery packs and number of series connected cells in a pack. This lightens the load on battery management system, as a smaller number of cells are managed individually which also improves the performance of the available cell balancing topologies. In addition, the distributed BESS is scalable and any voltage level can be satisfied by adjusting number of modules. With the bypassing ability of distributed BESS, the reliability is further increased. The independent connection of the battery packs enables to control charging / discharging current of individual battery packs, which in turn improves the power sharing capabilities of the structure. This dissertation briefly discusses the power sharing controller for distributed-BESS aiming different purposes in chapter 3. The SoC balancing performance is evaluated for a case study with six battery packs, and the poor light load performance is highlighted and discussed. Then, an adaptive power sharing controller is proposed, which improves the light load balancing speed and efficiency. In addition, the efficiency reduction after the peak efficiency point is limited with the proposed control method. However, the performance of the proposed adaptive power sharing controller relies on the SoC mismatch level, and when there is no imbalance there will be no an efficiency improvement. Therefore, the proposed method may be suitable for the distributed-BESS consisting of pre-used battery packs, where high imbalance is expected.

In chapter 4, an improved efficiency-based optimised power sharing controller is proposed. The bypassing ability of the distributed-BESS is utilised to improve the light load efficiency further. The genetic algorithm is used as an offline algorithm, and lookup table is used for the real-time implementation. The results shows that the proposed power-sharing control improves the light load efficiency up to 5.05% in discharging mode, and 4.8% in charging mode. Rather than keeping all modules SoC at equal state, this strategy keeps all modules very close to each other and improves the total system conversion efficiency.

This dissertation also considers the cost of the distributed-BESS which requires numerous components including passive components, switches, sensing and drive circuits. Thus, in chapter 5, a multi-port converter based partially-distributed BESS is proposed. The partially-distributed BESS requires less component than that of the fully-distributed BESS, and cheaper. It also has higher reliability than its counterparts as the dependency of the system to the series connected submodules is reduced. A power sharing controller with two-level decoupled balancing functions is proposed in both discharging and charging mode to manage the SoC of each battery packs. The simulation results validate the proposed control methods in both discharging and charging modes in chapter 5.

The development of the experimental hardware is explained in detail in chapter 6. To verify the proposed control methods six single port DC-DC bidirectional converter are used in the fully-distributed BESS. Six LiFePo4 battery packs are charged / discharged in a fully-distributed structure with both SoC-based power sharing controller and proposed efficiency-based optimised power sharing controller. Then, dual-port converter based partially-distributed BESS is experimentally tested to charge six LiFePo4 batteries. The results validate the effectiveness of the proposed algorithm in both charging and discharging mode.

7.2 Future Work

It is possible to extend the research in the following directions:

- The adaptive power sharing controller is effective when there is continuous balancing required. In the literature the SoH balancing controller for the pre-used batteries has been proposed. On the other hand, compared to the SoC balancing where balancing can be achieved in one cycle, balancing the SoH requires many charging / discharging cycles. In addition, in each cycle there should be continuous power difference among the battery packs to balance the SoH. The proposed adaptive sharing controller can be effectively implemented for this system. As a case study the total energy save can be estimated and compared with the conventional SoH balancing method.

- The number of ports in the partially distributed BESS affects the system performance in many aspects. On the one hand, when the ports number increases for a given battery pack voltage, the number of converters, circuit components, sensing and drive circuitries, and thus the cost of the system decrease. On the other hand, the power sharing flexibility reduces as higher number of battery packs are charged / discharged with the same current, and the voltage ratings of the multi-port converter increases. The reliability of the system also varies with different number of ports and battery packs as shown in chapter 5. Therefore, there is a trade-off between the size of the passive components, cost, reliability, and power sharing flexibilities. Thus, a multi-objective optimisation can be done for a case study. The different priority scenarios can be used depending on the system requirements.

- The different battery packs chemistry can be explored in the partially-distributed BESS. The same chemistry battery packs can be connected to the same multi-port converters, and different chemistry batteries can be connected to different multi-port converters. The proposed power sharing controller can be extended to apply the desired charging / discharging current for different battery packs.

Appendix A

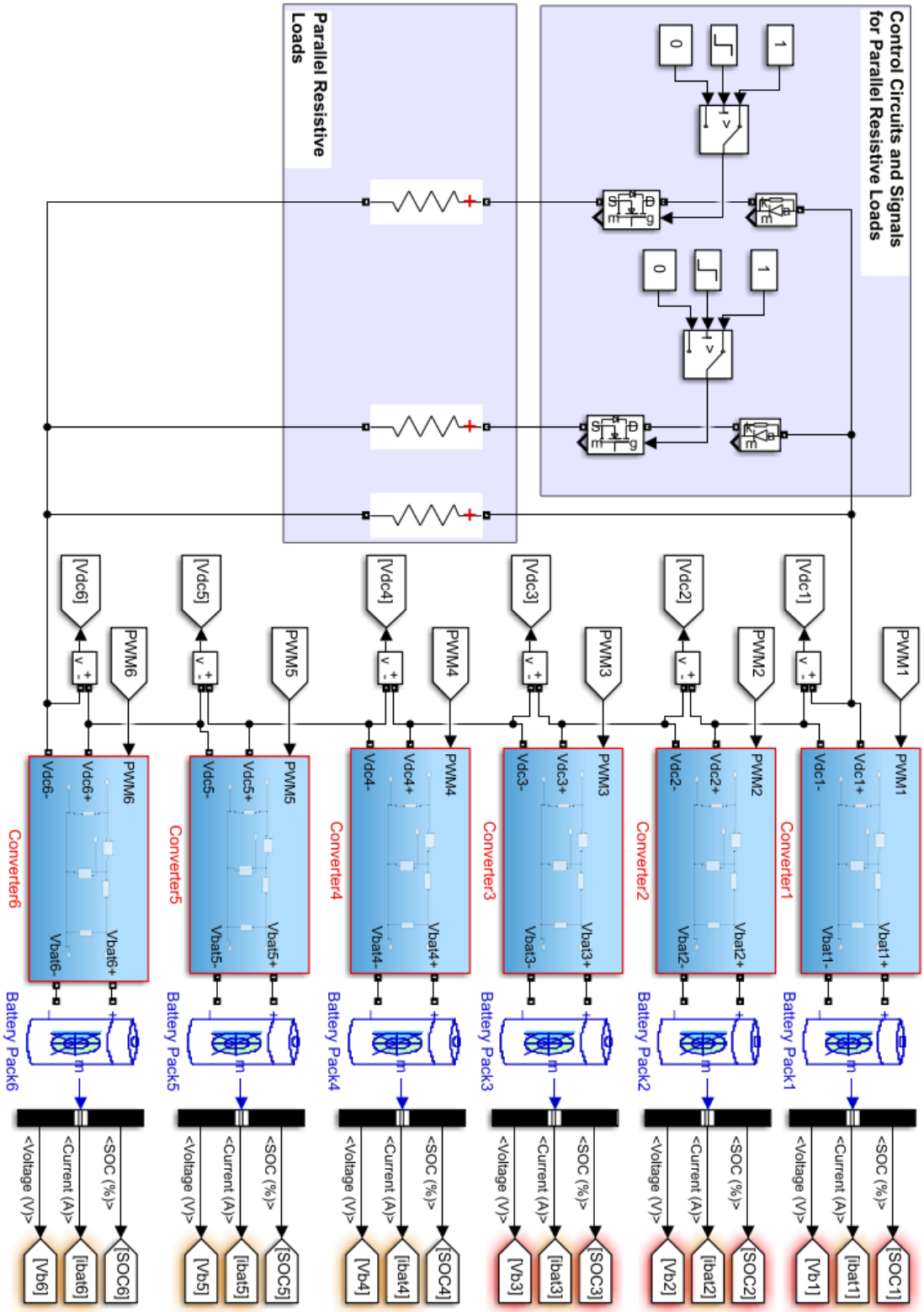

Figure A1: Simulink Model of Distributed Battery Energy Storage Systems

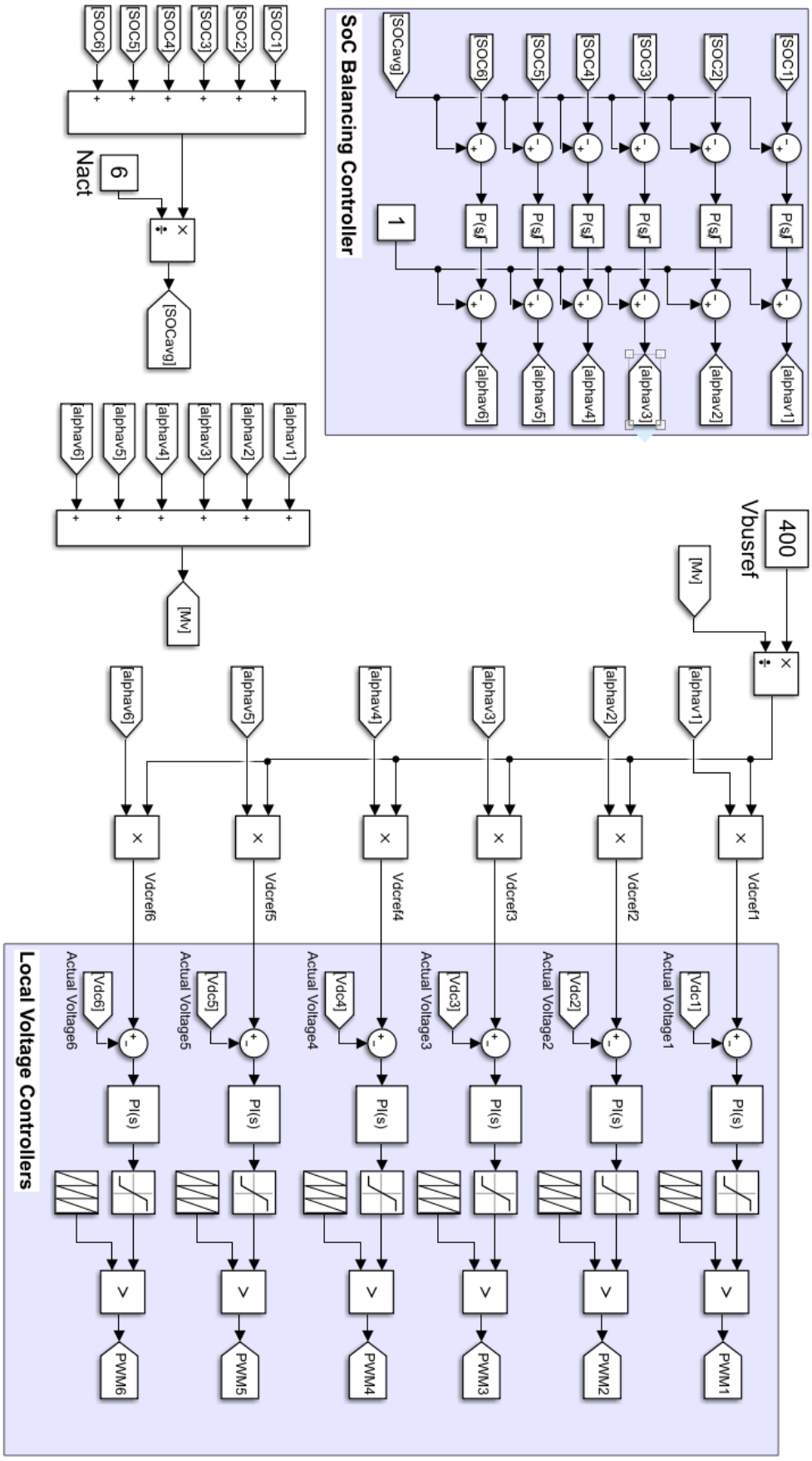

Figure A2: Simulink Model of SoC-based Power Sharing Controller

Appendix B

Table B1: Important Parameters of Converters Components used in Efficiency Calculation in Section 3.2

Components / Parameters	MOSFET (SIR606BDP)	DIODE (V40PW10C)	INDUCTOR (7443763540220)
On-state resistance, Rds,on (mΩ)	17.4	-	-
DC Series Resistance, DCR (mΩ)	-	-	3.2
Diode on state voltage drop, Vsd (V)	1.1	0.89	-
Rise Time, tr (ns)	5	-	-
Fall Time, tf (ns)	5	-	-
Total gate Charge, Qg (nC)	20	-	-
Output capacitance, Coss (pF)	132	-	-

Table B2: Important Parameters of Converters Components used in Efficiency Calculation in Section 4.3

Components / Parameters	MOSFET (TK18E10K3)	INDUCTOR (IHLP-8787MZ5A)
On-state resistance, Rds,on (mΩ)	33	-
DC Series Resistance, DCR (mΩ)	-	15.1
Diode on state voltage drop, Vsd (V)	1.2	-
Rise Time, tr (ns)	9	-
Fall Time, tf (ns)	7	-
Total gate Charge, Qg (nC)	33	-
Output capacitance, Coss (pF)	200	-

References

[1] H. Mahmood, D. Michaelson, and J. Jiang, "A Power Management Strategy for PV/Battery Hybrid Systems in Islanded Microgrids," *IEEE Journal of Emerging and Selected Topics in Power Electronics,* vol. 2, no. 4, pp. 870-882, 2014.

[2] M. T. Lawder *et al.*, "Battery Energy Storage System (BESS) and Battery Management System (BMS) for Grid-Scale Applications," *Proceedings of the IEEE,* vol. 102, no. 6, pp. 1014-1030, 2014.

[3] M. Stecca, L. R. Elizondo, T. B. Soeiro, P. Bauer, and P. Palensky, "A Comprehensive Review of the Integration of Battery Energy Storage Systems Into Distribution Networks," *IEEE Open Journal of the Industrial Electronics Society,* vol. 1, pp. 46-65, 2020.

[4] M. J. Rana and M. A. Abido, "Energy management in DC microgrid with energy storage and model predictive controlled AC–DC converter," *IET Generation, Transmission & Distribution,* https://doi.org/10.1049/iet-gtd.2016.1934 vol. 11, no. 15, pp. 3694-3702, 2017/10/01 2017.

[5] Z. Yi, W. Dong, and A. H. Etemadi, "A Unified Control and Power Management Scheme for PV-Battery-Based Hybrid Microgrids for Both Grid-Connected and Islanded Modes," *IEEE Transactions on Smart Grid,* vol. 9, no. 6, pp. 5975-5985, 2018.

[6] S. A. Hamidi, J. S. Katcha, and A. Nasiri, "Design and implementation of a DC line-interactive uninterruptible power supply (UPS) with load leveling," in *2015 IEEE Energy Conversion Congress and Exposition (ECCE)*, 2015, pp. 1248-1254.

[7] M. Kerler, P. Burda, M. Baumann, and M. Lienkamp, "A concept of a high-energy, low-voltage EV battery pack," in *2014 IEEE International Electric Vehicle Conference (IEVC)*, 2014, pp. 1-8.

[8] I. Aghabali, J. Bauman, P. J. Kollmeyer, Y. Wang, B. Bilgin, and A. Emadi, "800-V Electric Vehicle Powertrains: Review and Analysis of Benefits, Challenges, and Future Trends," *IEEE Transactions on Transportation Electrification,* vol. 7, no. 3, pp. 927-948, 2021.

[9] C. Jung, "Power Up with 800-V Systems: The benefits of upgrading voltage power for battery-electric passenger vehicles," *IEEE Electrification Magazine,* vol. 5, no. 1, pp. 53-58, 2017.

[10] B. G. Carkhuff, P. A. Demirev, and R. Srinivasan, "Impedance-Based Battery Management System for Safety Monitoring of Lithium-Ion Batteries," *IEEE Transactions on Industrial Electronics,* vol. 65, no. 8, pp. 6497-6504, 2018.

[11] Z. B. Omariba, L. Zhang, and D. Sun, "Review of Battery Cell Balancing Methodologies for Optimizing Battery Pack Performance in Electric Vehicles," *IEEE Access,* vol. 7, pp. 129335-129352, 2019.

[12] Y. Xing, E. W. M. Ma, K. L. Tsui, and M. Pecht, "Battery Management Systems in Electric and Hybrid Vehicles," vol. 4, no. 11, pp. 1840-1857, 2011.

[13] W. Huang and J. A. A. Qahouq, "Energy Sharing Control Scheme for State-of-Charge Balancing of Distributed Battery Energy Storage System," *IEEE Transactions on Industrial Electronics,* vol. 62, no. 5, pp. 2764-2776, 2015.

[14] Y. Li and Y. Han, "Evaluation of a module-integrated distributed battery energy storage system," in *2015 IEEE Energy Conversion Congress and Exposition (ECCE)*, 2015, pp. 1351-1358.

[15] F. Altaf, B. Egardt, and L. J. Mårdh, "Load Management of Modular Battery Using Model Predictive Control: Thermal and State-of-Charge Balancing," *IEEE Transactions on Control Systems Technology*, vol. 25, no. 1, pp. 47-62, 2017.

[16] Y. Li and Y. Han, "Used-battery management with integrated battery building block system," in *2015 IEEE Applied Power Electronics Conference and Exposition (APEC)*, 2015, pp. 3177-3182.

[17] N. Mukherjee and D. Strickland, "Control of Second-Life Hybrid Battery Energy Storage System Based on Modular Boost-Multilevel Buck Converter," *IEEE Transactions on Industrial Electronics*, vol. 62, no. 2, pp. 1034-1046, 2015.

[18] C. Liu, N. Gao, X. Cai, and R. Li, "Differentiation Power Control of Modules in Second-Life Battery Energy Storage System Based on Cascaded H-Bridge Converter," *IEEE Transactions on Power Electronics*, vol. 35, no. 6, pp. 6609-6624, 2020.

[19] V. Karthikeyan and R. Gupta, "Multiple-Input Configuration of Isolated Bidirectional DC–DC Converter for Power Flow Control in Combinational Battery Storage," *IEEE Transactions on Industrial Informatics*, vol. 14, no. 1, pp. 2-11, 2018.

[20] Q. Sun, J. Wu, C. Gan, J. Si, J. Guo, and Y. Hu, "Cascaded Multiport Converter for SRM-Based Hybrid Electrical Vehicle Applications," *IEEE Transactions on Power Electronics*, vol. 34, no. 12, pp. 11940-11951, 2019.

[21] Y. H. Hsieh, T. J. Liang, S. M. O. Chen, W. Y. Horng, and Y. Y. Chung, "A Novel High-Efficiency Compact-Size Low-Cost Balancing Method for Series-Connected Battery Applications," *IEEE Transactions on Power Electronics*, vol. 28, no. 12, pp. 5927-5939, 2013.

[22] G. Wu, R. Lu, C. Zhu, and C. C. Chan, "State of charge Estimation for NiMH Battery based on electromotive force method," in *2008 IEEE Vehicle Power and Propulsion Conference*, 2008, pp. 1-5.

[23] M. Thingvad, L. Calearo, A. Thingvad, R. Viskinde, and M. Marinelli, "Characterization of NMC Lithium-ion Battery Degradation for Improved Online State Estimation," in *2020 55th International Universities Power Engineering Conference (UPEC)*, 2020, pp. 1-6.

[24] X. Wang and Y. Liu, "Analysis of Energy Storage Technology and Their Application for Micro Grid," in *2017 International Conference on Computer Technology, Electronics and Communication (ICCTEC)*, 2017, pp. 972-975.

[25] R. Zhang, J. Wu, R. Wang, R. Yan, Y. Zhu, and X. He, "A Novel Battery Management System Architecture Based on an Isolated Power/Data Multiplexing Transmission Bus," *IEEE Transactions on Industrial Electronics*, vol. 66, no. 8, pp. 5979-5991, 2019.

[26] S. A. Hamidi, "DC line-interactive uninterruptible power supply (UPS) with load leveling for constant power and pulse loads," The University of Wisconsin-Milwaukee, 2017.

[27] LinearTechnology, "LTC6804-1/LTC6804-2 Multicell Battery Monitors," [Online] Available: https://www.analog.com/media/en/technical-documentation/data-sheets/680412fc.pdf.

[28] X. Wu, X. Li, and J. Du, "State of Charge Estimation of Lithium-Ion Batteries Over Wide Temperature Range Using Unscented Kalman Filter," *IEEE Access,* vol. 6, pp. 41993-42003, 2018.

[29] J. Xu, B. Cao, J. Cao, Z. Zou, C. C. Mi, and Z. Chen, "A Comparison Study of the Model Based SOC Estimation Methods for Lithium-Ion Batteries," in *2013 IEEE Vehicle Power and Propulsion Conference (VPPC)*, 2013, pp. 1-5.

[30] R. Xiong, J. Cao, Q. Yu, H. He, and F. Sun, "Critical Review on the Battery State of Charge Estimation Methods for Electric Vehicles," *IEEE Access,* vol. 6, pp. 1832-1843, 2018.

[31] M. Cacciato, G. Nobile, G. Scarcella, and G. Scelba, "Real-time model-based estimation of SOC and SOH for energy storage systems," in *2015 IEEE 6th International Symposium on Power Electronics for Distributed Generation Systems (PEDG)*, 2015, pp. 1-8.

[32] T.-H. Wu and C.-S. Moo, "State-of-Charge Estimation with State-of-Health Calibration for Lithium-Ion Batteries," *Energies,* vol. 10, no. 7, 2017.

[33] K. Movassagh, A. Raihan, B. Balasingam, and K. Pattipati, "A Critical Look at Coulomb Counting Approach for State of Charge Estimation in Batteries," *Energies,* vol. 14, no. 14, 2021.

[34] C. Hou, J. Chen, J. Hu, H. Wang, and S. Xu, "An online calibration algorithm of SOC for LiFePO4 battery by using characteristic curve," in *2015 5th International Conference on Electric Utility Deregulation and Restructuring and Power Technologies (DRPT)*, 2015, pp. 2108-2112.

[35] I. Baccouche, S. Jemmali, A. Mlayah, B. Manai, and N. Essoukri Ben Amara, "Implementation of an Improved Coulomb-Counting Algorithm Based on a Piecewise SOC-OCV Relationship for SOC Estimation of Li-IonBattery," *International Journal of Renewable Energy Research,* vol. 8, pp. 178-187, 03/27 2018.

[36] R. Xiong, Q. Yu, and F. Sun, "A study on the inflence of two OCV tests on state of charge estimation of lithium ion battery," in *2017 12th IEEE Conference on Industrial Electronics and Applications (ICIEA)*, 2017, pp. 608-612.

[37] Y. Li, H. Guo, F. Qi, Z. Guo, and M. Li, "Comparative Study of the Influence of Open Circuit Voltage Tests on State of Charge Online Estimation for Lithium-Ion Batteries," *IEEE Access,* vol. 8, pp. 17535-17547, 2020.

[38] L. Ju, G. Geng, Q. Jiang, Y. Gong, and C. Qin, "An Adaptive OCV-SOC Curve Selection Classifier for Battery State-of-Charge Estimation," in *2021 3rd International Conference on Smart Power & Internet Energy Systems (SPIES)*, 2021, pp. 457-463.

[39] D. N. T. How, M. A. Hannan, M. S. H. Lipu, and P. J. Ker, "State of Charge Estimation for Lithium-Ion Batteries Using Model-Based and Data-Driven Methods: A Review," *IEEE Access,* vol. 7, pp. 136116-136136, 2019.

[40] W. Zhou, Y. Zheng, Z. Pan, and Q. Lu, "Review on the Battery Model and SOC Estimation Method," *Processes,* vol. 9, no. 9, 2021.

[41] R. Zhang *et al.*, "A Study on the Open Circuit Voltage and State of Charge Characterization of High Capacity Lithium-Ion Battery Under Different Temperature," *Energies,* vol. 11, no. 9, 2018.

[42] J. P. Rivera-Barrera, N. Muñoz-Galeano, and H. O. Sarmiento-Maldonado, "SoC Estimation for Lithium-ion Batteries: Review and Future Challenges," *Electronics,* vol. 6, no. 4, 2017.

[43] H. He, R. Xiong, and J. Fan, "Evaluation of Lithium-Ion Battery Equivalent Circuit Models for State of Charge Estimation by an Experimental Approach," *Energies,* vol. 4, no. 4, 2011.

[44] G. Saldaña, J. I. San Martín, I. Zamora, F. J. Asensio, and O. Oñederra, "Analysis of the Current Electric Battery Models for Electric Vehicle Simulation," *Energies,* vol. 12, no. 14, 2019.

[45] X. Guo, X. Xu, J. Geng, X. Hua, Y. Gao, and Z. Liu, "SOC Estimation with an Adaptive Unscented Kalman Filter Based on Model Parameter Optimization," *Applied Sciences,* vol. 9, no. 19, 2019.

[46] Z. He, Z. Yang, X. Cui, and E. Li, "A Method of State-of-Charge Estimation for EV Power Lithium-Ion Battery Using a Novel Adaptive Extended Kalman Filter," *IEEE Transactions on Vehicular Technology,* vol. PP, pp. 1-1, 10/20 2020.

[47] J. Li, M. Ye, S. Jiao, W. Meng, and X. Xu, "A Novel State Estimation Approach Based on Adaptive Unscented Kalman Filter for Electric Vehicles," *IEEE Access,* vol. 8, pp. 185629-185637, 2020.

[48] F. Sun, X. Hu, Y. Zou, and S. Li, "Adaptive unscented Kalman filtering for state of charge estimation of a lithium-ion battery for electric vehicles," *Fuel and Energy Abstracts,* vol. 36, pp. 3531-3540, 05/01 2011.

[49] Q. Yu, R. Xiong, and C. Lin, "Online Estimation of State-of-charge Based on the H infinity and Unscented Kalman Filters for Lithium Ion Batteries," *Energy Procedia,* vol. 105, pp. 2791-2796, 2017/05/01/ 2017.

[50] J. Xu, C. C. Mi, B. Cao, J. Deng, Z. Chen, and S. Li, "The State of Charge Estimation of Lithium-Ion Batteries Based on a Proportional-Integral Observer," *IEEE Transactions on Vehicular Technology,* vol. 63, no. 4, pp. 1614-1621, 2014.

[51] I. S. Kim, "A Technique for Estimating the State of Health of Lithium Batteries Through a Dual-Sliding-Mode Observer," *IEEE Transactions on Power Electronics,* vol. 25, no. 4, pp. 1013-1022, 2010.

[52] B. Ning, J. Xu, B. Cao, B. Wang, and G. Xu, "A Sliding Mode Observer SOC Estimation Method Based on Parameter Adaptive Battery Model," *Energy Procedia,* vol. 88, pp. 619-626, 2016/06/01/ 2016.

[53] Y. Xu *et al.*, "State of charge estimation for lithium-ion batteries based on adaptive dual Kalman filter," *Applied Mathematical Modelling,* vol. 77, pp. 1255-1272, 2020/01/01/ 2020.

[54] J. Meng, D. Stroe, M. Ricco, G. Luo, and R. Teodorescu, "A Simplified Model-Based State-of-Charge Estimation Approach for Lithium-Ion Battery With Dynamic Linear Model," *IEEE Transactions on Industrial Electronics,* vol. 66, no. 10, pp. 7717-7727, 2019.

[55] M. S. Hossain Lipu *et al.*, "Data-driven state of charge estimation of lithium-ion batteries: Algorithms, implementation factors, limitations and future trends," *Journal of Cleaner Production,* vol. 277, p. 124110, 2020/12/20/ 2020.

[56] Y. Wei and L. Ling, "State of Charge Estimation for Lithium-Ion Battery based on Artificial Neural Network," in *2021 IEEE 5th Advanced Information Technology, Electronic and Automation Control Conference (IAEAC)*, 2021, vol. 5, pp. 2454-2458.

[57] M. Ismail, R. Dlyma, A. Elrakaybi, R. Ahmed, and S. Habibi, "Battery state of charge estimation using an Artificial Neural Network," in *2017 IEEE Transportation Electrification Conference and Expo (ITEC)*, 2017, pp. 342-349.

[58] E. Ipek, M. K. Eren, and M. Yilmaz, "State-of-Charge Estimation of Li-ion Battery Cell using Support Vector Regression and Gradient Boosting Techniques," in *2019 International Aegean Conference on Electrical Machines and Power Electronics (ACEMP) & 2019 International Conference on Optimization of Electrical and Electronic Equipment (OPTIM)*, 2019, pp. 604-609.

[59] Y. Chen, B. Long, and X. Lei, "The Battery State of Charge Estimation Based Weighted Least Squares Support Vector Machine," in *2011 Asia-Pacific Power and Energy Engineering Conference*, 2011, pp. 1-4.

[60] C.-T. Ma, "Design and Implementation of a Hybrid Real-Time State of Charge Estimation Scheme for Battery Energy Storage Systems," *Processes*, vol. 8, no. 1, 2020.

[61] S. Yang *et al.*, "A parameter adaptive method for state of charge estimation of lithium-ion batteries with an improved extended Kalman filter," *Scientific Reports*, vol. 11, no. 1, p. 5805, 2021/03/11 2021.

[62] M. Naguib, P. Kollmeyer, and A. Emadi, "Lithium-Ion Battery Pack Robust State of Charge Estimation, Cell Inconsistency, and Balancing: Review," *IEEE Access*, vol. 9, pp. 50570-50582, 2021.

[63] Y. Song, D. Liu, and Y. Peng, "Series-connected lithium-ion battery pack health modeling with cell inconsistency evaluation," in *2019 IEEE International Instrumentation and Measurement Technology Conference (I2MTC)*, 2019, pp. 1-6.

[64] D. Lin, Z. Li, Y. Feng, X. Wang, and S. Li, "Research on Inconsistency Identification of Lithium-ion Battery Pack Based on Operational Data," in *2021 4th IEEE International Conference on Industrial Cyber-Physical Systems (ICPS)*, 2021, pp. 498-502.

[65] I. Aizpuru, U. Iraola, J. Mari, and A. Goikoetxea, "Comparative Study and Evaluation of Passive Balancing Against Single Switch Active Balancing Systems for Energy Storage Systems," in *PCIM Europe 2016; International Exhibition and Conference for Power Electronics, Intelligent Motion, Renewable Energy and Energy Management*, 2016, pp. 1-9.

[66] J.Qi and D.D.-C.Lu,"Review of battery cell balancing techniques," in *2014 Australasian Universities Power Engineering Conference (AUPEC)*, 2014, pp. 1-6.

[67] M. Daowd, N. Omar, P. V. D. Bossche, and J. V. Mierlo, "Passive and active battery balancing comparison based on MATLAB simulation," in *2011 IEEE Vehicle Power and Propulsion Conference*, 2011, pp. 1-7.

[68] D. J. Park, S. Y. Choi, R. Y. Kim, and D. S. Kim, "A novel battery cell balancing circuit using an auxiliary circuit for fast equalization," in *IECON 2014 - 40th Annual Conference of the IEEE Industrial Electronics Society*, 2014, pp. 2933-2938.

[69] A. B. Ahmad, C. A. Ooi, and D. Ishak, "State-of-Charge Balancing Control for Optimal Cell Utilisation of a Grid-Scale Three-Phase Battery Energy Storage System Using Hybrid Modular Multilevel Converter Topology Without Redundant Cells," *IEEE Access*, vol. 9, pp. 53920-53935, 2021.

[70] Q. Ouyang, J. Chen, J. Zheng, and H. Fang, "Optimal Cell-to-Cell Balancing Topology Design for Serially Connected Lithium-Ion Battery Packs," *IEEE Transactions on Sustainable Energy*, vol. 9, no. 1, pp. 350-360, 2018.

[71] B. Yildirim, M. Elgendy, A. Smith, and V. Pickert, "Evaluation and Comparison of Battery Cell Balancing Methods," in *2019 IEEE PES Innovative Smart Grid Technologies Europe (ISGT-Europe)*, 2019, pp. 1-5.

[72] W. C. Lee, D. Drury, and P. Mellor, "Comparison of passive cell balancing and active cell balancing for automotive batteries," in *2011 IEEE Vehicle Power and Propulsion Conference*, 2011, pp. 1-7.

[73] M. Kim, J. Kim, and G. Moon, "Center-Cell Concentration Structure of a Cell-to-Cell Balancing Circuit With a Reduced Number of Switches," *IEEE Transactions on Power Electronics*, vol. 29, no. 10, pp. 5285-5297, 2014.

[74] Y. Wang, H. Yin, S. Han, A. Alsabbagh, and C. Ma, "A novel switched capacitor circuit for battery cell balancing speed improvement," in *2017 IEEE 26th International Symposium on Industrial Electronics (ISIE)*, 2017, pp. 1977-1982.

[75] A. C. Baughman and M. Ferdowsi, "Double-Tiered Switched-Capacitor Battery Charge Equalization Technique," *IEEE Transactions on Industrial Electronics*, vol. 55, no. 6, pp. 2277-2285, 2008.

[76] M. Kim, C. Kim, J. Kim, and G. Moon, "A Chain Structure of Switched Capacitor for Improved Cell Balancing Speed of Lithium-Ion Batteries," *IEEE Transactions on Industrial Electronics*, vol. 61, no. 8, pp. 3989-3999, 2014.

[77] M. Kim, C. Kim, J. Kim, D. Kim, and G. Moon, "Switched capacitor with chain structure for cell-balancing of lithium-ion batteries," in *IECON 2012 - 38th Annual Conference on IEEE Industrial Electronics Society*, 2012, pp. 2994-2999.

[78] Y. Ye, K. W. E. Cheng, Y. C. Fong, X. Xue, and J. Lin, "Topology, Modeling, and Design of Switched-Capacitor-Based Cell Balancing Systems and Their Balancing Exploration," *IEEE Transactions on Power Electronics*, vol. 32, no. 6, pp. 4444-4454, 2017.

[79] T. H. Phung, J. C. Crebier, A. Chureau, A. Collet, and V. Nguyen, "Optimized structure for next-to-next balancing of series-connected lithium-ion cells," in *2011 Twenty-Sixth Annual IEEE Applied Power Electronics Conference and Exposition (APEC)*, 2011, pp. 1374-1381.

[80] S. Park, T. Kim, J. Park, G. Moon, and M. Yoon, "A New Buck-boost Type Battery Equalizer," in *2009 Twenty-Fourth Annual IEEE Applied Power Electronics Conference and Exposition*, 2009, pp. 1246-1250.

[81] S. Li, C. C. Mi, and M. Zhang, "A High-Efficiency Active Battery-Balancing Circuit Using Multiwinding Transformer," *IEEE Transactions on Industry Applications*, vol. 49, no. 1, pp. 198-207, 2013.

[82] N. H. Kutkut, D. M. Divan, and D. W. Novotny, "Charge equalization for series connected battery strings," *IEEE Transactions on Industry Applications*, vol. 31, no. 3, pp. 562-568, 1995.

[83] N. H. Kutkut, H. L. N. Wiegman, D. M. Divan, and D. W. Novotny, "Design considerations for charge equalization of an electric vehicle battery system," *IEEE Transactions on Industry Applications*, vol. 35, no. 1, pp. 28-35, 1999.

[84] Y. Chen, X. Liu, Y. Cui, J. Zou, and S. Yang, "A MultiWinding Transformer Cell-to-Cell Active Equalization Method for Lithium-Ion Batteries With Reduced Number of Driving Circuits," *IEEE Transactions on Power Electronics*, vol. 31, no. 7, pp. 4916-4929, 2016.

[85] D. V. Cadar, D. M. Petreus, and T. M. Patarau, "An energy converter method for battery cell balancing," in *33rd International Spring Seminar on Electronics Technology, ISSE 2010*, 2010, pp. 290-293.

[86] H. S, "Overview of cell balancing methods for Li-ion battery technology," vol. 3, no. 2, p. e203, 2021.

[87] Q. Ouyang, J. Chen, J. Zheng, and Y. Hong, "SOC Estimation-Based Quasi-Sliding Mode Control for Cell Balancing in Lithium-Ion Battery Packs," *IEEE Transactions on Industrial Electronics*, vol. 65, no. 4, pp. 3427-3436, 2018.

[88] L. Yuang-Shung, D. Chun-Yi, C. Guo-Tian, and Y. Shen-Ching, "Battery Equalization Using Bi-directional Cuk Converter in DCVM Operation," in *2005 IEEE 36th Power Electronics Specialists Conference*, 2005, pp. 765-771.

[89] X. Cui, W. Shen, Y. Zhang, C. Hu, and J. Zheng, "Novel active LiFePO4 battery balancing method based on chargeable and dischargeable capacity," *Computers & Chemical Engineering*, vol. 97, pp. 27-35, 2017/02/02/ 2017.

[90] C. Kim, M. Kim, H. Park, and G. Moon, "A Modularized Two-Stage Charge Equalizer With Cell Selection Switches for Series-Connected Lithium-Ion Battery String in an HEV," *IEEE Transactions on Power Electronics*, vol. 27, no. 8, pp. 3764-3774, 2012.

[91] C. Kim, M. Kim, Y. Kim, and G. Moon, "A modularized charge equalizer using battery monitoring IC for series connected Li-Ion battery strings in an electric vehicle," in *8th International Conference on Power Electronics - ECCE Asia*, 2011, pp. 304-309.

[92] M. Uno and K. Tanaka, "Single-switch cell voltage equalizer using voltage multipliers for series-connected supercapacitors," in *2012 Twenty-Seventh Annual IEEE Applied Power Electronics Conference and Exposition (APEC)*, 2012, pp. 1266-1272.

[93] Y. Li and Y. Han, "A module-integrated distributed battery energy storage and management system," *IEEE Transactions on Power Electronics*, vol. 31, no. 12, pp. 8260-8270, 2016.

[94] Y. Li and Y. Han, "Power electronics integration on battery cells," in *2014 IEEE Applied Power Electronics Conference and Exposition - APEC 2014*, 2014, pp. 3318-3322.

[95] W. Huang and J. A. A. Qahouq, "Distributed battery energy storage system architecture with energy sharing control for charge balancing," in *2014 IEEE Applied Power Electronics Conference and Exposition - APEC 2014*, 2014, pp. 1126-1130.

[96] Y. Li and Y. Han, "Control of input-series and output-independent power converter building block system based on buck converter topology," in *2015 IEEE Applied Power Electronics Conference and Exposition (APEC)*, 2015, pp. 422-429.

[97] H. Bahrami, S. Farhangi, H. Iman-Eini, and E. Adib, "A New Interleaved Coupled-Inductor Nonisolated Soft-Switching Bidirectional DC–DC Converter With High Voltage Gain Ratio," *IEEE Transactions on Industrial Electronics*, vol. 65, no. 7, pp. 5529-5538, 2018.

[98] L. Jiang, C. C. Mi, S. Li, M. Zhang, X. Zhang, and C. Yin, "A Novel Soft-Switching Bidirectional DC–DC Converter With Coupled Inductors," *IEEE Transactions on Industry Applications*, vol. 49, no. 6, pp. 2730-2740, 2013.

[99] H. Wu, K. Sun, L. Chen, L. Zhu, and Y. Xing, "High Step-Up/Step-Down Soft-Switching Bidirectional DC–DC Converter With Coupled-Inductor and Voltage Matching Control for Energy Storage Systems," *IEEE Transactions on Industrial Electronics*, vol. 63, no. 5, pp. 2892-2903, 2016.

[100] A. Ayachit, S. U. Hasan, Y. P. Siwakoti, M. Abdul-Hak, M. K. Kazimierczuk, and F. Blaabjerg, "Coupled-Inductor Bidirectional DC-DC Converter for EV Charging Applications with Wide Voltage Conversion Ratio and Low Parts Count," in *2019 IEEE Energy Conversion Congress and Exposition (ECCE)*, 2019, pp. 1174-1179.

[101] C. Hong, L. Yang, T. Liang, and J. Chen, "Novel bidirectional DC-DC converter with high step-up/down voltage gain," in *2009 IEEE Energy Conversion Congress and Exposition*, 2009, pp. 60-66.

[102] M. Aamir, S. Mekhilef, and H. Kim, "High-Gain Zero-Voltage Switching Bidirectional Converter With a Reduced Number of Switches," *IEEE Transactions on Circuits and Systems II: Express Briefs*, vol. 62, no. 8, pp. 816-820, 2015.

[103] S. Waffler and J. W. Kolar, "A Novel Low-Loss Modulation Strategy for High-Power Bidirectional Buck + Boost Converters," *IEEE Transactions on Power Electronics*, vol. 24, no. 6, pp. 1589-1599, 2009.

[104] F. Caricchi, F. Crescimbini, and A. D. Napoli, "20 kW water-cooled prototype of a buck-boost bidirectional DC-DC converter topology for electrical vehicle motor drives," in *Proceedings of 1995 IEEE Applied Power Electronics Conference and Exposition - APEC'95*, 1995, vol. 2, pp. 887-892 vol.2.

[105] M. A. Khan, A. Ahmed, I. Husain, Y. Sozer, and M. Badawy, "Performance Analysis of Bidirectional DC–DC Converters for Electric Vehicles," *IEEE Transactions on Industry Applications*, vol. 51, no. 4, pp. 3442-3452, 2015.

[106] H. S. Lee and J. J. Yun, "High-Efficiency Bidirectional Buck–Boost Converter for Photovoltaic and Energy Storage Systems in a Smart Grid," *IEEE Transactions on Power Electronics*, vol. 34, no. 5, pp. 4316-4328, 2019.

[107] M. Nasir, H. A. Khan, A. Hussain, L. Mateen, and N. A. Zaffar, "Solar PV-Based Scalable DC Microgrid for Rural Electrification in Developing Regions," *IEEE Transactions on Sustainable Energy*, vol. 9, no. 1, pp. 390-399, 2018.

[108] A. Kloenne and T. Sigle, "Bidirectional ZETA/SEPIC converter as battery charging system with high transfer ratio," in *2017 19th European Conference on Power Electronics and Applications (EPE'17 ECCE Europe)*, 2017, pp. P.1-P.7.

[109] H. Y. Lee, T. J. Liang, J. F. Chen, and K. H. Chen, "Design and implementation of a bidirectional SEPIC-Zeta DC-DC Converter," in *2014 IEEE International Symposium on Circuits and Systems (ISCAS)*, 2014, pp. 101-104.

[110] S. A. Gorji, H. G. Sahebi, M. Ektesabi, and A. B. Rad, "Topologies and Control Schemes of Bidirectional DC–DC Power Converters: An Overview," *IEEE Access*, vol. 7, pp. 117997-118019, 2019.

[111] T. Jiang, J. Zhang, X. Wu, K. Sheng, and Y. Wang, "A Bidirectional LLC Resonant Converter With Automatic Forward and Backward Mode Transition," *IEEE Transactions on Power Electronics*, vol. 30, no. 2, pp. 757-770, 2015.

[112] A. R. R. Alonso, J. Sebastian, D. G. Lamar, M. M. Hernando, and A. Vazquez, "An overall study of a Dual Active Bridge for bidirectional DC/DC conversion," in *2010 IEEE Energy Conversion Congress and Exposition*, 2010, pp. 1129-1135.

[113] Y. Liu *et al.*, "A Simple Phase-Shift Modulation Using Parabolic Carrier for Dual Active Bridge DC–DC Converter," *IEEE Transactions on Power Electronics*, vol. 35, no. 8, pp. 7729-7734, 2020.

[114] X. Liu *et al.*, "Novel Dual-Phase-Shift Control With Bidirectional Inner Phase Shifts for a Dual-Active-Bridge Converter Having Low Surge Current and Stable Power Control," *IEEE Transactions on Power Electronics*, vol. 32, no. 5, pp. 4095-4106, 2017.

[115] S. S. Muthuraj, V. K. Kanakesh, P. Das, and S. K. Panda, "Triple Phase Shift Control of an LLL Tank Based Bidirectional Dual Active Bridge Converter," *IEEE Transactions on Power Electronics*, vol. 32, no. 10, pp. 8035-8053, 2017.

[116] W. Jiang, L. Kai, R. Hu, and W. Chen, "Novel Modeling and Design of a Dual Half Bridge DC-DC Converter Applied in Supercapacitor Energy Storage System," *Electric Power Components and Systems*, vol. 42, no. 13, pp. 1398-1408, 2014/10/03 2014.

[117] F. Z. Peng, L. Hui, S. Gui-Jia, and J. S. Lawler, "A new ZVS bidirectional DC-DC converter for fuel cell and battery application," *IEEE Transactions on Power Electronics*, vol. 19, no. 1, pp. 54-65, 2004.

[118] B.-R. Lin and G.-Y. Wu, "Bidirectional Resonant Converter with Half-Bridge Circuits: Analysis, Design, and Implementation," *Energies*, vol. 11, no. 5, 2018.

[119] G. Ma, W. Qu, G. Yu, Y. Liu, N. Liang, and W. Li, "A Zero-Voltage-Switching Bidirectional DC–DC Converter With State Analysis and Soft-Switching-Oriented Design Consideration," *IEEE Transactions on Industrial Electronics*, vol. 56, no. 6, pp. 2174-2184, 2009.

[120] Y. Du, M. Wang, R. T. Meitl, S. Lukic, and A. Q. Huang, "High-frequency high-efficiency DC-DC converter for distributed energy storage modularization," in *IECON 2010 - 36th Annual Conference on IEEE Industrial Electronics Society*, 2010, pp. 1832-1837.

[121] R. Morrison and M. G. Egan, "A new power-factor-corrected single-transformer UPS design," *IEEE Transactions on Industry Applications*, vol. 36, no. 1, pp. 171-179, 2000.

[122] C. Bai, B. Han, B. Kwon, and M. Kim, "Highly Efficient Bidirectional Series-Resonant DC/DC Converter Over Wide Range of Battery Voltages," *IEEE Transactions on Power Electronics*, vol. 35, no. 4, pp. 3636-3650, 2020.

[123] K. L. Jorgensen, M. C. Mira, Z. Zhang, and M. A. E. Andersen, "Review of high efficiency bidirectional dc-dc topologies with high voltage gain," in *2017 52nd International Universities Power Engineering Conference (UPEC)*, 2017, pp. 1-6.

[124] B. M. Reddy and P. Samuel, "A comparative analysis of non-isolated bi-directional dc-dc converters," in *2016 IEEE 1st International Conference on Power Electronics, Intelligent Control and Energy Systems (ICPEICES)*, 2016, pp. 1-6.

[125] K. Tytelmaier, O. Husev, O. Veligorskyi, and R. Yershov, "A review of non-isolated bidirectional dc-dc converters for energy storage systems," in *2016 II International Young Scientists Forum on Applied Physics and Engineering (YSF)*, 2016, pp. 22-28.

[126] M. M. U. Rehman, "Modular, Scalable Battery Systems with Integrated Cell Balancing and DC Bus Power Processing,", PhD Thesis, Utah State University, 2018.

[127] Y. Li and Y. Han, "A new perspective on battery cell balancing: Thermal balancing and relative temperature control," in *2016 IEEE Energy Conversion Congress and Exposition (ECCE)*, 2016, pp. 1-5.

[128] R. Xiong, Y. Zhang, J. Wang, H. He, S. Peng, and M. Pecht, "Lithium-Ion Battery Health Prognosis Based on a Real Battery Management System Used in Electric Vehicles," *IEEE Transactions on Vehicular Technology*, vol. 68, no. 5, pp. 4110-4121, 2019.

[129] N. Mukherjee and D. Strickland, "Analysis and Comparative Study of Different Converter Modes in Modular Second-Life Hybrid Battery Energy Storage Systems," *IEEE Journal of Emerging and Selected Topics in Power Electronics*, vol. 4, no. 2, pp. 547-563, 2016.

[130] N. Li, F. Gao, T. Hao, Z. Ma, and C. Zhang, "SOH Balancing Control Method for the MMC Battery Energy Storage System," *IEEE Transactions on Industrial Electronics*, vol. 65, no. 8, pp. 6581-6591, 2018.

[131] Y. Ting, K. Huang, S. W. H. d. Haan, and J. A. Ferreira, "A comparison of module shutdown methods in an input-series and output-parallel connected modular DC-DC converter," in *7th IET International Conference on Power Electronics, Machines and Drives (PEMD 2014)*, 2014, pp. 1-6.

[132] N. Mukherjee and D. Strickland, "Control of Cascaded DC–DC Converter-Based Hybrid Battery Energy Storage Systems—Part I: Stability Issue," *IEEE Transactions on Industrial Electronics*, vol. 63, no. 4, pp. 2340-2349, 2016.

[133] Y. Ting, S. d. Haan, and J. A. Ferreira, "A modular DC-DC converter with collapsible input voltage of series connected modules without additional bypass switch," in *2013 IEEE Energy Conversion Congress and Exposition*, 2013, pp. 2341-2346.

[134] J. Depew, "Efficiency analysis of a synchronous buck converter using Microsoft® Office® Excel®-based loss calculator," *Microchip Technology Inc.*, pp. 1-14, 2012. [Online]. Available: http://ww1.microchip.com/downloads/en/Appnotes/01471A.pdf. .

[135] Z. Chen, B. Xia, C. C. Mi, and R. Xiong, "Loss minimization-based charging strategy for lithium-ion battery," in *2014 IEEE Energy Conversion Congress and Exposition (ECCE)*, 2014, pp. 4306-4312.

[136] J. Ahn and B. K. Lee, "High-Efficiency Adaptive-Current Charging Strategy for Electric Vehicles Considering Variation of Internal Resistance of Lithium-Ion Battery," *IEEE Transactions on Power Electronics*, vol. 34, no. 4, pp. 3041-3052, 2019.

[137] F. Díaz-González, D. Heredero-Peris, M. Pagès-Giménez, E. Prieto-Araujo, and A. Sumper, "A Comparison of Power Conversion Systems for Modular Battery-Based Energy Storage Systems," *IEEE Access*, vol. 8, pp. 29557-29574, 2020.

[138] M. Čepin, *Assessment of power system reliability: methods and applications*. Springer Science & Business Media, 2011.

[139] Broadcom, "ACPL-C87B, ACPL-C87A, ACPL-C870 Precision Optically Isolated Voltage Sensor " [Online] Available: https://docs.broadcom.com/doc/AV02-3563EN.